Quantitative proteomic analysis of natural dendritic cell subsets

A thesis submitted to the University of Dublin for the degree of Doctor of Philosophy (Ph.D.)

By
Simon David O'Shaughnessy
B.A. (Mod)
School of Biochemistry and Immunology
Trinity College Dublin
2024

Under the supervision of Dr. David Finlay

Thesis Declaration

I declare that this thesis has not been submitted as an exercise for a degree at this or any other university, and it is entirely my own work, except where duly acknowledged.

I agree to deposit this thesis in the University's open access institutional repository or allow the Library to do so on my behalf, subject to Irish Copyright Legislation and Trinity College Library conditions of use and acknowledgement.

I consent to the examiner retaining a copy of the thesis beyond the examining period, should they so wish (EU GDPR May 2018)

Simon O'Shaughnessy B.A. (Mod)

Declaration of Collaborative Input

For quantitative proteomics data presented in Chapters 3-5, sample processing and mass-spectrometry were performed by the staff of the Proteomics Unit at the University of Dundee, UK.

Analysis of raw mass-spectrometry data was performed by Dr. Alejandro Brenes in collaboration with the Cantrell and Lamond labs at the University of Dundee, UK.

Transferrin experiments in Chapter 5 were performed by Ms Carrie Corkish (Finlay lab, Trinity College Dublin), as noted in the figure legend.

Publications

Metabolic requirements of NK cells during the acute response against retrovirus infection

Elisabeth Littwitz-Salomon, Diana Moreira, Joe N. Frost, Chloe Choi, Kevin T. Liou, David K. Ahern, **Simon D. O'Shaughnessy**, Bernd Wagner, Christine A. Biron, Ulf Dittmer, David K. Finlay

(Nature Communications, 2021)

QUAS-R: An SLC1A5-mediated glutamine uptake assay with single-cell resolution reveals metabolic heterogeneity with immune populations

Leonard R. Pelgrom, Gavin M. Davis, **Simon D. O'Shaughnessy**, Emilie JM. Wezenberg, Sander L. Van Kasteren, David K. Finlay, Linda V. Sinclair

(Cell Reports, 2023)

Recognition of yeast β-glucan particles triggers immunometabolic signalling required for trained immunity

Cian JH. Horneck Johnson, Anna E. Ledwith, Mimmi LE. Lundahl, Hugo Charles-Messance, Emer E. Hackett, **Simon D. O'Shaughnessy**, Jonah Clegg, Hannah Prendeville, John P. McGrath, Aaron M. Walsh, Sarah Case, Hollie Austen Byrne, Parth Gautam, Elaine Dempsey, Sinead C. Corr, Frederick J. Sheedy

(iScience 2024)

Iron is critical for mucosal-associated invariant T cell metabolism and effector functions

Eimear Ryan, Christy Clutter, Conor DeBarra, Benjamin J. Jenkins, **Simon D. O'Shaughnessy**, Odhran Ryan, Chloe McKenna, Helen Heneghan, Fiona Walsh, David K. Finlay, Linda V. Sinclair, Nicholas Jones, Daniel T. Leung, Donal O'Shea, Andrew E. Hogan

(Journal of Immunology (JI), 2024. Under review)

Oral Presentations

Short talk

Immunometabolism Forum – Trinity College Dublin

(March 2021)

Short talk – “PHD Brightsparks”

BSI Immunometabolism – Fuelling the immune response II

(May 2022)

Short talk – Workshop 1: Fundamentals of Immunometabolism

Keystone Symposia – Immunometabolism at the Crossroads of Obesity and Cancer

(September 2022)

Poster Presentations

BSI Congress

Edinburgh, UK

(November 2021)

Abstract

Dendritic cells (DCs) are a critical bridge between innate and adaptive immunity. They are a heterogeneous population composed of various subsets that modulate different aspects of the immune response. It is now clear that immunometabolism underpins all aspects of DC biology, from development to maturation and disease response. However, detailed characterisation of the metabolic phenotypes that dictate natural DC function is still in its infancy. The goal of immunometabolism research is to translate basic metabolic findings to generate novel therapeutic approaches in the treatment of infection and disease. As DCs orchestrate both innate and adaptive responses, striking the balance between tolerance and inflammation, they are prime candidates for immunotherapeutic interventions.

In recent years, quantitative proteomics has emerged as a powerful technique to investigate immune cell metabolism and function. The ability to simultaneously characterise the expression of thousands of proteins allows detailed mechanistic analysis of the metabolic machinery, revealing novel metabolic regulators of immune function. This project applies quantitative proteomics to study the immunometabolic features of natural type-1 conventional dendritic cells (cDC1), type-2 conventional dendritic cells (cDC2) and plasmacytoid dendritic cells (pDC). This approach reveals substantial metabolic heterogeneity between cDC1s and cDC2s. In particular, it was revealed that the differential activity of the amino acid transporter, SLC7A5, controls antigen processing and presentation by modulating the activity of the kinase mechanistic target of rapamycin complex 1 (mTORC1). Finally, this project identifies that pDCs have conserved enrichment of the iron transporter, the transferrin receptor (Tfrc). However, *in silico* and functional analysis of iron utilisation by pDCs indicates an iron-independent role of Tfrc.

Overall, the data presented in this thesis contribute to the field by providing mechanistic insight into the metabolic processes that underpin natural DC biology and identifying, as of yet, undescribed regulators of DC function.

Acknowledgements

First, I would like to thank my supervisor, Dr. David Finlay, for his supervision and support throughout this project. I could not have hoped for a better mentor to guide me through this process. You provided encouragement and direction at times when it was absolutely needed. Our long chats in your office, where we would continuously go off topic just following the science, were always enjoyable and highly motivational.

To the current and past members of the Finlay lab, thank you for making the last four years so enjoyable. The lab exemplifies the idea of work-life balance. I'm so lucky to have gotten to work with such talented people who have become some of my closest friends along the way. Chloe, my oldest friend in the lab, you're an amazing and thorough scientist, and you always knew how to keep me in check. Aisling, Carrie and Cathal thank you for your support and friendship in and out of the lab. The daily life updates at lunch were a constant source of entertainment. In particular, I would like to thank Carrie for all of your work on the pDC project and for putting up with my ineptitude in managing the mouse colonies. Cris and Maxim, you are the post-docs I aspire to be. Thank you for sharing your knowledge and kindness. Diana, you were my first mentor in the lab. Your knowledge and passion for science really motivated me at the beginning of this project.

To my extended TBSI friend group, past and present. In particular, Gearoid you have become one of my best friends. One day you will figure out what on earth glutamine is doing in those NK cells! Jamie, you are an incredible scientist and a close friend. Our time spent outside of the lab was a real highlight of this PHD.

To my friends, Aaron, Fionn, Fearghal, James, Rory, Peter, Robin, Fergus, Eoghan and their better halves Andrea, Annie, Louise, Maude, Emma, Rhianne, Aideen and Dervla. I hope I havn't forgotten anyone! I am so lucky to have met such a great group. It's crazy that random room allocation in Halls

brought us all together! Thank you for your friendship and support over the years!

I would also like to thank my family for their support and encouragement throughout all of my academic career. To my parents, you always supported me in whatever path I decided to take in life. For that, I will always be grateful. To Luke and Marcus, thanks for putting up with me. To my grandparents, I hope I made you proud.

Finally, Julia, the most important person in my life. You have seen me grow over the course of this process and have supported me through the highs and lows. Your ability to make me laugh and pick me up on bad days got me through this. I love you.

Table of Contents

List of Tables

List of Figures

List of Abbreviations

2DG	2-Deoxyglucose
ADP	Adenosine diphosphate
AHA	Azidohomoalanine
AMPK	AMP-activate protein kinase
APC	Antigen presenting cell
ATAC	Assay for transposase-accessible chromatin
ATP	Adenosine triphosphate
BCAA	Branched chain amino acid
BCH	2-Amino-2-norbornanecarboxylic acid
BCR	B cell receptor
BMDM	Bone marrow derived macrophage
BSA	Bovine serum albumin
cDC	Conventional dendritic cell
CDP	Common dendritic cell precursor
CLR	C-type lectin receptor
cMoP	Common monocyte progenitor
CMP	Common myeloid progenitor
CpG	Cytosine guanosine dinucleotide
CSFR	Colony stimulating factor receptor
CTL	Cytotoxic T lymphocyte
DAMP	Danger associated molecular pattern
DC	Dendritic cell
DC3	Type-3 dendritic cell
DDA	Data dependent acquisition
DFO	Deferoxamine
DIA	Data independent acquisition
ENO1	Enolase 1
ER	Endoplasmic reticulum
ESI	Electrospray ionisation
FAO	Fatty acid oxidation
FAS	Fatty acid synthesis
FCCP	Carbonyl cyanide-p-trifuoromethoxyphenylhydrazone

FE-S	Iron-sulphur
FLDC	Flt3l derived bone marrow dendritic cell
FLT3	FMS-like tyrosine kinase
FLT3L	FMS-like tyrosine kinase ligand
FPN	Ferroportin
GM-CSF	Granulocyte-macrophage colony stimulating factor
GM-MACS	GM-CSF-derived macrophage
GMDC	GM-CSF-derived dendritic cell
GO	Gene ontology
GSEA	Gene set enrichment analysis
HIF1α	Hypoxia inducible factor 1 alpha
HKII	Hexokinase 2
HPG	Homopropargylglycine
Immgen	Immunological Genome Project
iNOS	Inducible nitric oxide synthase
ISG	Interferon stimulated gene
iTRAQ	Isobaric tag for relative and absolute quantification
JAK	Janus kinase
KEGG	Kyoto Encyclopedia of Genes and Genomes
LC	Langerhans cell
LCMS	Liquid chromatograhy mass spectrometry
LDH	Lactate dehdrogenase
LKB1	Liver kinase 1
LPS	Lipopolysaccharide
M-CSF	Macrophage colony stimulating factor
M/Z	Mass to charge ratio
MCT	Monocarboxylate transporter
MDP	Monocyte dendritic cell progenitor
MGI	Mouse Genome Informatics
MHCI	Major histocompatibility complex 1
MHCII	Major histocompatibility complex 2
moDC	Monocyte derived dendritic cell
MPC1	Mitochondrial pyruvate carrier 1

MS	Mass spectrometry
MTG	Mitotracker Green
mTORC1	Mechanistic target of rapamycin complex 1
mTORC2	Mechanistic target of rapamycin complex 2
NADPH	Nicotinamide adenine dinucleotide phosphate
NK	Natural killer cell
NLR	NOD-like receptors
O-GlcNAc	O-linked-N-acetylglucosamine
OPP	O-Propargyl-puromycin
OXPHOS	Oxidative phosphorylation
PAMP	Pathogen associated molecular pattern
pDC	Plasmacytoid dendritic cell
PDH	Pyruvate dehydrogenase
PLC	Peptide loading complex
PPP	Pentose phosphate pathway
PRR	Pathogen recognition receptor
PTM	Post-translational modification
RLR	Rig-I-like receptor
ROS	Reactive oxygen species
SILAC	Stable isotope labelling by amino acids in cell culture
SLC	Solute carrier protein
STAT	Signal transducer and activator of transcription
TCA	Tricarboxylic acid cycle
TCR	T cell receptor
tDC	Transitional dendritic cell
TFEB	Transcription factor EB
TLR	Toll-like receptor
TME	Tumour microenvironment
TMRM	Tetramethylrhodamine methyl ester
TMT	Tandem mass tag

Chapter 1 – General introduction

1.1 The Immune System

Over millions of years, humans have evolved to survive in a world that constantly threatens our wellbeing. These threats include alterations in nutrient and water supplies, physical stress, temperature changes, infections, and malignancies (Medzhitov, 2008). Pathogenic and non-pathogenic microbes heavily populate our planet alongside many stimuli that promote cancer. Despite this, we rarely become ill. This is because we have developed a complex system of molecules, cells, and tissues collectively known as the immune system. The primary role of the immune system is to recognise and eliminate pathogenic microorganisms and abnormal or damaged cellular material to re-establish homeostasis without causing excessive damage to healthy cells and tissues (Paludan et al., 2021).

During infection, the immune system responds rapidly to limit pathogen replication and harm to the host. The early response to infection is mediated by the innate immune system, which includes barrier tissues such as the skin, innate immune cells, including macrophages, innate lymphocytes, and granulocytes, and the antimicrobial products they produce. Innate immune cells express pathogen recognition receptors (PRRs) that recognise conserved pathogen-associated molecular patterns (PAMPs) that are generally absent in the host (Janeway & Medzhitov, 2002). Over millions of years of evolution, pathogens have co-evolved with the host and developed complex immune evasion strategies that undermine the immune response. As such, the innate immune response alone is often insufficient in the clearance of infection. Mammals have evolved an adaptive immune system whose activation depends on innate immune cells and mediates specific and long-term defence against pathogens. The adaptive immune system is composed of T and B lymphocytes, which promote effective immune responses (CD4+ helper T cells), kill infected and malignant cells (cytotoxic CD8+ T cells (CTLs)) and generate antibodies (Flajnik & Kasahara, 2010).

In contrast to PRR expression on innate immune cells, T and B cells express highly specific antigen detection receptors, the T cell receptor (TCR) and B cell receptor (BCR), which recognise specific peptide sequences (antigens). As the potential number of antigens expressed by pathogens is exceedingly high, the protein chains composing the TCR and BCR are variant, undergoing a process termed V(D)J recombination during development, allowing the recognition of a broad range of antigens (Bassing et al., 2002). While variant receptor generation aids in recognising pathogens, it also carries the danger of self-reactivity, which leads to autoimmunity. To combat this challenge, the immune system has tolerance mechanisms to delete self-lymphocytes before they enter the circulation (central tolerance) and after (peripheral tolerance) (Nemazee, 2017).

1.1.1 Antigen Presenting Cells

The TCR and BCR must recognise their cognate antigen to induce an adaptive immune response. Due to receptor rearrangement, the number of lymphocytes with an antigen-specific receptor is limited. As such, the chances of an adaptive immune cell interacting with its cognate antigen are exceedingly rare if it relies on migration alone. To enhance the efficiency of antigen recognition, lymphocytes concentrate in the lymphoid system, composed of the spleen, lymph nodes, and bloodstream. Professional antigen-presenting cells (APCs) are innate cells that monitor tissues for infection or malignancy and are specialised in capturing and delivering antigens from the periphery to the lymphoid organs. Thus, by restricting the antigen contact site to the lymphoid organs, APCs significantly increase the probability of cognate antigen recognition by lymphocytes.

1.2 Dendritic Cells

Dendritic cells (DCs) are the most potent APCs, serving as a critical bridge between innate and adaptive immunity. They are a rare population diversely located in tissues throughout the body (Cabeza-Cabrerizo et al., 2021). Their primary function is to capture, process, and present both self- and foreign antigens. Antigens are presented as short peptides derived from processed antigens by major histocompatibility complex (MHC) molecules and displayed

on the surface of DCs. Akin to TCR and BCR variability, MHC molecules are polygenic and highly polymorphic, allowing the presentation of a vast repertoire of peptides (Piertney & Oliver, 2006). Two classes of antigens are typically presented by DCs: those that originate within the cell (endogenous) and those that are captured from the extracellular environment (exogenous). Endogenous antigens are presented by MHC class I (MHCI) molecules to the TCR of cognate CD8 T cells. Exogenous antigens are presented by MHC class II (MHCII) molecules to the TCR of cognate CD4 T cells. Exogenous antigens can also be presented by MHCI in a process called cross-presentation (Neefjes et al., 2011). MHCI is expressed by all nucleated cells, which constantly present endogenous antigens to maintain peripheral tolerance and prevent “non-self” targeting by natural killer cells (NKs) (V. Kumar & McNerney, 2005). The expression of MHCII is primarily limited to APCs, including DCs and macrophages, but it is also expressed in B cells. In addition to MHCII, DCs also express costimulatory molecules such as CD80 and CD86 and produce cytokines, which are required to provide additional activation stimulus to induce T cell activation **(Fig. 1.1)**.

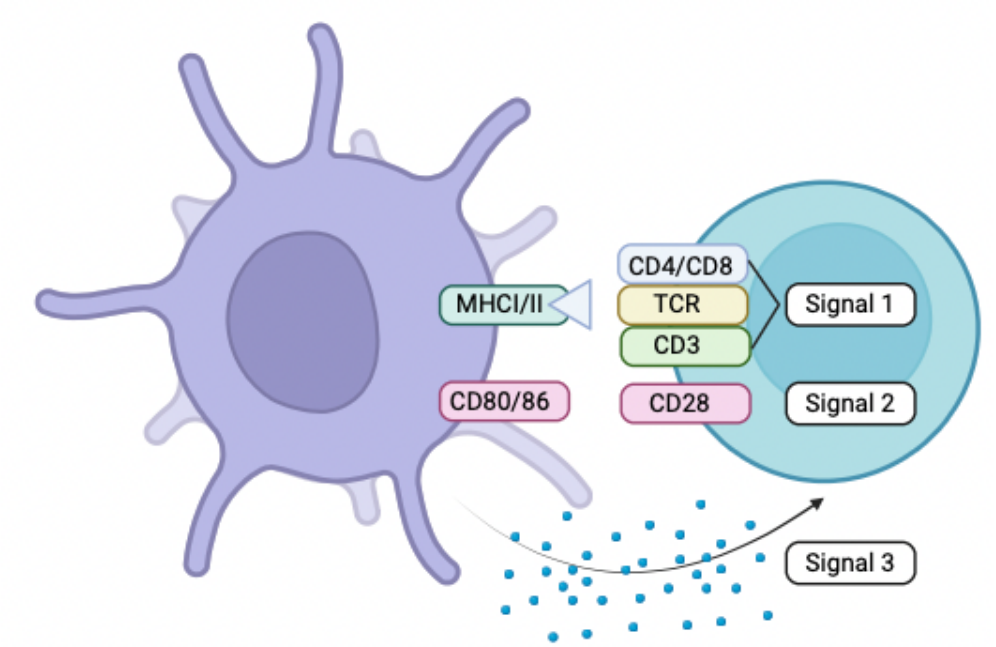

Figure 1.1 DC-mediated T cell activation.
Illustration of DC-T cell interaction. Signal 1: The CD3:TCR complex and CD4 or CD8 on T cells interact with the MHCI/II-peptide complex. Signal 2: Co-stimulation by CD80 and CD86 molecules. Signal 3: Cytokine interaction between DC and T cell. The Illustration was made with Biorender.

In the steady state, DCs have relatively low expression of MHC molecules and costimulatory markers and constantly present self-antigens to naïve T cells. MHC-TCR interaction without co-stimulation maintains T cells in a quiescent state, contributing to peripheral tolerance (Hasegawa & Matsumoto, 2018). Upon antigen encounter, DCs integrate environmental signals, including PAMPs, danger-associated molecular patterns (DAMPs) and local cytokine signals, to undergo an activation programme termed DC maturation, which converts them from a “pro-sensing” and “pro-tolerance” to a “pro-presenting” and proinflammatory phenotype **(Fig. 1.2)**. DC maturation is characterised by increased MHC and costimulatory molecule expression and a reduced capacity to capture antigens by downregulating endocytosis and macropinocytosis (Hammer & Ma, 2013; Sallusto et al., 1995). This ensures that DCs precisely deliver the antigen encountered at the site of infection to promote activation and expansion of the correct cognate T cells. Additionally, mature DCs upregulate the chemokine receptor, CC motif

chemokine receptor 7 (CCR7), which promotes migration from the site of infection to the lymph node to deliver the antigen to lymphocytes. Finally, DC maturation promotes cytokine production, essential to mediate T-cell polarisation to generate an appropriate response to the detected pathogen.

Thus, DCs are essential mediators of the adaptive immune response, acquiring, processing, and delivering antigens from the periphery to the lymphoid organs. Through DC maturation, the context of antigen capture is translated to precisely tailor the appropriate T-cell response by producing polarising cytokines. Therefore, DCs represent a critical control point in maintaining tolerance during homeostasis and fine-tuning adaptive immune responses during infection.

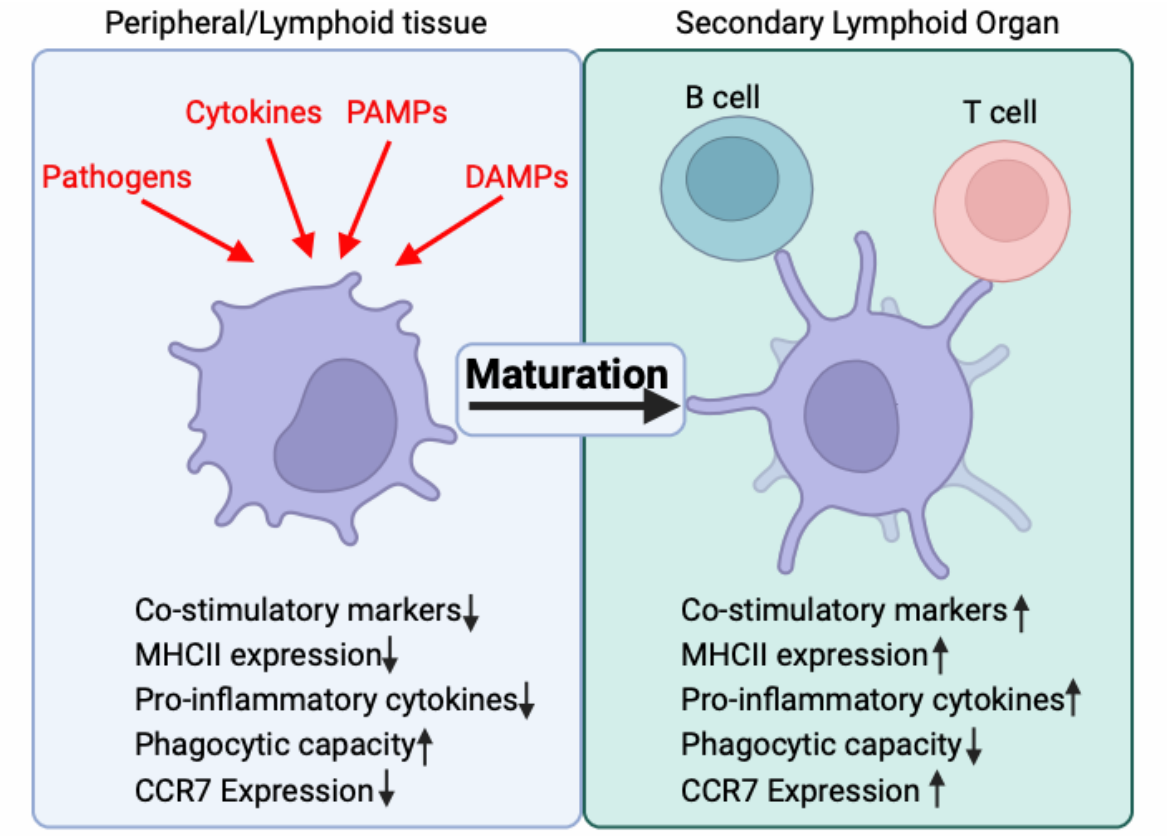

Figure 1.2 – Dendritic cell maturation
Illustration of the general phenotypic changes associated with DC maturation. Upon recognising pathogens, pathogen-associated molecular patterns (PAMPs) or interaction with danger-associated molecular patterns (DAMPs), DCs undergo phenotypical changes that transition from a pro-sensing to a pro-antigen presentation phenotype. DC maturation is associated with increased expression of costimulatory markers, MHCII and the production of proinflammatory cytokines. Maturation is also accompanied by a reduction in phagocytic capacity and increased expression of the chemokine receptor CCR7, which promotes migration from the site of infection to secondary lymphoid organs to interact with adaptive immune cells. The illustration was made with Biorender.

1.2.1 Dendritic Cell Subsets

DCs were first identified by Steinman and Cohn as stellate cells that could induce a mixed lymphocyte reaction *in vitro* (Steinman & Witmer, 1978). Subsequently, it is now recognised that DCs are a highly heterogeneous population composed of various subsets with specific phenotypic and functional characteristics. As our immune system coevolved with an incredibly diverse array of pathogenic threats, DC subsets likely arose, with different functional programmes to meet these needs. DCs must contend with several variables to effectively induce immunity, including the type of pathogen, the site of infection and the direction of an appropriate adaptive immune response. As such, DC subsets have diverse properties that specialise in combating different immunogenic threats, including PRR expression, tissue localisation (Resident vs Migratory), antigen presentation and cytokine production. As DCs are instrumental in directing T-cell responses, there is a need to better understand DC heterogeneity, allowing the generation of more specific therapeutic approaches to modulate immunity.

Due to the heterogeneous nature of the DC compartment, a universal classification system has proven challenging. In recent years, classification based on cellular ontogeny has been the most successful (Guilliams et al., 2014). Based on this simplified classification, DCs are routinely subdivided into four groups: conventional DC (cDC), plasmacytoid DC (pDC), monocyte-derived DC (moDC), and Langerhans cells (LC).

1.2.2 Conventional Dendritic Cells

cDCs are defined as cells that develop from the common dendritic cell progenitor (CDP) in the bone marrow and are characterised by the expression of the integrin CD11c and MHCII (Cabeza-Cabrerizo et al., 2021). cDCs are commonly divided into two phenotypically and functionally distinct subsets: type-1 conventional DCs (cDC1s) and type-2 conventional DCs (cDC2s). cDCs rely on the growth factor FMS-like tyrosine kinase 3 ligand (Flt3l) for their development in the bone marrow (Waskow et al., 2008). While both subsets arise from the CDP, cDC1s develop through a committed precursor called pre-cDC1s, and cDC2s arise from pre-cDC2s (Naik et al., 2007;

Schlitzer et al., 2015). cDC1 commitment during development involves the expression of the transcription factors IRF8, BATF3 and ID2 (Bagadia et al., 2019; Grajales-Reyes et al., 2015; Hildner et al., 2008), while cDC2s rely on IRF4 expression (Persson et al., 2013; Schlitzer et al., 2013). In mice, lymphoid resident cDC1s are characterised by the expression of XCR1 (Crozat et al., 2010, 2011) and CLEC9A (Poulin et al., 2012) and migratory cDC1 are identified by CD103 expression (Ginhoux et al., 2009). cDC2s are typically identified by the expression of CD172a (SIRPα) and CD11b (Guilliams et al., 2016). cDC2s are a more heterogenous population than cDC1s. Two subgroups of cDC2s have been characterised based on the differentiation requirements for Notch2 and KLF4 (Lewis et al., 2011; Satpathy et al., 2013; Tussiwand et al., 2015). They have also been subdivided based on their expression of the transcription factor T-bet (cDC2A) and RORγt (cDC2b) (Brown et al., 2019). A recent study has demonstrated that cDC2a corresponds to Notch-dependent cells and cDC2b are KLF-dependent cells (Minutti et al., 2024).

In addition to developmental and phenotypic differences, cDC1s and cDC2s specialise in the direction of different immune responses. cDC1s excel at the cross-presentation of antigens and the induction of type 1 immune responses by promoting CTL and CD4 T helper 1 (Th1) responses (Den Haan et al., 2000; Harpur et al., 2019; Schnorrer et al., 2006). Thus, cDC1s have been implicated in mediating the immune response against virally infected and malignant cells and certain bacterial infections (Cabeza-Cabrerizo et al., 2021; Heras-Murillo et al., 2024). cDC2s, on the other hand, specialise in the induction of type 2 and type 3 immunity and are important in the defence against bacterial, fungal and helminth infections (Gao et al., 2013; T.-T. Liu et al., 2022; Tussiwand et al., 2015) **(Fig. 1.3)**.

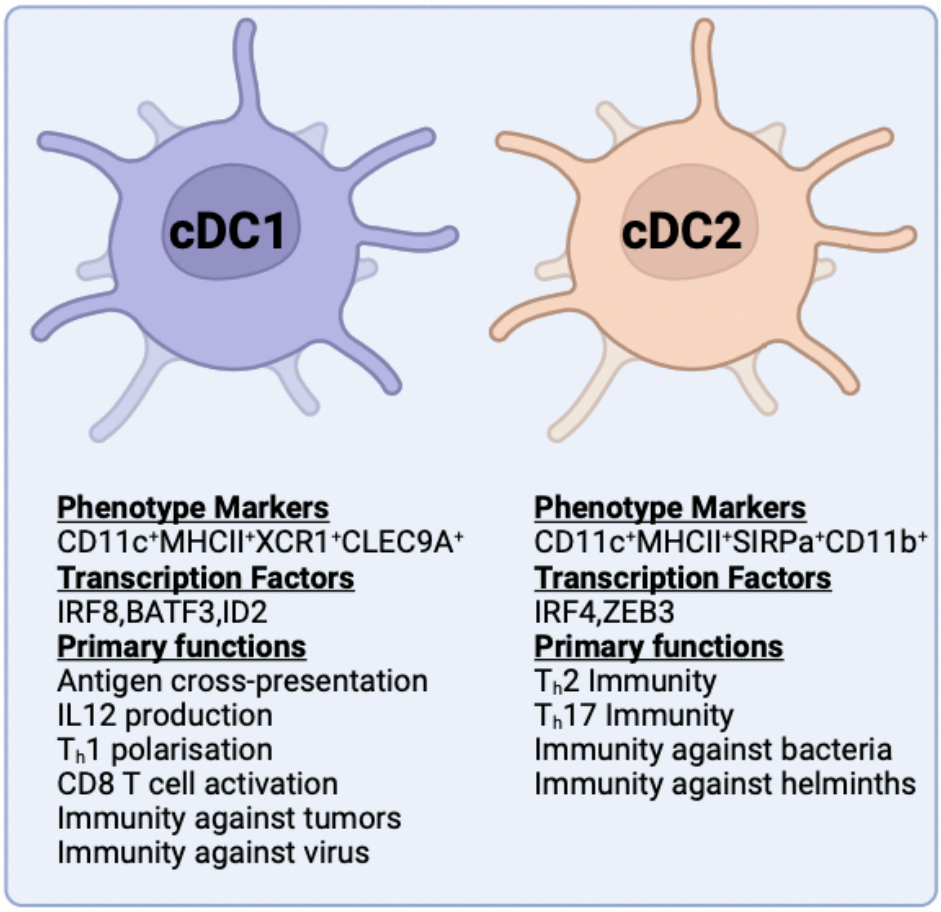

Figure 1.3 – Phenotype and functional features of cDC1s and cDC2s
Illustration of the surface phenotype markers, transcription factors and primary functions associated with cDC1s and cDC2s. cDC1s are identified by the surface expression of XCR1 and CLEC9A, and cDC2s are identified by SIRPα and CD11b. IRF8, BATF3 and ID2 are required for cDC1 development, while cDC2s depend on IRF4 and ZEB3. cDC1s specialised in antigen cross-presentation and the induction of Th1 T cell responses and are associated with anti-viral and anti-tumoral immunity. cDC2s specialise in polarising Th2 and Th17 responses and mediate immunity against extracellular bacteria and helminths. The illustration was made with Biorender.

1.2.3 Plasmacytoid Dendritic Cells

pDCs are a unique subset that shares common features with cDCs, including reliance on Flt3l for their development and the ability to present antigens to T cells upon maturation, although with lower efficiency (Reizis, 2019). pDCs can arise from both myeloid and lymphoid progenitors in the bone marrow (Rodrigues & Tussiwand, 2020). Myeloid-derived pDCs differentiate from the CDP and develop through a committed pre-pDC precursor (Naik et al., 2007; Onai et al., 2007, 2013). Recent studies have investigated the lymphoid origin of pDCs, differentiating from the common lymphoid progenitor (CLP) (Dress et al., 2019; Herman et al., 2018; Rodrigues et al., 2018). The contribution of myeloid and lymphoid cells to the mature pDC pool *in vivo* is currently unknown (Reizis, 2019). Transcriptionally, pDCs rely on the expression of the transcription factors TCF4 and IRF8 for their development (Cisse et al., 2008; Sichien et al., 2016). Steady-state pDCs specialise in detecting viral antigens and highly express the endosomal toll-like receptors (TLR), TLR7 and TLR9. Upon immunogenic stimulation, they rapidly produce large quantities of type-1 interferons, including IFNβ and subtypes of IFNα. They also produce IFNγ and additional proinflammatory cytokines, including TNFα and IL-6. Thus, pDCs are important mediators in anti-viral defences and have been implicated in the pathogenesis of autoimmune disease (Reizis, 2019).

1.2.4 Other Dendritic Cell Subsets

LCs are a population of myeloid DC-like cells located in the epidermal layer of the skin. Like cDCs, LCs express MHCII and can stimulate a mixed leukocyte reaction when cultured with T cells *in vitro* (Schuler & Steinman, 1985). Due to these DC properties, LCs were long considered prototypical examples of migratory DCs. However, in contrast to cDCs, LCs do not arise from bone marrow precursors but from erythro-myeloid progenitors that self-renew in the tissue (Collin & Milne, 2016). Their development is independent of Flt3l but relies on colony stimulatory factor 1 receptor (CSFR1) ligation akin to macrophages (Greter et al., 2012). Thus, LCs are generally considered more closely related to tissue-resident macrophages than DCs.

Monocyte-derived DCs (MoDCs), also termed “inflammatory DCs”, arise from monocyte progenitors that gain DC properties during inflammation (Cheong et al., 2010). Due to their shared lineage, MoDCs share numerous properties with monocyte-derived macrophages, including the expression of inducible nitric oxide synthase (iNOS) and high levels of TNFα production upon activation (Serbina et al., 2003). Phenotypically, MoDCs have a stellate DC morphology, have similar expression of surface markers including CD11c, MHCII and CD11b and have the ability to capture and process antigens in the periphery and migrate to present antigens to T cells within lymphoid organs (Cabeza-Cabrerizo et al., 2021). In contrast to cDCs, moDC development is independent of Flt3l, and they do not arise from the CDP. While moDC numbers are limited in the steady state, upon inflammation, Ly6C$^+$ monocytes are recruited from the bone marrow, where they differentiate into moDCs under the control of the growth factor Macrophage Colony Stimulating Factor (M-CSF) (Briseño et al., 2016; Croxford et al., 2015).

With advancements in single-cell profiling of immune cells, new DC subsets have been identified. A population that expresses a mixed cDC2-monocyte transcriptomic and phenotypic profile, termed DC3s, has been described (Bourdely et al., 2020; Z. Liu et al., 2023; Villani et al., 2017). These cells are efficient inducers of CD4 T cell activation *ex vivo* and can secrete cytokines, including IL12p70 and IL23, similar to cDCs and large amounts of IL-1β, similar to monocytes (Bourdely et al., 2020; Dutertre et al., 2019). Another DC subtype recently described is termed transitional DCs (tDCs) (Alcántara-Hernández et al., 2017; Leylek et al., 2019; Villani et al., 2017). These cells are identified as AXL$^+$SIGLEC6$^+$ cells with a mixed pDC-cDC transcriptomic profile (Leylek et al., 2019; Sulczewski et al., 2023). Functionally, tDCs share many features with cDC2s, including CD4 T cell stimulatory capacity (Sulczewski et al., 2023). Rodrigues et al. recently demonstrated that tDCs are distinct circulating precursors distinct from the CDP, with cDC2 differentiation potential. They show that a substantial proportion of cDC2s arise from these pDC-like precursor cells with a bias towards generating

ESAM^{-} cDC2B cells under the direction of the transcription factor KLF4 (Rodrigues et al., 2023) **(Fig. 1.4)**.

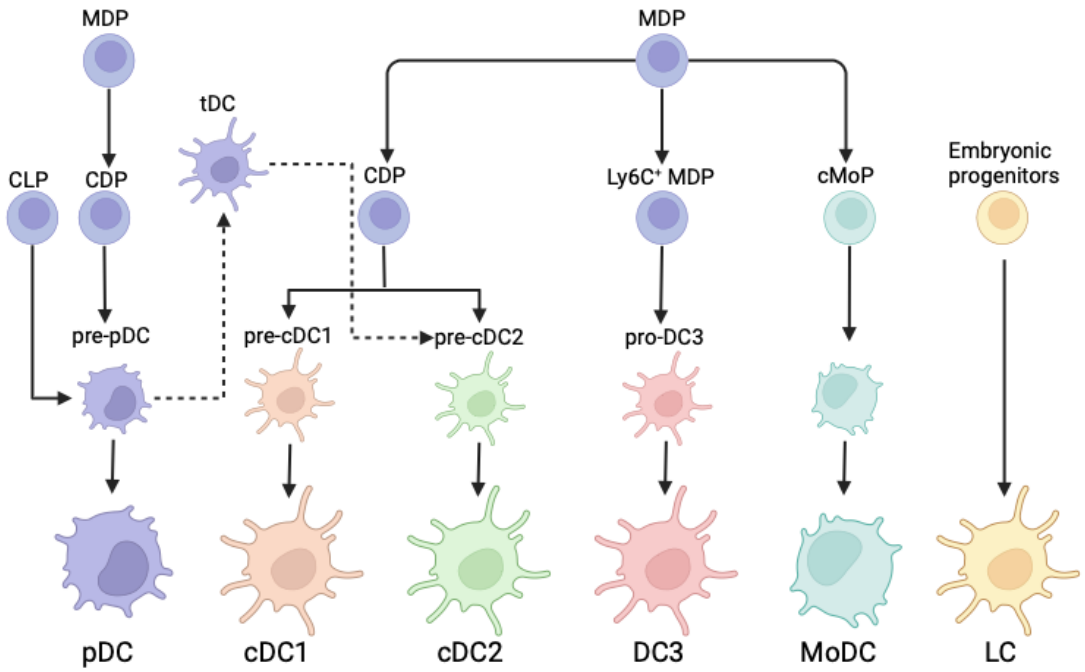

Figure 1.4 – Dendritic cell ontogeny and subsets
Illustration of dendritic cell ontogeny and known subsets in the steady state. Plasmacytoid DCs (pDCs) arise from immediate pre-pDC precursors, which can differentiate from both Common Lymphoid Progenitors (CLPs) and Common DC progenitors (CDPs). Transitional DCs (tDCs) share a developmental origin with pDCs, have an intermediate pDC-cDC2 phenotype and can differentiate into ESAM cDC2s. cDC1s and cDC2s develop from pre-cDC1s and pre-cDC2s, respectively, which differentiate from CDPs before leaving the bone marrow. Type 3 DCs (DC3s) differentiate from pro-DC3 precursors, which derive from the Macrophage-Dendritic cell precursor (MDP) independently of CDP differentiation. Monocyte-derived DCs (MoDCs) derive from the MDP through the Common Monocyte Progenitor (cMoP), which becomes prevalent during inflammatory conditions. Langerhans cells (LCs) are epidermal resident macrophages from embryonic tissue precursors. LCs have traditionally been included in the DC family due to functional similarities. The illustration was made with Biorender and adapted from (Heras-Murillo et al., 2024).

1.3 Immunometabolism

Immunometabolism defines the area of study investigating the interface between immunology and cellular metabolism. It has long been appreciated that systemic and cellular metabolism plays a role in disease pathogenesis (Warburg, 1956). Conversely, inflammation contributes to the pathogenesis of metabolic disorders such as obesity and type-2 diabetes (Hotamisligil et al., 1993). Over the past twenty years, a renewed interest has been in understanding the relationship between immunity and metabolism (O'Neill et al., 2016; Pearce & Pearce, 2013). Improvements in technical approaches have greatly accelerated our understanding and appreciation of the importance of cellular metabolism in immune cell function and how dysregulation of metabolism during disease can undermine our immune defences (Verberk et al., 2022; Voss et al., 2021). Characterisation of the metabolic profiles of immune cells during homeostasis and disease opens a new repertoire of therapeutic targets to modulate immunity.

1.3.1 Dendritic Cell Metabolism

Our knowledge of DC immunometabolism has significantly expanded in recent years (Guo & Chi, 2023; Møller et al., 2022; Wculek et al., 2019). Due to their rarity *in vivo* and technical limitations associated with DC viability and spontaneous activation in culture, many advancements in DC metabolism have come from *in vitro*-generated culture models (Vremec et al., 2011, 2015). However, there is a growing appreciation that the nutrient levels within traditional culture media can reprogram the metabolism of cells (Cantor et al., 2017; Kaymak et al., 2022). Thus, extended culture in non-physiological media can confound metabolic observations using these models.

Two *in vitro* culture models have primarily been used to investigate DC metabolism. The most widely used model for *in vitro* DC generation relies on the addition of granulocyte-macrophage colony-stimulating factor (GM-CSF) to bone marrow precursors (Lutz et al., 1999). This approach leads to the generation of predominantly $CD11c^{+}$ cells with heterogenous expression of MHCII. This heterogeneity was initially ascribed to differences in the maturation state. However, it is now known that this culture model generates

two phenotypically and functionally distinct populations, which the authors termed GM-DC and GM-Macs (Helft et al., 2015). Thus, it is important to take metabolic observations using this culture with caution. A second culture model involves treating bone marrow precursors with the cytokine Flt3l (Naik et al., 2007). This model leads to the generation of three DC subsets, including cDC1s, cDC2s and pDCs, which functionally resemble their splenic counterparts. DCs generated by this approach are termed FLDC. Despite resembling natural DC phenotypes more closely, FLDCs lack many key phenotype markers associated with natural DCs, including XCR1 and CD8a. These cells are also poorly immunogenic relative to their natural DC counterparts (Naik et al., 2006, 2007). A modified protocol, which involves the co-culture of Flt3l bone marrow cells with OP9 stromal cells expressing Notch ligand delta-like 1 (OP9-DL1), has been shown to generate cDC1-like cells that more closely resemble the phenotype of *ex vivo* cDC1s (Kirkling et al., 2018). Finally, Mayer and colleagues described a protocol to generate a homogenous population of CD103+ migratory cDC1s, which requires both GM-CSF and Flt3l during the culture (Mayer et al., 2014).

Despite these limitations, the application of these models, particularly GM-CSF-derived and Flt3l-derived bone marrow DCs, have contributed significantly to our understanding of DC metabolism and thus will be included in the following discussion. For clarity, cells generated using GM-CSF will be termed GMDCs, cells generated using Flt3L will be termed FLDCs and studies involving *ex vivo* natural DC subsets will be termed cDC1s, cDC2s and pDCs.

1.3.2 Immunometabolism of DC activation

Glycolysis

DCs undergo profound phenotypic and functional changes upon immunogenic stimulation to promote effective adaptive immune responses. This transition requires enhanced bioenergetic and biosynthetic demands, which are met by metabolic reprogramming. Initial investigations into the metabolism of DC activation revealed that enhanced glycolytic metabolism is a characteristic feature of maturation. PRR activation of GMDCs with the

TLR4 ligand lipopolysaccharide (LPS) or the TLR2 ligand zymosan promoted increased glycolytic flux proportional to the activation stimulus's amplitude (Krawczyk et al., 2010). Various studies have investigated the impact of inhibiting glycolytic metabolism in GMDCs by pharmacological inhibition using 2-deoxyglucose (2DG) or genetic deficiency of the glycolytic enzyme enolase 1 (ENO1) (Everts et al., 2014; Ryans et al., 2017). In both studies, inhibition of glycolysis abrogated GMDC maturation, reducing costimulatory marker expression, cytokine production and migration. Pharmacological inhibition of glycolysis has also been shown to inhibit cDC maturation, reducing cDC-mediated CD4 and CD8 T cell activation in response to LPS stimulation (Everts et al., 2014).

Mechanistically, it has been shown that GMDCs stimulated with TLR agonists activate the TANK-binding kinase 1 (TBK1) and IκB kinase ε (IKKε) pathway, which phosphorylates protein kinase B (AKT) promoting hexokinase II (HKII) association with the mitochondrial outer membrane, activating glycolysis (Everts et al., 2014). Thus, the early enhancement in glycolytic flux is independent of mechanistic target of rapamycin complex 1 (mTORC1) activity. mTORC1 is a kinase that integrates environmental signals to coordinate intracellular metabolism, discussed in greater detail below. In line with the rapid induction of glycolytic metabolism in GMDCs, Thwe and colleagues demonstrated that the expression of the glucose transporter GLUT1 (SLC2A1) increases after the early induction of glycolysis (Thwe et al., 2017). The authors show that GMDCs maintain intracellular glycogen stores that are degraded upon LPS stimulation to fuel glycolysis. Accordingly, inhibition of the rate-limiting enzyme in glycogen catabolism, glycogen phosphorylase (PYG), abrogated GMDC maturation. In contrast, prolonged glycolytic activity in GMDCs in response to LPS stimulation has been reported to require mTORC1 signalling (Amiel et al., 2012, 2014; Lawless et al., 2017). Pharmacological inhibition of mTORC1 signalling in GMDCs in response to LPS stimulation for 20 hours inhibits the upregulation of glycolytic enzymes and glycolytic flux (Amiel et al., 2012).

Mitochondria

In addition to glycolytic reprogramming, GMDCs have been reported to modulate their mitochondrial activity during activation. Prolonged stimulation of GMDCs with LPS dramatically reduces mitochondrial flux relative to unstimulated cells (Krawczyk et al., 2010). After 24h of LPS stimulation, GMDCs have reduced oxygen consumption and mitochondrial membrane potential and are insensitive to the ATP synthase inhibitor oligomycin (Everts et al., 2012; Thwe et al., 2017). Mitochondrial inhibition was subsequently shown to be caused by nitric oxide (NO) production by the GMDC culture (Everts et al., 2012). The source of NO is macrophage contamination within the GMDC culture system (Helft et al., 2015). As nitric oxide synthase (iNOS) is not expressed in natural DC subsets, interpretation of these results should be taken with caution. To address this limitation, Everts et al. utilised iNOS-deficient GMDCs during LPS activation and reported maintenance of mitochondrial metabolism required to support GMDC-mediated T cell activation (Everts et al., 2012). However, these studies indicate that increased mitochondrial flux is a feature of early GMDC activation (Everts et al., 2012, 2014). LPS stimulation for 6 hours before NO induction increased oxygen consumption and mitochondrial membrane potential. Notably, 2DG treatment abrogated mitochondrial flux in this system, indicating that glycolysis-derived pyruvate is the primary mitochondrial fuel source (Everts et al., 2014).

In human $CD1c^+$ mDCs (equivalent to murine cDC2s), TLR7/8 ligation for 6 hours with a complex of protamine and mRNA (pRNA) down-regulated the expression of OXPHOS-related genes and mitochondrial content (Basit et al., 2018). Further, it was demonstrated that TLR activation induced mitophagy, which supported the metabolic reprogramming towards a glycolytic phenotype. In contrast, the same stimulation conditions promoted increased mitochondrial mass and fusion, enhancing OXPHOS in pDCs (Basit et al., 2018). Extended stimulation of human pDCs *ex vivo* with influenza or rhinovirus displayed a mild reduction in oxygen consumption rate (OCR) relative to untreated cells (Bajwa et al., 2016). Data from the Pearce lab show that Flt3l-cultured pDCs from mouse bone marrow have elevated OXPHOS after 24 hours of CpG dinucleotide stimulation (Wu et al., 2016).

Mechanistically, IFNAR signalling promoted enhanced FAO to support mitochondrial flux through the transcription factor peroxisome proliferator-activated receptor alpha (PPARα). In mice, cDC1s utilise the Hippo pathway kinases Mst1 and Mst2, which have been reported to control oxidative metabolism (X. Du et al., 2018). Depletion of Mst kinases dysregulates mitochondrial metabolism, disrupting cDC1s but not cDC2s, resulting in abrogated IL-12p40 production and inhibiting cDC1-mediated T-cell responses. In another study, inhibition of mitochondrial function prevents the cross-presentation of dead-cell antigens in splenic cDC1s (Chougnet et al., 2015). Conversely, stimulation of total splenic DCs with the TLR3 agonist poly(I:C) reduces mitochondrial membrane potential and oxygen consumption in an interferon alpha receptor (IFNAR)-dependent manner (Pantel et al., 2014).

Lipids

Glycolytic flux induction upon DC activation has been reported to support fatty acid synthesis (FAS) in GMDCs. Pharmacological inhibition of the mitochondrial pyruvate carrier 1 (MPC1), which facilitates the entry of glycolysis-derived pyruvate into the mitochondria restrains GMDC maturation and cytokine production (Everts et al., 2014). De novo FAS is hypothesised to support the expansion of the endoplasmic reticulum (ER) and Golgi membranes to facilitate the enhanced biosynthetic burden associated with DC cytokine production as pharmacological inhibition of FAS abrogated GMDC maturation in response to LPS (Everts et al., 2014). In support of this idea, the knockdown of glucose-6-phosphate dehydrogenase (G6PDH), the rate-limiting step in the PPP, limits NADPH production required for FAS abrogating LPS-induced GMDC maturation (Everts et al., 2014). In contrast, inhibition of FAS upon immunogenic stimulation of FLDCs with CpG or mycobacterial infection does not affect costimulatory marker expression or cytokine production (Stüve et al., 2018). This study shows that FAS inhibition increases the uptake of extracellular lipids in FLDCs, which may negate the impact of de novo lipid synthesis inhibition. In addition, the accumulation of lipids into intracellular organelles called lipid bodies as a result of FAS or extracellular

lipid accumulation promotes antigen cross-presentation in GMDCs, FLDCs and cDC1s (Bougnères et al., 2009; Den Brok et al., 2016; Herber et al., 2010). Notably, cDC1s, which excel at cross-presentation, were shown to have more lipid bodies than cDC2s. Conversely, lipid body formation inhibits CD103+ migratory cDC1 cross-presentation within the tumour microenvironment due to an enrichment of oxidatively truncated lipids (Veglia et al., 2017). Thus, the role of lipid metabolism in DC function is cell-type and context-specific.

Amino Acids

Amino acids are the fundamental building blocks of protein synthesis. In addition, amino acid metabolism contributes to mitochondrial ATP production and acts as a carbon and nitrogen source for biomass synthesis, redox metabolism and metabolic signalling (Kelly & Pearce, 2020). Several studies have investigated amino acid metabolism in moDCs. For example, lowering the amino acid concentration in traditional culture media to physiological concentrations in human plasma increased moDC differentiation (Kakazu et al., 2009). Conversely, culturing moDCs in media with imbalanced amino acid concentrations mirroring those found in patients with liver cirrhosis had decreased IL-12p40 production, costimulatory marker expression and migratory capacity (Kakazu et al., 2013). In another study, LPS-stimulated moDCs increased the uptake of the branched-chain amino acids (BCAA) valine, leucine and isoleucine. Depletion of valine from the culture medium impaired moDC maturation and T cell priming capacity in response to LPS stimulation (Kakazu et al., 2007). The mTORC1 kinase is a known sensor of the availability of certain BCAA, and indeed, mTORC1 signalling was found to be impaired in this study when BCAAs were limiting. These data argue that BCAA and mTORC1 signalling influences moDC function. BCAA metabolism has also been implicated in regulating moDC function in response to TLR7/8 pRNA stimulation. In contrast to LPS, pRNA treatment enhanced FAO-dependent mitochondrial respiration, which required BCAA availability (Kakazu et al., 2013). In addition to moDCs, Grzes and colleagues have demonstrated a role for the system-L neutral amino acid transporter SLC7A5, which transports BCAA, in activating human pDCs. This study demonstrates

that IL3 signalling induces JAK2-STAT5 signalling, upregulating SLC7A5 and its heterodimeric binding partner, SLC3A2. Amino acid uptake through SLC7A5 supports mTORC1 signalling upon TLR stimulation, which is required for optimal cytokine production (Grzes et al., 2021).

Glutamine is a critical amino acid required for immune cell function (Cruzat et al., 2018). It has been shown that depleting glutamine from GMDC culture medium does not affect DC maturation after 6 hours of LPS stimulation (Thwe et al., 2017). In contrast, GMDCs stimulated with the TLR7/8 agonist imiquimod are sensitive to glutamine deprivation and pharmacological inhibition of glutaminolysis (Mogilenko et al., 2019). In this case, the absence of glutamine promoted mitochondrial reactive oxygen species (ROS), which enhanced IL-23 production. A recent study from the lab of Hongbo Chi revealed that metabolic competition for glutamine in the tumour microenvironment (TME) between cDC1s and tumour cells is mediated through the transporter SLC38A2. It was shown that blocking glutamine uptake via SLC38A2 or inhibiting glutamine signalling through the FLCN-TFEB axis abrogated the antigen presentation capacity of cDC1s, resulting in weak T-cell responses and poor control of tumour growth (Guo et al., 2023). Overall, this study demonstrates that glutamine is important for cDC1 function, but the extent to which this is true is context-dependent.

1.3.3 Nutrient sensing pathway in DCs

mTOR

The mechanistic target of rapamycin (mTOR) is a serine/threonine protein kinase that forms the catalytic subunit of two protein complexes, termed mTOR complex 1 (mTORC1) and mTOR complex 2 (mTORC2). mTORC1 coordinates intracellular metabolism with environmental signals, including nutrient and oxygen availability, growth factors and the energy status of the cells and is a critical mediator of protein synthesis and autophagy. In contrast, mTORC2 is insensitive to nutrient availability and primarily promotes proliferation, survival and cytoskeletal remodelling in response to growth factor signalling (Saxton & Sabatini, 2017) **(Fig. 1.5)**. The role of mTOR, particularly mTORC1, has been studied extensively in DCs (Snyder & Amiel,

2019; Sukhbaatar et al., 2016). However, the exact role of mTORC1 in mediating DC metabolism and function is complex, as it has been reported to mediate both pro- and anti-inflammatory functions.

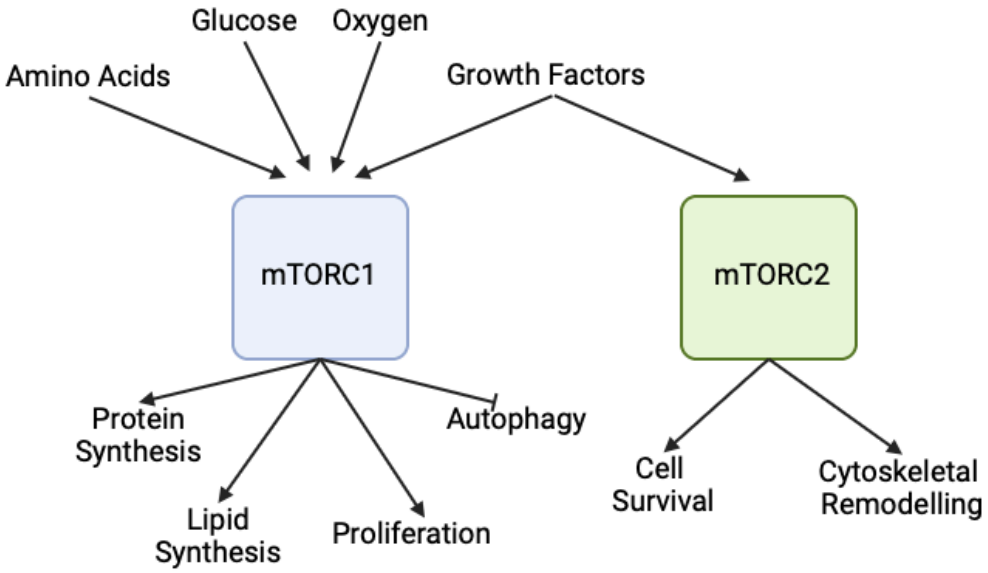

Figure 1.5 – mTORC1 and mTORC2
Illustration of the environmental regulators and functional outputs of mTORC1 and mTORC2 signalling. mTORC1 senses nutrients (Amino acids, glucose) and oxygen availability and is responsive to growth factor signalling, controlling anabolic and catabolic processes, including protein and lipid biosynthesis and autophagy. mTORC2 is activated by growth factors and controls cell survival and cytoskeletal remodelling. The illustration was made with Biorender.

mTORC1 signalling is activated downstream of the growth factor PI3K/AKT signalling pathway and promotes glycolysis and FAS (Linke et al., 2017). While the early induction of glycolytic metabolism is independent of mTORC1 in GMDCs, sustained glycolytic flux depends on mTORC1-mediated hypoxia-inducible factor 1 alpha (HIF1α) signalling (Everts et al., 2014; Lawless et al., 2017). In response to LPS stimulation for 24 hours, rapamycin, a highly specific inhibitor of mTORC1, reduced GMDC maturation by limiting HIF-1α-iNOS signalling. Further, genetic ablation of iNOS in GMDCs prevented the late glycolytic induction in GMDCs, reducing proinflammatory cytokine

production in response to LPS stimulation (Jantsch et al., 2008). In addition, *in vivo* administration of rapamycin impairs DC costimulatory marker expression, proinflammatory cytokine production and T cell stimulatory capacity (Hackstein et al., 2003). Further, Fekete and colleagues show that rapamycin impairs the upregulation of glycolysis and proinflammatory cytokine production in human moDCs in response to retinoic acid-inducible gene-I-like (RIG-I) stimulation (Fekete et al., 2018). In murine pDCs, mTORC1 was demonstrated to support IFNα production in response to CpG stimulation by promoting the interaction between TLR9 and its adaptor MyD88 to activate IRF7 signalling effectively (Cao et al., 2008). A recent study in line with this finding showed that mTORC1 activity controlled by SLC7A5 amino acid uptake is required for IFNα production in human pDCs (Grzes et al., 2021).

mTORC1 has also been reported to restrain DC function. Amiel and colleagues show that mTORC1 signalling in GMDCs limits DC lifespan by limiting cellular energy levels by repressing OXPHOS (Amiel et al., 2012). A subsequent study from the same group shows that rapamycin treatment extends DC lifespan by preserving mitochondrial function through the upregulation of FAO (Amiel et al., 2014). mTORC1 inhibition in GMDCs and human $CD1c^+$ (cDC2) has been reported to enhance the production of proinflammatory cytokines in response to LPS stimulation (Ohtani et al., 2008; Weichhart et al., 2008). Accordingly, GMDCs with constitutively active mTORC1 signalling have reduced IL-12p40 production and enhanced IL-10 secretion in response to LPS stimulation. Moreover, genetic knockout of tuberculosis sclerosis 1 (TSC1), an upstream inhibitor of mTORC1 in $CD11c^+$ DC, restrains DC-mediated T cell responses (Shi et al., 2019; Wang et al., 2013). Thus, in many cases, mTORC1 promotes an anti-inflammatory DC phenotype. Indeed, mTORC1 inhibition reverses the anti-inflammatory effects of glucocorticoids in myeloid DCs (Weichhart et al., 2011).

mTORC1 signalling also regulates DC function in a tissue-specific manner. In a genetic model of mTOR deficiency in $CD11c^+$ cells, cDC1s are depleted

specifically in the lungs and the skin. In the same model, mTOR-deficient cDC2s have elevated FAO and increased IL-23 production, which promotes Th17 immunity, contributing to allergic inflammation in a model of asthma (C. Sinclair et al., 2017). Thus, mTOR signalling restrains cDC2 inflammation within the lung. A recent study by Pelgrom and colleagues utilised a CD11c-specific knockout of the mTORC1 complex component RAPTOR to investigate the role of mTORC1 in cDC1s and cDC2s (Pelgrom et al., 2022). This study revealed impaired mTORC1 signalling inhibited splenic cDC1 glycolysis and maturation while enhancing the accumulation of $EpCAM^{+}$ migratory cDC1s in the skin, draining lymph nodes, and promoting favourable responses to Listeria infection.

AMPK

AMP-activated protein kinase (AMPK) is a highly conserved metabolic sensor sensitive to cellular ATP levels. When ATP levels are low, AMPK negatively regulates mTORC1 signalling, inhibiting anabolic processes while simultaneously activating catabolic programmes, including autophagy. Thus, AMPK and mTORC1 function in concert to mediate the balance between anabolism and catabolism in response to the environment (Herzig & Shaw, 2018). AMPK activation inhibits anabolic pathways, including protein and lipid biosynthesis, and promotes catabolic pathways, such as glycolysis, FAO, OXPHOS and nutrient generation by autophagy and mitophagy **(Fig. 1.6)**.

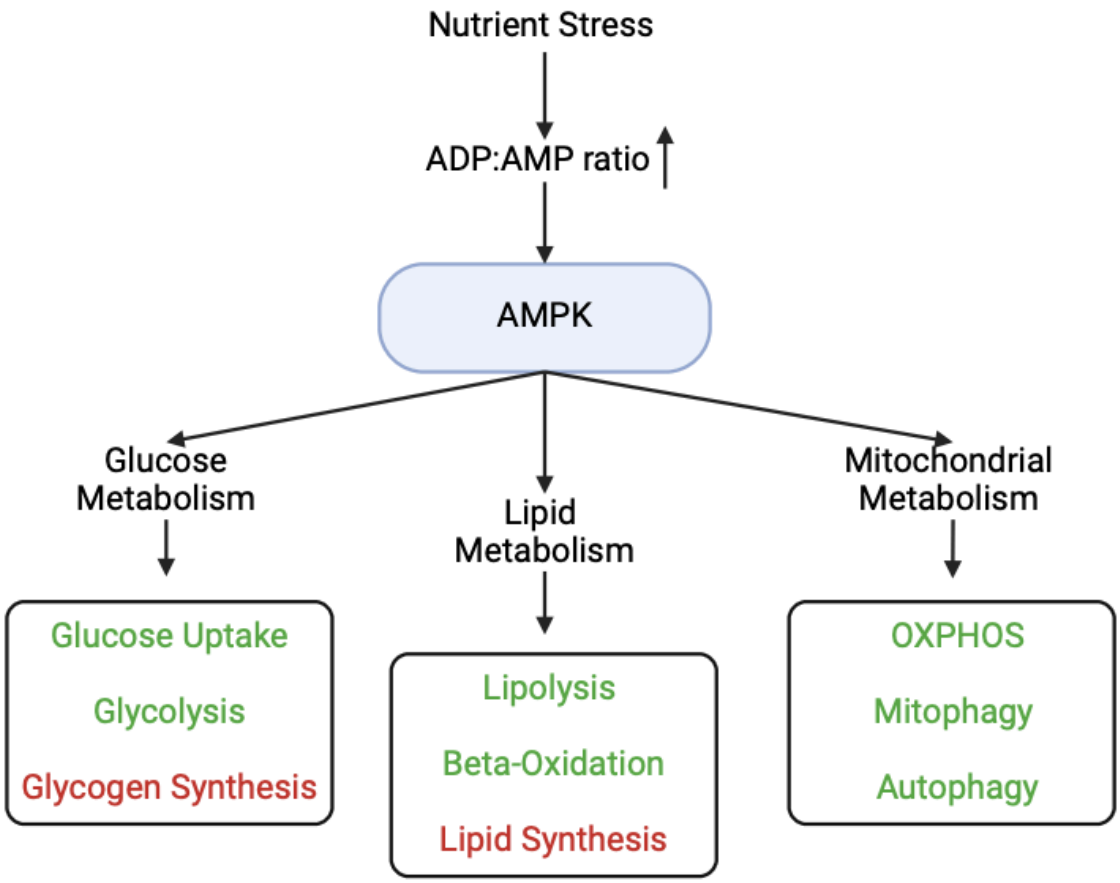

Figure 1.6 – AMPK activation promotes catabolic pathways
Illustration of metabolic pathways influenced by AMPK activation. Nutrient stress increases the ADP:AMP ratio, which induces AMPK activation. AMPK promotes the activation of metabolic pathways that generate ATP to restore cellular energy balance while inhibiting ATP-consuming anabolic pathways. AMPK promotes metabolic pathways coloured green, and those in red are inhibited. The illustration was made using Biorender.

In LPS-stimulated GMDCs, shRNA knockdown of AMPK enhanced IL-12p40 production and costimulatory marker expression, indicating it functions as a negative regulator of proinflammatory DC maturation (Krawczyk et al., 2010). In support of this, pharmacological induction of AMPK using aminoimidazole-4-carboxamide ribonucleotide (AICAR) abrogates glycolysis induction and DC maturation in response to LPS stimulation (Krawczyk et al., 2010). Genetic deficiency of the AMPK-activating kinase liver kinase B 1 (LKB1) in $CD11c^{+}$ DCs, which inhibits AMPK signalling, reduces mitochondrial mass and membrane potential and promotes upregulation of costimulatory markers

in the absence of stimulation in cDC1s and cDC2s (Pelgrom et al., 2019). Thus, AMPK appears to control mitochondrial fitness and the maintenance of quiescence in steady-state DCs. Interestingly, despite LKB1 deficiency promoting a proinflammatory phenotype, AMPK-deficient mice have impaired responses to immunisation (OVA + Poly (I:C) + incomplete Freund's adjuvant (IFA)) and control of tumour growth. This was shown to be a result of increased T regulatory cell (Treg) expansion *in vivo* due to enhanced thymic cDC2 activation (Pelgrom et al., 2019). In another study, LKB1 deletion in DCs was shown to impair anti-tumour immunity by promoting the expansion of Tregs (Wang et al., 2019). Further, it was revealed that LKB1 acts in a mTORC1-dependent manner to maintain DC quiescence and DC-mediated control of Tregs. Thus, AMPK mediates the balance between pro- and anti-inflammatory responses in DCs.

1.3.4 Nutrient competition and DC function

Nutrients are the fuel of metabolism. Upon metabolic reprogramming, immune cells dynamically regulate their nutrient acquisition to meet the demands associated with alterations in metabolic flux (Kedia-Mehta & Finlay, 2019; H. J. Weiss & Angiari, 2020). Accordingly, nutrient availability regulates cellular metabolism and immune cell function. It is now emerging that under different physiological circumstances, nutrients are not equally available to all immune cells, suggesting a complex interplay of immune regulation. For example, imaging of tumours using positron emission tomography (PET) reveals that tumours have the greatest capacity to take up glutamine in the tumour microenvironment (TME) compared to lymphocytes and myeloid cells (Reinfeld et al., 2021). In contrast, it was shown that myeloid and T cells have preferential acquisition of glucose in the TME relative to tumour cells. These data argue for the partitioning of nutrients between different cell types within the TME. A recent study by Guo and colleagues reveals that local glutamine deprivation within the TME restrains cDC1 anti-tumour responses (Guo et al., 2023). Notably, despite the requirement for glutamine by tumour cells, intra-tumoral glutamine supplementation restricted tumour growth by promoting cDC1-mediated T-cell responses. In contrast to glutamine, which enhances tumour DC function, it has been shown that tumour-infiltrating DCs have

elevated arginine metabolism associated with abrogated CD8 T cell responses (Norian et al., 2009). Thus, metabolic competition for different amino acids within the TME influences DC function.

In addition to the TME, a study from the Finlay lab has shown that nutrient competition between GMDCs and CD8 T cells influences DC function (Lawless et al., 2017). Upon antigenic activation, T cells upregulate glucose uptake and metabolism to support proliferation and the acquisition of effector function (Chapman & Chi, 2022). Activated T cells outcompete GMDCs for glucose, which enhances DC-mediated T cell responses by repressing mTORC1-HIF1α-iNOS signalling in GMDCs (Lawless et al., 2017). Quantitative proteomic studies of T cells have revealed significant upregulation of amino acid transporters upon activation (Howden et al., 2019; Marchingo et al., 2020). Thus, considering the control of cDC1 function by glutamine availability (Guo et al., 2023), further research is required to understand the influence of amino acid competition between DCs and T cells during inflammation.

In summary, significant progress has been made in elucidating the metabolic pathways and nutrient sensors engaged upon DC activation and how manipulating these can modulate function. Despite this, most studies reported are performed in bone marrow-derived GMDCs, which are intrinsically limited and do not offer insight into subset-specific metabolic profiles. Since cDC1s and cDC2s instigate different immune responses, further research is required to characterise their subset-specific metabolic characteristics.

1.4 Quantitative Proteomics as a tool to study immune cell function

Proteomics is the large-scale study of proteins, their structures, functions, interactions, and abundances within a biological system (Schubert et al., 2017). In recent years, applying proteomic techniques to clinical and immunological research has complemented our understanding of disease pathogenesis and how the immune system works (Urbiola-Salvador et al., 2022). While the application of proteomic studies has lagged behind transcriptomic approaches, mainly due to intrinsic challenges associated with

proteomics, including sample preparation, complex analysis, cost and throughput, the rapid advancements in mass-spectrometry technology and analysis pipelines in recent years have dramatically enhanced both the accessibility and quality of proteomics in the interrogation of immune cell function.

1.4.1 Mass-spectrometry-based proteomics

Liquid chromatography-mass spectrometry (LCMS) is an analytic technique that identifies and quantifies a broad range of analytes (Pitt, 2009). In LCMS, samples are first separated by liquid chromatography, and the products are subsequently analysed by mass spectrometry (MS). Mass spectrometers comprise three primary components: an ionisation source, a mass analyser, and a detector. To commence analysis, samples are converted from the liquid phase to the gaseous phase by procedures such as electrospray ionisation (ESI) prior to entering the mass spectrometer (Ho et al., 2003). Within the mass spectrometer, ions are accelerated and deflected in a magnetic field. Separation of ions within the magnetic field depends on the molecule's mass and its charge. Thus, the primary readout of MS is the molecule's mass-to-charge (m/z) ratio. Finally, the separated ions are detected, generating a spectral readout of m/z versus signal intensity **(Fig. 1.7)** (Pitt, 2009). Due to its ability to analyse a broad range of analytes, from small molecules to large biomolecules, MS is commonly used in applications such as proteomics and metabolomics.

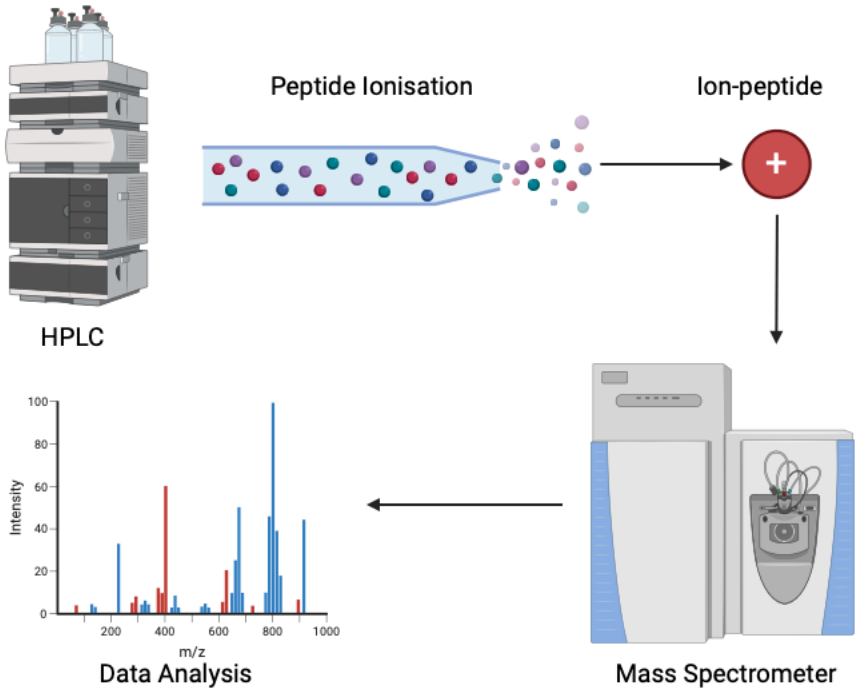

Figure 1.7 – LC/MS workflow for quantitative proteomics
Illustration of the workflow of LC/MS proteomics. Samples are separated using high-performance liquid chromatography before electrospray ionisation. Ionised molecules are separated based on their M/Z ratio in the mass spectrometer and detected for subsequent analysis. Illustration made using Biorender.

MS-based proteomic studies typically use two primary experimental approaches: a top-down approach, which analyses intact proteins, and a bottom-up approach, which enzymatically digests proteins into peptides before analysis **(Fig. 1.8)** (Toby et al., 2016). The top-down approach allows the analysis of intact proteins, which provides several advantages, including complete protein sequences, locating and characterising post-translational modifications (PTMs), and the identification of protein isoforms (Toby et al., 2019). However, due to limitations in instrumentation and technical difficulties associated with whole protein analysis, top-down analysis lags behind the bottom-up approach in terms of proteome coverage, sensitivity and throughput.

Bottom-up proteomics begins with the enzymatic digestion of proteins into peptides prior to separation by LCMS (Zhang et al., 2013). In contrast to the analysis of complete proteins, peptides are more easily separated and ionise well. As peptide fragments are analysed, proteins are typically identified by comparing the peptide spectra against a database of known peptide sequences (Zhang et al., 2013). Protein inference, the process of aligning digested peptides to theoretical whole protein sequences, is complicated because it involves identifying and quantifying proteins that may contain similar peptide sequences, leading to ambiguities (Amunugama et al., 2013). While this ambiguity is a limitation of bottom-up proteomics, this approach is most commonly applied to immunological samples due to its high sensitivity, proteome coverage and ease of analysis relative to the top-down approach.

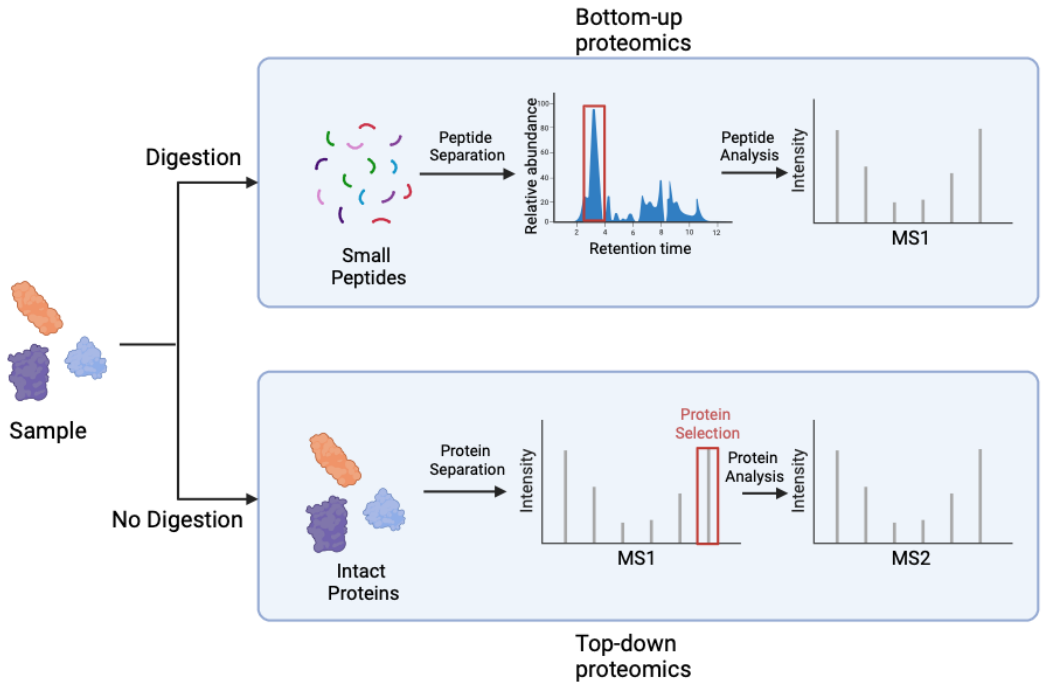

Figure 1.8 – Experimental approaches used in LC/MS quantitative proteomics
Illustration showing the analysis pipeline of two main non-targeted proteomics methods. Bottom-up proteomics analyses peptides after they have been digested and injected into the mass cytometer, while top-down proteomics analyses intact proteins without digestion. Illustration made using Biorender and adapter from (Brenes, 2023).

1.4.2 Data Acquisition Strategies

In analysing the bottom-up MS approach, two common data acquisition strategies for peptide identification and quantification are data-dependent acquisition (DDA) and data-independent acquisition (DIA) **(Fig. 1.9)**. DDA was the first acquisition method routinely used for bottom-up proteomics analysis (Pandey & Mann, 2000). In DDA, ions (peptides) are selected for fragmentation and MS/MS analysis based on predefined criteria, typically the most abundant ions in the MS1 spectrum. Once the chosen ions have been fragmented, the mass spectrometer moves on to the next set of ions, after which the process is iteratively repeated until a sufficient number of peptides have been identified and quantified (Michalski et al., 2011). A key benefit of DDA is the ease of analysis of the MS2 spectra, as this typically contains ions from the same peptide. This allows effective and accurate quantification of abundant peptides and is commonly used in discovery proteomics experiments to identify novel peptides and proteins. The primary disadvantage of DDA is the inconsistent quantification of peptides across samples due to the selection of precursor ions based on abundance rather than uniform coverage. In addition, low-abundance peptides are often missed in DDA experiments as they are not selected for fragmentation due to competition with more abundant ions (Davies et al., 2021).

In contrast to DDA, DIA does not have any predefined ion selection criteria and involves the systematic fragmentation of all precursor ions within predefined mass/charge (m/z) windows across the entire mass range rather than selecting specific ions for fragmentation (Gillet et al., 2012). While DIA leads to more complex MS2 spectra, increasing the computational power required for analysis, this approach leads to more consistent identification and proteins across samples, fewer missing values due to the analysis of all peptides, and increased sensitivity to lowly abundant peptides. Thus, as computational approaches have improved to deconvolute complex DIA spectra effectively, DIA is the preferred data acquisition strategy for targeted quantification and reproducible analysis in large-scale quantitative proteomics experiments (Dowell et al., 2021).

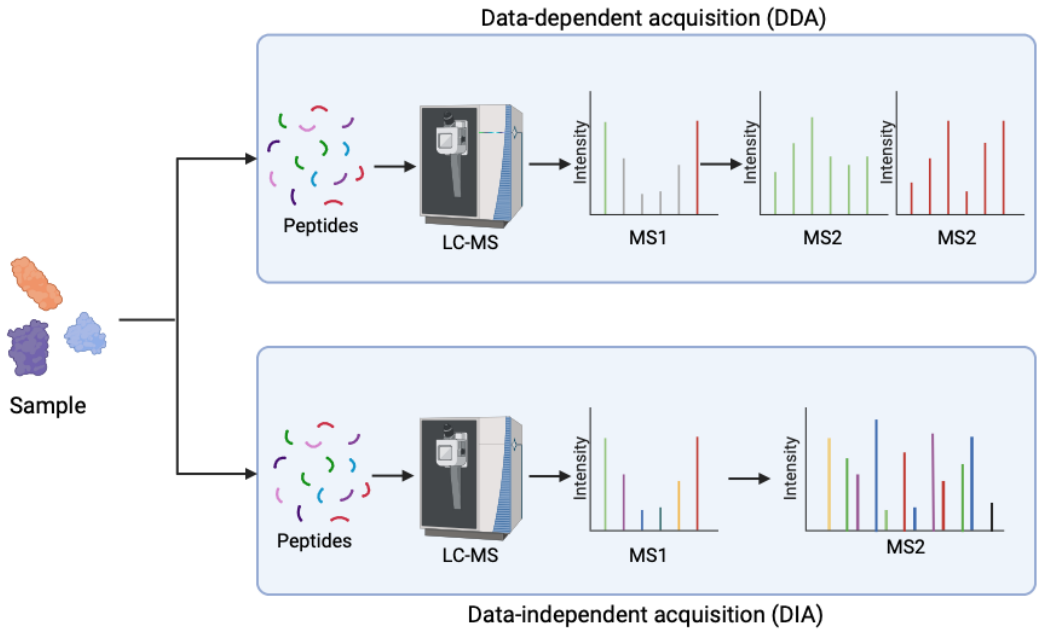

Figure 1.9 – Data acquisition strategies in Bottom-up proteomics
Illustration of the analysis pipeline showing the two main bottom-up proteomics workflows. Data-dependent acquisition (DDA) involves the selection of specific ions, typically the most abundant in the MS1 spectrum, which is iteratively analysed in the MS2 spectra. Data-independent acquisition (DIA) involves systematically fragmenting all precursor ions in a sample rather than selecting specific ions for fragmentation. Illustration made with Biorender and adapted from (Brenes, 2023)

1.4.3 Labelling-free and labelled quantification

The acquisition strategies discussed above (DIA and DDA) are examples of label-free quantification. In label-free experiments, samples of each condition are run individually in separate MS runs. While this approach involves less sample preparation, the requirement for numerous runs significantly reduces throughput and is more prone to error. Various metabolic and chemical labelling strategies have been developed to address this, allowing numerous samples to be run simultaneously (Chen et al., 2021; Gouw et al., 2010). The most frequently used metabolic labelling strategy is stable isotope labelling of amino acids in cell culture (SILAC) (Ong et al., 2002). This method involves culturing cells in media that contains isotope-labelled amino acids. SILAC labelling can increase throughput by labelling samples with light, medium and

heavy isotopes (Ong et al., 2002). Chemical labelling involves isobaric tags, which chemically bind to peptides and proteins and have varying distributions of heavy isotopes in their structure, allowing labelled samples to be distinguished in the MS2 spectrum. The most commonly used isobaric labelling methods include tandem mass tags (TMT) and isobaric tags for relative and absolute quantification (iTRAQ) (Ross et al., 2004; Thompson et al., 2003). In DDA experiments, isobaric tags are added to each sample after protein digestion. As each sample is labelled with a unique tag, all samples are combined and analysed in a single MS run. Currently, TMT labelling allows the simultaneous analysis of up to 18 samples in a single experiment (Y. Du et al., 2021).

1.4.4 Quantitative proteomics in the study of immune cell function

As technological approaches in proteomic profiling have improved, allowing the capacity for multiplexing samples and high-throughput experimental pipelines, the application of proteomics in studying immune cell function has expanded in recent years. For example, quantitative proteomics has been applied extensively to studying T-cell metabolism and function (Howden et al., 2019; Hukelmann et al., 2016; Marchingo et al., 2020). A key benefit of proteomics is directly quantifying protein abundance rather than using mRNA as a surrogate marker for protein expression. While transcriptional profiling has been instrumental in advancing the understanding of immune cell function, it is now apparent that mRNA abundance does not always reflect protein abundance due to the complex network of post-transcriptional and post-translational regulatory mechanisms associated with protein expression (Howden et al., 2019; Hukelmann et al., 2016). Hukelmann et al. analysed the relationship between the transcriptome and proteome of cytotoxic T lymphocytes (CTLs), identifying a weak positive correlation between mRNA transcript abundance and corresponding protein abundance (Hukelmann et al., 2016). This study revealed that CTLs have active mTORC1 signalling and that pharmacological inhibition of mTORC1 with rapamycin controls the protein expression of a subset of proteins associated with metabolic and effector functions in CTLs. Notably, a high proportion of the proteins significantly downregulated in response to rapamycin treatment were not

affected at the transcriptional level, highlighting the importance of direct proteomic analysis for cell phenotyping (Hukelmann et al., 2016).

In the study of immune cell function, quantitative proteomics allows the mechanistic characterisation of cellular state during development and activation. For example, Tan et al. characterised proteomic features associated with mouse T cell activation in response to anti-CD3 and anti-CD28 stimulation during different phases of T cell activation (Tan et al., 2017). This study found that after 2h of stimulation, while there were limited changes in overall protein abundance, there was significant remodelling of the phosphoproteome, indicating the induction of signalling events. Extensive proteomic remodelling occurred between 8-16h of stimulation, leading to changes in protein translation and metabolic functions. Subsequent analysis identified proteomic signatures associated with naïve T cell exit from quiescence, including the downregulation of MAPK signalling pathways and the DNA damage response. This study highlights the value of proteomic profiling in identifying the molecular circuitry associated with T-cell activation, which has important implications for T-cell maintenance and survival (Tan et al., 2017).

In the study of immunometabolism, quantitative proteomics allows the ability to simultaneously quantify the abundance of proteins involved in metabolic pathways, the transcription factors that induce their expression and the nutrient transporters that supply metabolic fuels. For example, a study by Howden and colleagues used quantitative proteomics to compare CD4 and CD8 T cell proteome remodelling during activation to determine how mTORC1 influenced metabolism and function (Howden et al., 2019). This study identified how environmental signalling pathways integrated antigen and cytokine signalling to ensure appropriate immune responses. The authors detailed the expression and dynamic remodelling of nutrient transporter abundance in T cells, identifying cell-specific transporter preferences. For example, CD8 T cells have a striking enrichment of the glutamine transporter SLC1A5 compared to CD4 T cells. Additionally, CD8 T cells have higher expression of protein translation machinery and nutrient transporters, which

likely supports their enhanced proliferative capacity. Interestingly, while both cells induce mTORC1 signalling upon activation, CD4 T cells were found to be specifically dependent on mTORC1 activity for cell-cycle regulation (Howden et al., 2019). In another study, the same group investigated the impact of the proto-oncogenic transcription factor cMYC on CD4 and CD8 T cell activation (Marchingo et al., 2020). This study revealed that cMYC is a critical regulator of proteomic remodelling in T cells, promoting amino acid transporter expression required for T cell bioenergetic and biosynthetic programs. The researchers identified a feed-forward loop whereby enhanced amino acid transport sustained cMYC stability, further promoting amino acid transporter expression.

1.4.5 Proteomic Analysis in the Study of DCs

The Mann group performed the first comprehensive analysis of the dendritic cell proteome over a decade ago (Luber et al., 2010). This study conducted a quantitative proteomic analysis of steady-state murine cDC1s, cDC2s and pDCs from the splenocytes directly *ex vivo*, identifying subset-specific differences in pathogen recognition receptors. They show that cDC2s are enriched for the expression of the viral RNA-recognition molecules RIG-I and MDA5, conferring cDC2s with enhanced sensitivity to viral infection with Sendai virus (Luber et al., 2010). In a more recent publication, Worah et al. apply quantitative proteomics to study human blood dendritic cells (Worah et al., 2016). The authors performed proteomics and transcriptomics on circulating pDCs, BDCA3+ cDC1s and CD1C+ cDC2s to identify differentially expressed proteins and transcripts between subsets. They show a weak positive correlation between mRNA transcript abundance and protein abundance, which supports the utility of direct protein measurement. Analysing conserved signatures at both the transcript and protein level, they reveal that pDCs lack caspase-1 expression, which reflects a lack of inflammasome activity in pDCs (Worah et al., 2016). In addition, Arya et al. examined the proteomic changes in moDCs in response to LPS for 6 and 24 hours (Arya et al., 2019). The authors report significant enrichment of proteins associated with cytokine signalling, ER-phagosome pathway and antigen presentation in response to LPS treatment.

While informative, these studies have their limitations. For example, these reports do not quantify absolute protein abundance but rather compare relative expression across subsets. As a result, these studies do not determine global proteome features between subsets or how these are remodelling upon maturation. The proteomic remodelling associated with cDC maturation is yet to be determined. Finally, as discussed above, quantitative proteomics is a valuable technique for investigating immunometabolic profiles of immune cells. None of these studies investigate in detail metabolic features at the proteomic level either between subsets or during DC maturation.

1.4.6 Limitations of proteomic analysis

While quantitative proteomics is a compelling approach to mechanistically understanding cellular function, its mainstream application remains challenging. In contrast to genomic and transcriptomic approaches, where thousands of genes can be sequenced rapidly, proteomics has a lower throughput. In addition, the instrumentation required for genomics and transcriptomics is currently more readily available than for proteomics. Despite advancements in MS technologies, the detection sensitivity of proteomics is less than that of transcriptomics, particularly for low-abundance and membrane-bound proteins. Further, the analysis of proteomic data is complex and computationally intensive. Thus, there is a need to develop accessible data analysis pipelines for proteomic studies (Solt, 2022).

A fundamental issue that hinders the mainstream use of proteomics is the amount of cellular material required for analysis. Technologies, including single-cell RNA sequencing (scRNA-seq) and Assay for Transposase-Accessible Chromatin (ATAC)-seq, have enabled the interrogation of biological questions in small numbers of cells. The number of cells currently required for proteomic analysis far outpaces that of these assays, limiting our ability to investigate rare immune cell populations directly *ex vivo*. Recent advances in applying MS quantitative proteomics at the single-cell level have been reported (Schoof et al., 2021; Specht et al., 2021). While still in its

infancy, applying proteome profiling to single cells has the potential to revolutionise immunological studies. This approach may be particularly valuable in the case of DCs, whose subsets show a high degree of heterogeneity.

1.5 Single-cell nutrient uptake assays to interrogate immunometabolism

While quantitative proteomics allows the characterisation of metabolic machinery, including proteins involved in intermediary metabolism and nutrient transport, it does not directly describe metabolic flux or nutrient utilisation. Thus, combinatorial approaches to studying metabolic flux, including stable isotope metabolic tracing, metabolite quantification, and nutrient uptake, provide a more complete picture of a cell's immunometabolic profile.

Using radiolabelled metabolites has provided valuable insights into nutrient transport dynamics, transporter specificity and affinity in immune cells. However, the application of radiolabelled tracer assays is limited in the specific equipment and training required and the necessity to perform experiments on bulk cell populations (L. V. Sinclair et al., 2020). Thus, this approach does not allow the resolution of nutrient uptake in single cells or subpopulations present in a complex mixture of cells. To address this, fluorescently labelled nutrient analogues such as bodipy labelled lipids or 7-nitrobenzofurazan-labelled glucose (NBDG) have been used to interrogate nutrient uptake at the single-cell level by flow cytometry. However, while still frequently reported in the literature, growing evidence has questioned the utility of these assays. The attachment of fluorophores to nutrients can dramatically change the transport activity of the labelled nutrient, making this approach inaccurate. For example, bodipy-labelled lipids accumulate in different compartments than lipids modified with smaller detectable groups (Laguerre & Schultz, 2018). Furthermore, NBDG was previously thought to be taken up by the glucose transporters SLC2A1 and SLC2A3, which are prominently expressed in immune cells. However, Sinclair and colleagues recently showed that NBDG is not outcompeted by glucose uptake in T cells, indicating that it is not transported through these transporters (L. V. Sinclair

et al., 2020). In the case of amino acids, the naturally fluorescent tryptophan metabolite, kynurenine, has been shown to be transported by the system-L family of amino acid transporters, including SLC7A5 (L. V. Sinclair et al., 2018). While many fluorescent amino acid analogues have been synthesised, the transporter specificity of these compounds needs to be better understood. To circumvent the limitations associated with nutrient uptake specificity due to fluorophore ligation, approaches to chemically attach fluorescent probes after nutrient uptake are gaining traction. Work from the Finlay lab and collaborators have recently described a single-cell uptake assay for the glutamine transporter SLC1A5 using biorthogonal “click” chemistry to label non-natural amino acids after cellular uptake (Pelgrom et al., 2023).

1.5.2 Bioorthogonal “Click” Chemistry

Bioorthogonal “Click” chemistry is an approach in which a biomolecule with a small reactive chemical group can be ligated to a detectable group. This methodology was first reported by Saxon and Bertozzi, whose contributions were recently recognised with the 2022 Nobel Prize in Chemistry (Saxon & Bertozzi, 2000). In practical applications, this involves a small molecule such as an amino acid, lipid or metabolite that is minimally modified with a chemical group (handle) that does not affect its biological function, thus making a “bioorthogonal” molecule. The “handle” is then attached to a second detectable molecule, such as a fluorescent tag, which allows any process in the cell that uses the minimally modified molecule to be visualised, quantified or selectively isolated (Van Kasteren & Rozen, 2023). For example, the amino acid methionine can be modified by the addition of a reactive amine group (Homopropargylglycine (HpG)) or azide group (Azidohomoalanine (Aha)) to create selectively reactive non-natural amino acids. Both HpG and Aha have been shown to incorporate into nascent peptide chains in the place of methionine during protein synthesis and have thus been used to measure protein synthesis rates both *in vitro* and *in vivo* (Steward et al., 2020).

1.5.3 Application of Click Chemistry to Measure Nutrient Uptake

The application of bioorthogonal reagents to study cellular biology has developed significantly in recent years. This approach has been used to label

many cellular components, such as glycans, lipids, DNA, and RNA, as well as whole animals such as zebrafish and mice (Jao & Salic, 2008; Laughlin et al., 2008; Saxon & Bertozzi, 2000; Suazo et al., 2021). The addition of “clickable” fluorescent tags to amino acids, referred to as BONCAT (bioorthogonal non-canonical amino acid tagging), has frequently been used in studying protein synthesis, protein localisation and enzyme activity studies (Van Kasteren & Rozen, 2023). HpG and Aha are among the most frequently used non-natural amino acids in protein synthesis studies; however, despite their broad application, their transport mechanism was only recently determined (Pelgrom et al., 2023). Work from the Finlay lab and collaborators revealed that HpG and Aha are actively transported through the sodium-dependent neutral amino acid transporter, SLC1A5 and not through the methionine transporter, SLC7A5. It was revealed that short-term incubation of immune cells with HpG and Aha, before incorporating these amino acids into proteins, provides a measure of SLC1A5 transport activity both *in vitro* and *in vivo* **(Fig. 1.10)**. SLC1A5 has been identified as a critical glutamine transporter in activated immune cells and tumour cells. Thus, the ability to measure SLC1A5 transport activity in a heterogeneous population of cells is of broad immunological and therapeutic interest.

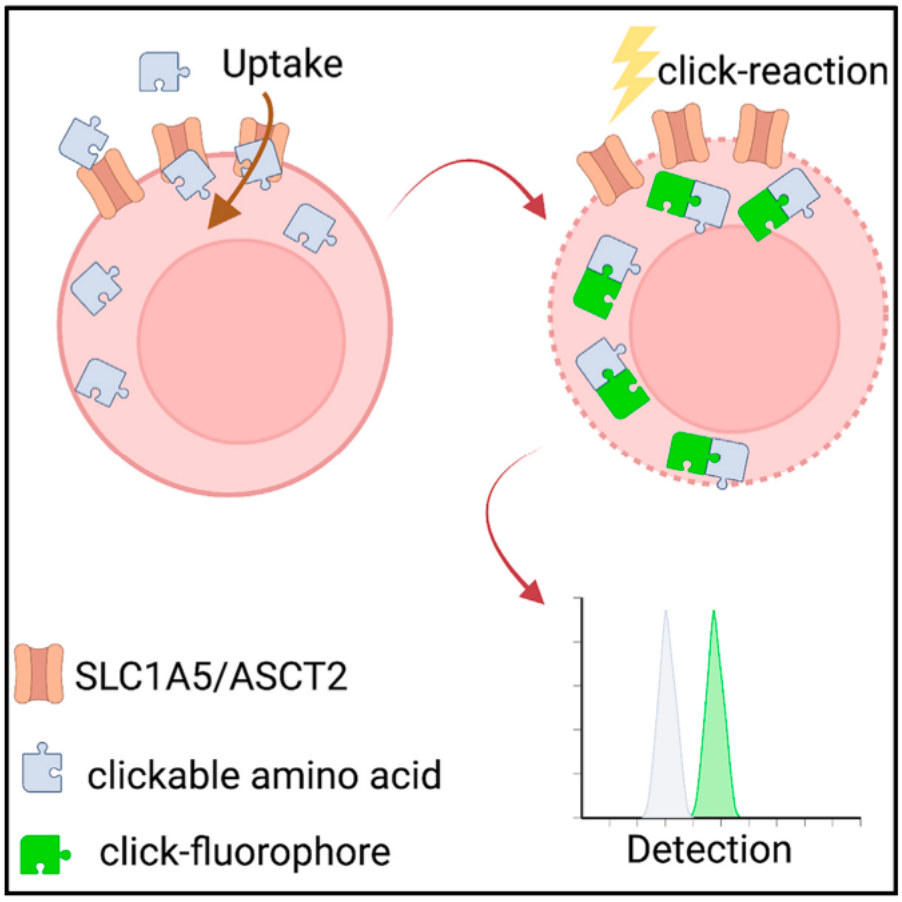

Figure 1.10 –Bioorthogonal SLC1A5 nutrient uptake assay
The short-term incubation of immune cells with “clickable” amino acids (HpG/Aha) measures Slc1a5 transport activity. A “clickable” fluorophore specifically binds to the non-natural amino acids within the cells to detect uptake by flow cytometry.

Image Credit - (Pelgrom et al., 2023)

1.6 Thesis aims

This project aims to characterise the proteomic features of splenic dendritic cell subsets in the steady state and after immunogenic activation. While proteomics has been applied to the study of DC biology, with the advancement of mass-spectrometry technology and advanced analysis pipelines, this project provides an updated and comprehensive characterisation of cDC1, cDC2 and pDC proteomes identifying novel regulators of dendritic cell function. In particular, the differential expression of nutrient transporters is identified across subsets. While the regulation of immune function by nutrient transporters has been highlighted in various immune cells, their role in DC metabolism and function remains unclear. I utilise single-cell nutrient uptake assays, both established and novel, to determine differential rates of nutrient acquisition in DC subsets and the implication of this on DC metabolism and function.

The specific aims of this project are as follows:

1. Apply quantitative proteomics to study the metabolism of cDC1s and cDC2s in the steady state and after immunogenic activation.
2. Quantify the nutrient transport machinery of cDC1s and cDC2s and investigate how amino acid transport influences mTORC1 signalling and cDC function.
3. Investigate the pDC proteome to identify novel regulators of function.

Chapter 2 – Materials and Methods

2.1 Materials

2.1.1 – Cell Culture Reagents

Dulbecco's Modified Eagle Medium (DMEM) (61965026), RPMI medium 1640 (1X) [+] L-Glutamine (61870010), RPMI medium 1640 (1X) [-] L-Glutamine (21870076), Dulbecco's phosphate-buffered saline (PBS) (10010023), Penicillin-Streptomycin (151401122), MEM-vitamin solution (100X) (11120037), L-Glutamine solution (100X) (25030149), Trypsin (0.25%) phenol red (25300104), Hanks' Balanced Salt Solution (HBSS) (15373571) were purchased from Thermofisher. Heat-inactivated Fetal Bovine Serum (FBS) was purchased from Labtech International. β-Mercaptoethanol (31350) and red cell lysis buffer (A1049201) were purchased from Gibco. Optiprep density gradient media (07820) was purchased from Stemcell.

2.1.2 – Cell Culture Equipment

Pipettes, pipette tips, Pasteur pipettes, filtered pipette tips, cell culture strainers (70µm), 2ml syringes, filters (20µm), tissue culture dishes, tissue culture flasks, falcon tubes and Eppendorf tubes were obtained from Cruinn Diagnostics Ltd. P1000, P200, P20, P10 pipettes are from Gilson. Haemocytometers were purchased from Hausser Scientific**.** Steri-cycle CO_2 Incubator, serological pipettes, pipette boy, insulin needles and needles were from Fisher Scientific. Anti-XCR1 Microbead kit (130-115-721) was purchased from Merck. MojoSort CD8 T cell isolation kit (480007) was purchased from Biolegend.

2.1.3 Cell stimulants and treatments

ODN1826 (CpG-B) (tlr-1826), ODN1585 (CpG-A) (tlr-1585) and OVA 257-264 (vac-sin) were purchased from InvivoGen. Ovalbumin (9006-59-1) was purchased from Worthington. 2-Deoxyglucose (25972), Oligomycin (495455), FCCP (C2920), DMSO (D8418), 2-Amino2norbornanecarboxylic acid (BCH) (A7902), Chloroquine (C6628), rapamycin (37094) and bovine serum albumin (BSA) (A2153) were purchased from Merck. CB839 (S7655) was purchased

from Selleckchem. Deferoxamine (D9533) was purchased from Sigma-Aldrich.

2.1.4 Buffers and Solutions

Media/Buffer	Composition
DC culture media	RPMI medium 1640 (+) L-Glutamine, FCS (10%), Penicillin/Streptomycin (1%), 50μM β –mercaptoethanol
B16-Flt3l culture media	DMEM (+) L-Glutamine, FCS (10%), Penicillin/ Streptomycin (1%)
FACS buffer	Dulbecco's PBS supplemented to contain sodium azide (0.1%) and BSA (0.25%)
Acid wash	PBS supplemented with 150mM NaCl and 20mM citric acid, pH5
Wash buffer	Dulbecco's PBS supplemented with 10% FBS
Permeabilisation buffer (Click Chemistry)	Dulbecco's PBS supplemented with 1% BSA and 0.01% Saponin.

Table 2.1 – List of buffers and solutions

2.1.5 Biological material

C57BL/6J were purchased from Harlan (Bicester, U.K.) or Charles River or were bred in-house. All mice used for this project were between 8 and 12 weeks of age, male or female. Experiments were conducted in compliance with the Finlay lab project license, with ethical approval from the Trinity College Dublin University ethics committee and the Animal Research Ethics Committee from the Health Products Regulatory Authority (HPRA). Animals were culled by CO_2 inhalation or cervical dislocation. Organs were harvested in the comparative medicine unit (CMU), and carcasses were disposed of in accordance with the guidelines described by the TCD CMU.

2.1.6 Cell lines and primary cells

Flt3l-producing B16 melanoma cells were kindly gifted by Professor Bart Everts (Leiden University). Primary splenocytes were isolated from spleens of C57BL/6J mice (Strain code: 623) (Charles River) for dendritic cell experiments and OT-I (C57BL/6-Tg(TcraTcrb)1100Mjb/Crl) (Strain code: 642) (Charles River) for dendritic cell – T cell co-culture experiments.

2.1.7 Flow Cytometry Reagents

Collagenase D (11088866001) was purchased from Roche. DNase I (D4513) was purchased from Sigma-Aldrich. LIVE/DEAD Aqua (L34965) and LIVE/DEAD Yellow (L34959), pHrodo Green dextran (P10361), Dextran AF-647 (D22914), BSA-AF647 (A34785), Ovalbumin AF647 (O34784), Lysotracker Deep Red (L12492), DQ-Ovalbumin (D12053), Foxp3/Transcription factor staining buffer set (00-5523-00) were purchased from Thermofisher. 4% paraformaldehyde (PFA) (SC281692) was purchased from Santa Cruz. Cytofix/Cytoperm fixation/permeabilisation kit (554714) and GolgiPlug (555029) were purchased from BD Biosciences. Mitotracker Green FM (M7514) and TMRM (T668) were purchased from Invitrogen.

2.1.8 Click Chemistry Reagents

L-homopropargylglycine (HPG) (CLK-1067-25), AF488-Alkyne (CLK-1277-1), AF488-Azide (CLK-1275-1) and Tris-hydroxypropyltriazolylmethylamine (THPTA) (CLK-1010-25) were purchased from Jena Biosciences. Aminoguanidine (81530) was purchased from Caymen Chemicals. Copper(II) sulfate pentahydrate (209198) and sodium ascorbate (A7631) were purchased from Sigma-Aldrich. O-propargyl-puromycin (C10459) was purchased from Thermo Fischer. Saponin (558255) was purchased from Merck.

2.1.9 List of Antibodies

Target	Fluorchrome	Supplier	Clone
CD11b	BV605	BIOLEGEND #101257	M1/70
CD11c	BV421	BD #562782	HL3
CD19	BV650	BD #563235	1D3

CD19	PECY7	BD #552854	1D3
CD24	BV421	BIOLEGEND #101825	M1/69
CD3	PerCP	Miltenyi 130-120-826	REA641
CD317	BV650	BD #747605	927
CD69	APCEFLUOR780	BIOLEGEND #104526	H1.2F3
CD71	PE	BD#553267	C2
CD80	BV605	BIOLEGEND #104729	16-10A1
CD86	PE	BD #553692	GL1
CD98	PE	EBIOSCIENCES #12-0981-83	RL388
F4/80	AF700	BIORAD #MCA497A700	BM8.1
H2kB-SIINFEKL	APC	BIOLEGEND #141606	25-D1.16
IFNα	FITC	BIOTECHNE (R&D) #22100-3	RMMA-1
IL12p40	BV421	BD #561456	C15.6
IL6	PE	BIOLEGEND #504504	MP5-20F3
IRF4	AF488	BIOLEGEND #646405	IRF4.3E4
IRF8	APC	EBIOSCIENCE #17-9852-80	V3GYWCH
Ly6G	BV510	BIOLEGEND #127633	1A8
MHCII (I-A/I-E)	APCEFLUOR780	EBIOSCIENCES #47-5321-82	M5/114.15.2
NKp46	PERCPEFLUOR710	INVITROGEN 46-3351-82	29A1.4
PDL1	APC	BIOLEGEND #124312	10F.9G2
pEIF4BP1/2	PE	ABCAM	Y329
pS6	PE	CELL SIGNALLING #S235/236	D57.2.2E
Siglec-H	FITC	BIOLEGEND #129603	551
SIRPα	AF594	BIOLEGEND #144020	P84
TNFα	PECY7	INVITROGEN #25-7321-82	MP6-XT22
XCR1	BV785	BIOLEGEND #148225	ZET

Table 2.2 – List of flow cytometry antibodies

2.1.10 Software

FlowJo™ version 10.7 (FlowJo) was used to analyse flow cytometry data. Graphpad Prism 9.0 (Graphpad) was used to format data and perform statistical analysis. Microsoft Excel (Version 16.81), Phantasus (Version 1.21.5), g:Profiler, DAVID (v2023q4), and SRplot were used to analyse and present quantitative proteomic data. Graphical figures were made using BioRender.

2.2 Methods

2.2.1. *In vivo* dendritic cell expansion

To expand the dendritic cell compartment *in vivo*, mice were inoculated with $2.5x10^6$ B16-Flt3l secreting melanoma cells in 100μL PBS subcutaneously in the flank. After 10-12 days of tumour growth, mice were sacrificed, and the spleen was harvested and processed as described below.

2.2.2. B16-Ft3l murine melanoma cell culture

B16-Ft3l melanoma cells were cultured in DMEM supplemented with 10% heat-inactivated FBS and 1% penicillin/streptomycin at 37°C, 5% CO_2. Once confluent, the cells were passaged at a ratio of 1:10 by incubating with 0.25% trypsin for 5 mins at 37°C, 5% CO_2. After the incubation, the trypsin was neutralised by the addition of serum-containing DMEM. Cells were counted, and viability was assessed using Trypan Blue staining.

2.2.3. DC isolation and culture

Spleen from C56Bl/6J mice inoculated with B16-Flt3l secreting melanoma cells were mechanically disrupted using the back-end of a syringe before the addition of 50μL of collagenase D (final concentration = 1mg/ml) and DNase I (final concentration = 2000U/ml) for 30 mins at 37°C, 5% CO_2. After 30 mins, the cells were filtered through 70μm sterile filters and the filtered suspension was centrifuged. The resulting pellet was resuspended in ACK buffer for 5 mins to lyse red blood cells. Subsequently, RPMI was added to neutralise the ACK buffer and the cells were centrifuged. Following centrifugation, splenocytes were resuspended in complete RPMI.

For splenocyte experiments, $5x10^6$ splenocytes/ml were seeded in 96 well U-bottom cell culture plates in 200μL of complete RPMI. Where indicated, splenocytes were treated with CpG-A (4μg/ml), CpG-B (4μg/ml), rapamycin (20nM), BCH (25mM), 2-DG (100mM), Oligomycin (2μM) CB839 (4μg/ml) and Deferoxamine (20μg/ml).

For SLC7A5 inhibition experiments using BCH, splenocytes were cultured in a 1:1 mixture of cRPMI and Hanks balanced salt solution (HBSS). For glutamine deprivation experiments, splenocytes were cultured in RPMI

without glutamine supplemented with 10% dialysed heat-inactivated FCS, 50μM of β-mercaptoethanol, and 1% penicillin-streptomycin.

2.2.4 Flt3l Bone marrow-derived cells generation

Cell suspensions from bone marrow from C57Bl/6 mice were cultured in cRPMI in the presence of 100ng/ml Flt3l (R&D) for 7 days. $2x10^6$ bone marrow cells/ml were plated in 6-well culture plates. For iron chelation experiments, deferoxamine (20μg/ml) was added on Day 0, Day 3, or Day 5 of culture. FL-DC generation was determined on day 7 by flow cytometry.

2.2.5. Flow Cytometry

For analysis of surface markers, cells were first incubated with FC block for 5 mins in FACS buffer (PBS +0.25% BSA +0.1% Sodium azide) and then stained with the appropriate antibodies for 20 mins at room temperature in the dark. For intracellular cytokine detection, cells were stimulated for 6h with TLR9 agonists. cDC cytokine production was induced using 4μg/ml CpG-B. For intracellular IFNα detection in pDCs, cells were stimulated with 4μg/ml CpG-A. After 2h of stimulation, exocytosis was blocked using Golgi Plug (BD Biosciences, contains Brefeldin A) to capture intracellular cytokines. Cells were stained with surface markers before fixation and permeabilisation using Cytofix/Cytoperm (BD Biosciences) for 20 mins in the dark at 4°C. Intracellular antibody staining was performed in 1x Perm Wash (BD Biosciences) for 30 min at room temperature in the dark. Transcription factor staining was performed with a FOXP3/transcription factor staining buffer set (eBiosciences) according to the manufacturer's instructions. Samples were acquired on LSR Fortessa and analysed using FlowJo™ software (TreeStar).

2.2.6 Mitochondrial Staining

Mitochondrial mass was determined using Mitotracker Green (MTG, M715, Invitrogen) and mitochondrial membrane potential was measured using Tetramethylrhodamine methyl ester (TMRM, T668, Invitrogen) staining by flow cytometry. Cells were first stained with surface markers as described above. Subsequently, cells were incubated with a mastermix containing

100nM MTG and 100nM TMRM in cRPMI for 20 mins at 37°C, 5% CO_2. Oligomycin (2μM, Sigma) and FCCP (20μM) were added as positive and negative controls, respectively. After incubation, cells were washed in FACS buffer and acquired immediately on the BD LSRII Fortessa and analysed using FlowJo™ software (TreeStar).

2.2.7 Kynurenine uptake

Slc7a5 transport activity was determined by measuring the rate of kynurenine uptake into cells. Kynurenine is a naturally fluorescent metabolite that is transported by system-L amino acid transporters (L. V. Sinclair et al., 2018). Cells were stained with surface markers as described above. Subsequently, cells were resuspended in pre-warmed HBSS (37°C) and treated and incubated with kynurenine (final concentration 200μM) for 5 mins at 37°C, 5% CO_2. As controls, BCH (final 10mM), leucine (final 5mM) and lysine (final 5mM) were used as pharmacological (BCH) and competition controls (Leu, Lys). A separate control incubated on ice was used to inhibit active transport. After the incubation, uptake was stopped by the addition of 1% PFA. Cells were washed in FACS buffer and acquired on the BD LSRII Fortessa. Kynurenine fluorescence was measured using 405 nm excitation (violet laser) and bandpass filter 450 ± 50.

2.2.8 Transferrin uptake

Transferrin uptake was determined by measuring the uptake of Alexa fluor-conjugated transferrin by flow cytometry. Cells were washed in serum-free RPMI supplemented with 0.5% BSA. Subsequently, cells were incubated in RPMI + 5% BSA for 1 hour at 37°C, 5%. After incubation, cells were incubated with or without 5μg/ml Alexa Fluor-conjugated Transferrin for 10 minutes at 37°C, 5% CO_2. As controls, cells were also incubated with Holo-transferrin (500μg/ml), or uptake was performed on ice. Uptake was ceased by washing the cells with ice-cold acid wash (PBS supplemented with 150mM NaCl and 20mM citric acid, pH5) followed by washing in ice-cold RPMI + 0.5% BSA. Cells were stained with surface antibodies as described above, and samples

were acquired live on the BD LSRII Fortessa and analysed using FlowJo™ software (TreeStar).

2.2.9 Bioorthogonal amino acid uptake

Cells were stained with surface markers as described above. Following staining, cells were resuspended in a mixture containing a 1:1 ratio of HBSS and RPMI and centrifuged. Subsequently, cells were resuspended in HBSS + RPMI and warmed in the incubator at 37°C, 5% CO_2, excluding the cold control, which was kept on ice in the dark. In parallel, homopropargylglycine (HPG) (Final concentration = 200μM) was prepared in HBSS. Competition controls (L-Glutamine and L-Alanine, concentrations indicated in figure legends) were also prepared in HBSS. Uptake was performed in 96 well U-bottom plates by incubating $2x10^6$ cells with HPG +/- competition controls for 5 mins at 37°C, 5% CO_2 or on ice for the cold control. After the incubation, uptake was ceased by the addition of PFA (1% final concentration) for 30 min at room temperature in the dark. Subsequently, cells were centrifuged and washed three times in PBS. Finally, cells were resuspended in PBS and stored at 4°C prior to the click-chemistry reaction.

2.2.10 Click chemistry

To perform the click chemistry reaction, cells were first permeabilised by incubating the cells with saponin (0.01%) in PBS for 20 mins at room temperature. During the incubation, the click reaction mixture was prepared as follows. In a sequential order, sodium ascorbate (NaAsc) (final concentration = 10mM), tris-hydroxypropyltriazolylmethylamine (THPTA) (final concentration = 1mM), aminoguanidine (final concentration = 100mM), PBS and bio-orthogonal fluorophore (AZDye-488) (final concentration = 5mM) were added to copper sulfate (CuSO4) (final concentration = 1mM). After the incubation, the cells were centrifuged, the supernatant removed and resuspended in 30μl of click reaction mixture in a 96-well U-bottom plate and incubated for 1 hour at room temperature in the dark. After the incubation, cells were resuspended in PBS and centrifuged, followed by three washes in FACS buffer. Finally, cells were resuspended in PBS and samples were

acquired on the BD LSRII Fortessa and analysed using FlowJo™ software (TreeStar).

2.2.11 Measuring protein synthesis

O-propargyl-puromycin (OPP) was used to measure protein synthesis in cDC populations within splenocytes. Incorporation was measured using the Cu-catalysed click reaction as above to attach an azido-fluorophore. Fluorescence intensity reflects the level of protein synthesis. Cells were stained with surface antibodies as described above. Subsequently, cells were incubated with OPP (20mM final concentration) in cRPMI for 20 mins at 37°C, 5% CO_2. Following incubation, cells were fixed using PFA (1% final concentration) for 20 mins at room temperature in the dark. After the incubation, cells were washed three times in PBS. Permeabilization and the click chemistry reaction were performed as described above. Samples were acquired using the BD LSRII Fortessa and analysed using FlowJo™ software (TreeStar).

2.2.12 SCENITH

SCENITH was performed as previously described in (Argüello et al., 2020). Briefly, splenocytes were plated at a density of $5x10^6$ cells/ml in U-bottom 96-well plates (200μL final volume). Cells were treated with PBS (Control), 2-Deoxy-D-Glucose (2DG, final concentration 100mM), Oligomycin (Oligo, final concentration 2μM), CB839 (CB, final concentration, 4μg/ml) or a sequential combination of 2DG and Oligo for 20 minutes at 37°C, 5% CO_2. After 20 minutes of inhibitor incubation, OPP (20mM) was added for a further 20 minutes. After OPP treatment, cells were washed in cold PBS and stained with a combination of Fc receptor blockade and fluorescent cell viability dye, then primary conjugated antibodies against surface markers for DC identification. After washing, cells were fixed in 1% PFA and the OPP-click chemistry reaction was performed as discussed above. Samples were acquired using the BD LSRII Fortessa and analysed using FlowJo™ software (TreeStar).

2.2.13 Endocytosis assays

Endocytosis of fluorescently labelled macromolecules was determined by incubating cells with 10μg/ml BSA-AF647, 0.5mg/ml 10kDA dextran-AF647 or 1μg/ml OVA-AF647 for indicated periods. Subsequently, cells were washed three times in ice-cold PBS before surface antibody staining and fixation with 4% paraformaldehyde. After fixation, cells were acquired on the LSR Fortessa and analysed using FlowJo™ software (TreeStar).

2.2.14 DQ-ovalbumin degradation assay

Splenocytes were incubated with 10μg/ml DQ-Ovalbumin (DQ-OVA) for 1h in cRPMI at 37°C, 5% CO_2. After 1h, extracellular OVA was washed off, and splenocytes were replated in cRPMI and incubated for the indicated periods. After DQ-OVA incubation, cells were washed in cold PBS and stained for surface markers. Samples were acquired on LSR Fortessa and analysed using FlowJo™ software (TreeStar).

2.2.15 Lysosomal acidification assays

Lysosomal acidification was determined using 10kDA dextran beads conjugated to pHrodo green. Cells were incubated with 20ng/ml pHrodo Green Dextran for the indicated periods. Subsequently, cells were washed three times in ice-cold PBS before surface antibody staining and fixation with 4% paraformaldehyde. After fixation, cells were acquired on the LSR Fortessa and analysed using FlowJo™ software (TreeStar). For Lysotracker Red staining, cells were stained with surface antibodies as described after cell culture treatment. After surface staining, cells were incubated with 50nM Lysotracker red for 30 mins at room temperature in the dark. Subsequently, cells were washed 3 times in ice-cold PBS, and samples were acquired immediately on LSR Fortessa.

2.2.16 H2-KB cross-presentation assay

To determine cross-presentation in cDCs, Flt3l expanded splenocytes ($2x10^6$ cells/ml) were treated with OVA (20μg/ml) or the OVA peptide SIINFEKL (1μg/ml) in cRPMI at 37°C, 5% CO_2 for 3h or 18h. For the 18h experiments,

extracellular OVA/SIINFEKL was washed off after 6h, and the cells were replated in cRPMI for the remaining 12h. For SLC7A5 inhibition experiments, splenocytes were treated with BCH (25mM) in a 1:1 mixture of cRPMI and HBSS for the first 6h and replated in cRPMI for the remaining 12h. Cross-presentation was determined by measuring the surface expression of H2KB-SIINFEKL complexes on the cell surface by flow cytometry. After the incubation, cells were washed in cold PBS and stained for surface markers and H2KB-SIINFEKL as described above. Samples were acquired on LSR Fortessa and analysed using FlowJo™ software (TreeStar).

2.2.17 *In vitro* cDC1-mediated OT-1 T cell activation

$XCR1^+$ cDC1s were isolated from Flt3L-expanded spleens using an $XCR1^+$ Microbead kit (Miltenyi) according to the manufacturer's instructions. Briefly, DCs were enriched from expanded splenocytes using a density gradient (Optiprep, 60% iodixanol in water, density = 1.32g/ml). After density enrichment, a maximum of $1x10^8$ splenocytes in 900μl of MACS (PBS + 0.5% BSA + 2mM EDTA) buffer was incubated with 100ul of $XCR1^+$ microbeads for 10 min at 4°C. After incubation, labelled splenocytes were transferred to MS columns and placed in a magnetic column, retaining $XCR1^+$ cells. The eluent contains $XCR1^-$ cells. MS columns were removed from the magnet, and $XCR1^+$ cells were expelled using an MS plunger. An aliquot of cells was taken to confirm purity by flow cytometry. $2x10^4$ cDC1s were plated in 96 well U-bottom plates in 50:50 RPMI:HBSS stimulated with 4μg/ml CpG-B and 20μg/ml OVA or 1μg/ml SIINFEKL in the presence or absence of 25mM BCH. During the incubation, CD8 T cells were isolated from the spleens of OT-I mice using a naïve CD8 T cell isolation kit (Mojosort). Following incubation, OT-I T cells were co-cultured with cDC1s at a 1:1 DC:T cell ratio in cRPMI for 24 and 48 hours. Following the incubation, OT-I T cell viability and activation were determined by flow cytometry. Samples were acquired on LSR Fortessa and analysed using FlowJo™ software (TreeStar).

2.2.18 Preparation of cell pellets for quantitative proteomics

DCs were enriched from B16-Flt3l expanded splenocytes using a density gradient (Optiprep, 60% iodixanol in water, density = 1.32g/ml) before surface marker staining by flow cytometry. Cell sorting of DC subsets was performed using the FACS Aria cytometer. cDC1 were identified as LIVE/DEAD^{-},CD3^{-},CD19^{-},CD11c^{+},MHCII^{hi},XCR1^{+},SIRPα^{-} cells, cDC2s were identified as LIVE/DEAD^{-},CD3^{-},CD19^{-},CD11c^{+},MHCII^{hi},XCR1^{-},SIRPα^{+} and pDCs were identified as LIVE/DEAD^{-},CD3^{-},CD19^{-},CD11c^{int} ,CD317^{+} cells. Cells were collected from the cell sorter and resuspended in ice-cold HBSS in 1.5ml sterile Eppendorf tubes. Cells were washed three times in HBSS to remove residual serum. After the final wash, excess supernatant was removed, and the pellets were snap-frozen in liquid nitrogen and stored at -80^{o}C.

2.2.19 Mass Spectrometry Processing

Proteomics sample preparation was performed by the staff of the Proteomics Facility at the University of Dundee, UK. The following protocol is adapted from (Brenes et al., 2023; Howden et al., 2019; Lisci et al., 2021). Sample pellets were lysed in 400 µl lysis buffer (4% sodium dodecyl sulfate, 50 mM tetraethylammonium bromide (pH 8.5) and 10 mM tris(2-carboxyethyl)phosphine hydrochloride) and incubated at 22^{o}C for 5 min. Following incubation, the lysates were boiled for 5 min before sonication with a BioRuptor (30 cycles: 30s on and 30s off) before alkylation with 20 mM iodoacetamide for 1 h at 22 °C in the dark. The lysates were subjected to the SP3 procedure for protein clean-up before elution into digest buffer (0.1% sodium dodecyl sulfate, 50 mM tetraethylammonium bromide (pH 8.5) and 1 mM CaCl2). For each sample, 2µg of peptide was analysed. Samples were injected into a nanoscale C18 reverse-phase chromatography system and electrospray into an Orbitrap Exploris 480 mass-spectrometer (Thermo Fischer).

2.2.20 Processing and analysis of proteomic data

The data were processed, searched, and quantified using Spectronaut 14 using the directDIA option. The direct DIA data was searched against the

UniProt mouse database (SwissProt and Trembl). Protein copy number quantification was performed in the Perseus software package. Mean copy numbers were estimated using the "proteomic ruler" described in (Wiśniewski et al., 2014). The accuracy of quantification was established using the following guidelines: proteins categorised as high accuracy had more than eight unique and razor peptides and a ratio for unique/unique + razor of ≥0.75; proteins categorised as medium accuracy had at least three unique and razor peptides, and a ratio for unique/unique + razor of ≥0.5; and any proteins below these thresholds were classified as low accuracy.

Differential expression analysis was performed on $\log_2$ transformed copy number per cell using LIMMA (version 3.7). Heatmaps were generated using the Morpheus tool from the Broad Institute (https://software.broadinstitute.org/morpheus). GSEA was performed using DAVID (https://david.ncifcrf.gov), and GSEA plots were generated using the Phantasus web tool (https://ctlab.itmo.ru/phantasus/#). Volcano plots were made using GraphPad Prism or SRPlot, and bubble plots were created using SRplot. Radar plots were generated using Microsoft Excel. For comparing microarray data and human copy number data to murine proteomics data, $\log_2$ microarray counts and $\log_2$ copy numbers from the human dataset were aligned with $\log_2$ protein copy numbers per cell in Microsoft Excel. The mass of individual proteins was estimated using the following formula: $CN \times MW/NA = \text{protein mass (g cell}^{-1})$, where CN is the protein copy number, MW is the protein molecular weight (in Da), and NA is Avogadro's Constant. The total protein content per cell was determined as the sum of the individual mass of all proteins detected. Iron proteome analysis was performed as described in (Teh et al., 2021). Briefly, a list of murine iron interacting proteins derived from (Teh et al., 2021) was cross-referenced with the pDC proteomic dataset using Microsoft Excel. Iron interaction information for each iron-binding protein was derived from (Andreini et al., 2018). The total number of iron atoms per cell was estimated as the sum of the copy number of iron interacting proteins times the estimated number of iron ions binding that protein. In cases where the exact number of iron atoms bound was unknown, the following assumption was applied: Proteins that bind iron via a heme

group or directly have 1 iron atom, and proteins that utilise an iron-sulphur prosthetic group have 2 iron atoms.

2.2.21 Statistical Analysis

Details of the statistical analyses performed can be found in the figure legends. Data are expressed as mean +/- standard error of the mean (SEM) or standard deviation (SD) unless stated otherwise. P-values were calculated using a two-tailed Student's t-test for two-group comparisons. A one-sample t-test was used to compare more than two groups against one sample. To compare multiple samples, one-way ANOVA with Dunnet's, Tukey or Sidak's post-test or two-way ANOVA with Dunnet's post-test was used as indicated.

Chapter 3 – Proteomic analysis of natural cDC metabolism and function

3.1 Introduction

Conventional dendritic cells (cDCs) orchestrate the crosstalk between innate and adaptive immunity. Two primary subsets of cDCs, cDC1s and cDC2s, have been identified to have preferential capabilities to promote different adaptive immune responses. cDC1s have a superior ability to prime CD8 T cell and Th1 polarised CD4 T cells responses while cDC2s are more efficient in priming Th2 and Th17 CD4 T cell immunity (Cabeza-Cabrerizo et al., 2021). The mechanisms underpinning this division of labour still need to be fully understood. The role of immunometabolism in directing cDC1 and cDC2 responses has been poorly characterised relative to other immune cells. To date, most metabolic studies have been performed on *in vitro* DCs generated from bone marrow cultures. The phenotype and metabolic profiles of these cells poorly reflect that of natural DC subsets (Helft et al., 2015; Wculek et al., 2019). In light of a growing number of studies indicating the potential of natural cDCs in tumour immunotherapy, there is a need to better understand the metabolic profiles of these cells (Heras-Murillo et al., 2024; Wculek et al., 2020).

Detailed proteomic analysis in T cells has proven to be a useful approach to interrogate immunometabolism (Howden et al., 2019; Hukelmann et al., 2016; Marchingo et al., 2020). Repositories, including Immpres (http://immpres.co.uk) and ProteomicDB (https://www.proteomicsdb.org), to disseminate these datasets have proven to be valuable collaborative resources for the immunometabolism research community (Brenes et al., 2023). Over a decade ago, the first proteomic characterisation of cDC subsets was performed by Luber and colleagues, who identified viral recognition pathways specific to cDC2s (Luber et al., 2010). Since then, technical advancements in proteomic techniques have allowed greater depth and accuracy in proteomic quantification. Chapter 3 will explore the proteomes of both cDC1s and cDC2s in immature and mature states. Due to the large

quantity of data generated and the relative lack of metabolic evidence supporting cDC subset function, this chapter will focus on immunometabolic features of the cDC proteomes.

3.2 The cDC Proteome

cDCs are a rare immune cell population comprising approximately 0.05% of lymphocytes in the spleen (Cabeza-Cabrerizo et al., 2021). To have sufficient cell numbers to perform quantitative proteomics, the DC compartment was expanded *in vivo* by inoculating mice with B16-Flt3l melanoma cells that secrete the DC growth factor Flt3l, as described previously (Mach et al., 2000). After 10-12 days of tumour growth, mice were sacrificed, and splenic DCs were quantified **(Fig. 3.1 A)**. cDC1s were identified as $CD11c^{+}MHCII^{+}XCR1^{+}SIRP\alpha^{-}$ cells and cDC2s were identified as $CD11c^{+}MHCII^{+}XCR1^{-}SIRP\alpha^{+}$ cells **(Fig. 3.1 B)**. B16-Flt3l expansion led to a significant increase in total splenic cDC numbers (increased from 5% to 35% of live Lin^{-} splenocytes) with a particular enrichment of the cDC1 subset (enriched from 20% to 65% of total DC) **(Fig. 3.1. A-C)**. I next confirmed by flow cytometry that the expansion model does not specifically induce DC maturation in either subset. Analysis of cDC phenotype markers **(Fig. 3.2 A)**, co-stimulatory markers **(Fig. 3.2 B)** and lineage transcription factors **(Fig. 3.2 C)** in cDC1s and cDC2s shows the expected expression of phenotype markers and transcription factors associated with each cell type, while costimulatory marker expression is comparable between cDC1s and cDC2s. To further confirm that the *in vivo* expansion model does not induce DC maturation, I compared the expression of cDC phenotype markers and co-stimulatory markers between C57Bl/6 mice and mice bearing B16-Flt3l cells in cDC1 **(Fig. 3.3 A)** and cDC2 **(Fig. 3.3 B)**.

After *in vivo* DC expansion, mice were injected intravenously with 50μg/kg CpG oligodeoxynucleotide B (CpG-B) or PBS (vehicle control) and spleens were harvested for proteomic analysis of cDC subsets after 18 hours. DC preparations from pooled spleens consistently yielded $>1x10^{6}$ DCs/condition as measured using the cell sorter with a purity >95%, resulting in >20 μg of

total protein per condition. The experiment was repeated twice, with different pools of spleens resulting in biological triplicates with a Pearson Correlation Coefficient above 0.94 for cDC1 **(Fig. 3.4 A)** and 0.95 for cDC2 **(Fig. 3.5 A)**. 6529 proteins were detected in all three biological replicates, with a small number of outliers detected in each replicate **(Fig. 3.5 B) (Fig. 3.6 B)**.

Several studies have investigated the transcriptome of cDC subsets. However, due to post-transcriptional and post-translational regulation of gene and protein expression, the gene transcript abundance does not always correlate with protein abundance (Ghazalpour et al., 2011). This discrepancy may confound the interpretation of cDC transcriptional studies. To investigate the relationship between the cDC transcriptome and proteome, I compared microarray gene transcript abundance acquired from the Immunological Genome Project (Immgen) (GSE15907) to the protein copy number per cell for the corresponding protein. This analysis identified 5960 gene-protein pairs for cDC1 **(Fig. 3.6 A)** and 5947 for cDC2 **(Fig. 3.6 B)**. Linear regression analysis of gene transcript abundance and protein abundance shows a weak correlation for cDC1s (R^2=0.44) **(Fig. 3.6 A)** and cDC2s (R^2=0.42) **(Fig. 3.6 B)**. I next investigated the relationship between transcript expression and protein abundance for proteins involved in different cellular processes. For example, the gene expression of many cDC1 phenotype markers correlates well with protein abundance **(Fig. 3.7 A)**. By contrast, gene expression overestimates the expression of glucose and amino acid transporters, including the glutamine transporters SNAT1 (Slc38a1) and SNAT2 (Slc38a2) **(Fig. 3.7 B)**. Similarly, comparing transcript and protein abundance of cellular organelles, including ribosomes (GO:0005840) **(Fig. 3.7 C)** and proteasomes (GO:0000502) **(Fig. 3.7 D),** shows that transcript accurately predicts ribosomal protein abundance but underestimates the abundance of proteasomal proteins.

Comparing global proteome features between cDC1s and cDC2s shows that cDC1s have a significantly higher total protein content than cDC2s **(Fig. 3.8 A)**. Total protein content is a good metric to determine cellular size. Forward scatter signal, a commonly accepted proxy for cell size, using flow cytometry

confirms this observation, showing that cDC1s are significantly larger than cDC2s **(Fig. 3.8 B,C)**. I next investigated the contribution of different proteins to the total protein mass of the cell. Cumulative protein analysis shows that a small number of highly expressed proteins account for the majority of the total protein content of cDCs. 44 proteins (0.64%) in cDC1 **(Fig. 3.9 A)** and 18 proteins (0.26%) in cDC2 **(Fig. 3.9 B)** account for 50% of total protein. These highly expressed proteins are shared between cDC subsets and are primarily composed of histone and cytoskeleton proteins **(Table 3.1)**. To better understand the functional consequences of protein expression between cDC1s and cDC2s, I examined the distribution of proteins into different cellular compartments in cDC1s **(Fig. 3.10 A)** and cDC2 **(Fig. 3.10 B)**. The protein expression of each compartment was measured as a percentage of total protein content per cell. Using this approach, both cDC1s and cDC2s were found to have similar protein distributions of plasma membrane (GO:0005886), mitochondrial (GO:0005739) and nuclear envelope (GO:0005635) proteins as a percentage of their total protein content. By contrast, cDC1s have significantly higher expression of endoplasmic reticulum (GO:0005783) proteins than cDC2 **(Fig. 3.11 A)**. GSEA confirms that ER proteins are enriched in the cDC1 proteome **(Fig. 3.11 B).** The expanded ER proteome in cDC1s is consistent with studies showing that cDC1s have constitutive ER stress signalling, even without stress stimuli**,** which promotes ER expansion and supports cDC1 cross-presentation ability (Osorio et al., 2014; Tavernier et al., 2017). In line with this, the abundance of the ER stress sensors IRE1a, ATF6 and PERK are enriched in cDC1s **(Fig. 3.11 C)**.

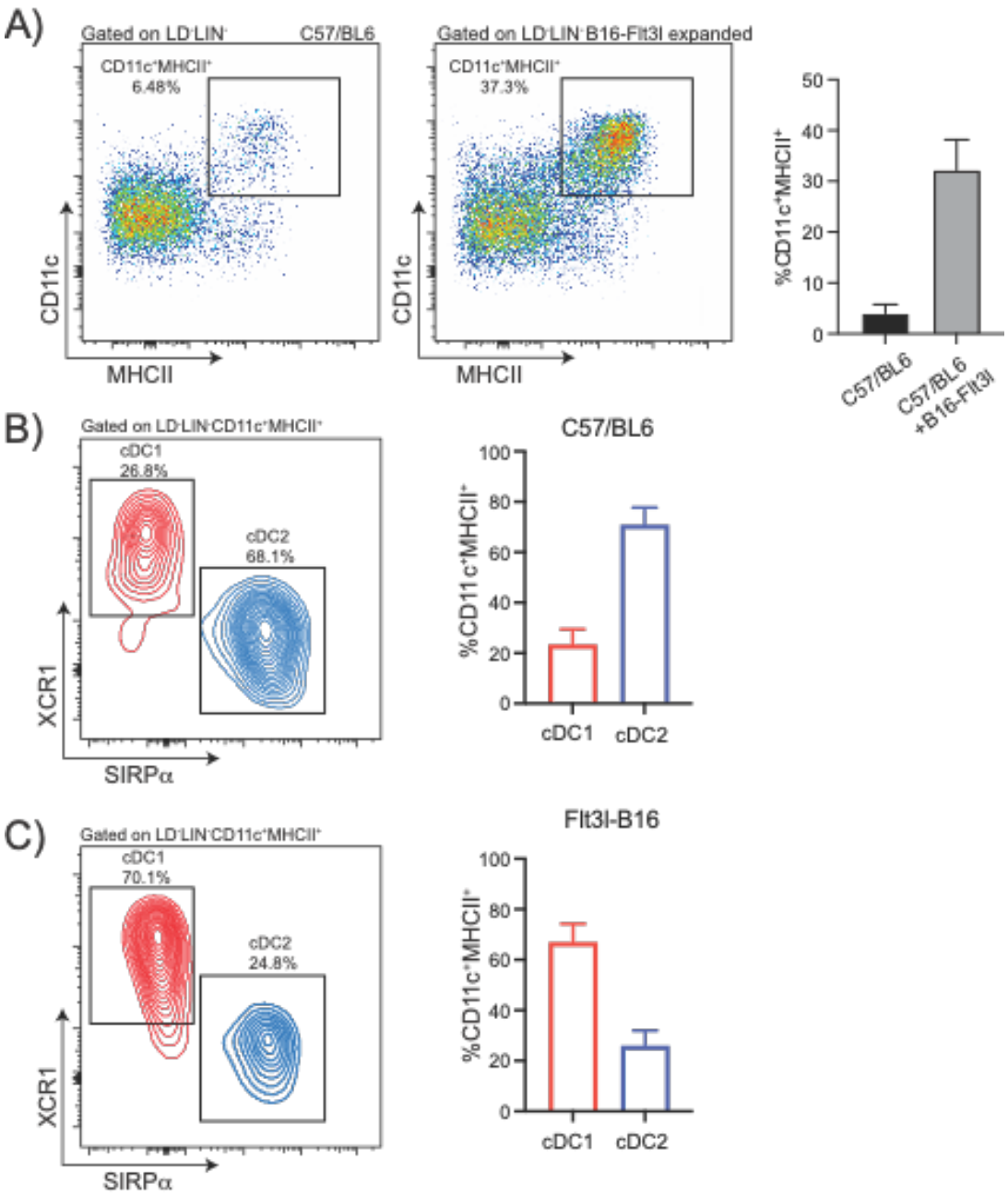

Figure 3.1 – Mice bearing B16-Flt3l tumour show expansion of CD11c$^+$MHCII$^+$ splenic dendritic cells.

(A-C) C57/BL6 mice were inoculated subcutaneously with 2.5x10^6 Flt3l-secreting B16 melanoma cells (B16-Flt3l). After ten days, spleens were harvested, and DC enrichment was determined by flow cytometry. **(A)** Representative dot plot (left) showing the frequency of cDCs in C57Bl/6 mice versus those bearing B16-Flt3l cells after excluding lineage markers ((CD3$^-$, CD19$^-$, F4/80$^-$, NK1.1$^-$,LY6G$^-$) (middle). Histogram showing pooled data for the total frequency of CD11c$^+$MHCII$^+$ cells in splenocytes (right). **(B,C)** Representative contour plots of cDC1s (red) and cDC2s (blue) indicating the % of CD11c$^+$MHCII$^+$ cells in **(B)** C57Bl/6 mice and **(C)** C57Bl/6 mice inoculated with B16-Flt3l cells. cDC1 were identified as XCR1$^+$SIRPa$^-$ cells and cDC2 were identified as XCR1$^-$SIRPa$^+$ cells. Data are representative (left) or mean +/- SEM (right) from 4 independent experiments.

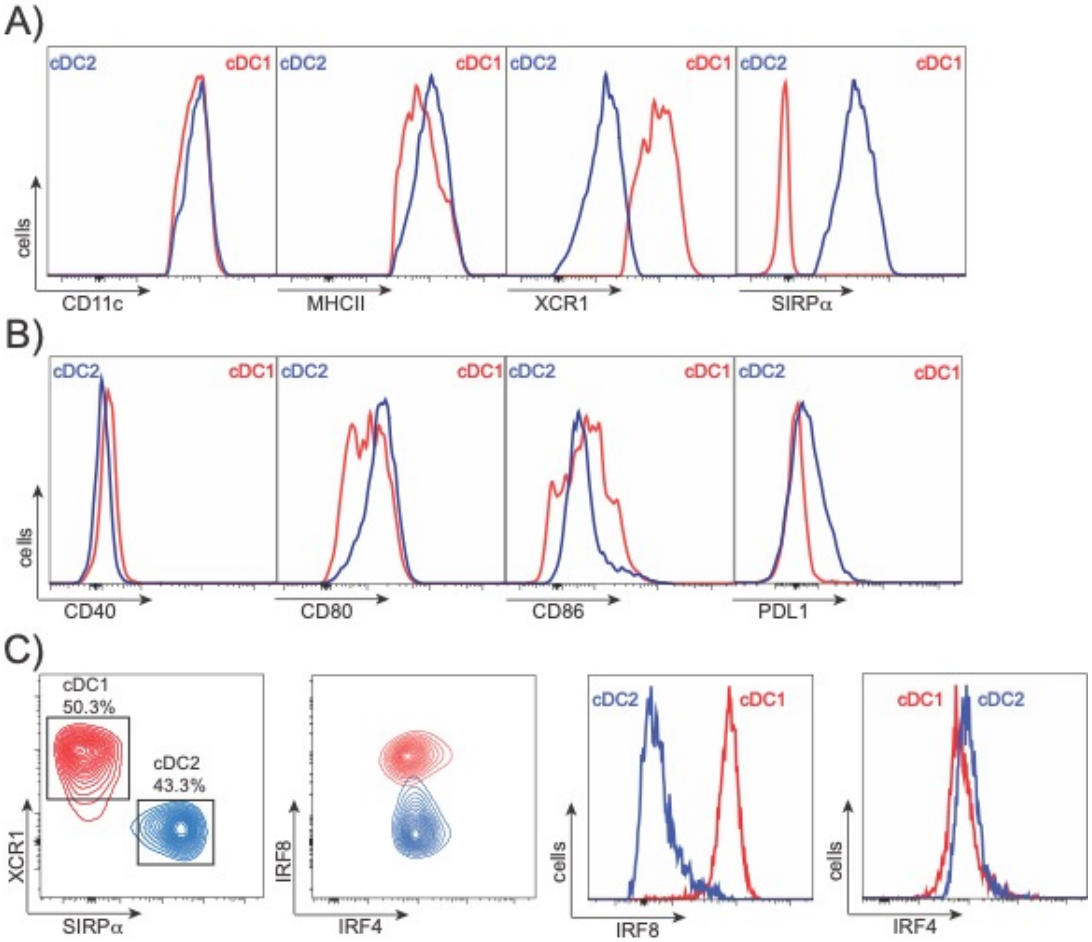

Figure 3.2 – Characterisation of cDCs in C57Bl/6 mice inoculated with B16-Flt3l cells

(A-E) Flow cytometry analysis of splenocytes from C57Bl/6 mice inoculated with B16-Flt3l cells analysing Lin^-, $CD11c^+$, $MHCII^+$ cDCs comparing cDC1s ($XCR1^+SIRP\alpha^-$) and cDC2s ($XCR1^-SIRP\alpha^+$). **(A,B)** Representative histograms showing the expression of surface phenotype markers **(A)** and surface activation markers (**B)** on cDC1s and cDC2s. **(C)** Representative dot plots (left) and histograms (right) showing the intracellular expression of **(D)** IRF8 and **(E)** IRF4 transcription factors in cDC1s and cDC2s. Data are representative of 4 **(A,B)** and 3 **(C-E)** independent experiments.

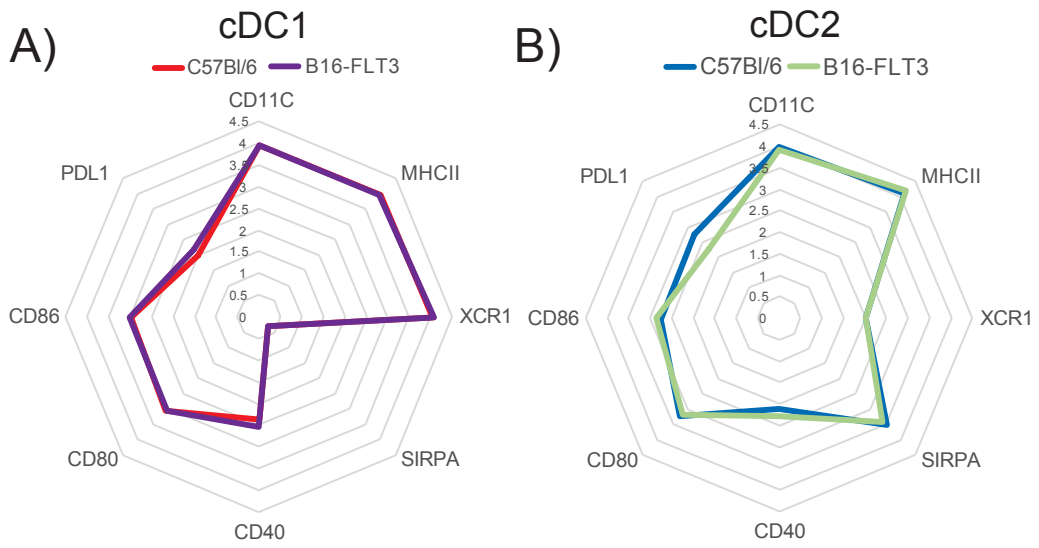

Figure 3.3 – Inoculation with B16-Flt3l cells does not induce cDC maturation

(A,B) Flow cytometry analysis of splenocytes from C57Bl/6 mice inoculated with B16-Flt3l cells analysing Lin^-, $CD11c^+$, $MHCII^+$ cDCs comparing cDC1s ($XCR1^+SIRP\alpha^-$) and cDC2s ($XCR1^-SIRP\alpha^+$). Radar plots compare the expression of phenotype and costimulatory markers in mice with and without inoculation with B16-Flt3l cells in **(A)** cDC1s and **(B)** cDC2s. Data are presented as log_2-transformed mean fluorescent intensity (MFI) values of each protein. Data are representative of three independent experiments.

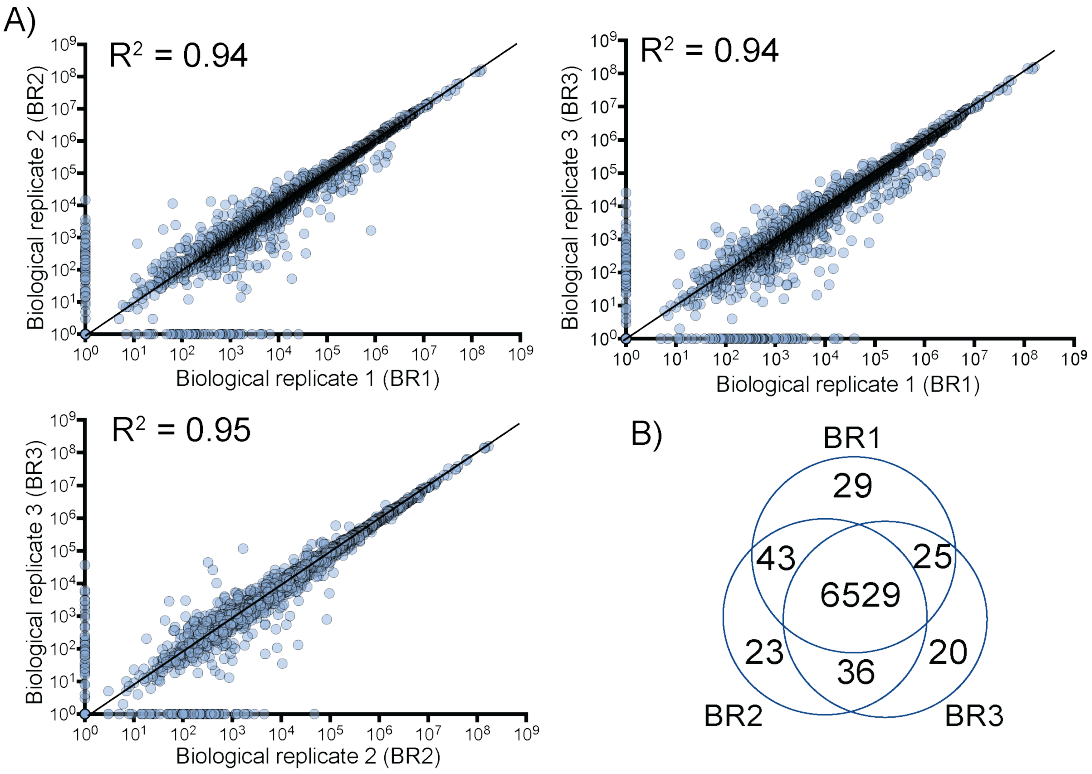

Figure 3.4 – cDC1 biological replicates show a high degree of similarity **(A,B)** Quantitative proteomics was performed on C57Bl/6 mice inoculated with B16-Flt3l secreting cells, analysing the degree of similarity in Lin^- $CD11c^+MHCII^+XCR1^+SIRP\alpha^-$ cDC1 biological replicates. **(A)** Linear regression analysis of cDC1 comparing the protein copy number in each biological replicate (BR). **(B)** Venn diagram illustrating the overlap of proteins detected in each biological replicate. Data were analysed using linear regression and R^2 =Pearson's correlation coefficient.

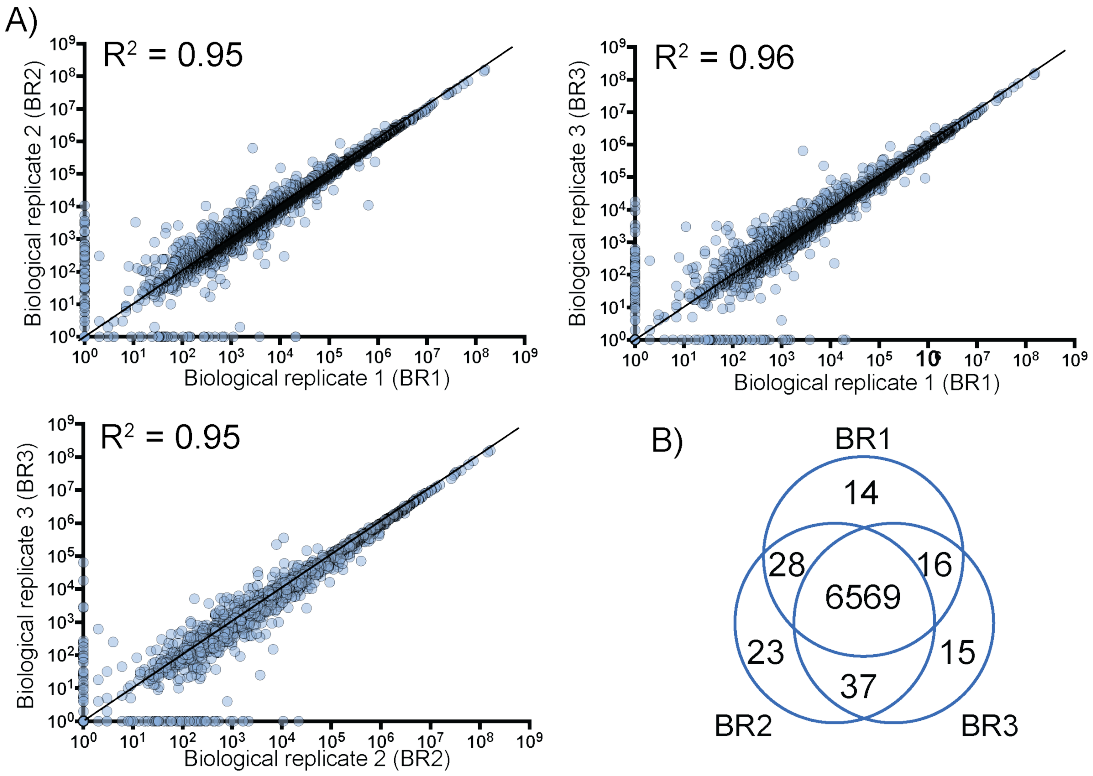

Figure 3.5 – cDC2 biological replicates show a high degree of similarity **(A,B)** Quantitative proteomics was performed on C57Bl/6 mice inoculated with B16-Flt3 secreting cells, analysing the degree of similarity in $Lin^-CD11c^+MHCII^+XCR1^-SIRP\alpha^+$ cDC2 biological replicates. **(A)** Linear regression analysis of cDC1 comparing the protein copy number in each biological replicate (BR). **(B)** Venn diagram illustrating the overlap of proteins detected in each biological replicate. Data were analysed using linear regression and R^2 =Pearson's correlation coefficient.

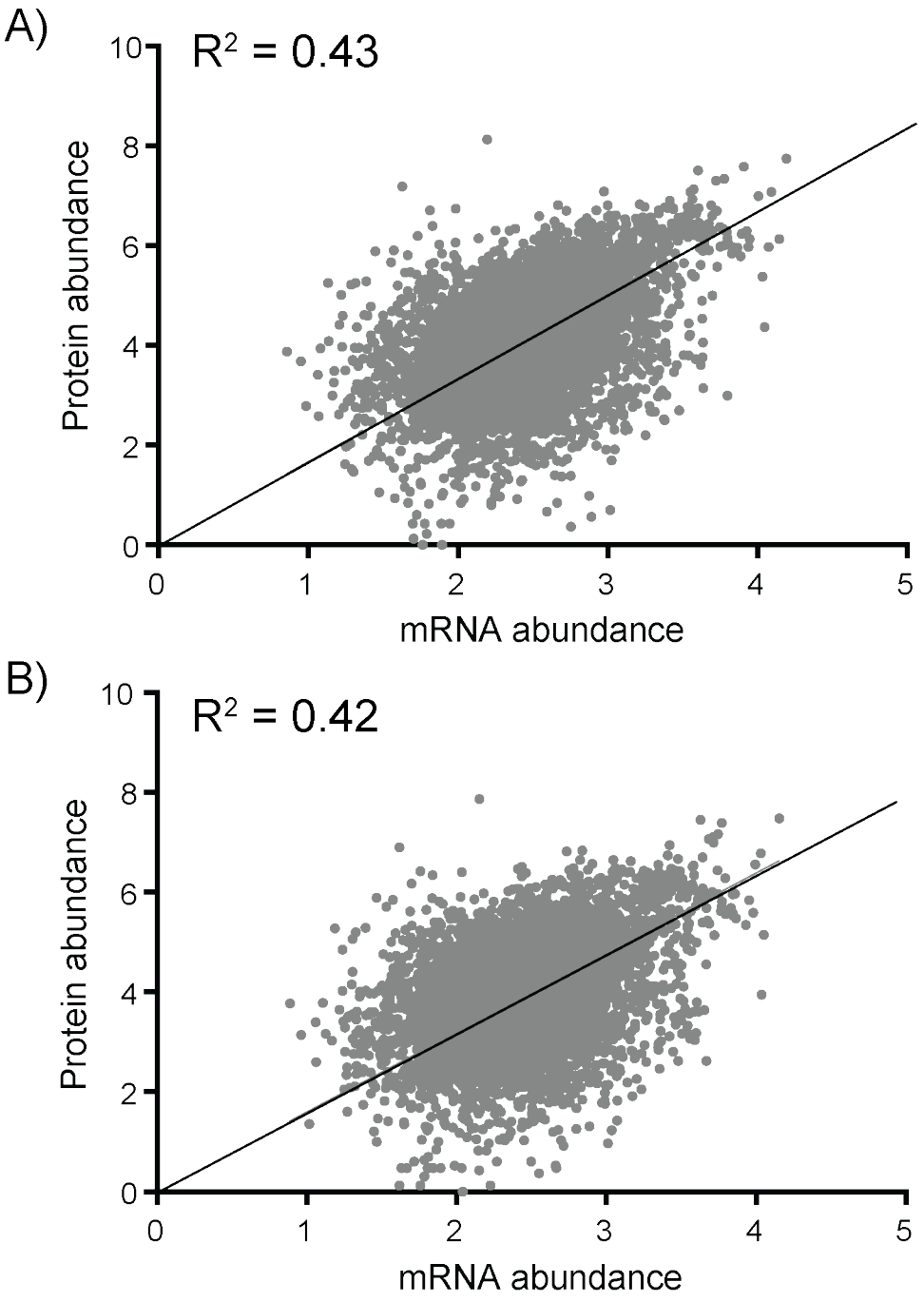

Figure 3.6 – Weak correlation between cDC transcriptome and proteome
(A,B) Transcript intensity (mean value, Affymetrix microarray) acquired from the Immunological Genome Project dataset (GSE15907) plotted against the corresponding copy number per cell for **(A)** cDC1 and **(B)** cDC2. Data was analysed using linear regression, and R^2 = Coefficient of determination. Quantitative proteomics was performed on three biological replicates, and microarray data was reanalysed from three biological replicates.

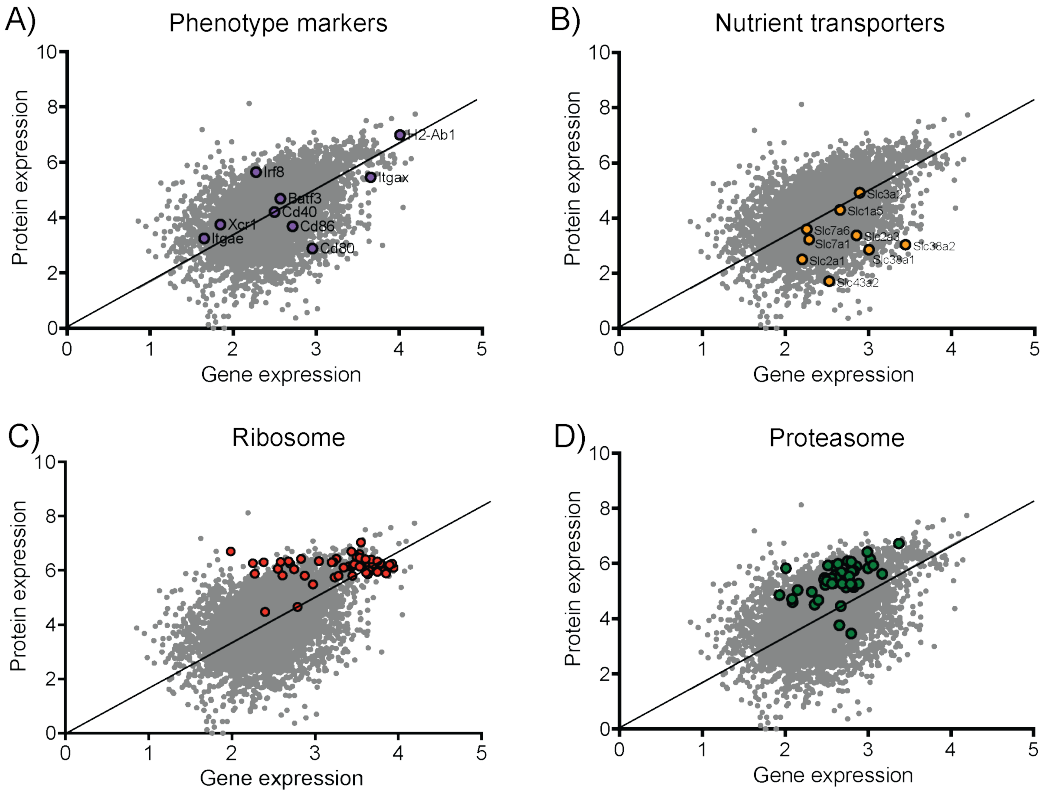

Figure 3.7 – Linear regression analysis of functional groups in the cDC1 transcriptome and proteome

(A-D) Transcript intensity (as in **Fig. 3.6**) and copy number for cDC phenotype markers, **(A)** plasma membrane nutrient transporters, **(B)** ribosomal proteins and **(C)** proteasomal proteins **(D)**. Quantitative proteomics was performed on three biological replicates. Microarray data was reanalysed from three biological replicates.

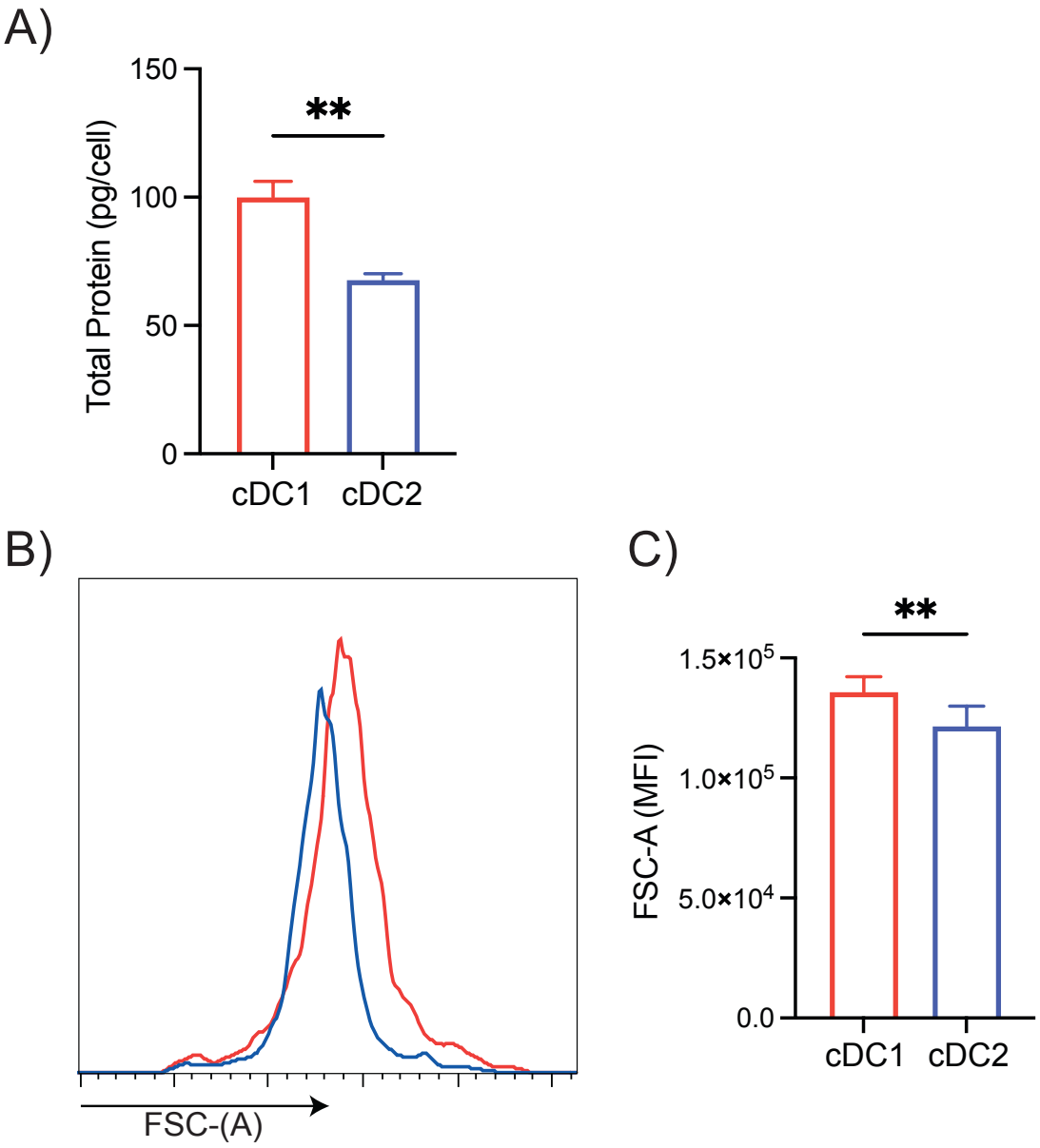

Figure 3.8 – cDC1s have a higher total protein content than cDC2s
(A-C) Quantitative proteomics was performed on C57Bl/6 mice inoculated with B16-Flt3 secreting cells, analysing the total protein content and cell size in cDC1s and cDC2s. **(A)** Total protein content (pg/cell) in cDC1s and cDC2s. **(B,C)** Flow cytometry analysis of splenocytes from C57Bl/6 mice inoculated with B16-Flt3l secreting cell analysing cell size by forward scatter (FSC-(A)) in cDC1s and cDC2s. **(B)** Representative histogram and **(C)** pooled MFI of FSC-(A) in cDC1s and cDC2s. Total protein content per cell was calculated as $\Sigma((CN \times MW)/N))$ where CN = Protein copy number, MW = Protein molecular weight, N = Avogadro's constant. Data are representative **(B)** or mean +/- SEM of 3 independent experiments **(A,C)**. Statistical analysis was performed using student's t-test. (**p<0.01)

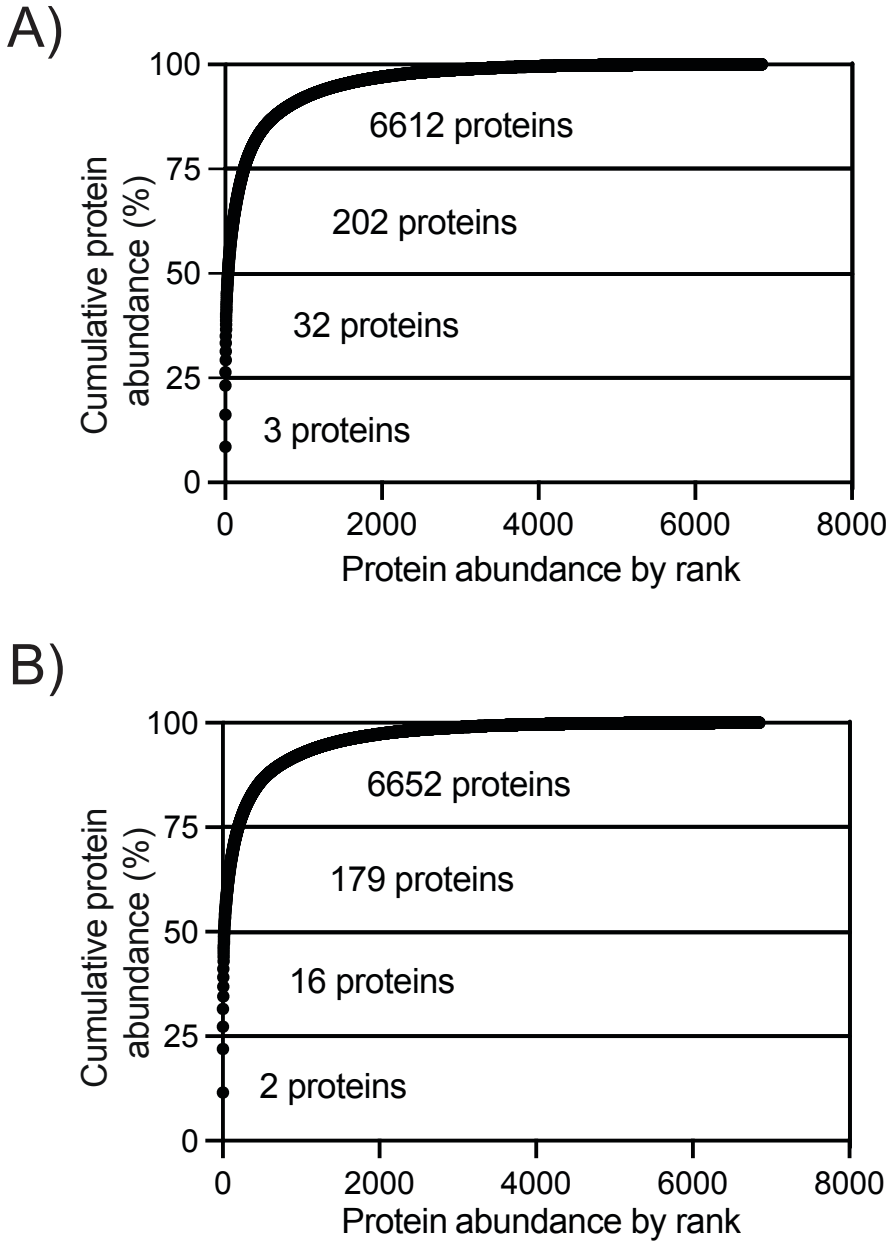

Figure 3.9 – A small number of highly expressed proteins account for the majority of the total protein content in cDC1s and cDC2s
(A,B) Quantitative proteomics was performed on cDC1s and cDC2s from C57Bl/6 mice inoculated with B16-Flt3l secreting cells, analysing cumulative protein abundance. Proteins were ranked in order of abundance (copy number) and plotted against cumulative protein abundance (% of total protein copies per cell) in **(A)** cDC1s and **(B)** cDC2s. The numbers represent the number of proteins in each quartile. Quantitative proteomics was performed on three biological replicates.

A)

Top 20 most highly expressed proteins in cDC1

Rank	Gene Symbol	Protein	Copies	%	Cum %
1	H4c1	Histone 4C1	1.62E+08	8.59%	8.59%
2	H2bc7	Histone BC7	1.44E+08	7.58%	16.17%
3	Actc1	Actin alpha, cardiac muscle 1	1.33E+08	7.03%	23.20%
4	Hist1h2af	Histone H2A	6.03E+07	3.19%	26.39%
5	Actb	Actin beta	5.51E+07	2.91%	29.31%
6	H1-3	H1.3 linker histone	3.84E+07	2.03%	31.34%
7	Tmsb4x	Thymosin beta	3.81E+07	2.01%	33.35%
8	Pfn1	Profilin 1	3.20E+07	1.69%	35.04%
9	H3c2	H3 clustered histone 2	2.98E+07	1.58%	36.62%
10	Ppia	Peptidylprolyl Isomerase a	2.16E+07	1.14%	37.76%
11	Cfl1	Cofilin 1	1.99E+07	1.05%	38.81%
12	Actbl2	Actin beta like 2	1.52E+07	0.80%	39.62%
13	Lcp1	Lympocyte cytosolic protein 1	1.33E+07	0.71%	40.32%
14	Ptma	Prothymosin alpha	1.28E+07	0.68%	41.00%
15	H1-5	H1.5 linker histone	1.24E+07	0.66%	41.66%
16	Tuba1a	Tubulin alpha 1A	1.21E+07	0.64%	42.30%
17	Eef1a1	Eukaryotic translation elongation factor 1 alpha 1	1.19E+07	0.63%	42.92%
18	Rps27a	Ribosomal protein S27a	1.18E+07	0.62%	43.55%
19	H2-Ab1	Histocompatibility 2, class 2 antigen A, beta 1	9.81E+06	0.52%	44.07%
20	Gapdh	Glyceraldehyde-3-phosphate dehydrogenase	9.12E+06	0.48%	44.55%

B)

Top 20 most highly expressed proteins in cDC2

Rank	Gene Symbol	Protein	Copies	%	Cum %
1	H4c1	Histone 4C1	1.59E+08	11.55%	11.55%
2	H2bc7	Histone BC7	1.43E+08	10.43%	21.98%
3	Actc1	Actin alpha, cardiac muscle 1	7.34E+07	5.35%	27.33%
4	Hist1h2af	Histone H2A	5.77E+07	4.21%	31.53%
5	H1-3	H1.3 linker histone	4.07E+07	2.97%	34.50%
6	H3c2	H3 clustered histone 2	3.32E+07	2.42%	36.91%
7	Actb	Actin beta	3.01E+07	2.19%	39.11%
8	Pfn1	Profilin 1	2.82E+07	2.05%	41.16%
9	Tmsb4x	Thymosin beta	2.44E+07	1.78%	42.94%
10	Ppia	Peptidylprolyl Isomerase a	1.46E+07	1.06%	44.00%
11	Cfl1	Cofilin 1	1.28E+07	0.93%	44.93%
12	Lcp1	Lympocyte cytosolic protein 1	1.17E+07	0.85%	45.78%
13	H1-5	H1.5 linker histone	1.04E+07	0.76%	46.54%
14	Mdh2	Malate dehydrogenase 2	9.87E+06	0.72%	47.26%
15	Rps27a	Ribosomal protein S27a	8.73E+06	0.64%	47.89%
16	H1-2	Histone 1.2 linker histone	8.46E+06	0.62%	48.51%
17	Actbl2	Actin beta like 2	7.93E+06	0.58%	49.09%
18	Tuba1a	Tubulin alpha 1A	6.86E+06	0.50%	49.59%
19	S100a4	S100 calcium binding protein A4	6.60E+06	0.48%	50.07%
20	Gapdh	Glyceraldehyde-3-phosphate dehydrogenase	6.25E+06	0.46%	50.52%

Table 3.1 – The top 20 most highly abundant proteins in cDC1s and cDC2s

Table ranking the top 20 most abundant proteins by copy number in **(A)** cDC1s and **(B)** cDC2s. % = Protein copy number as a percentage of the total copy number per cell. Cum % = Cumulative sum of protein copy number as a percentage of the total copy number per cell.

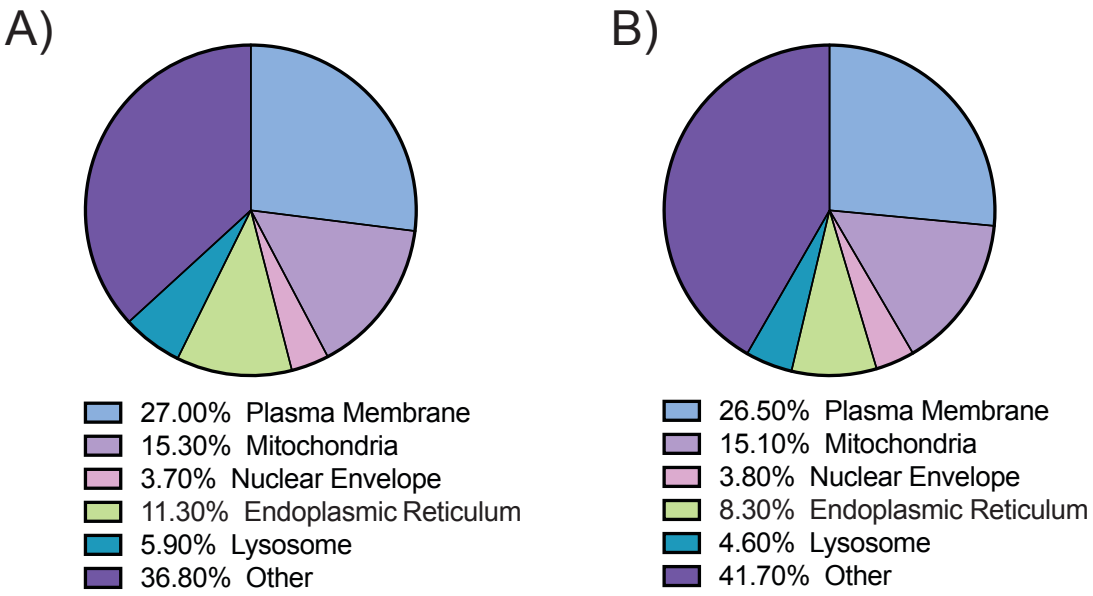

Figure 3.10 – Distribution of proteins into cellular compartments in cDC1s and cDC2s

(A,B) Quantitative proteomics was performed on cDC1s and cDC2s from C57Bl/6 mice inoculated with B16-Flt3l secreting cells, analysing the distribution of proteins into subcellular compartments. The protein content of plasma membrane (GO:0005886), mitochondria (GO:0005739), nuclear envelope (GO:0005635), endoplasmic reticulum (GO:0005783) and lysosome (GO:0005764) as a percentage of total protein mass in **(A)** cDC1s and **(B)** cDC2s. Quantitative proteomics was performed on three biological replicates.

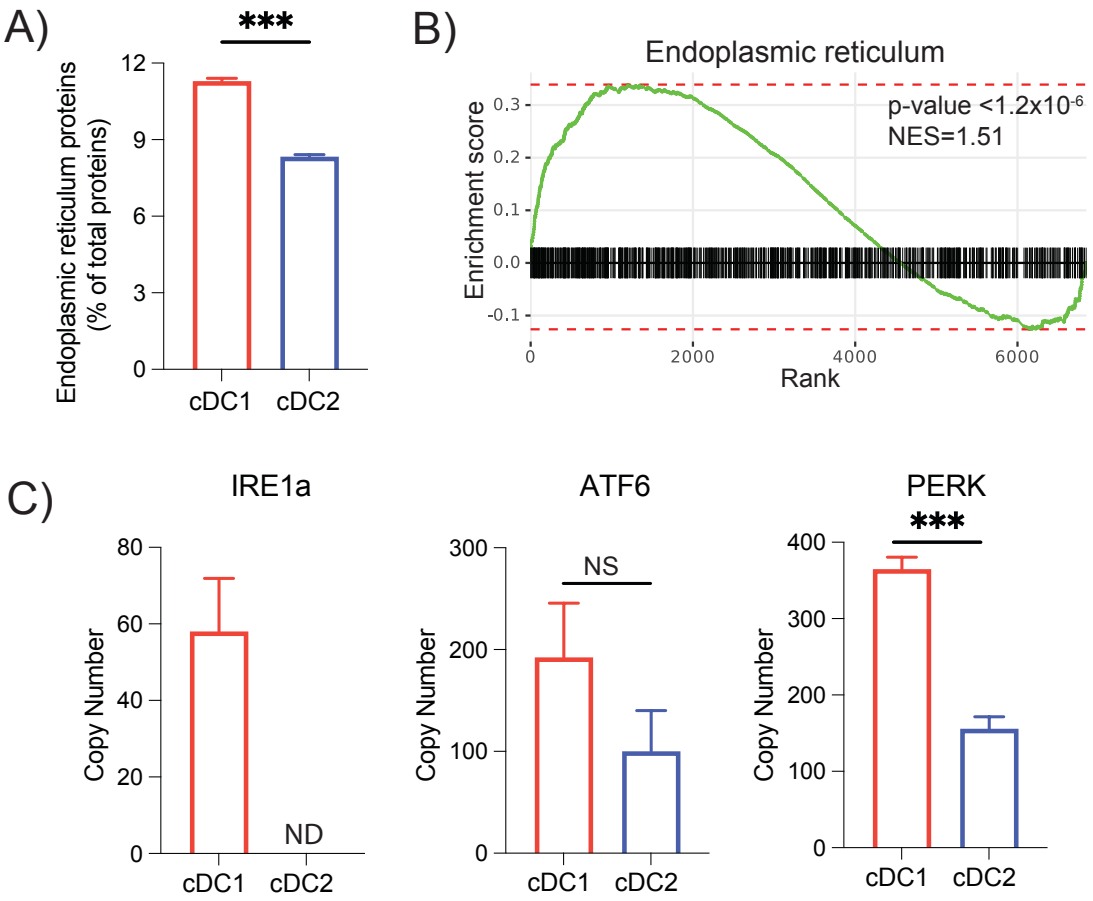

Figure 3.11 – Enrichment of endoplasmic reticulum proteins in cDC1s
(A-C) Quantitative proteomics was performed on cDC1s and cDC2s from C57Bl/6 mice inoculated with B16-Flt3l secreting cells**,** analysing the abundance of endoplasmic reticulum (ER) associated proteins and ER stress sensors. **(A)** Total ER-associated protein (GO:0005783) abundance as a percentage of total cellular protein abundance in cDC1s and cDC2s. **(B)** Gene set enrichment analysis (GSEA) plot of ER proteins in the cDC proteome. Proteins are ranked by Log_2FC from differential expression analysis. NES = Normalised enrichment score. **(C)** Copy number per cell of ER stress response signalling proteins in cDC1s and cDC2s. Data is presented as mean +/- SEM of three independent experiments. Data was analysed using a paired student's t-test. (NS = $p>0.05$,***$p<0.001$) ND = Not detected

3.3 Differential expression analysis identifies an anabolic phenotype in cDC1s

To directly interrogate the proteome differences between cDC1s and cDC2s, I performed a differential expression analysis of the protein copy numbers between both cDC subsets **(Fig. 3.12 A)**. This analysis identified 1442 significantly upregulated proteins in cDC1s and 185 significantly upregulated proteins in cDC2s. Differentially expressed proteins are designated as significant if they have a $\log_2$ fold change >+1/<-1 and an adjusted p-value <0.05. The large number of significantly upregulated proteins in cDC1s versus cDC2s is attributed to the larger total protein content in cDC1s. The normalisation of protein copy number per cell by cellular total protein content can be used to correct this bias **(Fig. 3.12 B)**. However, as the un-normalised data represents actual protein abundance, it is a more useful approach for determining functional outcomes. To investigate the functional consequences of the differentially expressed proteins, I performed a gene set enrichment analysis (GSEA) on the significantly upregulated proteins in cDC1s **(Fig. 3.13 A,B)**. GSEA, using the KEGG **(Fig. 3.13 A)** and Reactome **(Fig. 3.13 B)** databases, identified enrichment for translation and protein synthesis pathways. This result supports the observations in **(Fig. 3.11),** as an expanded ER compartment is required to support increased protein folding demands associated with higher protein synthesis rates. The most significantly upregulated KEGG pathway in cDC1s is the ribosome. Ribosomes are the cellular site of protein synthesis. Indeed, cDC1s have a significantly higher abundance of all proteins that compose both the large (60S) and small (40S) ribosomal subunits compared to cDC2 **(Fig. 3.14 A-C)**. In addition, cDC1s also have significantly higher protein abundance of all 5' translation initiation complex subunits than cDC2s **(Fig. 3.15 A-C)**. As protein synthesis is regulated by several factors, including cellular energy status, anabolic signalling, and amino acid availability, I confirmed the proteomic observations by measuring protein synthesis rates in cDC1s and cDC2s. I determined the protein synthesis rate by measuring the incorporation of puromycin into nascent peptide chains using flow cytometry **(Fig. 3.16 A,B)**. In accordance with the proteomic data, cDC1s have a significantly higher rate of protein synthesis than cDC2s.

Protein synthesis is the most energetically demanding cellular process (Buttgereit & Brand, 1995a). As such, the significant difference in protein synthesis rates observed between cDC subsets suggested that there may be different metabolic programmes in cDC1s and cDC2s. I next investigated the metabolic proteome in cDC1s and cDC2s. Two recent studies have shown that cDC1s have more active mitochondrial metabolism than cDC2s (X. Du et al., 2018; Pelgrom et al., 2022). In agreement with these studies, cDC1s have significantly higher mitochondrial protein content than cDC2s, indicating larger mitochondrial mass **(Fig. 3.17 A)**. Using Mitotracker Green staining, which measures mitochondrial mass by flow cytometry, I confirmed that cDC1s have significantly higher mitochondrial mass than cDC2s **(Fig. 3.17 B,C)**. Mitochondrial mass alone does not indicate whether a cell uses oxidative metabolism for energy generation. A proxy for mitochondrial activity is the mitochondrial membrane potential, often indicative of mitochondrial metabolic flux. To measure mitochondrial membrane potential, I stained the cDCs with the TMRM flow cytometry stain **(Fig. 3.17 D-F)**. TMRM staining shows that cDC1s have significantly higher mitochondrial membrane potential than cDC2s, indicating enhanced mitochondrial metabolism.

Considering the higher rate of mitochondrial metabolism in cDC1s, I next investigated the abundance of proteins associated with pathways that fuel the TCA cycle. Three primary catabolic pathways converge on the TCA cycle to provide NADH and FADH synthesis substrates, including glycolysis, glutaminolysis and fatty acid beta-oxidation. As glucose is the preferred fuel source for most immune cells, I first investigated the abundance of glycolytic proteins in cDC1s and cDC2s (Wolowczuk et al., 2008) **(Fig. 3.18 A-D)**. Glucose uptake across the plasma membrane is the first rate-limiting step of glycolytic metabolism. Two plasma membrane glucose transporters (GLUTs) are expressed in cDC1s and cDC2s, GLUT1 (Slc2a1) **(Fig. 3.18 A)** and GLUT3 (Slc2a3) **(Fig. 3.18 B)**. GLUT1 has been described as a critical regulator of immunometabolic reprogramming in many immune cells (Chapman & Chi, 2022). GLUT1 expression in resting cells is low but is highly inducible during immunogenic stimulation. In line with this, immature cDC1s

and cDC2s have low GLUT1 abundance, with less than 500 copies per cell **(Fig. 3.18 A)**. Interestingly, GLUT3 is significantly more highly expressed in cDC2s, suggesting the potential for higher glucose uptake rates in this subset **(Fig. 3.18 B)**. Despite this, cDC1s have a higher total protein abundance of the enzymes that catalyse the ten steps of glycolytic metabolism **(Fig. 3.18 C)** and an overall enrichment of glycolytic proteins in their proteome **(Fig.3.18 D).**

Pyruvate, the primary metabolite product of glycolysis, can be metabolised into two products depending on the cellular context. Anaplerosis of pyruvate into the TCA cycle requires transport into the mitochondria by the heterodimeric mitochondrial pyruvate carrier (MPC1/MPC2), followed by the conversion of pyruvate to acetyl-CoA by the pyruvate dehydrogenase complex (PDH). cDC1s have significantly higher protein abundance of both MPC1 **(Fig. 3.19 A)** and MPC2 **(Fig. 3.19 B)** proteins relative to cDC2. In line with the elevated abundance of glycolytic machinery in cDC1s, this suggests that cDC1s have a higher capacity to transport pyruvate into the mitochondria for energy generation. Interestingly, despite lower MPC abundance, cDC2s have a significantly higher abundance of the catalytic subunit of the pyruvate dehydrogenase complex A1 (PDHA1) **(Fig. 3.19 C)** while pyruvate dehydrogenase complex B1 (PDHB1) is similarly expressed in both subsets **(Fig. 3.19 D)**.

During high biosynthetic demand, many immune cells metabolise pyruvate to lactate to regenerate NAD^+ to perform substrate-level phosphorylation to generate ATP, a process termed aerobic glycolysis (Pearce & Pearce, 2013). Lactate production is catalysed by the reversible action of the enzyme lactate dehydrogenase (LDH). LDH comprises two isoenzymes: LDHA, which catalyses the conversion of pyruvate to lactate coupled to the hydrolysis of NADH to NAD+, and LDHB, which catalyses the reverse reaction. The expression of LDH isoenzymes in cDCs shows that LDHA is significantly more abundant than LDHB, suggesting that both cDC subsets favour pyruvate conversion to lactate **(Fig. 3.20 A)**. cDC1s have significantly higher expression of LDHA than cDC2s, suggesting an increased capacity to

perform aerobic glycolysis **(Fig. 3.20 A)**. Conversely, cDC2s have significantly higher expression of LDHB **(Fig. 3.20 A)**. However, considering that LDHA is substantially more abundant than LDHB in both cDC1s and cDC2s, this does not suggest that lactate conversion to pyruvate is a primary fuel source.

Lactate is actively transported out of cells by the proton-coupled monocarboxylate (MCT) transporters MCT1 (Slc16a1) and MCT4 (Slc16a3). MCT1 has high and MCT4 low lactate affinity (Km ~ 3.5-10mmol/L and ~22-28mmol/L, respectively) (Halestrap, 2013). MCT1 is, therefore, particularly well-suited for inward lactate transport and MCT4 for the export of lactate from glycolytic cells. Interestingly, MCT1 is significantly more abundant in cDC1s **(Fig. 3.20 B)**, while MCT4 is significantly more abundant in cDC2s **(Fig. 3.20 C)**.

Amino acids, notably glutamine, can also be metabolised for ATP production (Cruzat et al., 2018). Glutamine is the most abundant amino acid in serum and has been described as a key fuel in many immune cells (Yoo et al., 2020). To investigate whether glutamine metabolism is involved in fuelling TCA metabolism in cDCs, I first examined the expression of plasma membrane glutamine transporters in cDC1s and cDC2s **(Fig. 3.21 A)**. Several transporter families mediate glutamine influx, including ASCT and SNATs. cDC1s have significantly higher expression of all glutamine transporters detected than cDC2s, indicating increased glutamine uptake in cDC1s **(Fig. 3.21 A)**. This supports the observation that cDC1s have a higher rate of protein synthesis than cDC2s, as glutamine is a substrate for protein synthesis and is important for ER protein folding by promoting O-linked N-acetylglucosamine (O-GlcNAc) acylation (Cruzat et al., 2018). To enter the TCA cycle, glutamine is first converted to glutamate, catalysed by the enzyme glutaminase (GLS). Glutamate is then converted to α-ketoglutarate by oxidative deamination catalysed by glutamate dehydrogenase 1 (GLUD1). To investigate whether glutamine may be used as a fuel for the TCA cycle and oxidative metabolism, I compared the expression of GLS **(Fig. 3.21 B)** and GLUD1 **(Fig. 3.21 C)** in

cDC1s and cDC2s. cDC1s have significantly higher GLS expression, indicating the capacity for increased glutamate synthesis in cDC1s **(Fig. 3.21 B)**. Interestingly, despite increased glutamine transporter and GLS expression, cDC1s have significantly lower GLUD1 expression than cDC2s **(Fig. 3.21 C)**. This may suggest that cDC2s may have a greater propensity to utilise glutamine for ATP generation than cDC1s. However, considering that GLUD1 is highly abundant (~$1x10^6$ copies) in both cDC1s and cDC2s, it is likely that access to glutamine through plasma membrane transporters may be the limiting step in glutamine metabolism in cDC subsets.

To validate the proteomic findings, I performed SCENITH analysis on cDC1s **(Fig. 3.22 A,C)** and cDC2s **(Fig. 3.22 B,D).** SCENITH determines the relative contribution of different metabolic pathways for maintaining protein synthesis (Argüello et al., 2020). To perform SCENITH, I treated splenocytes with 100mM 2DG (DG), 2μM oligomycin (O) or 4μM CB839 for 20 minutes to inhibit glycolytic metabolism, OXPHOS and glutaminolysis, respectively and measured the protein synthesis rate by puromycin incorporation using flow cytometry **(Fig. 3.22 A,B)**. I also treated splenocytes with a combination of 2DG and oligomycin (DGO) to determine the background signal of the puromycin staining when both glycolysis and OXPHOS are inactivated. Glycolytic dependency **(Fig. 3.22 E)** is calculated as the percentage change in protein synthesis rate in response to 2DG treatment relative to DGO treatment. This analysis suggests similar dependence on glycolysis for ATP generation in both cDC1s and cDC2s. **(Fig. 3.22 E)**. On the other hand, as described in **(Fig. 3.17)**, cDC1s have significantly higher mitochondrial mass and mitochondrial membrane potential than cDC2s, indicating more active OXPHOS. In support of this, cDC1s have a significantly higher mitochondrial dependency than cDC2s **(Fig. 3.22 F).** Mitochondrial dependence is calculated as the percentage change in protein synthesis rate in response to O treatment relative to DGO treatment. In **(Fig. 3.21),** I analysed the cDC glutaminolysis machinery, which showed that despite cDC1s having significantly higher glutamine transporter expression, they have lower expression of the rate-limiting step of glutaminolysis GLUD1 than cDC2s.

SCENITH analysis, using the GLUD1 inhibitor CB839, shows that despite having lower GLUD1 expression, cDC1s have a higher glutaminolysis dependency for ATP production **(Fig. 3.22 G)**. This discrepancy is likely explained by cDC1s having a significantly higher reliance on mitochondrial metabolism than cDC2s. As glutaminolysis generates ATP by fuelling the TCA cycle and OXPHOS, disruption of glutaminolysis in cDC1s would impact overall cellular ATP production compared to cDC2s with low mitochondrial ATP production.

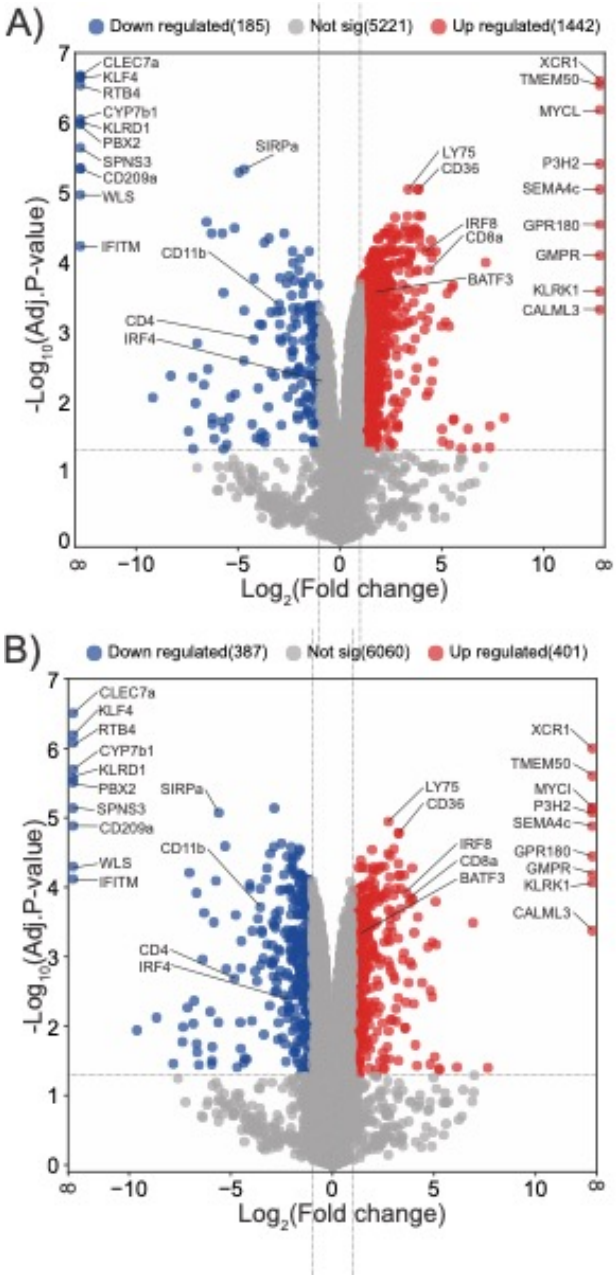

Figure 3.12 – Differential expression analysis of protein abundance in cDC1s and cDC2s

(A,B) Quantitative proteomics was performed on cDC1s and cDC2s from C57Bl/6 mice inoculated with B16-Flt3l secreting cells, analysing the differential expression of protein abundance in cDC1s and cDC2s. **(A)** Volcano plot of 6850 identified proteins displaying differences in relative abundance between cDC1s and cDC2s. The plot represents the $-\log_{10}$ of the adjusted p-value (Bonferroni) versus $\log_2$ of the fold change of protein abundance. Significantly differentially expressed proteins (red and blue) have a $\log_2$ fold change >1<-1 and a $-\log_{10}$(adj.p-value) > 1.35 (Q<0.05). Proteins highlighted in red are enriched in cDC1s, and those in blue are enriched in cDC2s. (**B)** Volcano plot of protein concentrations in cDC1s versus cDC2s. Protein concentration was calculated by normalising the protein copy number per cell to the total protein content of the cell. Quantitative proteomics was performed on three biological replicates.

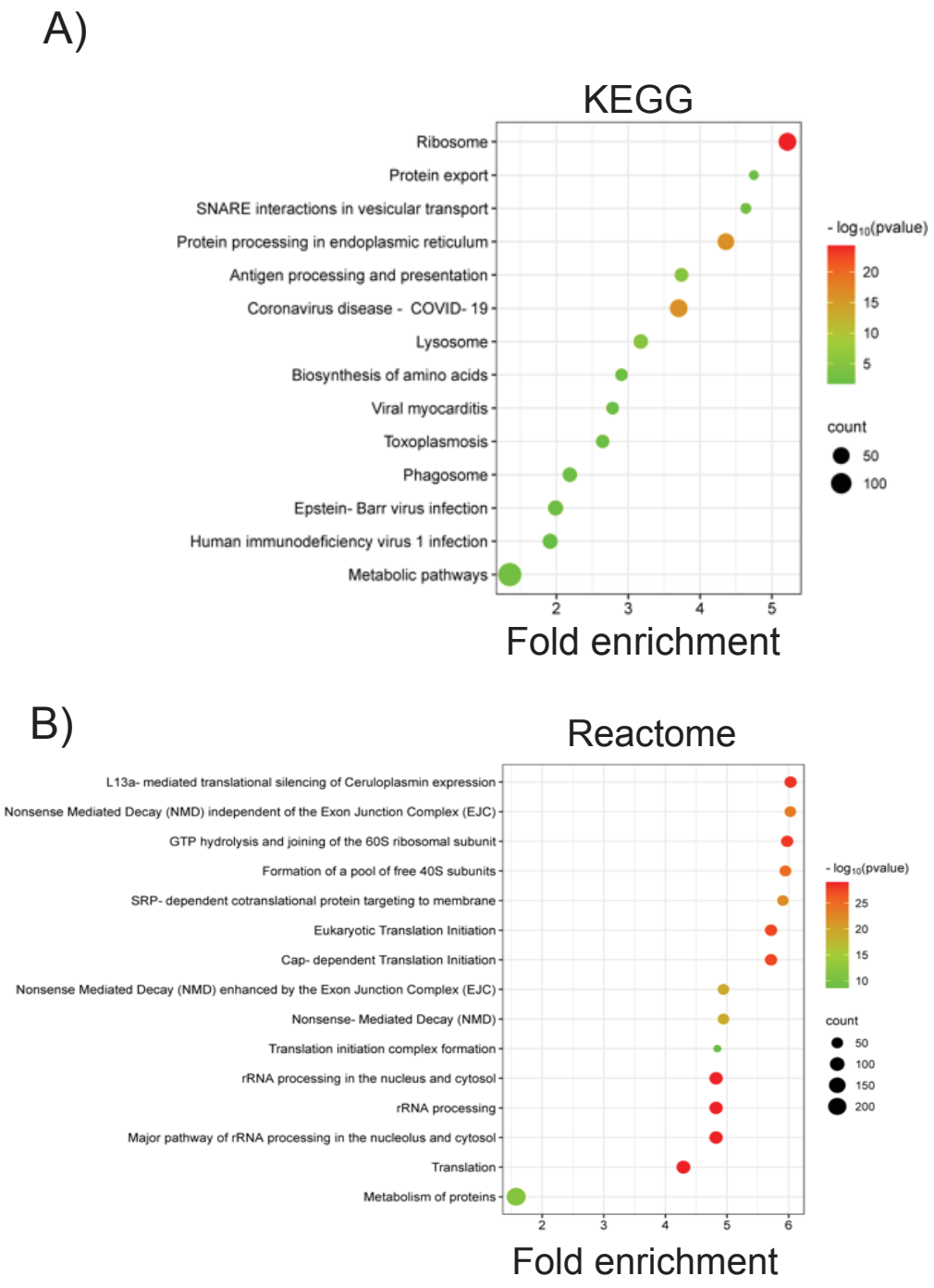

Figure 3.13 – Gene set enrichment analysis identifies an enrichment of metabolic proteins in cDC1s

(A,B) Quantitative proteomics was performed on cDC1s and cDC2s from C57Bl/6 mice inoculated with B16-Flt3l secreting cells, analysing the enriched functional pathways in cDC1s. GSEA was performed on significantly enriched proteins in cDC1s using **(A)** KEGG and **(B)** Reactome databases. The bubble plot X-axis represents fold enrichment, and the Y-axis represents the most enriched pathways from each database. Bubble size indicates the number of proteins associated with each pathway, and the colour indicates the adjusted p-value. Quantitative proteomics was performed on three biological replicates.

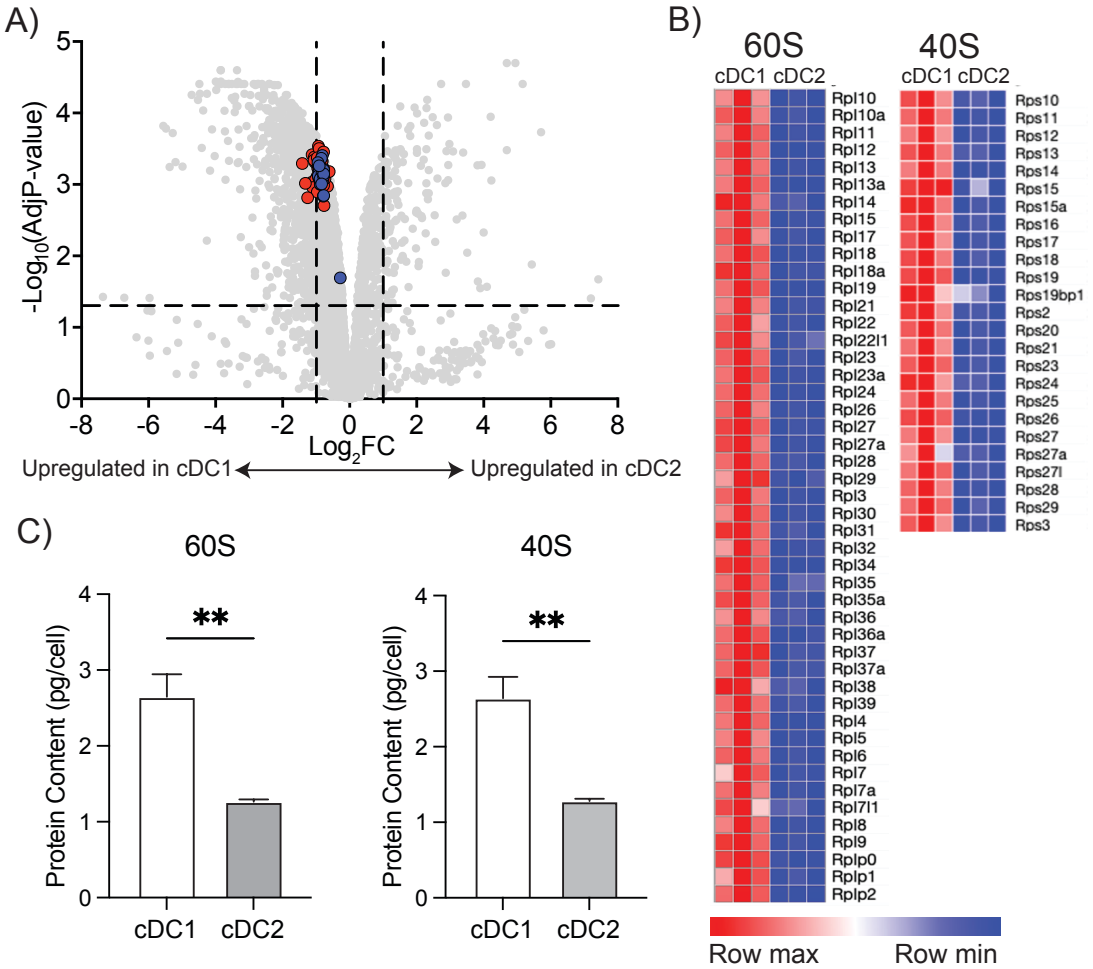

Figure 3.14 – cDC1s have significantly higher expression of ribosomal proteins than cDC2s

(A-C) Quantitative proteomics was performed on cDC1s and cDC2s from C57Bl/6 mice inoculated with B16-Flt3l secreting cells, analysing the abundance of ribosome proteins. **(A)** Volcano plot of the relative abundance of 60S (GO:0022625) (red) and 40S (GO:0022627) (blue) cytosolic ribosomal proteins in cDC1 and cDC2. The plot represents the -$\log_{10}$ of the adjusted p-value (Bonferroni) versus $\log_2$ of the fold change of protein abundance. The horizontal line represents a p-value >0.05, and the vertical lines represent a $\log_2$ fold change of 1. **(B)** Heat maps of the protein abundance of the 60S and 40S ribosomal proteins. Protein abundance is quantile normalised and graded from low (blue) to high (red) per row. **(C)** Bar plot of total protein abundance (pg/cell) of the 60S and 40S ribosomal proteins in cDC1s and cDC2s. Pooled data is presented as mean +/- SEM of three independent experiments **(C)**. Statistical analysis was performed using a paired student's t-test. (**p<0.01)

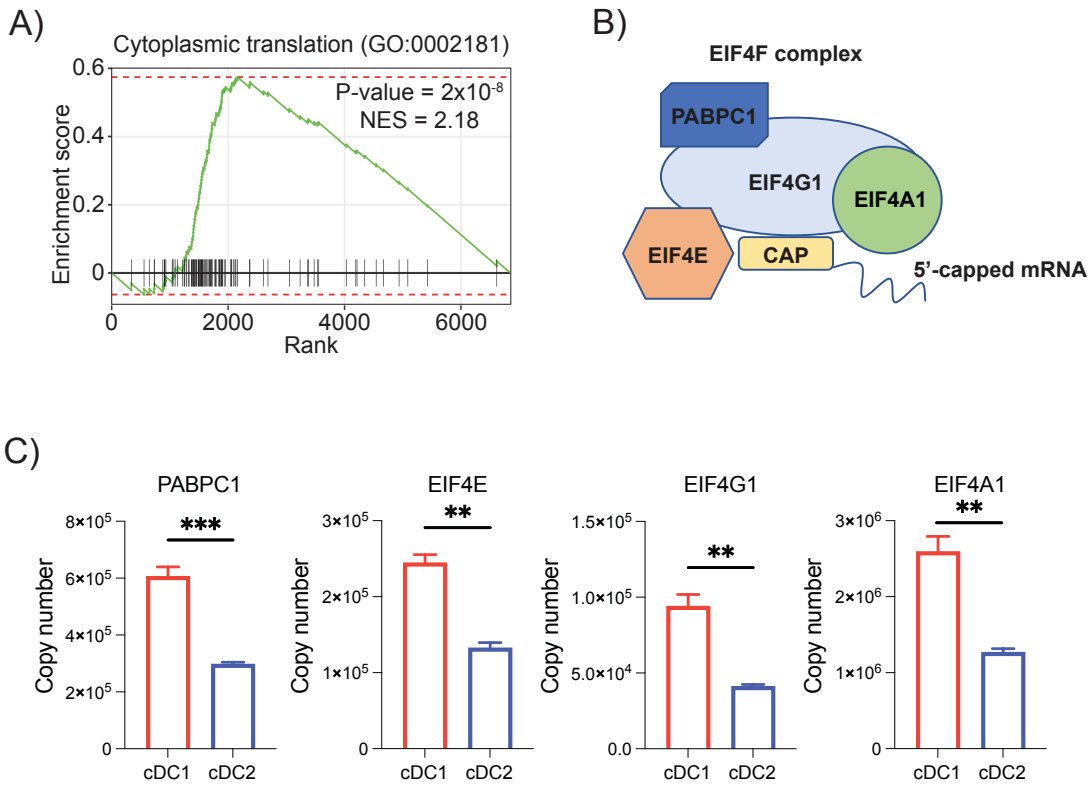

Figure 3.15 – cDC1s have a significant enrichment of proteins associated with protein synthesis than cDC2s

(A-C) Quantitative proteomics was performed on cDC1s and cDC2s from C57Bl/6 mice inoculated with B16-Flt3l secreting cells, analysing the abundance of 5'-translation initiation complex proteins. **(A)** GSEA plot of proteins involved in cytoplasmic translation (GO:0002181) in the cDC proteome. Proteins are ranked by Log_2FC from differential expression analysis. **(B)** Illustration of the proteins composing the 5'-translation initiation complex. **(C)** Copy number per cell of proteins in the 5'-translation initiation complex in cDC1s and cDC2s. Data is mean +/- SEM of three independent experiments. Statistical analysis was performed using a paired student's t-test. (**p<0.01, ***p<0.001)

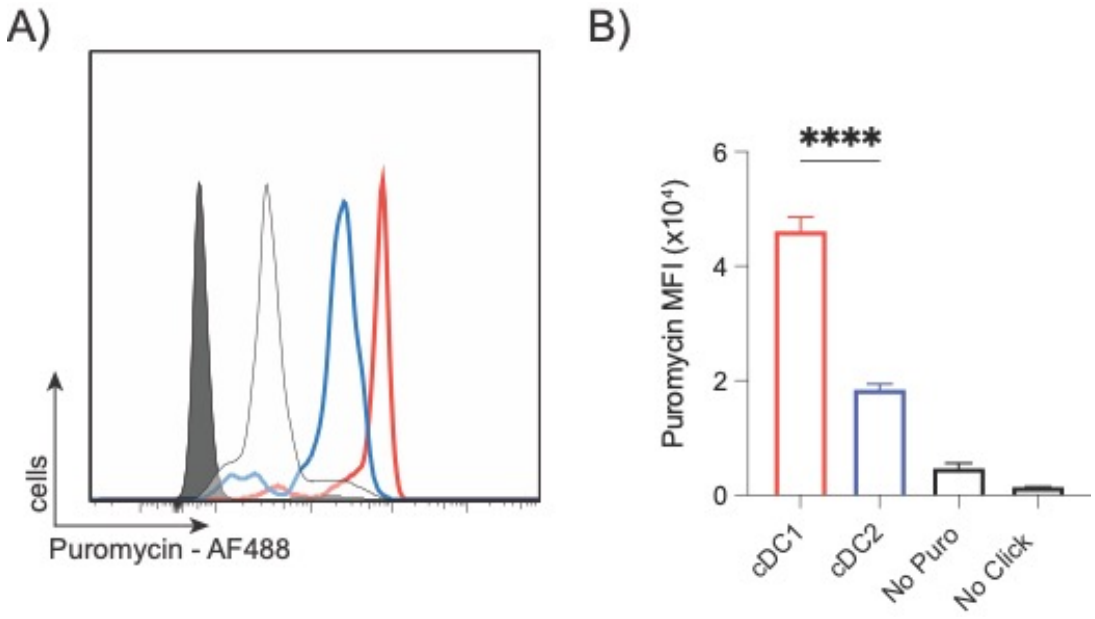

Figure 3.16 – cDC1s have a higher rate of protein synthesis than cDC2s (A,B) Flow cytometry was performed on splenocytes from C57Bl/6 mice inoculated with B16-Flt3l secreting cells, analysing the rate of protein synthesis in cDC1s and cDC2s. The protein synthesis rate was determined by administering puromycin to splenocytes and measuring incorporation into polypeptide chains. Puromycin staining was performed using a click-chemistry puromycin analogue (OPP). The click-chemistry reaction was performed without puromycin treatment in the no puro condition (black line). In the no-click condition (grey filled), cells were treated with puromycin, and the click-chemistry reaction was not performed. Data are representative **(A)** or mean +/- SEM **(B)** of four independent experiments. Statistical analysis was performed using a paired student's t-test. (****$p<0.001$)

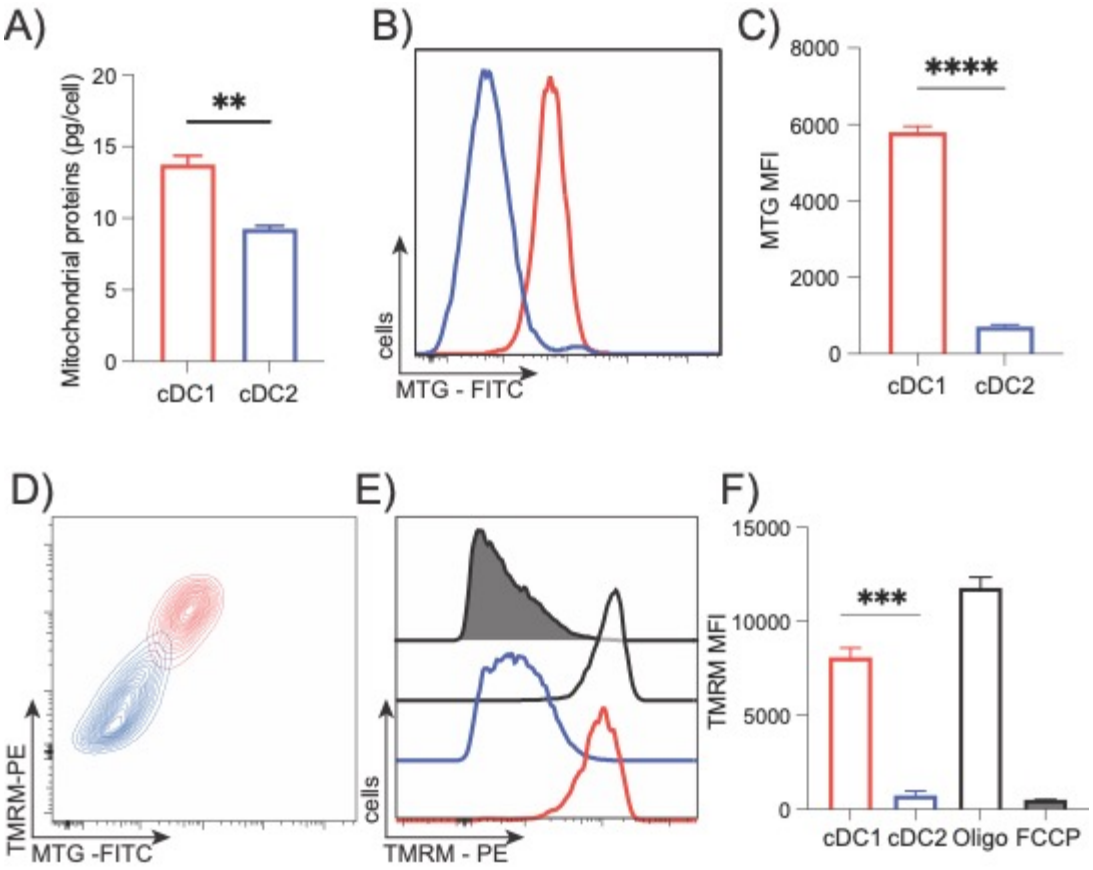

Figure 3.17 – Elevated mitochondrial activity in cDC1s
(A-F) Flow cytometry was performed on splenocytes from C57Bl/6 mice inoculated with B16-Flt3l secreting cells, analysing mitochondrial mass and membrane potential in cDC1s and cDC2s. **(A)** The total protein content of mitochondrial proteins (GO:0005739) in cDC1s and cDC2s. **(B,C)** Mitochondrial mass was determined using Mitotracker Green staining by flow cytometry in cDC1s and cDC2s. **(D-F)** Mitochondrial membrane potential was determined using TMRM staining in cDC1s and cDC2s. Data are representative **(B,D,E)** or mean +/- SEM **(A,C,F)** for three independent experiments. Statistical analysis was performed using a paired student's t-test **(A,C)** or one-way ANOVA followed by Tukey's multiple comparisons post-test **(F)**. (**p<0.01,***p<0.001,****p<0.0001)

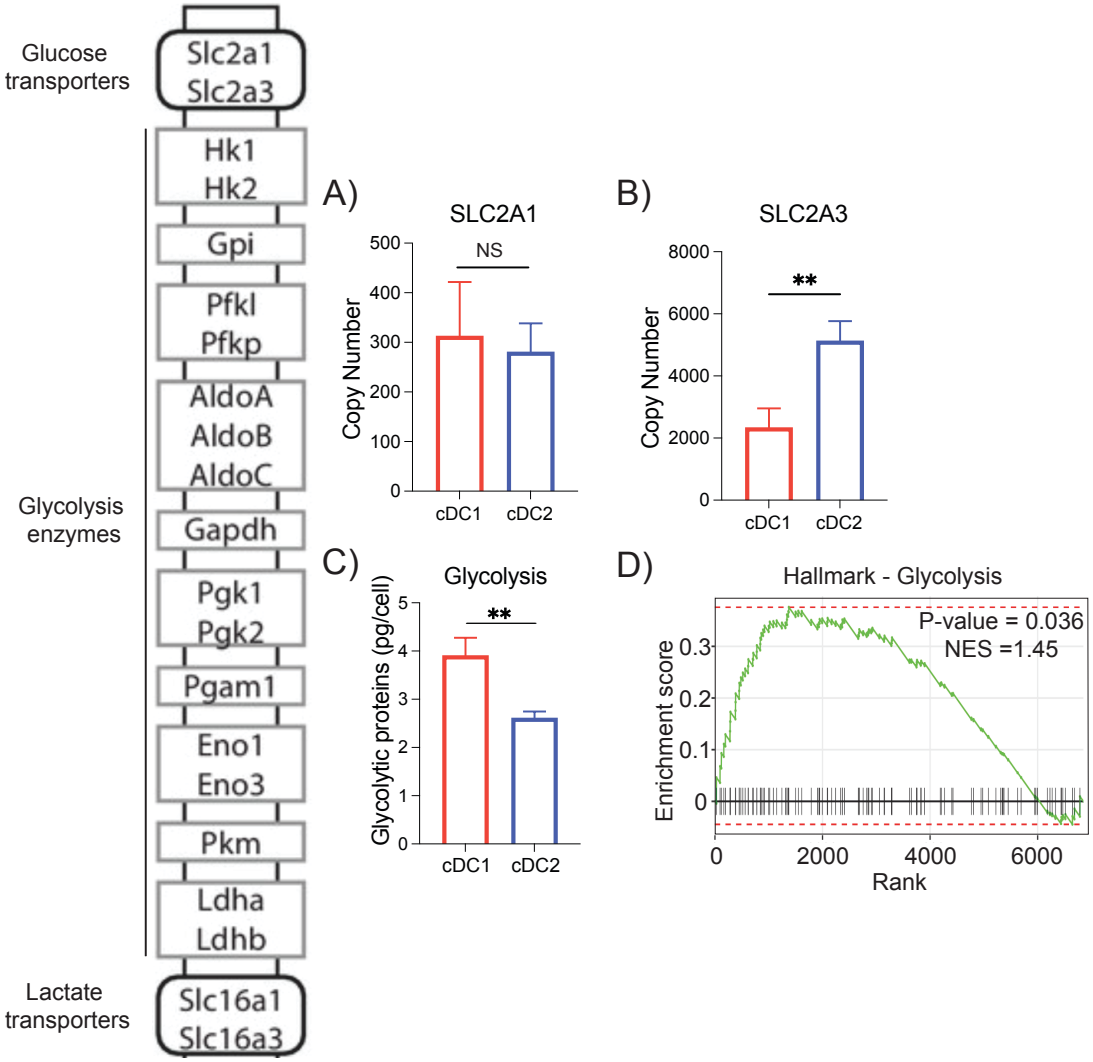

Figure 3.18 – Analysis of the glycolytic proteome in cDC1s and cDC2s
(A-D) Quantitative proteomics was performed on cDC1s and cDC2s from C57Bl/6 mice inoculated with B16-Flt3l secreting cells, analysing the abundance of glycolytic proteins. **(A,B)** Copy number per cell of glucose transporters GLUT1 (SLC2A1) **(A)** and GLUT3 (SLC2A3) **(B)** in cDC1s and cDC2s. **(C)** Total protein content (pg/cell) of glycolytic enzymes in cDC1s and cDC2s. **(D)** GSEA plot of glycolysis proteins (Hallmark-Glycolysis M5937) in the cDC1 proteome. Proteins are ranked by Log_2FC from differential expression analysis. NES = Normalised enrichment score. Data are mean +/- SEM of three independent experiments. Statistical analysis was performed using a paired student's t-test **(A-C)**. (NS = $p>0.05$, **$p<0.01$)

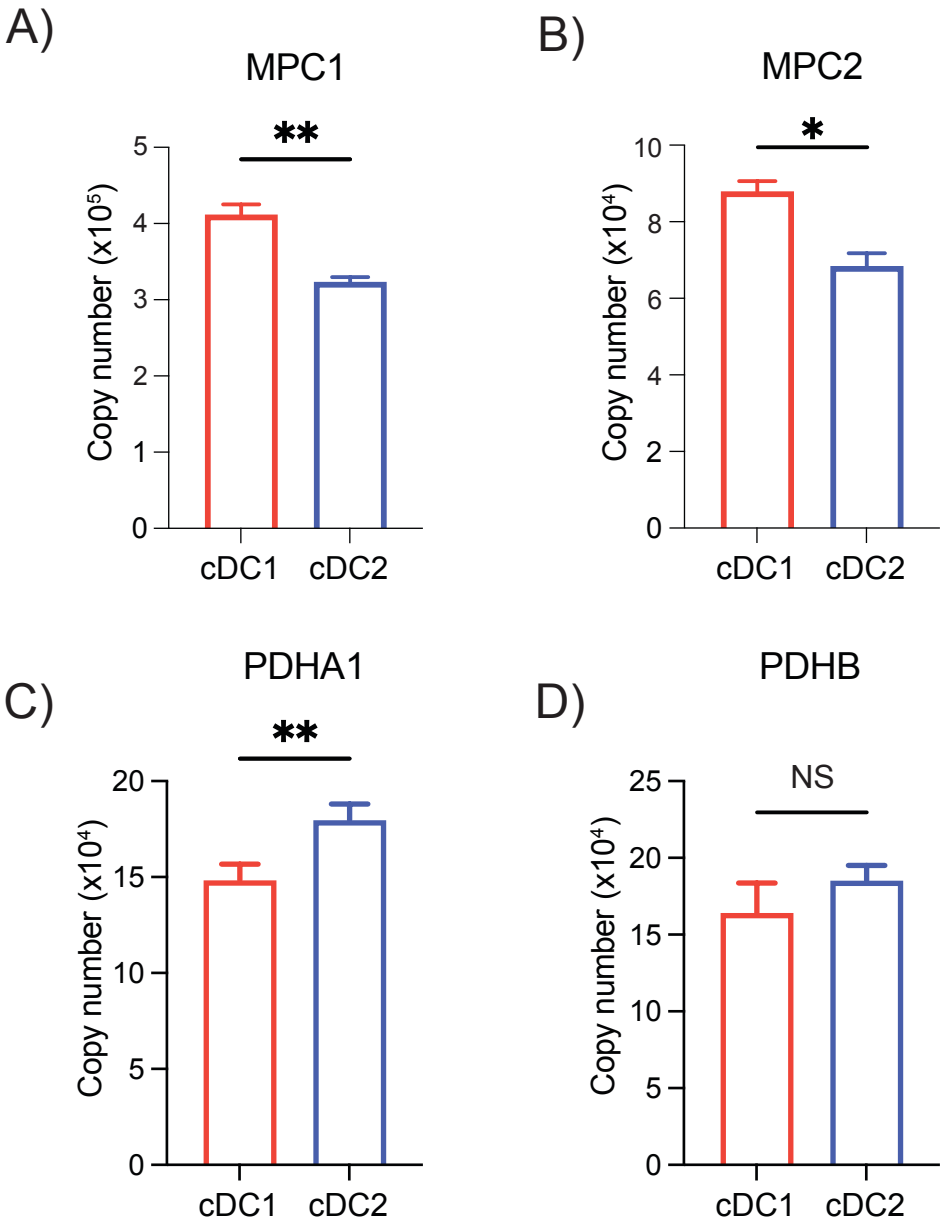

Figure 3.19 – Analysis of mitochondrial pyruvate metabolism in cDC1s and cDC2s

(A-D) Quantitative proteomics was performed on cDC1s and cDC2s from C57Bl/6 mice inoculated with B16-Flt3l secreting cells, analysing the abundance of proteins associated with mitochondrial pyruvate metabolism. **(A,B)** Copy number per cell of the mitochondrial pyruvate carrier (MPC) subunits, MPC1 **(A)** and MPC2 **(B)** in cDC1s and cDC2s. **(C,D)** Copy number per cell of the pyruvate dehydrogenase (PDH) subunits, PDHA1 **(A)** and PDHB **(B)** in cDC1s and cDC2s. Data are mean +/- SEM of three independent experiments. Statistical analysis was performed using a paired student's t-test (NS = $p>0.05$,*$p<0.05$,**$p<0.01$)

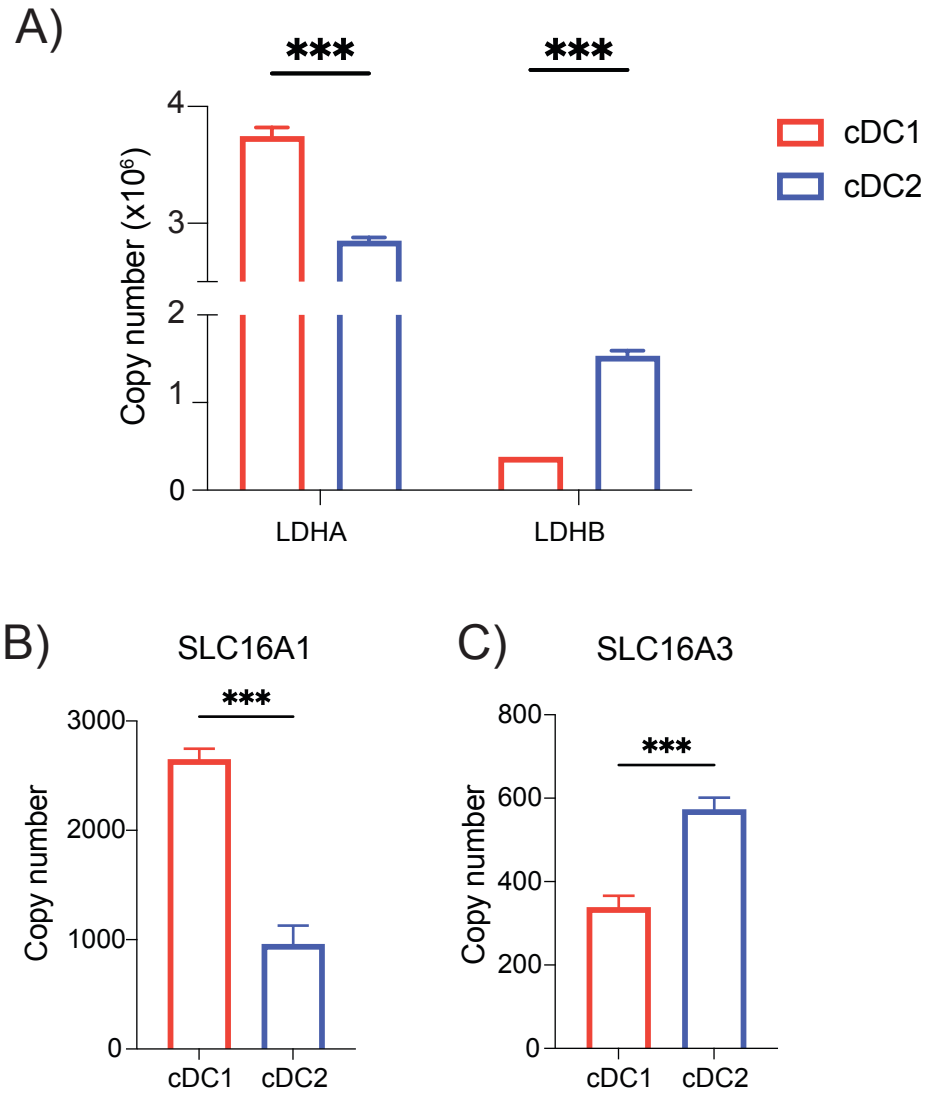

Figure 3.20 – cDCs have differential expression of LDH isozymes and lactate transporters

(A-C) Quantitative proteomics was performed on cDC1s and cDC2s from C57Bl/6 mice inoculated with B16-Flt3l secreting cells, analysing the abundance of proteins associated with lactate metabolism and export. **(A)** Copy number per cell of LDH isozymes in cDC1s and cDC2s. **(B,C)** Copy number per cell lactate transporters MCT1 (SLC16A1) **(B)** and MCT4 (SLC16A3) **(C)** in cDC1s and cDC2s. Data are mean +/- SEM of three independent experiments. Statistical analysis was performed using a two-way ANOVA and Sidak's post-test **(A)** or a paired student's t-test **(B,C)** (***p<0.001).

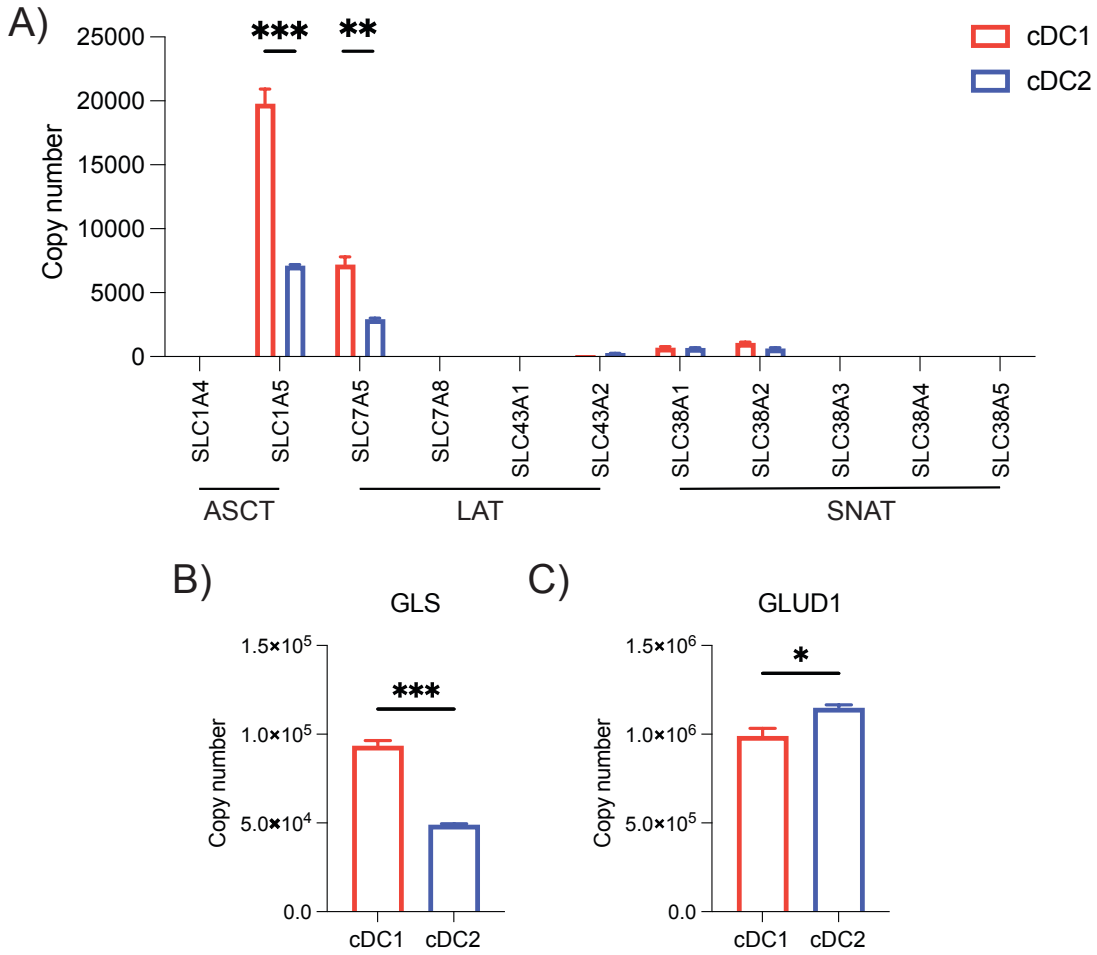

Figure 3.21 – Analysis of glutamine transporter and catabolism machinery in cDC1s and cDC2s

(A-C) Quantitative proteomics was performed on cDC1s and cDC2s from C57Bl/6 mice inoculated with B16-Flt3l secreting cells, analysing the expression of amino acid transporter expression and glutamine catabolism machinery. **(A)** Copy number per cell of amino acid transporters in cDC1s and cDC2s. **(B)** Copy number per cell of glutaminase (GLS) in cDC1s and cDC2s. **(C)** Copy number per cell of glutamate dehydrogenase (GLUD1) in cDC1s and cDC2s. Data are mean +/- SEM of three independent experiments. Statistical analysis was performed using a two-way ANOVA and Sidak's post-test **(A)** or a paired student's t-test **(B,C)** (*p<0.05,**p<0.01, ***p<0.001)

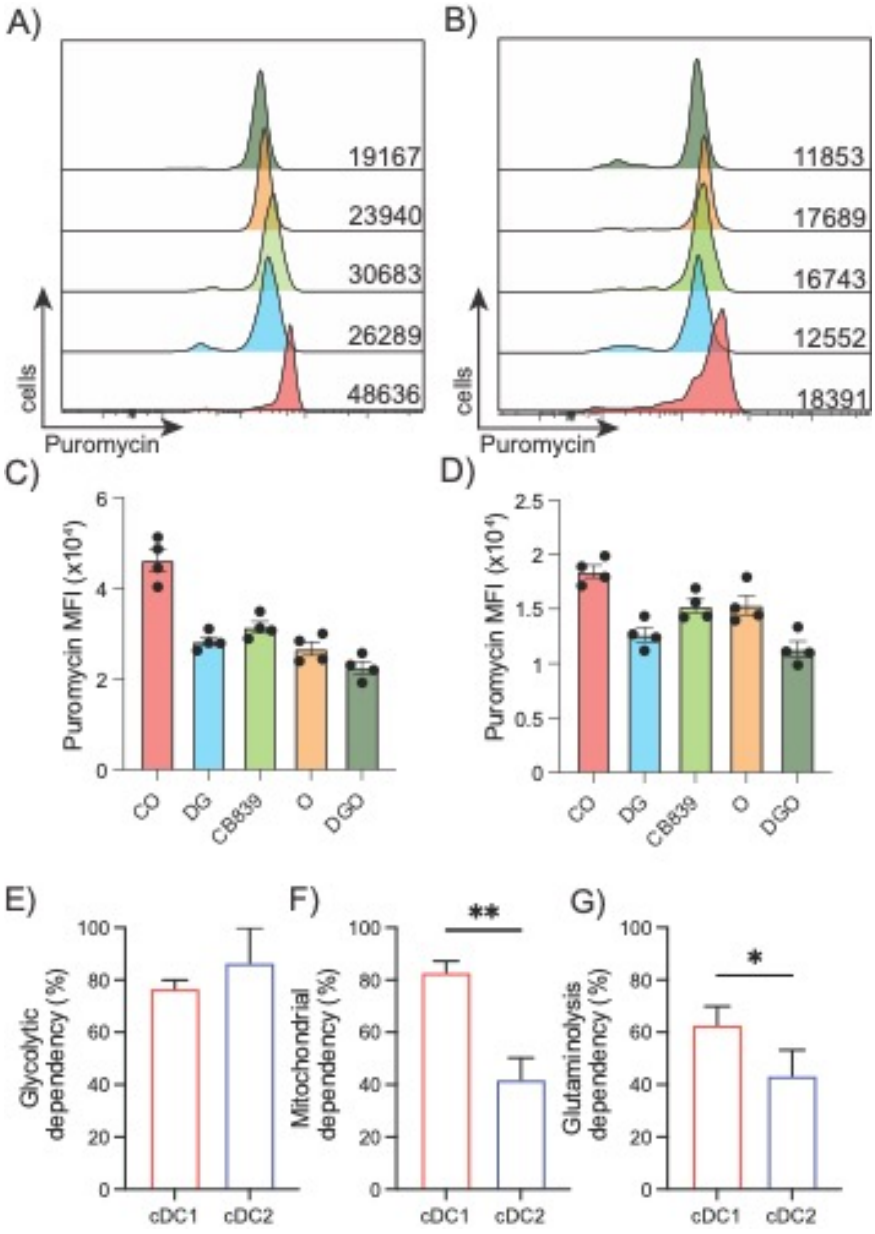

Figure 3.22 – SCENITH analysis confirms higher mitochondrial dependency in cDC1s than in cDC2s

(A-G) Splenocytes from C57Bl/6 mice inoculated with B16-Flt3l secreting cells were treated with PBS (CO, Vehicle control) or metabolic inhibitors (DG = 100mM 2DG, O =2μM Oligomycin, 4μM CB839, DGO = 2DG + Oligomycin) for 20 minutes and protein synthesis rate of cDCs was determined by puromycin incorporation by flow cytometry. **(A,B)** Representative histograms of puromycin incorporation in **(A)** cDC1s and **(B)** cDC2s. **(C,D)** Pooled puromycin MFI in **(C)** cDC1s and **(D)** cDC2s. **(E)** Glycolytic dependency was calculated as MFI 100(CO-DG)/(CO-DGO) for cDC1s and cDC2s. **(F)** Mitochondrial dependency was calculated as MFI 100(O-DG)/(CO-DGO) for cDC1s and cDC2s. **(G)** Glutaminolysis dependency was calculated as MFI 100(CB839-DG)/(CO-DGO) for cDC1s and cDC2s. Data are representative (**A,B)** or mean +/- SEM **(C-G)** of four independent experiments. Statistical analysis was performed using a paired student's t-test **(E-G)**. (*p<0.05,**p<0.01)

3.4 CpG-B stimulation induces functional and metabolic reprogramming of cDC subsets

Immunogenic stimulation is associated with metabolic reprogramming in many immune cells. Upon activation, DCs undergo DC maturation, which alters their phenotype to allow efficient antigen presentation while reducing antigen capture. Although numerous studies have investigated the transcriptional changes associated with DC maturation, a detailed examination of the proteome still needs to be provided. To investigate the proteomic remodelling associated with DC maturation, I injected B16-Flt3l expanded mice with 50μg/kg of the TLR9 agonist CpG-B or PBS (vehicle control) and harvested spleens for proteomic analysis of cDC subsets after 18 hours. CpG-B treatment induced proteomic remodelling in both cDC1s **(Fig. 3.23 A)** (191 proteins upregulated, 95 proteins downregulated) and cDC2s **(Fig. 3.24 A)** (252 proteins upregulated and 84 downregulated). I confirmed that stimulation-induced DC maturation by quantifying the upregulation of DC co-stimulatory markers, chemokine receptors and proinflammatory signalling pathway (STATs, NFκB) in both cDC1 **(Fig. 3.23 B)** and cDC2 **(Fig.3.24 B)**.

To understand the functional consequences of this proteomic remodelling, I performed GSEA on the significantly upregulated and downregulated proteins in cDC1 **(Fig. 3.25 A,B)** and cDC2 **(Fig. 3.26 A,B)**. Analysis of both GO biological processes (GO:BP) and Reactome pathway analysis shows that both cDC1 **(Fig. 3.25 A,B)** and cDC2 **(Fig. 3.26 A,B)** strongly upregulate proteins associated with response to viral infection, as may be expected when stimulated with a viral ligand such as CpG-B. The downregulated proteins responding to stimulation (blue) do not significantly associate with any GO: BPs or Reactome pathways. Notably, metabolic pathways do not feature highly in the GSEA in the upregulated or downregulated proteins.

Interferons are essential in direct anti-viral defence and linking innate and adaptive immune responses (McNab et al., 2015). Interferons signal through interferon receptors (IFNAR, IFNGR) and induce the upregulation of many

interferon-stimulated genes (ISGs), which promote anti-viral responses (Platanias, 2005). The pathway analyses **(Fig. 3.27 A,D)** show that the most upregulated pathways are dominated by response to interferon signalling. Indeed, analysis of the expression of ISGs in both cDC1s **(Fig. 3.27 B,C)** and cDC2s **(Fig. 3.27 E,F)** show that they are strongly enriched upon CpG-B treatment. A report by Pantel and colleagues has shown that *in vivo* TLR3 stimulation with poly I:C strongly inhibits the OCR of a mixed population of cDCs after 14h of stimulation. This was shown to depend on type-1 IFN signalling, as cDCs deficient in the IFNAR receptor have no abrogation of mitochondrial metabolism (Pantel et al., 2014). Similar observations have been reported in macrophages, showing that type-1 IFN and IFNAR signalling limit mitochondrial metabolism in response to mycobacterial infection (Olson et al., 2021). To investigate if CpG-B stimulation alters mitochondrial metabolism in cDCs, I analysed the mitochondrial proteome of both subsets **(Fig. 3.28).** GSEA analysis of mitochondrial proteins in response to CpG-B stimulation shows that the most significantly downregulated pathways in both cDC1 **(Fig. 3.28 A-C)** and cDC2 **(Fig. 3.28 D-F)** are associated with pathways that fuel the TCA cycle and OXPHOS including FAO and amino acid metabolism. In line with this, GO:BP and KEGG pathways analysis identified cellular respiration and OXPHOS as downregulated pathways in cDC1 and cDC2. Finally, analysis of the protein abundances of the proteins composing the ETC complexes shows a global reduction in expression in stimulated versus naïve cDC1s **(Fig. 3.29 A)** and cDC2s **(Fig. 3.29 B)**.

Overall, the proteomic data suggests that mitochondrial metabolism is repressed in TLR9-activated mature DCs. As discussed earlier, the protein synthesis rate is a good proxy for the energetic demands of a cell. A study by Lelouard and colleagues investigated the kinetics of translation induction upon LPS stimulation of GMDCs (Lelouard et al., 2007). This study showed that GMDCs rapidly increase their protein synthesis rate after 4 hours of stimulation, followed by a steady decline in translation at later time points. It was suggested that the early increase in translation is required for the biosynthetic demands associated with DC maturation, and a reduced rate of synthesis supported cell survival and longevity. In line with this, puromycin

incorporation in response to CpG-B stimulation shows an increased protein synthesis rate after 6h of stimulation, followed by a significant decline after 18h in cDC1 **(Fig. 3.30 A,B)** and cDC2 **(Fig. 3.30 C,D)**.

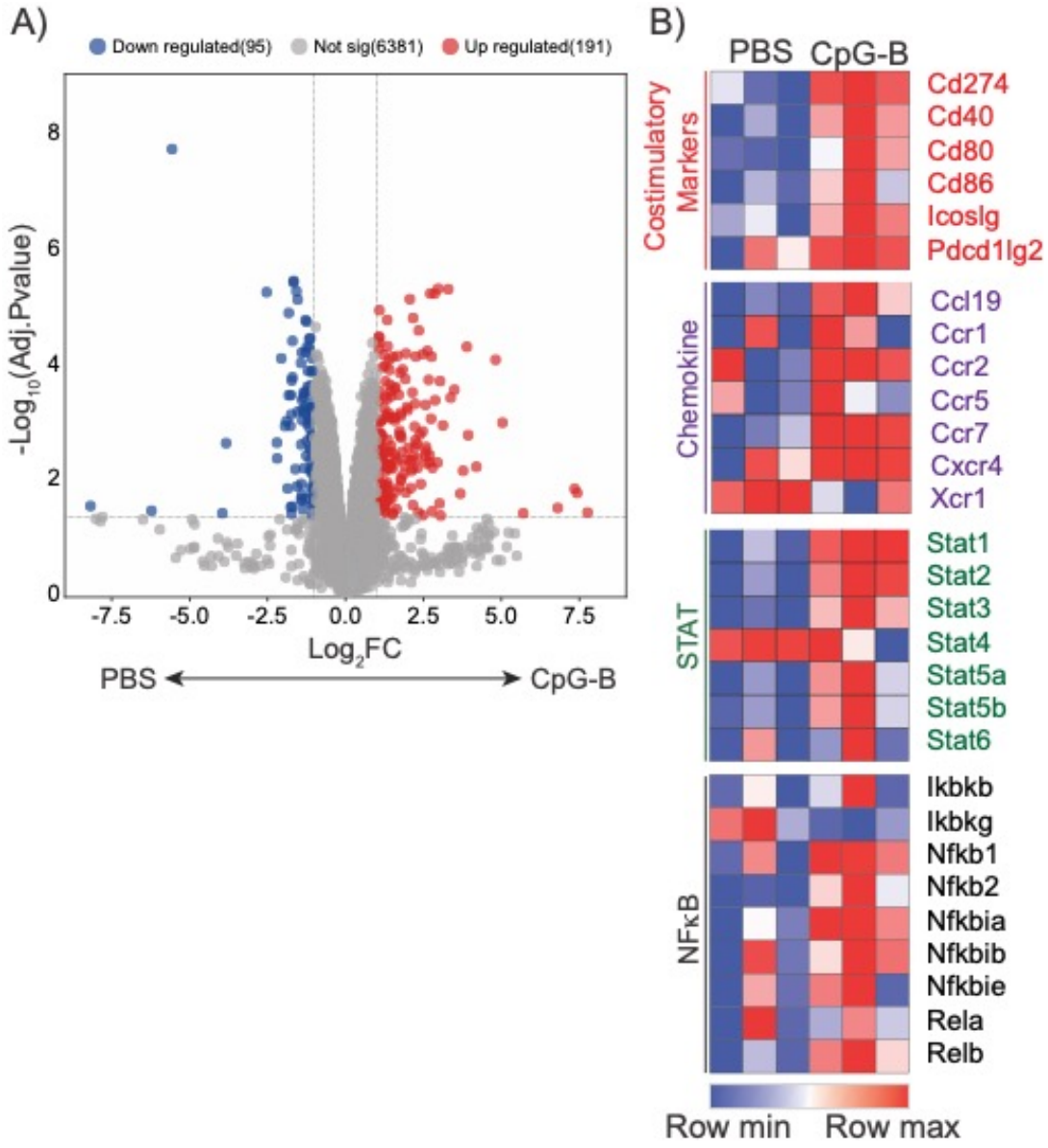

Figure 3.23 – CpG-B stimulation induces DC maturation and proteomic remodelling in cDC1s

(A,B) Quantitative proteomics was performed on cDC1s from C57Bl/6 mice inoculated with B16-Flt3l secreting cells, analysing proteomic remodelling in response to CpG-B stimulation. Mice were treated intravenously with PBS or 50μg/kg CpG-B for 18h. **(A)** Volcano plot of 6,667 identified proteins in cDC1s displaying differences in relative abundance between PBS and CpG-B stimulated groups. The plot represents the $-\log_{10}$ of the adjusted p-value (Bonferroni) versus $\log_2$ of the fold change of protein abundance. Significantly upregulated proteins (red) have a $\log_2$ fold change >1 and a $-\log_{10}$(adj.p-value) > 1.35 (Q<0.05) and downregulated proteins (blue) have a $\log_2$ fold change <1 and a $-\log_{10}$(adj.p-value) > 1.35 (Q<0.05). **(B)** Heatmap displaying the $\log_2$ copy number of proteins involved in DC maturation and inflammatory signalling in PBS and CpG-B groups. Quantitative proteomics was performed on three biological replicates.

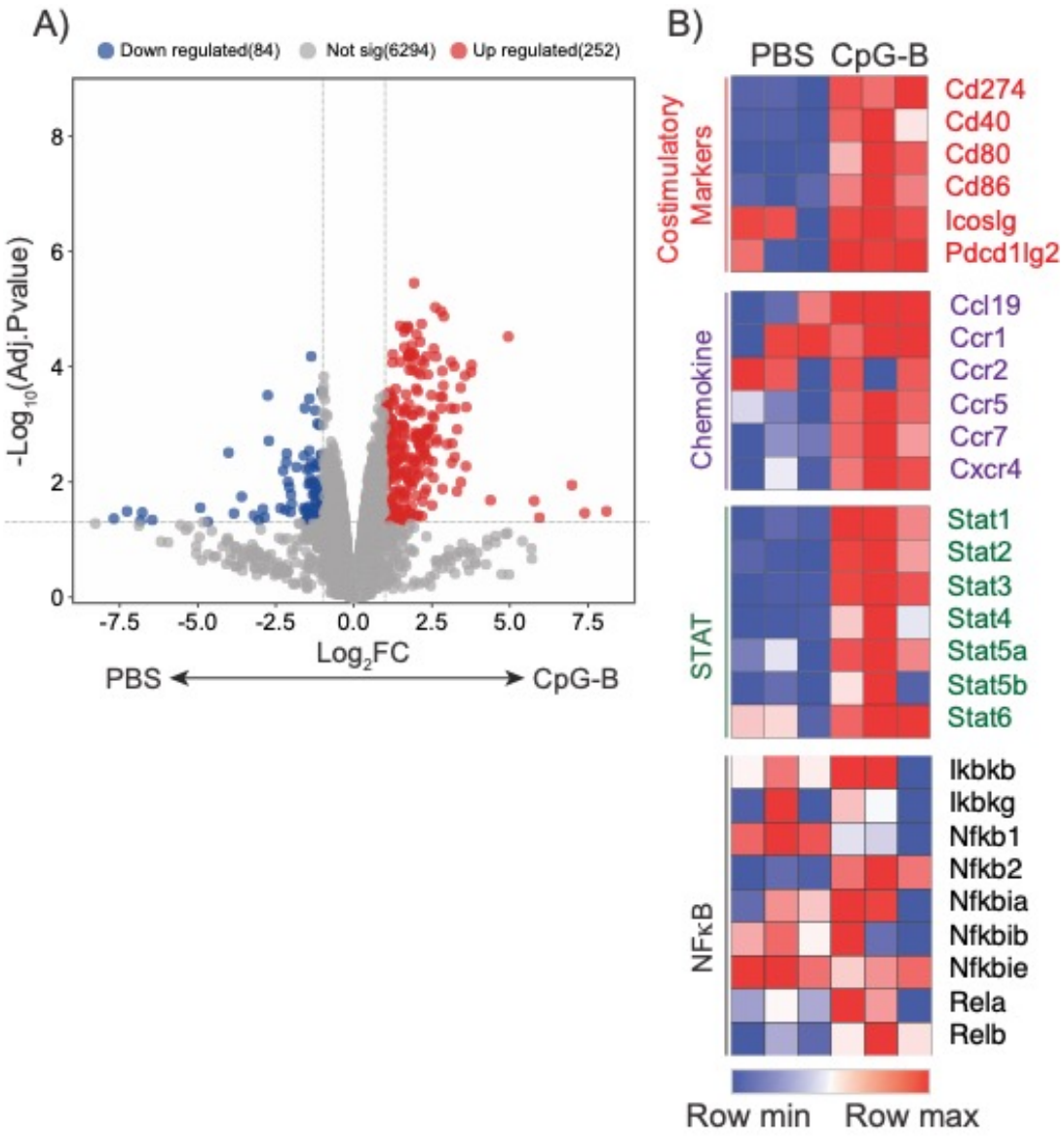

Figure 3.24 – CpG-B stimulation induces DC maturation and proteomic remodelling in cDC2s

(A,B) Quantitative proteomics was performed on cDC2s from C57Bl/6 mice inoculated with B16-Flt3l secreting cells, analysing proteomic remodelling in response to CpG-B stimulation. Mice were treated intravenously with PBS or 50μg/kg CpG-B for 18h. **(A)** Volcano plot of 6,667 identified proteins in cDC2s displaying differences in relative abundance between PBS and CpG-B stimulated groups. The plot represents the $-\log_{10}$ of the adjusted p-value (Bonferroni) versus $\log_2$ of the fold change of protein abundance. Significantly upregulated proteins (red) have a $\log_2$ fold change >1 and a $-\log_{10}$(adj.p-value) > 1.35 (Q<0.05) and downregulated proteins (blue) have a $\log_2$ fold change <1 and a $-\log_{10}$(adj.p-value) > 1.35 (Q<0.05). **(B)** Heatmap displaying the $\log_2$ copy number of proteins involved in DC maturation and inflammatory signalling in PBS and CpG-B groups. Quantitative proteomics was performed on three biological replicates.

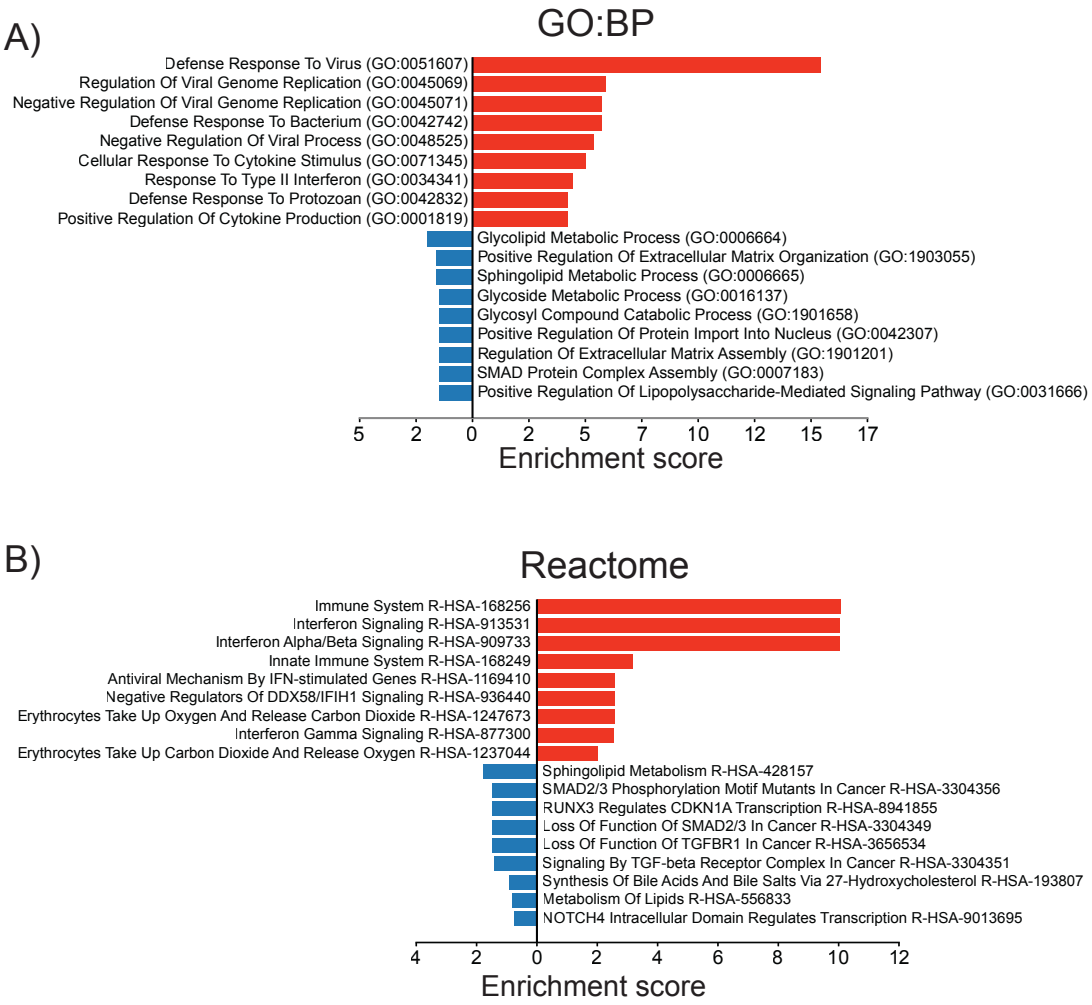

Figure 3.25 – Pathway analysis of differentially expressed protein in response to CpG-B stimulation in cDC1s

(A,B) Quantitative proteomics was performed on cDC1s from C57Bl/6 mice inoculated with B16-Flt3l secreting cells, analysing enriched biological processes and functional pathways in response to CpG-B stimulation. Mice were treated intravenously with PBS or 50μg/kg CpG-B for 18h. Significantly upregulated (Log_2FC >1, adj.p-value<0.05) and downregulated (Log_2FC<-1, adj.p-value<0.05) proteins were analysed for pathways enrichment using Gene ontology biological process (GO:BP) **(A)** and Reactome **(B)** databases in cDC1s. Pathways upregulated in response to CpG-B stimulation are shown in red and downregulated pathways in blue. Enrichment score = $-Log_{10}$Adj.p-value. Quantitative proteomics was performed on biological replicates.

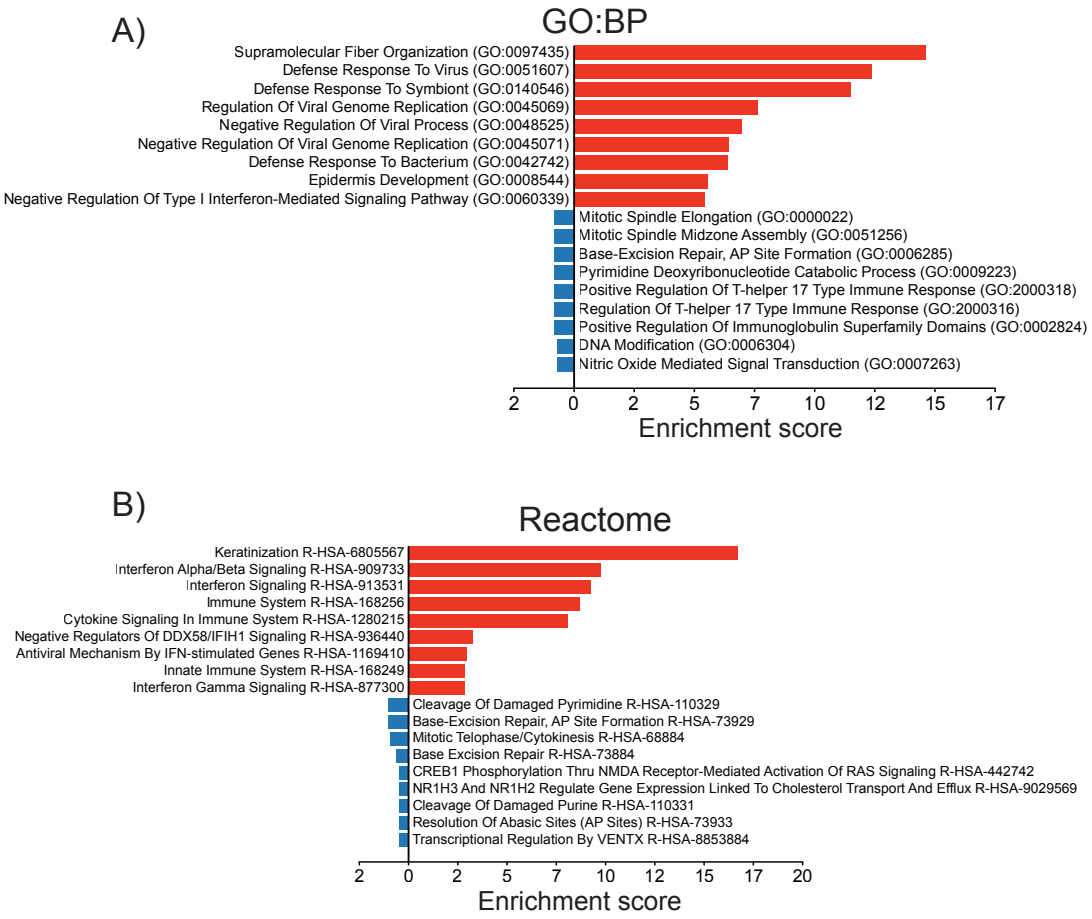

Figure 3.26 – Pathway analysis of differentially expressed protein in response to CpG-B stimulation in cDC2s

(A,B) Quantitative proteomics was performed on cDC1s from C57Bl/6 mice inoculated with B16-Flt3l secreting cells, analysing enriched biological processes and functional pathways in response to CpG-B stimulation. Mice were treated intravenously with PBS or 50μg/kg CpG-B for 18h. Significantly upregulated ($Log_2FC > 1$, adj.p-value<0.05) and downregulated ($Log_2FC < -1$, adj.p-value<0.05) proteins were analysed for pathways enrichment using Gene ontology biological process (GO:BP) **(A)** and Reactome **(B)** databases in cDC2s. Pathways upregulated in response to CpG-B stimulation are shown in red and downregulated pathways in blue. Enrichment score = $-Log_{10}$Adj.p-value. Quantitative proteomics was performed on biological replicates.

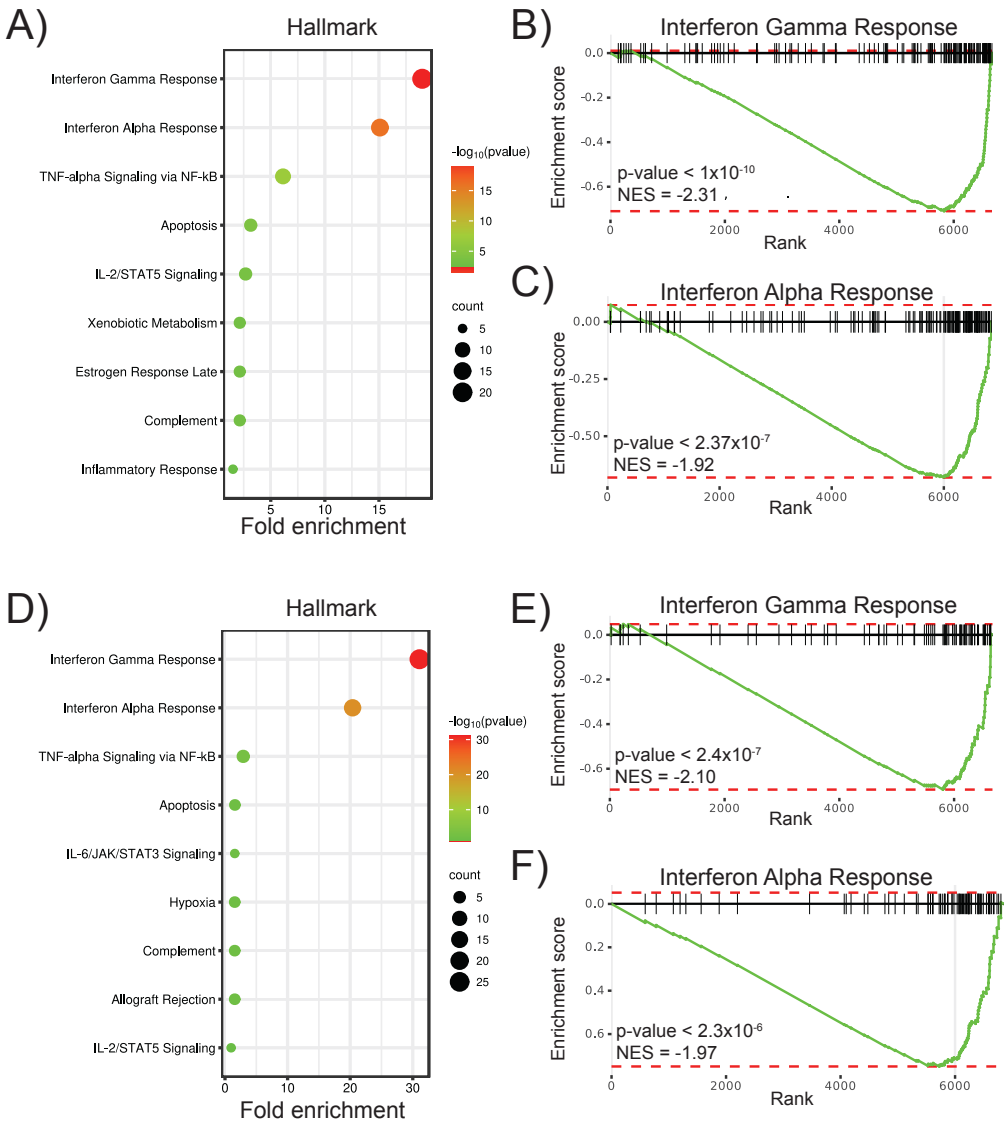

Figure 3.27 – CpG-B stimulation induces the expression of type-1 and type-2 interferon response genes in cDC1s and cDC2s

(A-F) Quantitative proteomics was performed on cDC1s and cDC2s from C57Bl/6 mice inoculated with B16-Flt3l-secreting cells, analysing the abundance of proteins involved in the response to IFNα and IFNγ signalling. Mice were treated intravenously with PBS or 50μg/kg CpG-B for 18h. Significantly upregulated proteins (Log_2FC >1, adj.p-value<0.05) in response to CpG-B stimulation were analysed using the Hallmark gene set database in cDC1s **(A)** and cDC2 **(D)**. The bubble plot X-axis represents fold enrichment, and the Y-axis represents the most enriched pathways from the Hallmark database. Bubble size indicates the number of proteins associated with each pathway, and the colour indicates the adjusted p-value. GSEA was performed for proteins involved in response to interferon-gamma (GO:0034341) and interferon-alpha (GO:0034340) in cDC1s **(B,C)** and cDC2s **(E,F)**. NES = normalised enrichment score. Quantitative proteomics was performed on biological replicates.

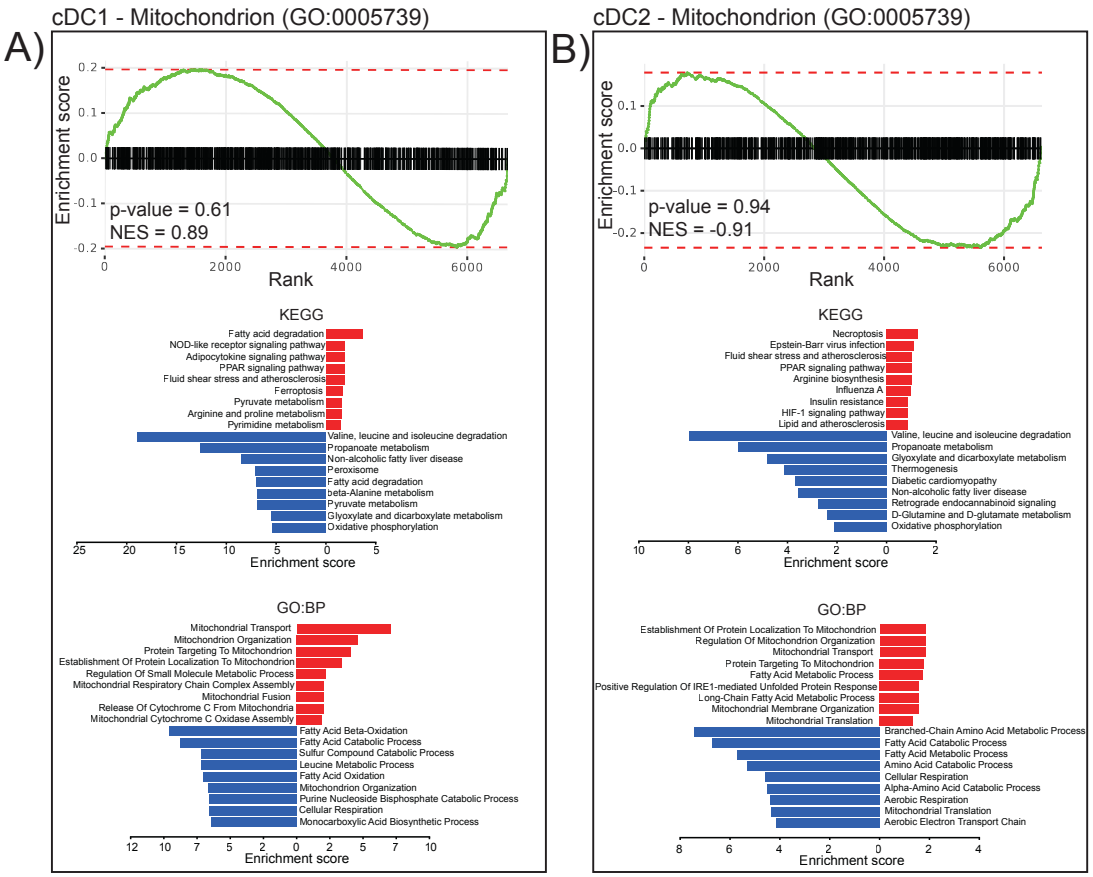

Figure 3.28 – CpG-B stimulation suppresses the expression of mitochondrial catabolic pathways in cDC1s and cDC2s

(A,B) Quantitative proteomics was performed on cDC1s and cDC2s from C57Bl/6 mice inoculated with B16-Flt3l secreting cells, analysing the enrichment of mitochondrial pathways in response to CpG-B stimulation. Mice were treated intravenously with PBS or 50μg/kg CpG-B for 18h. GSEA analysis was performed on mitochondrial proteins (GO:0005739) in cDC1 **(A)** and cDC2 **(B).** Significantly upregulated (Log_2FC >1, adj.p-value<0.05) and downregulated (Log_2FC<-1, adj.p-value<0.05), mitochondrial proteins in response to CpG-B stimulation were analysed using GO:BP and Reactome pathway analysis in cDC1 **(A)** and cDC2 **(B).** NES = normalised enrichment score. Quantitative proteomics was performed on biological replicates.

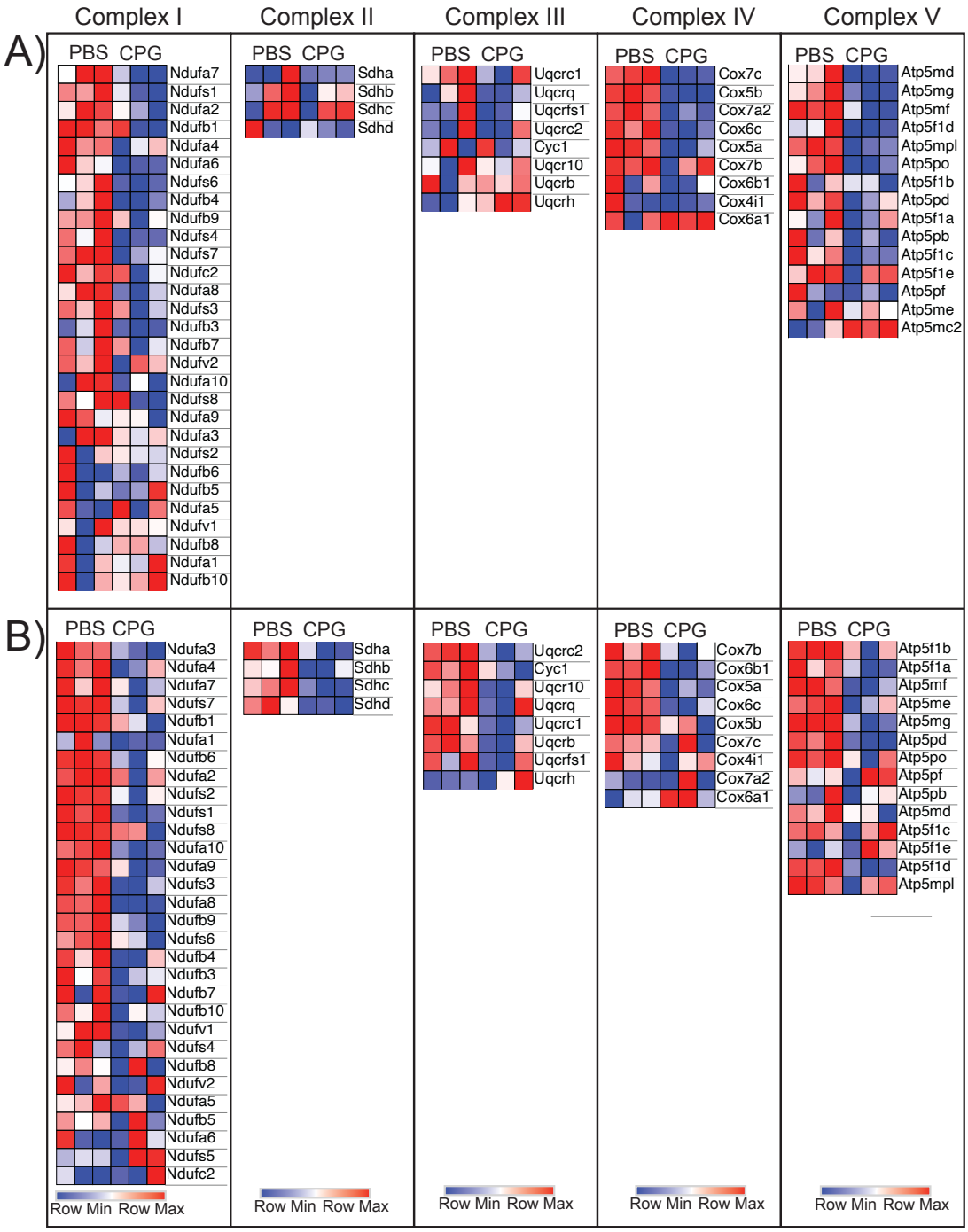

Figure 3.29 – CpG-B stimulation globally downregulates proteins involved in the ETC

(A,B) Quantitative proteomics was performed on cDC1s and cDC2s from C57Bl/6 mice inoculated with B16-Flt3l-secreting cells, analysing the abundance of proteins associated with the electron transport chain (ETC). Mice were treated intravenously with PBS or 50μg/kg CpGB for 18h. The expression of proteins in complex I (GO:0032981), complex II (GO:0042573), complex III (GO:0006122), complex IV (GO:0005751) and complex V (GO:0045259) were compared in cDC1s **(A)** and cDC2 **(B)** between PBS and CpG-B stimulated mice. Heatmaps represent the $\log_2$ copy number per cell of each protein. Quantitative proteomics was performed on biological replicates.

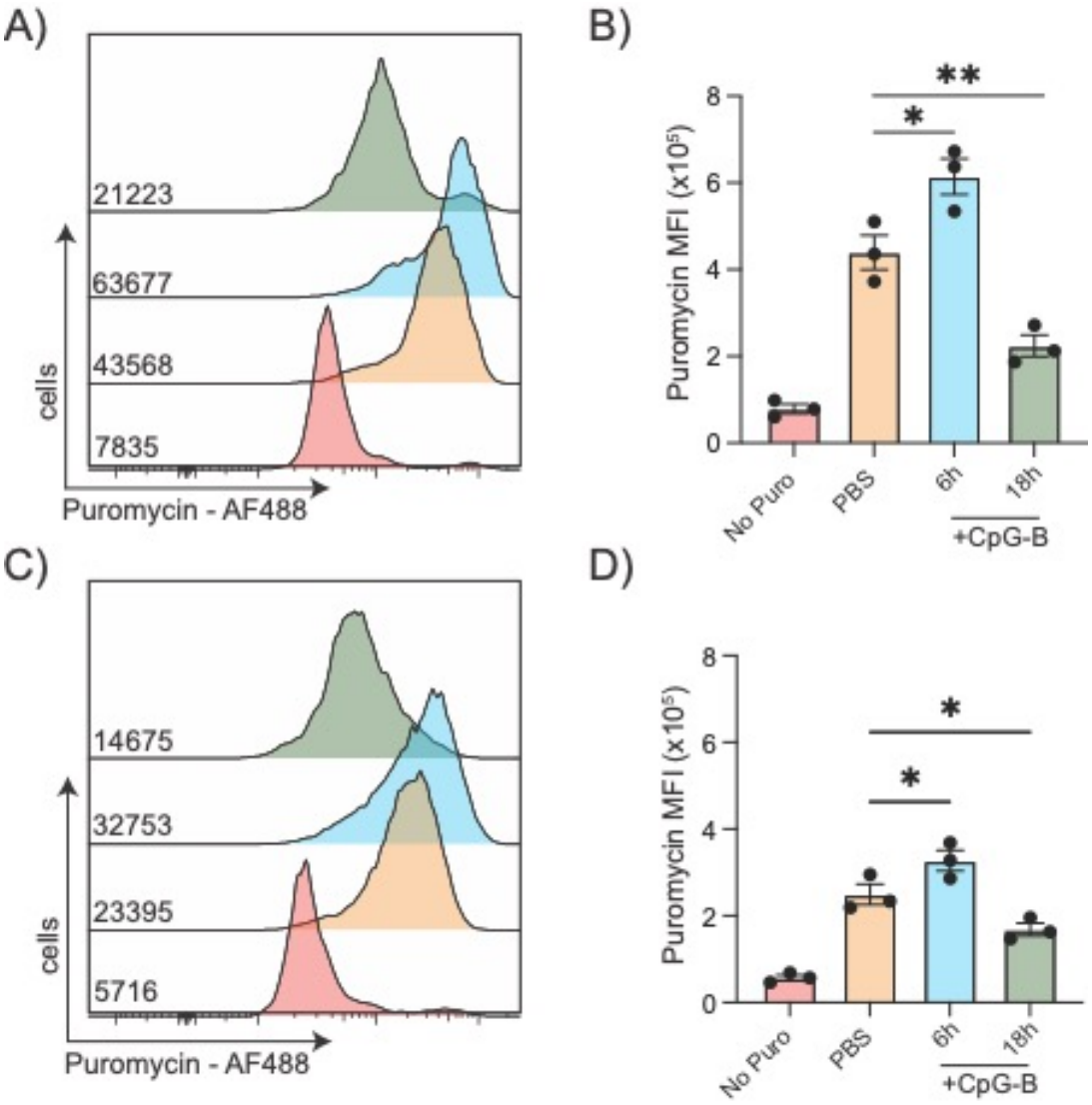

Figure 3.30 – Prolonged CpG-B stimulation *in vivo* reduces protein synthesis rate

(A-D) Flow cytometry was performed on splenocytes from C57Bl/6 mice inoculated with B16-Flt3l secreting cells, analysing the rate of protein synthesis in cDC1s **(A,B)** and cDC2s **(C,D)**. The protein synthesis rate was determined by administering puromycin to splenocytes and measuring incorporation into polypeptide chains by flow cytometry. Mice were stimulated by intravenous injection with 50μg/kg CpG-B for the indicated times prior to flow cytometry analysis. Data are representative **(A,C)** or mean +/-SEM of three biological replicates **(B,D)**. Data were analysed using one-way ANOVA followed by Tukey's multiple comparisons post-test. (*p<0.05, **p<0.01)

3.5 Discussion

cDCs are the primary antigen-presenting cells of the immune system, acting as a critical bridge between innate and adaptive immunity. Two primary subsets of cDCs, cDC1s and cDC2s, have been identified to have preferential capabilities to promote different adaptive immune responses. cDC1s have a superior ability to prime CD8 T cells, while cDC2s are more efficient in priming CD4 T cells (Cabeza-Cabrerizo et al., 2021). The mechanisms underpinning this division of labour are still not fully understood. The aim of Chapter 3 was to investigate the molecular basis of cDC function by examining the cellular proteome of cDC1s and cDC2s. Over a decade ago, a landmark study from Luber et al. demonstrated for the first time the potential of utilising high-resolution proteomics to study rare cell populations (Luber et al., 2010). This study examined proteomic features of splenic cDC1s and cDC2s, identifying essential viral recognition proteins to be exclusively expressed in cDC2s. While this current study is not the first attempt at such an approach, due to the advancement in mass spectrometry technology and protein quantification methodologies, my research presented in this chapter adds a new level of detail in determining the proteome of cDCs.

This study provides greater protein quantification depth, quantifying the abundance of approximately 6700 proteins in both cDC1s and cDC2s, while Luber et al. report the expression of approximately 5700 proteins (Luber et al., 2010). In addition, a distinct advantage of this study is the absolute quantification of protein copy number per cell as estimated by the proteomic histone ruler (Wiśniewski et al., 2014). This methodology allows the quantification of protein concentration and copy number per cell without the requirement for isotope-labelled spike-in references, cell counting and protein concentration measurements, thus reducing the number of error-prone steps and increasing the accuracy of quantification. Earlier proteomic studies compared MS signal intensity, which limits analysis to relative quantification between samples. Absolute protein quantification allows a more detailed analysis of proteome architecture, including the distribution of proteins into subcellular compartments and stoichiometric analysis of protein complexes.

This study provides for the first time a global characterisation of cDC proteomes.

Due to the rarity of cDCs, I used a DC expansion model to acquire enough cells to perform proteomic analysis by inoculating mice with B16-Flt3-secreting melanoma cells, which expands the DC compartment *in vivo* (Mach et al., 2000). This approach limited the number of mice required, thus refining the experimental approach and reducing experimental noise associated with pooling large numbers of mice. The benefit of this approach is demonstrated by the high degree of similarity between biological replicates in cDC1s and cDC2s, increasing the reliability and statistical power of the study. As previously reported, B16-Flt3l inoculation disproportionately increased the number of cDC1s relative to cDC2s (Mach et al., 2000). In light of this observation, it was important to ensure that B16-Flt3l treatment did not specifically impact the maturation status of cDC1s and cDC2s, which would affect the reliability of subsequent analysis. cDCs from B16-Flt3l mice had an equivalent expression of costimulatory markers in both cDC1s and cDC2s. Further, costimulatory marker expression was unchanged between mice with and without B16-Flt3l expansion, indicating that tumour inoculation did not induce DC maturation.

Numerous studies have investigated the relationship between mRNA transcript abundance and protein expression in murine and human cells (Ghazalpour et al., 2011; Gunawardana & Niranjan, 2013; Hukelmann et al., 2016). The general conclusion of these studies is that the transcriptome correlates poorly with actual protein abundance. For example, a study from the Cantrell lab analysed the relationship between the transcriptome and proteome of cytotoxic T lymphocytes (CTLs), finding a moderate positive correlation between mRNA abundance and protein abundance, with a coefficient of determination of 0.43 (Hukelmann et al., 2016). This observation aligns closely with both cDC1s and cDC2s, which had coefficients of determination of 0.43 and 0.42, respectively. This finding suggests substantial post-transcriptional regulatory mechanisms controlling gene expression in cDCs. Examples of discordance between mRNA abundance and protein

abundance include the finding that nutrient transporter expression is enriched at the mRNA level while proteasome expression is enriched at the protein level. There was a close correspondence between transcript abundance and protein abundance for some proteins, including DC phenotype markers and ribosomal proteins. Nevertheless, these data highlight the importance of direct measurement of protein, rather than measurement of the mRNA as a surrogate, for estimation of protein expression.

Investigating global proteome features between steady-state cDC subsets revealed substantial differences in the proteome architecture. cDC1s have a significantly higher total protein content than cDC2s, reflected in their larger cell size as determined by flow cytometry. Analysis of the composition of the cDC proteomes reveals that in both subsets, a small number of highly abundant proteins account for the majority of the total protein content of the cells. The abundance of these proteins is reflected by their roles in fundamental cellular processes, including DNA packaging, cellular organisation and protein synthesis. Importantly, the abundance of histone proteins used in the normalisation process of the proteomic histone method to calculate protein copy numbers is equivalent in cDC1s and cDC2s (Wiśniewski et al., 2014). This indicates that the difference in total protein content observed between cDC subsets does not result from bias in the normalisation process. Notably, while 35 proteins account for 50 per cent of the total protein content in cDC1s, only 18 highly abundant proteins make up this percentage in cDC2s. This indicates that the difference in total protein content between cDC1s and cDC2s is not solely related to the abundance of highly expressed “housekeeping” proteins.

Investigation of the distribution of proteins into subcellular compartments reveals insights into the location of the enriched proteins in cDC1s. While both subsets have a similar distribution of proteins associated with the plasma membrane, mitochondria, nuclear envelope and lysosome, cDC1s have significantly more proteins associated with the endoplasmic reticulum than cDC2s. This finding aligns with reports that cDC1s but not cDC2s have active ER stress signalling in the absence of ER stressors via the IREa-XBP1

signalling axis, which supports the ability of cDC1s to cross-present antigens (Osorio et al., 2014; Tavernier et al., 2017). In agreement with these findings, IRE1a expression was only detected in cDC1s. Genetic ablation of IRE1a in $CD11c^+$ cDCs has led to a dysregulated ER compartment in cDC1s but not cDC2s (Osorio et al., 2014). As IRE1a-mediated XBP1 signalling promotes the expression of ER proteins to manage increased protein folding requirements, it is plausible that the reported basal IRE1a activity in cDC1s accounts for the enrichment of ER proteins. This hypothesis is further supported by a study in pDCs, which also have constitutive XBP1 splicing in the steady-state and an expanded ER compartment, which is proposed to support the ability to manage the rapid increase in biosynthetic demand associated with type-I interferon production (Iwakoshi et al., 2007).

Differential expression analysis of cDC1 and cDC2 protein abundance in the steady-state reveals many statistically significant upregulated proteins in cDC1s versus cDC2s. This bias in cDC1s reflects the overall protein abundance in cDC1s and cDC2s. While normalising the protein copy number to the total protein content of the cell (protein concentration) corrects this bias, the copy number is a more accurate reflection of the actual biological state of the cell. For example, the concentration of proteins associated with the mitochondria is equivalent in cDC1s and cDC2s. However, flow cytometry analysis reveals that cDC1s have a significantly higher mitochondrial mass than cDC2s. Accordingly, the copy number per cell of proteins associated with the mitochondria is significantly higher in cDC1s than in cDC2s. The difference in total protein abundance between cDC subsets highlights the importance of protein scaling versus enrichment, which may affect the interpretation and functional relevance of protein quantification studies (Howden et al., 2019).

Gene set enrichment analysis of the significantly upregulated proteins in cDC1s identifies an enriched signature for pathways associated with protein biosynthesis, protein processing in the ER and metabolic pathways. This anabolic signature, exemplified by a global enrichment of ribosomal proteins and significantly higher expression of the 5’ translation initiation complex,

indicates that cDC1s either engage in or have the capacity for higher rates of protein biosynthesis than cDC2s. In fact, cDC1s have significantly higher rates of protein biosynthesis in the steady state as determined by puromycin labelling of nascent polypeptide chains. This finding aligns with the expanded ER compartment described, which would be required to handle the elevated protein folding demand associated with higher rates of protein biosynthesis. Further, this elevated rate of protein synthesis also likely accounts for the higher total protein content observed in cDC1s. In addition to having chronic IRE1a signalling in the steady-state, a report by Mendes et al. shows that cDC1s also have high rates of EIF2a phosphorylation as a result of chronic PERK signalling, even in the absence of putative ER stress signals (Mendes et al., 2021). This study also identifies elevated rates of protein biosynthesis in steady-state cDC1s. An apparent contradiction arises from observing parallel EIF2a phosphorylation alongside elevated protein synthesis rates, as phosphorylated EIF2a should inhibit translation initiation. This is addressed by Mendes et al., who propose that the escape of PERK-mediated translation inhibition is primarily attributed to the high abundance of the translation initiation factors EIF2a and EIF2b in cDCs, which is sufficient to counteract excessive EIF2a phosphorylation maintaining active translation during chronic ER stress (Mendes et al., 2021). The underlying mechanism driving chronic ER stress signalling in cDC1s is currently unknown. Considering that the accumulation of unfolded proteins in the ER activates ER stress signalling, the higher steady-state translation rate in cDC1s may provide an ER protein folding load conducive to the induction of chronic low-level ER stress activation. This hypothesis naturally raises the question of how (Eg. anabolic signalling) and why cDC1s maintain elevated rates of protein biosynthesis in the steady state.

While DCs have been reported to increase their protein synthesis rate in response to immunogenic stimulation, likely to facilitate the increased biosynthetic demand associated with DC maturation, the implication of a higher rate of protein synthesis in the steady state is unclear (Argüello et al., 2020; Lelouard et al., 2007). As protein synthesis is an highly energy-demanding process, it would be highly inefficient for cDC1s to maintain

elevated rates if it served no biological function. One possibility may relate to the specialisation of cDC1s in presenting endogenous antigens on MHCI. During development, CD8 T cells are educated in the thymus to recognise self-MHCI molecules presenting self-peptides. T cells with high affinity for self-peptides are deleted or undergo functional inactivation (anergy). Peripheral tissues express self-antigens, reinforcing tolerance by providing ongoing exposure to self-antigens (B. V. Kumar et al., 2018). Considering that the cellular MHCI peptidome reflects the proteins synthesised by that cell, the elevated protein synthesis rates in cDC1s may contribute to peripheral tolerance by maintaining a broad peptide repertoire for MHCI presentation (Rock et al., 2014). However, this appears unlikely, considering that all nucleated cells present self-antigens via MHCI and the rarity of both cDC1s and antigen-specific CD8 T cells in vivo. Indeed, a study by Macnabb et al. shows that genetic deletion of cDC1s in vivo has a negligible role in mediating CD8 T cell tolerance (MacNabb et al., 2019).

An alternative hypothesis relates to generating antigens in response to viral infection or treatment with mRNA vaccines. There is a discordance between the observed antigen presentation rate and the predicted antigen production rate when cells become virally infected (Yewdell et al., 1996). The presentation of viral antigens is a function of the half-life of viral proteins synthesised by the host cell. While the predicted half-life of viral proteins is approximately 24 hours, viral antigens are detected much earlier (Qian et al., 2006). This discordance was resolved by the identification of defective ribosomal products (DRiPs), proteins which are partially synthesised and immediately targeted for proteasomal degradation. The generation of DRiPs provides a mechanism to rapidly generate antigens, enhancing the kinetics of the anti-viral response. While the quantity of newly synthesised proteins for DRiP production remains controversial, ranging from 5% to 30% of nascent peptide chains, this mechanism directly links the rate of protein synthesis to antigen production (Princiotta et al., 2003). Thus, it is plausible that the enhanced steady-state protein biosynthesis observed in cDC1s allows the rapid generation of antigens in accordance with their described role as the preferential inducers of CD8 T cell responses.

In alignment with previous reports that cDC1s are more metabolically active than cDC2s in the steady state, the proteomic data reveals a distinct enrichment of metabolic proteins in cDC1s (X. Du et al., 2018; Pelgrom et al., 2022). In particular, cDC1s have significantly more mitochondrial proteins, reflected in their higher mitochondrial mass. In addition, analysis of mitochondrial membrane potential indicates that mitochondrial metabolism is more active in cDC1s than cDC2s. As protein synthesis is the most metabolically demanding cellular process, accounting for approximately 45% of the total ATP demand of a cell, it is perhaps no surprise that cDC1s are more metabolically active (Buttgereit & Brand, 1995b). In agreement with the enhanced rates of mitochondrial metabolism, SCENITH analysis confirms the higher reliance on mitochondrial ATP in cDC1s to maintain translation. A report by Du et al. identified the Hippo/Mst signalling axis acts as a molecular driver of mitochondrial metabolism in cDC1s, controlling both mitochondrial mass and dynamics, which was required for cDC1 IL-12 production and the effective induction of cDC1-mediated $CD8^+$ T cell responses (X. Du et al., 2018).

In addition to higher mitochondrial dependency, the SCENITH analysis identified a higher requirement for glutaminolysis-derived ATP to maintain translation in cDC1s. In agreement, cDC1s have significantly higher expression of the glutamine transporter SLC1A5 than cDC2s. Interestingly, a recent study by Guo et al. identified that tumour-infiltrating cDC1s are sensitive to limited glutamine availability in the tumour microenvironment (Guo et al., 2023). The authors demonstrate that glutamine competition between cDC1s and tumour cells mediated by the SNAT transporter, SLC38A2, is a metabolic checkpoint in cDC1 but not cDC2 function. Notably, SLC38A2 is lowly expressed in both splenic cDC subsets, particularly relative to SLC1A5. This potentially suggests different glutamine uptake mechanisms between lymphoid resident and tumour-infiltrating cDCs. Indeed, it is also possible that SLC38A2 expression is induced under a limiting concentration of extracellular glutamine.

Upon immunogenic stimulation, DCs undergo maturation, characterised by increased costimulatory marker expression and the production of cytokines to induce adaptive immune responses (Cabeza-Cabrerizo et al., 2021). This study characterises for the first time the proteomic remodelling associated with DC maturation in response to TLR9 ligation, mimicking an antiviral response. Differential expression analysis between steady-state and CpGB-stimulated cDCs shows low levels of proteomic remodelling during maturation, with only 4% and 5% of proteins significantly changing in abundance in cDC1s and cDC2s, respectively. As expected, DC maturation led to the upregulation of costimulatory markers and inflammatory signalling proteins in both cDC1s and cDC2s. Notably, GSEA analysis of significantly upregulated proteins in cDC1s and cDC2s was dominated by pathways associated with anti-viral responses and interferon regulation. In particular, interferon-stimulated genes (ISGs) were highly enriched in both cDC1s and cDC2s, indicating IFNAR-mediated signalling. Indeed, a study from Asselin-Paturel et al. showed that cDC maturation *in vivo* highly depends on IFNAR signalling in response to CpG but not LPS stimulation. It was shown that the majority of IFN produced in response to CpG treatment arose from pDCs rather than cDCs (Asselin-Paturel et al., 2005). Thus, the paracrine production of interferons by pDCs in response to CpG treatment leading to IFNAR induction in cDCs likely explains the proteomic phenotype observed.

Numerous studies have identified that metabolic reprogramming is a characteristic feature of DC maturation (Guo & Chi, 2023; Møller et al., 2022; Wculek et al., 2019). Most studies investigating DC metabolism have used *in vitro*-generated bone marrow dendritic cells. While these models have been a valuable resource for interrogating DC immunometabolism, it is now appreciated that they may not accurately reflect that of natural DCs (Helft et al., 2015; Mayer et al., 2014). Interestingly, pathway analysis of mitochondrial proteins in response to CpG-B stimulation shows that there is a general downregulation of processes that catabolise nutrients for mitochondrial ATP production, including fatty acid oxidation and branched-chain amino acid (BCAA) catabolism in both cDC1s and cDC2s. Strikingly, CpG-B stimulation leads to a global reduction in the expression of proteins associated with the

electron transport chain (ETC) complexes. These data suggest a general repression in mitochondrial metabolism in mature cDC1s and cDC2s. Studies in GMDCs have shown that DC maturation *in vitro* is associated with repressed mitochondrial function occurring after eight hours of stimulation (Everts et al., 2012, 2014). This effect is attributed to nitric oxide (NO) production by macrophage-like cells within the GMDC culture system (Helft et al., 2015; Thwe & Amiel, 2018). Natural DCs do not express inducible nitric oxide synthase (iNOS), so they cannot produce NO endogenously. Thus, it is unlikely that NO production is interfering with cDC metabolism in this system. Additionally, considering that NO inhibits mitochondrial respiration by interfering with complex four activity, this does not explain the global reduction in the expression of ETC proteins (Giuffrè et al., 1996).

A study from Pantel et al. investigated the role of IFNAR signalling in cDCs in response to *in vivo* PolyI:C stimulation (Pantel et al., 2014). This study revealed that PolyI:C induced transcriptional repression of mitochondrial proteins, including proteins involved in oxidative phosphorylation, which was reversed in mice lacking the expression of the IFNAR. This suggests that interferon signalling negatively regulates mitochondrial metabolism in cDCs. Notably, IFNAR-mediated mitochondrial repression has also been reported in macrophages responding to mycobacterial infection (Olson et al., 2021). Considering the strong ISG signature in cDCs in response to CpG-B stimulation, the repressed mitochondrial proteome in cDCs may result from IFNAR-mediated signalling.

Overall, proteins involved in intermediary metabolism were not significantly enriched in cDC1s or cDC2s in response to CpG-B stimulation. For example, in addition to the repressed mitochondrial phenotype observed, there was no apparent upregulation of glycolytic proteins. Although glucose and lactate transports showed a moderate increase in expression upon stimulation, possibly suggesting an increase in aerobic glycolysis, the magnitude of this change was small. In total, these data do not indicate that cDCs are very metabolically active 18h after *in vivo* CpG-B stimulation. Indeed, the protein synthesis rate of cDCs, a good parameter for ATP demand at this later time

point, is lower than that of steady-state cDCs. This observation aligns with the findings of Leluoard et al., who show that BMDC undergoes enhanced protein synthesis upon LPS stimulation, which peaks 8h after stimulation and returns to below baseline after 18h of stimulation (Lelouard et al., 2007). Thus, it is likely that metabolic rewiring is a feature of early cDC activation, which becomes more quiescent after prolonged stimulation. Whether this metabolic repression is related to the interferon response still needs to be determined.

Chapter 4 – SLC7A5-mediated amino acid uptake controls mTORC1 signalling in cDC subsets

4.1 Introduction

Amino acids are the fundamental building blocks of protein synthesis and contribute to many intracellular metabolic pathways, including ATP generation, nucleotide synthesis and redox balance to support cellular function (Kelly & Pearce, 2020). As immune cell function depends on these pathways, amino acids have emerged as critical regulators of cellular function. Plasma membrane transporters mediate amino acid acquisition from the extracellular environment. As such, the repertoire of transporters expressed by a cell reflects its nutrient requirements. Accordingly, immune cells reconfigure their transporter expression during metabolic reprogramming to meet these metabolic demands (Howden et al., 2019; Marchingo et al., 2020). It has been shown that within the TME, amino acids are not equally available to all cells (Reinfeld et al., 2021). Indeed, recent evidence suggests that amino availability and uptake through Slc38a2 controls cDC1 function (Guo et al., 2023). This is the first evidence that amino acid transporter expression regulates cDC subset-specific function. However, a detailed characterisation of the expression of amino acid transporters in cDC subsets is currently lacking. Thus, this Chapter aims to characterise the amino acid transporter repertoires of cDC1 and cDC2s to identify subset-specific regulators of function.

In addition to supporting protein synthesis, amino acids directly modulate metabolic reprogramming through mTORC1 and cMYC. While cMYC is repressed during cDC development (Kc et al., 2014), mTORC1 has been extensively studied in regulating DC metabolism and function (Møller et al., 2022; Snyder & Amiel, 2019). mTORC1 controls DC development and has been shown to promote pro-inflammatory and anti-inflammatory responses in DCs. However, how amino availability regulates mTORC1 function in cDCs is currently unknown. To address this, Chapter 4 investigates the relationship between amino acid uptake and mTORC1 signalling in cDC1s and cDC2s.

4.2 cDC1s have an enrichment of amino acid transporter expression relative to cDC2s

Amino acid transporter expression is a critical metabolic checkpoint in regulating immune cell function (Kelly & Pearce, 2020). However, the abundance of amino acid transporters and their functional relevance in cDCs have yet to be determined. Amino acid transport in mammalian cells is mediated by >60 different transporters that are primarily members of the solute carrier (SLC) family of proteins (Gauthier-Coles et al., 2021). These are distributed into different groups depending on their mode of action (Uniport, symport, antiport) and the nature of the substrates they transport (Cationic, neutral). To determine the amino acid transporter expression in cDC subsets, I performed quantitative proteomics on cDC1s and cDC2s. This analysis shows that both cDC1s and cDC2s express a limited number of amino acid transporters, including members of the ASCT, CAT, SNAT, LAT and y^+LAT transporter families **(Fig. 4.1 A,B)**. The sodium-dependent neutral amino acid transporter, Slc1a5, and the LNAA transporter, Slc7a5, are the most abundant transporters in cDC1s and cDC2s. Interestingly, while both cDC1s and cDC2s express the same amino acid transporters, differential expression analysis reveals that cDC1s have a general enrichment of amino acid transporters relative to cDC2s **(Fig. 4.2 A)**. As amino acids are the building blocks of protein synthesis, this observation aligns with the finding in Chapter 3 that cDC1s maintain higher rates of protein synthesis than cDC2s in the steady state. Significantly enriched transporters in cDC1s include the Slc1a5 and Slc38a2, which primarily mediate glutamine uptake, Slc7a5, which mediates neutral amino acid uptake and Slc7a1, which uptakes cationic amino acids, including arginine **(Fig. 4.2 B)**.

Amino acid uptake through Slc1a5 and Slc7a5 has been described to control the metabolic reprogramming associated with highly proliferative cells, including blasting lymphocytes and malignant cells (Marchingo et al., 2020; Nachef et al., 2021; Nakaya et al., 2014). To investigate whether elevated transporter expression in cDC1s directly relates to differences in amino acid uptake, I utilised single-cell nutrient uptake assays to determine amino acid uptake in cDC1s and cDC2s. A recent publication from the Finlay lab and

collaborators shows that the non-natural amino acid homopropargylglycine (HPG) is a transport substrate for Slc1a5 (Pelgrom et al., 2022). HPG is a methionine analogue that contains a reactive alkyne group not present within other biomolecules within the cell **(Fig. 4.3 A).** The presence of the alkyne reactive group facilitates the copper-catalysed "click chemistry" cycloaddition of a fluorophore after HPG has been transported into the cell by Slc1a5 **(Fig. 4.3 B)**. Thus, HPG fluorescence is directly proportional to the rate of uptake by Slc1a5. To determine whether HPG is actively transported in cDC1s, I stained splenocytes with surface markers prior to treatment HPG (200μM) for 2 minutes at either 37°C or 4°C, followed by fixation and copper-click addition of azide-AF488 **(Fig. 4.3 C)**. At 4°C, HPG uptake is significantly inhibited, indicating that it is actively transported into cDC1s. Further, HPG uptake in the presence of increasing concentrations of the Slc1a5 substrates glutamine **(Fig. 4.4 A)** and alanine **(Fig. 4.4 B)** effectively outcompete HPG uptake in cDC1s, indicating the specificity of the assay. In line with the enhanced Slc1a5 expression observed in cDC1s, a comparison of HPG uptake in cDC1s and cDC2s shows that cDC1s have significantly higher Slc1a5 mediated amino acid transport relative to cDC2s **(Fig. 4.5 A,B)**.

To catalyse amino acid uptake, SLC7A5 forms a heterodimer with CD98 (Slc3a2). Proteomic and flow cytometry analysis confirms the expression of both SLC7A5 and CD98 in cDC1s and cDC2s **(Figure 4.6).** In line with the enhanced biosynthesis observed, cDC1s have higher expression of CD98 **(Fig 4.6 A-C)** and SLC7A5 **(Fig 4.6 D)** than cDC2s**.** To confirm SLC7A5 activity in cDCs, I performed a kynurenine uptake assay by flow cytometry. Kynurenine is a metabolite substrate for system-L amino acid transporters (LAT1-4), which fluoresces when excited by the 450nm laser of the flow cytometer (L. V. Sinclair et al., 2018). As SLC7A5 is the only system-L transporter expressed by cDC1s and cDC2s **(Fig. 4.1 A,B),** the rate of kynurenine uptake is proportional to SLC7A5 activity. To confirm the specificity of kynurenine uptake, I treated splenocytes with the SLC7A5 inhibitor BCH or with a saturating concentration of a competing SLC7A5 substrate, in this case, leucine. Both BCH treatment and leucine competition

effectively inhibit kynurenine uptake in cDC1s **(Fig 4.7 A,B)** and cDC2s **(Fig 4.7 C,D)**. By contrast, treating splenocytes with a saturating concentration of lysine, which is not a SLC7A5 substrate, has no impact on kynurenine uptake. Thus, the rate of kynurenine uptake is an effective measure of SLC7A5 activity in cDCs. To investigate whether the higher expression of the SLC7A5 heterodimer in cDC1s results in enhanced activity, I compared the rate of kynurenine uptake in cDC1s and cDC2s **(Fig 4.8 A,B)**. In accordance, steady-state cDC1s have higher kynurenine uptake than cDC2s.

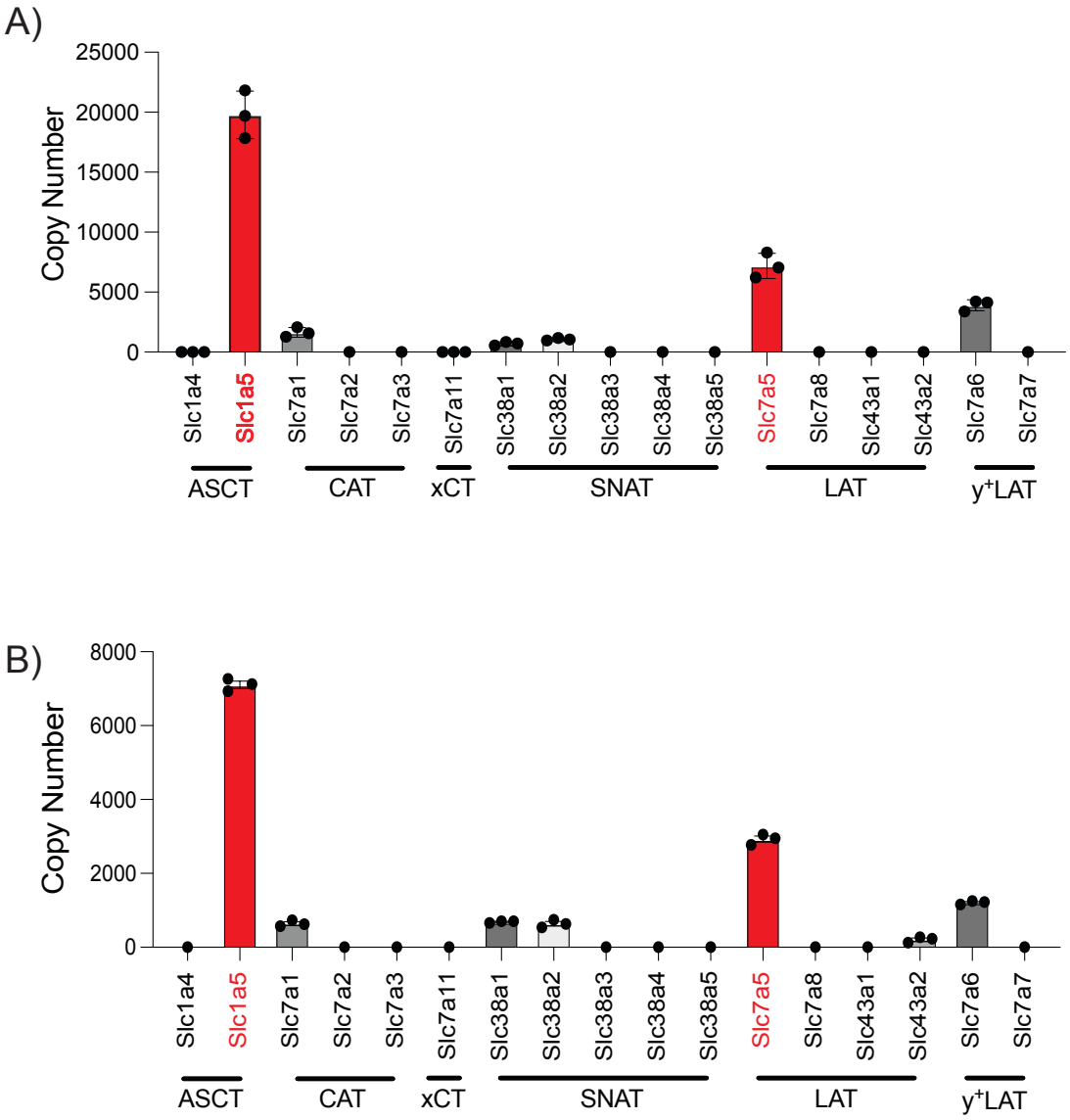

Figure 4.1 – Amino acid transporter expression in splenic cDC subsets
(A,B) Quantitative proteomic analysis was performed on splenic cDC1s and cDC2s from C57Bl/6 mice inoculated with B16-Flt3l cells, analysing the abundance of amino acid transporters. Copy number per cell of amino acid transporters in **(A)** cDC1s and **(B)** cDC2s. Data are mean +/- SEM of three independent experiments.

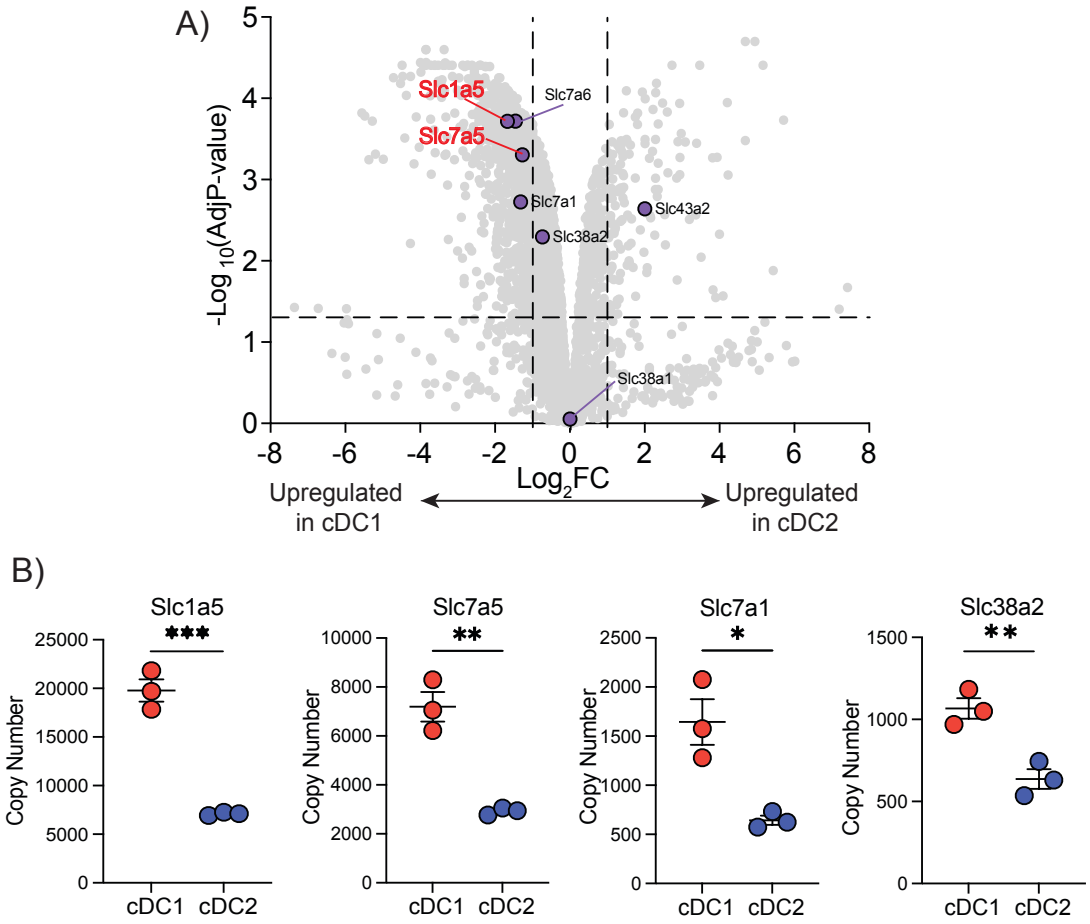

Figure 4.2 – cDC1s in the steady state have an enrichment of amino acid transporters compared to cDC2s

(A,B) Quantitative proteomic analysis was performed on splenic cDC1s and cDC2s from C57Bl/6 mice inoculated with B16-Flt3l cells, analysing the relative abundance of amino acid transporters. **(A)** Differential expression analysis of amino acid transporters in cDC1s and cDC2s. The volcano plot represents the Log_2 fold change (X-axis) versus the $-Log_{10}$ adjusted P-Value. The vertical broken lines indicate a Log_2 fold change >1 or <-1, and the horizontal broken line indicates an adjusted P-value <0.05. **(B)** Copy number per cell of amino acid transporters in cDC1s and cDC2s. Data are presented as mean +/- SEM of three independent experiments **(B)**. Data were analysed using paired students' t-tests (*p<0.05, **p<0.01, ***p<0.001)

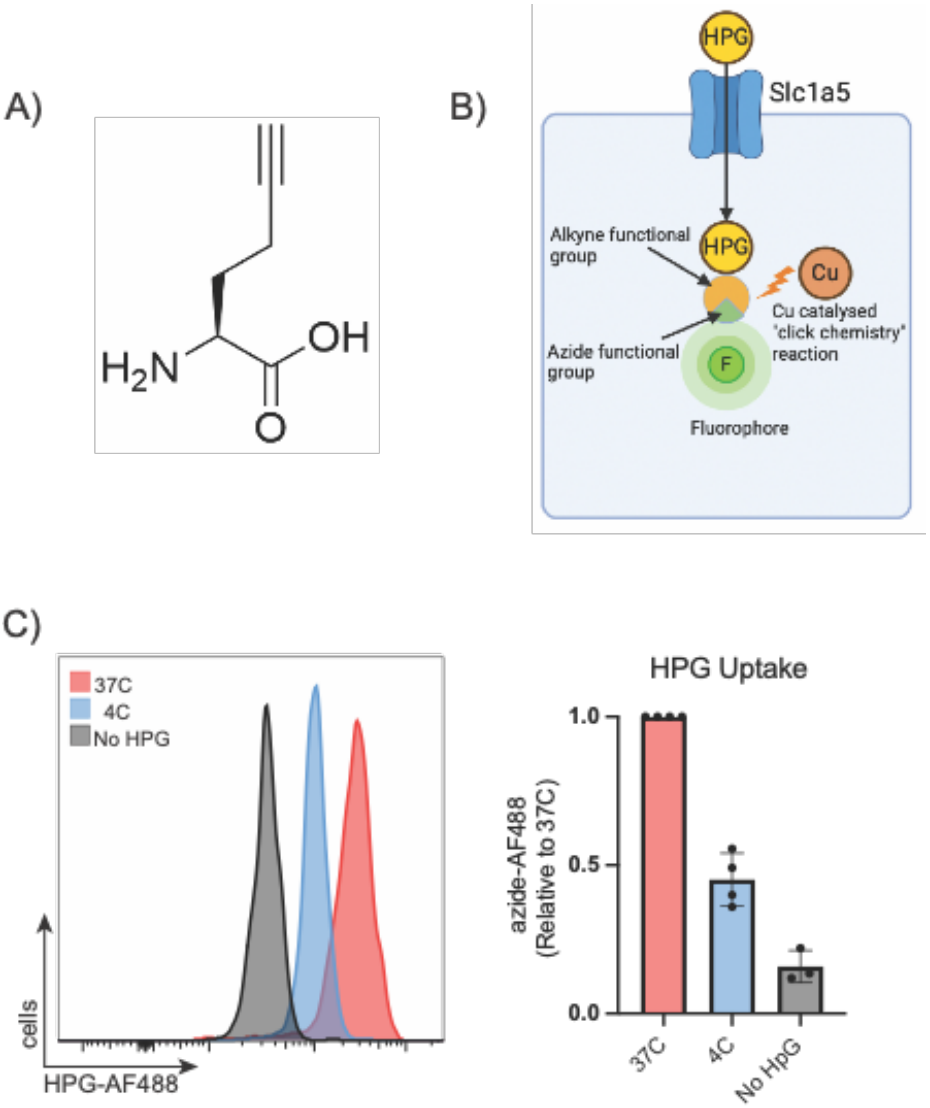

Figure 4.3 – The non-natural amino acid homopropargylglycine (HPG) is actively transported into cDC1s

(A-C) Flow cytometry analysis of splenocytes from C57Bl/6 mice inoculated with B16-Flt3l cells analysing the uptake of HPG into cDC1s. Splenocytes were stained with surface antibodies prior to 2 min HPG (200μM) uptake at either 37°C or 4°C, followed by fixation and copper-click addition of azide-AF488. **(A)** Chemical structure of HPG. **(B)** Illustration of HPG uptake and ligation of AF-488 by copper-click addition. **(C)** Representative histogram (left) and pooled data (right) of HPG-AF488 fluorescence in $MHCII^{high}$, $CD11c^{+}$, $XCR1^{+}$ cDC1s. Data are representative **(C)** (left) or mean +/- SEM of at least three independent experiments **(C)** (right). Pooled data are presented as MFI relative to 37°C condition. Data were analysed using one-sample t-tests against a theoretical value of 1. (**p<0.01)

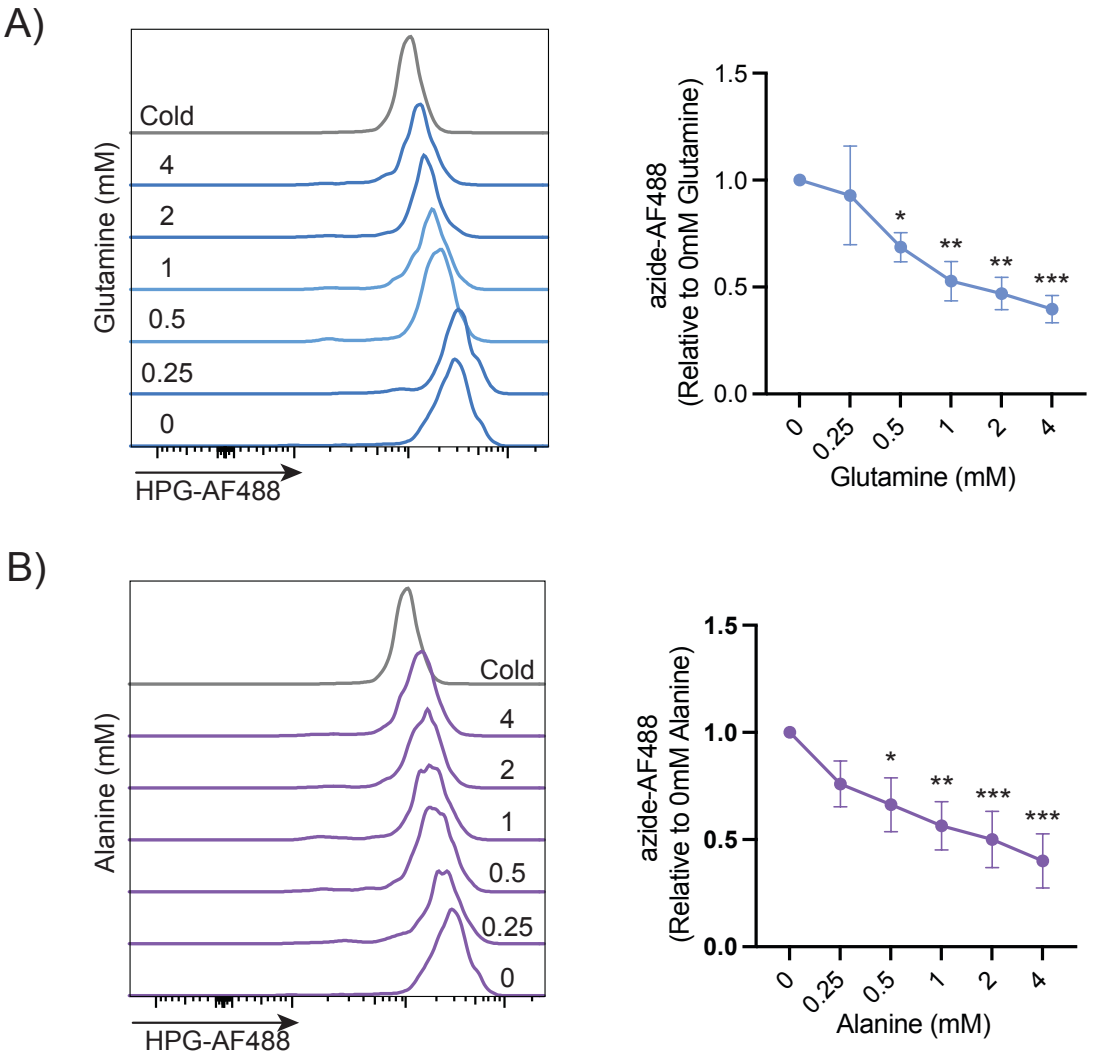

Figure 4.4 – HPG uptake competes with Slc1a5 substrates
(A,B) Flow cytometry analysis of splenocytes from C57Bl/6 mice inoculated with B16-Flt3l cells analysing the uptake of HPG into cDC1s. Splenocytes were stained with surface antibodies prior to 2 min uptake of HPG (200μM) in the presence of increasing concentrations of **(A)** glutamine and **(B)** alanine, followed by fixation and copper-click addition of azide-AF488. Representative histograms **(A,B)** (left) and pooled data (right) of HPG-AF488 fluorescence in the presence of increasing concentrations of glutamine **(A)** and alanine **(B)**. Data are representative (left) or mean +/- SEM of three independent experiments. Data are analysed using multiple one-sample t-tests against a theoretical value of 1. (*p<0.05, **p<0.01, ***p<0.001)

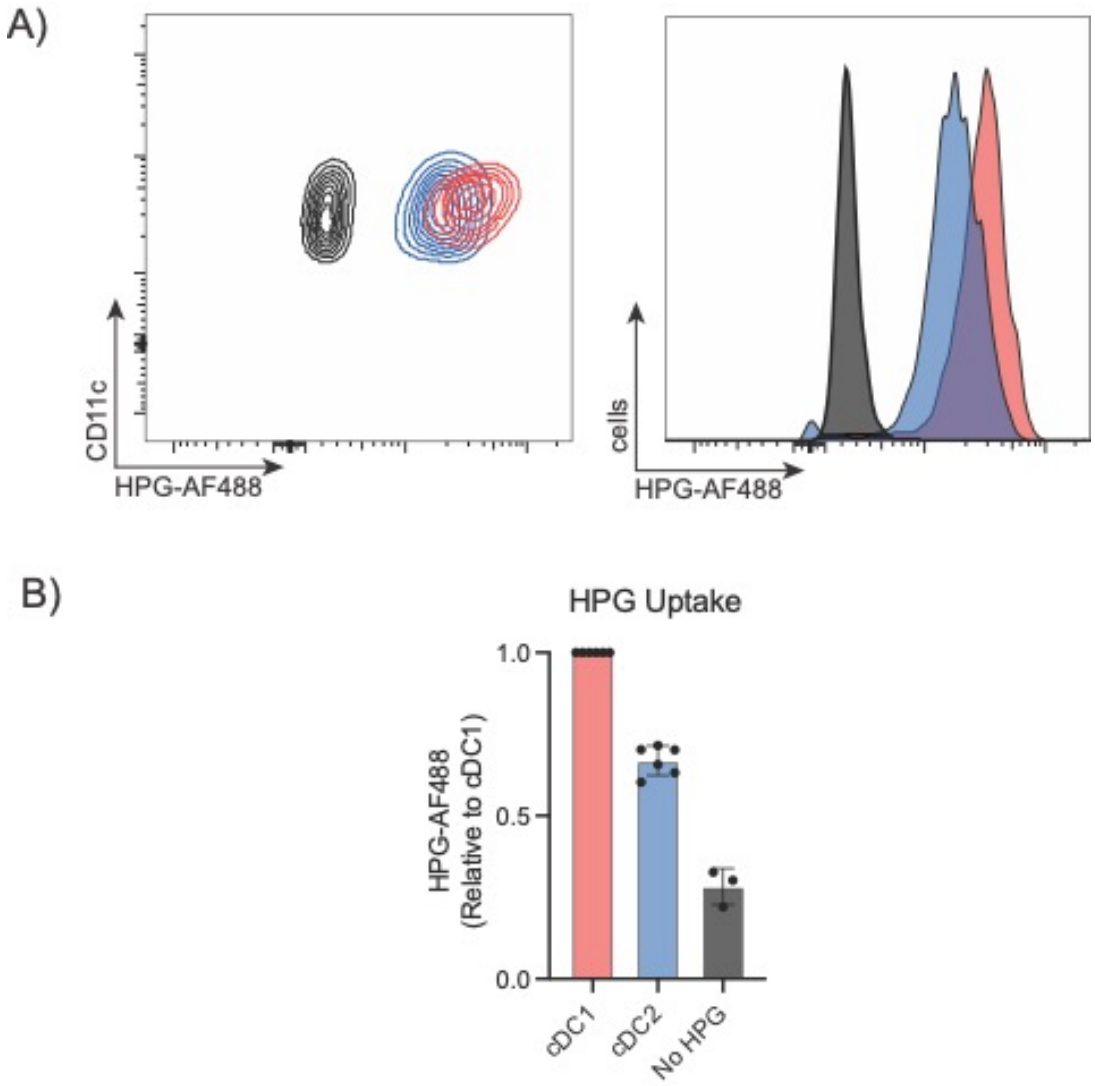

Figure 4.5 – cDC1s have higher HPG uptake than cDC2s in the steady state.

(A,B) Flow cytometry analysis of splenocytes from C57Bl/6 mice inoculated with B16-Flt3l cells analysing the uptake of HPG into cDC1s. Splenocytes were stained with surface antibodies prior to 2 min uptake of HPG (200μM) followed by fixation and copper-click addition of azide-AF488. **(A)** Representative contour plot (left) and histogram (right) of HPG-AF488 fluorescence in cDC1s and cDC2s. **(B)** Pooled data of HPG-AF488 fluorescence in cDC1s and cDC2s. Data are representative **(A)** or mean +/- SEM of at least 3 independent experiments. Pooled data are presented as MFI relative to the cDC1 condition. Data are analysed using a one-sample t-test against a theoretical value of 1. (**p<0.01)

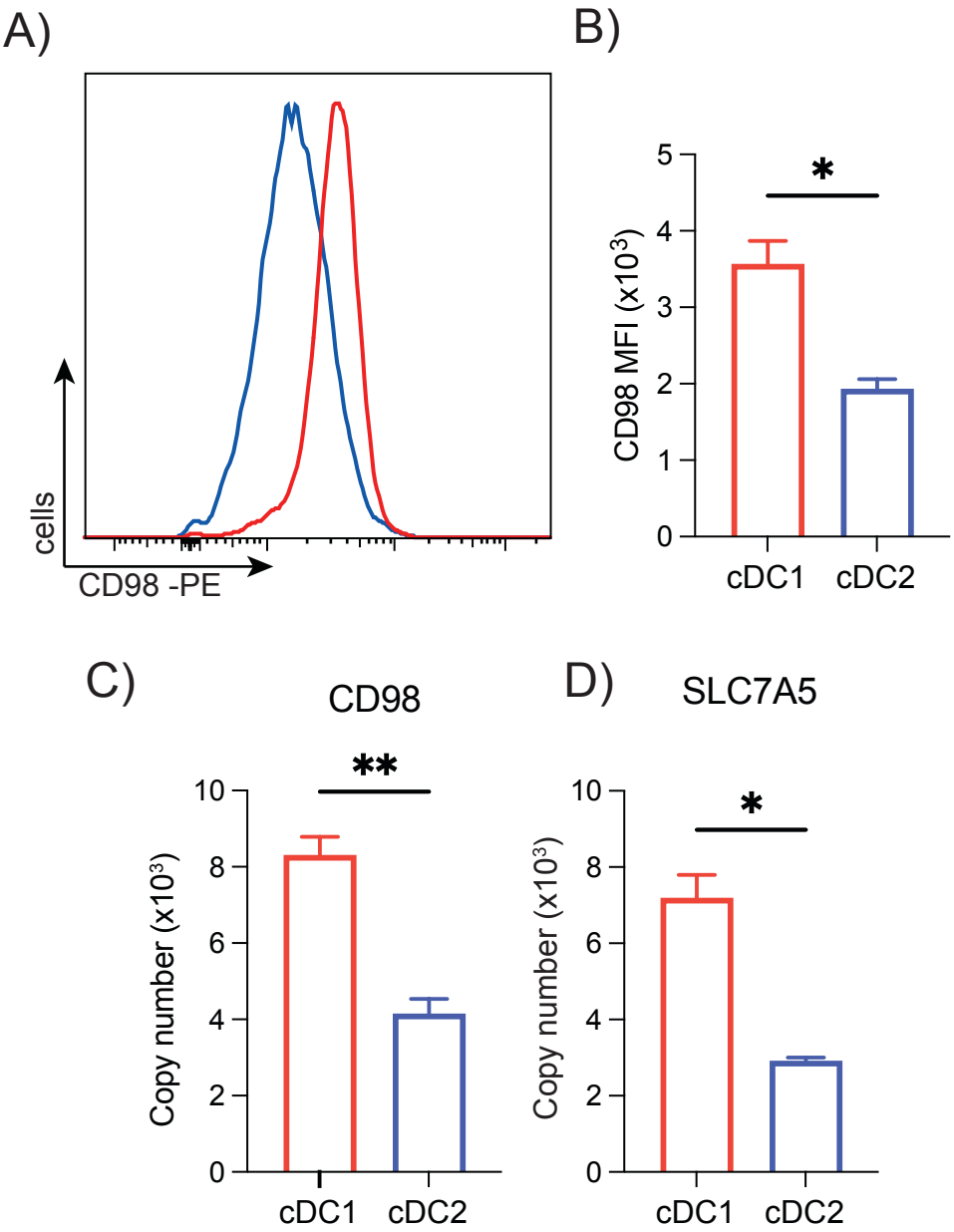

Figure 4.6 – cDC1s have higher expression of the LNAA heterodimer LAT1 than cDC2s

(A,B) Flow cytometry analysis of splenocytes from C57Bl/6 mice inoculated with B16-Flt3l cells analysing the expression of CD98 in cDC1s and cDC2s. **(C,D)** Copy number per cell of the LAT1 heterodimer CD98 **(C)** and SLC7A5 **(D)**. Data are representative **(A)** or mean +/- SEM of **(B)** three biological replicates and **(C,D)** three independent experiments. Data were analysed using paired students' t-tests. (*p<0.05, **p<0.01)

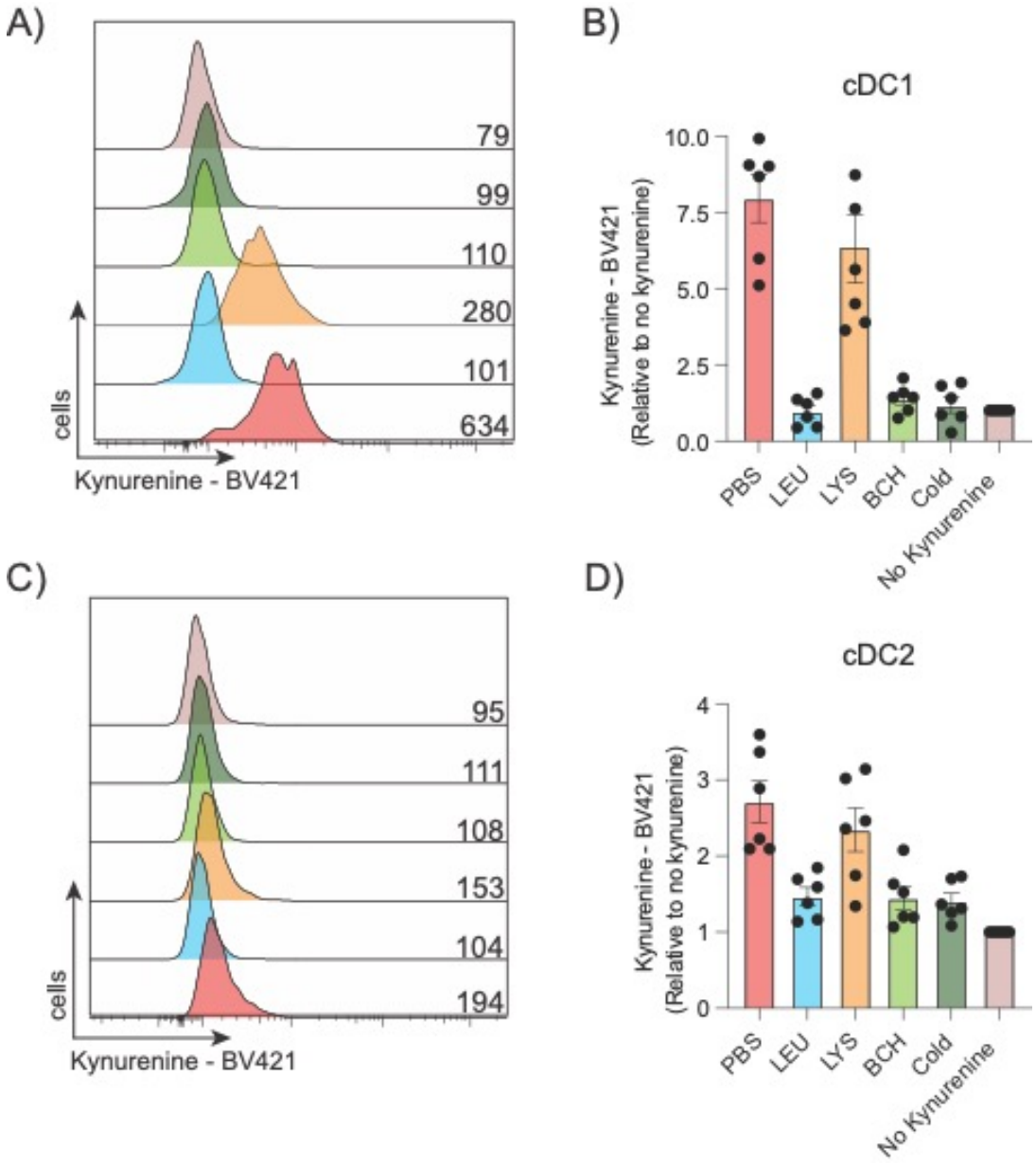

Figure 4.7 – Kynurenine is a transport substrate for SLC7A5 in cDCs
(A-D) Flow cytometry analysis of splenocytes *ex vivo* from C57Bl/6 mice inoculated with B16-Flt3l cells analysing SLC7A5 amino acid transport by monitoring kynurenine uptake. Data are representative **(A,C)** with a cold control (inhibits active transport), leucine competition control (system-L transporters transport leucine), BCH (system-L inhibitor), lysine control (y+L transporters transport lysine) and no kynurenine control (background control). Pooled data is mean +/- SEM **(B,D)** of six biological replicates.

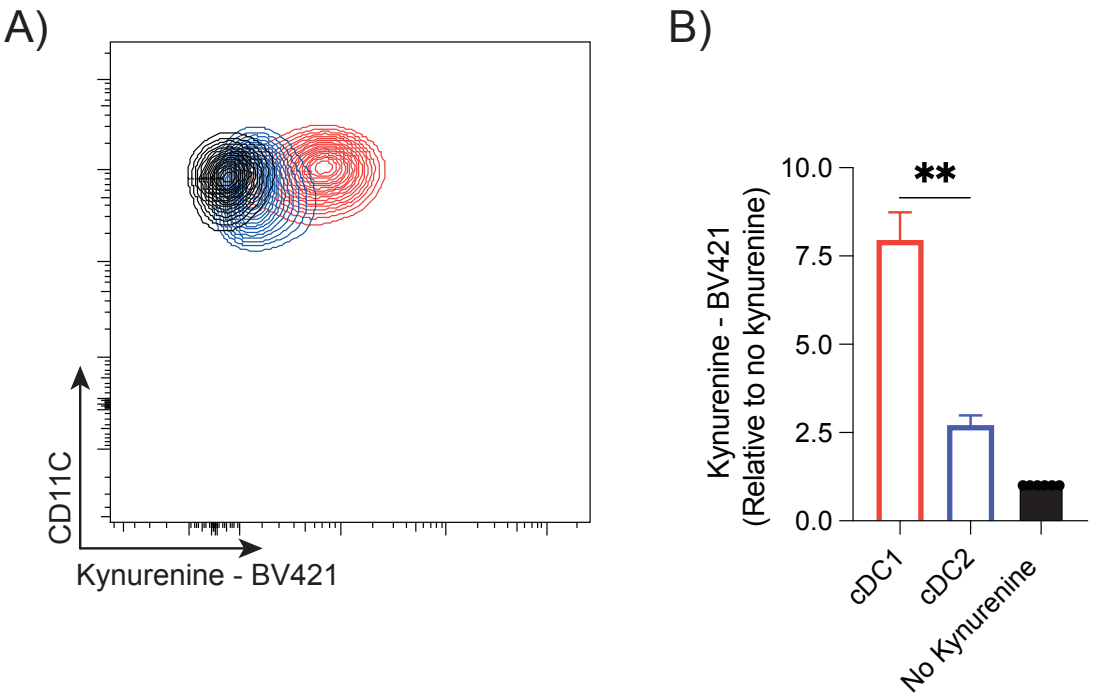

Figure 4.8 – cDC1s have significantly higher SLC7A5 transport activity than cDC2s

(A,B) Flow cytometry analysis of splenocytes *ex vivo* from C57Bl/6 mice inoculated with B16-Flt3l cells analysing SLC7A5 amino acid transport by monitoring kynurenine uptake. Data are representative **(A)** or mean +/- SEM **(B)** of six biological replicates. Data were analysed using one-way ANOVA with Tukey's post-test. (**p<0.01)

4.3 cDC1s in the steady-state have more active mTORC1 signalling than cDC2s.

In Chapter 3, I identified that cDC1s are more metabolically active than cDC2s in the steady state, characterised by higher protein synthesis rates and a greater dependence on mitochondrial metabolism for energy generation. mTORC1 signalling controls the rate of protein translation by phosphorylating proteins involved in regulating translation initiation, including the ribosomal protein S6K1 and the eukaryotic translation initiation factor 4E binding proteins EIF4EBP1 and EIF4EBP2 **(Fig. 4.9 A)**. In line with the higher rate of protein synthesis, cDC1s have a higher protein abundance of the components of the mTORC1 complex than cDC2s **(Fig. 4.9 B)**. Similarly, cDC1s have significantly higher expression of the mTORC1 target S6K1 while there is no significant difference in expression of EIF4EBP2 between subsets. **(Fig. 4.9 C)**. As mTORC1 primarily controls translation by modulating the activity of these target proteins by phosphorylation, I next investigated the phosphorylation levels of these proteins using flow cytometry **(Fig. 4.10)**. Phospho-flow analysis of S6 **(Fig. 4.10 A,B)** and EIF4EBP1/2 **(Fig. 4.10 C,D)** show higher phosphorylation of these proteins in cDC1s than in cDC2s. To confirm that the phosphorylation observed was mTORC1 mediated, I treated the cells with the mTORC1 inhibitor rapamycin, which significantly reduces the phosphorylation of both proteins, confirming the phosphorylation is mTORC1 mediated **(Fig. 4.10 A-D).** To investigate whether mTORC1 signalling regulates protein synthesis in cDCs, I measured protein synthesis using puromycin incorporation into nascent peptide chains by flow cytometry in the presence or absence of rapamycin **(Fig. 4.11)**. Treatment with rapamycin for 1h significantly reduces the protein synthesis rate in cDC1s **(Fig. 4.11 A,B)** and trends downwards in cDC2s **(Fig. 4.11 C,D),** confirming the role of mTORC1 signalling in supporting translation.

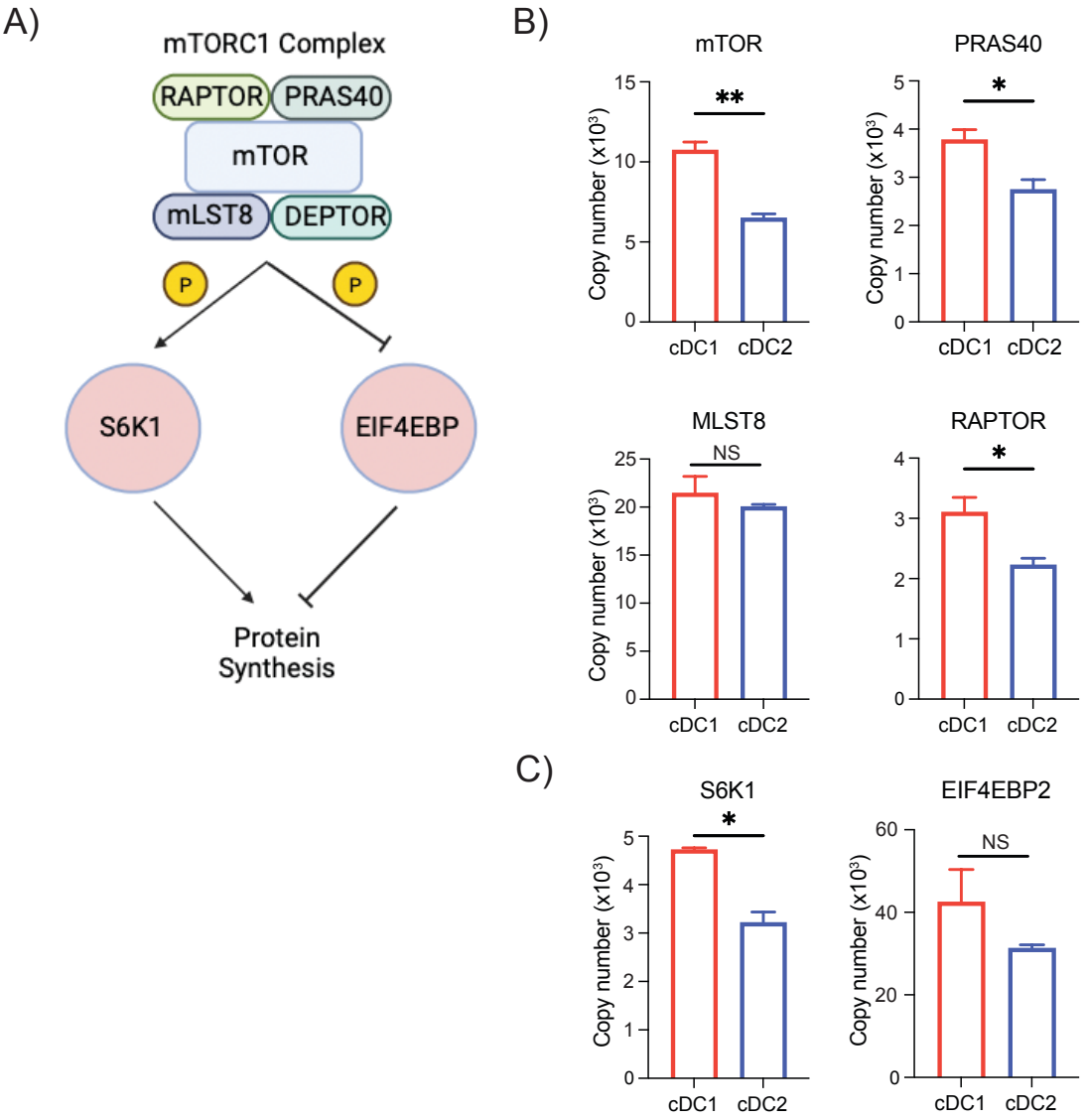

Figure 4.9 – cDC1s have higher expression of the mTORC1 complex than cDC2s

(A-C) Quantitative proteomic analysis was performed on splenic cDC1s and cDC2s from C57Bl/6 mice inoculated with B16-Flt3l cells, analysing the abundance of mTORC1 complex proteins. **(A)** Illustration of the mTORC1 complex subunits and phosphorylation targets that control protein synthesis. **(B)** Copy number per cell of mTORC1 complex proteins in cDC1s and cDC2s. **(C)** Copy number per cell of mTORC1 phosphorylation targets involved in protein synthesis regulation. Quantitative proteomics was performed on three biological replicates. Data is mean +/- SEM. Data were analysed using paired students' t-tests. (*p<0.05, **p<0.01, NS=Not significant)

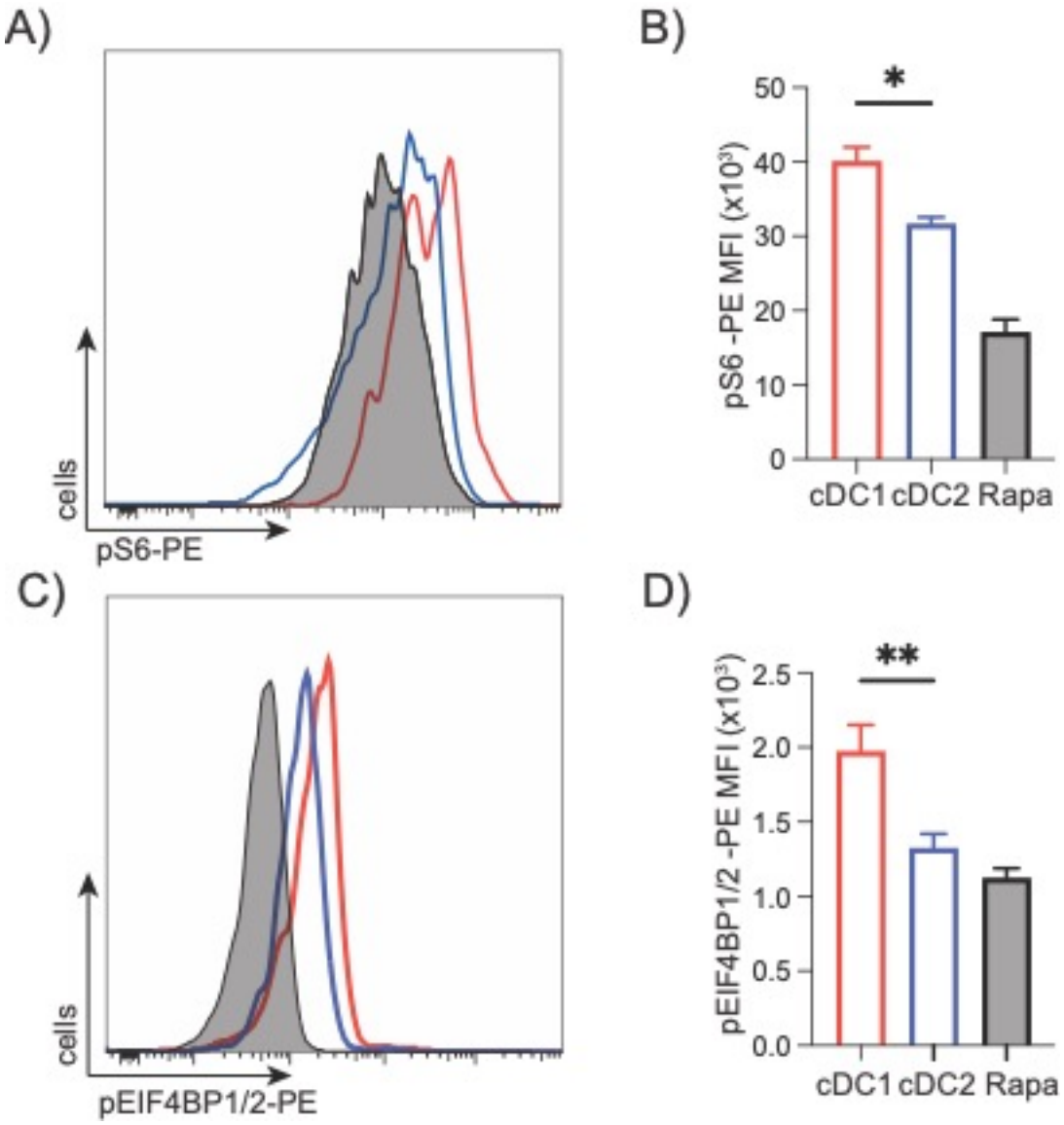

Figure 4.10 – cDC1s have more active mTORC1 signalling in the steady-state

(A-D) Flow cytometry analysis of splenocytes from C57Bl/6 mice inoculated with B16-Flt3l cells analysing the phosphorylation of mTORC1 targets S6 **(A)** and EIF4BP1/2 **(B)** in cDC1s and cDC2s. Splenocytes were treated with 20nM rapamycin for 20 minutes at 37°C to inhibit mTORC1 activity. Data are representative **(A,C)** or mean +/- SEM **(B,D)** of three independent experiments. Data were analysed using one-way ANOVA with Tukey's post-test. (*p<0.05, **p<0.01)

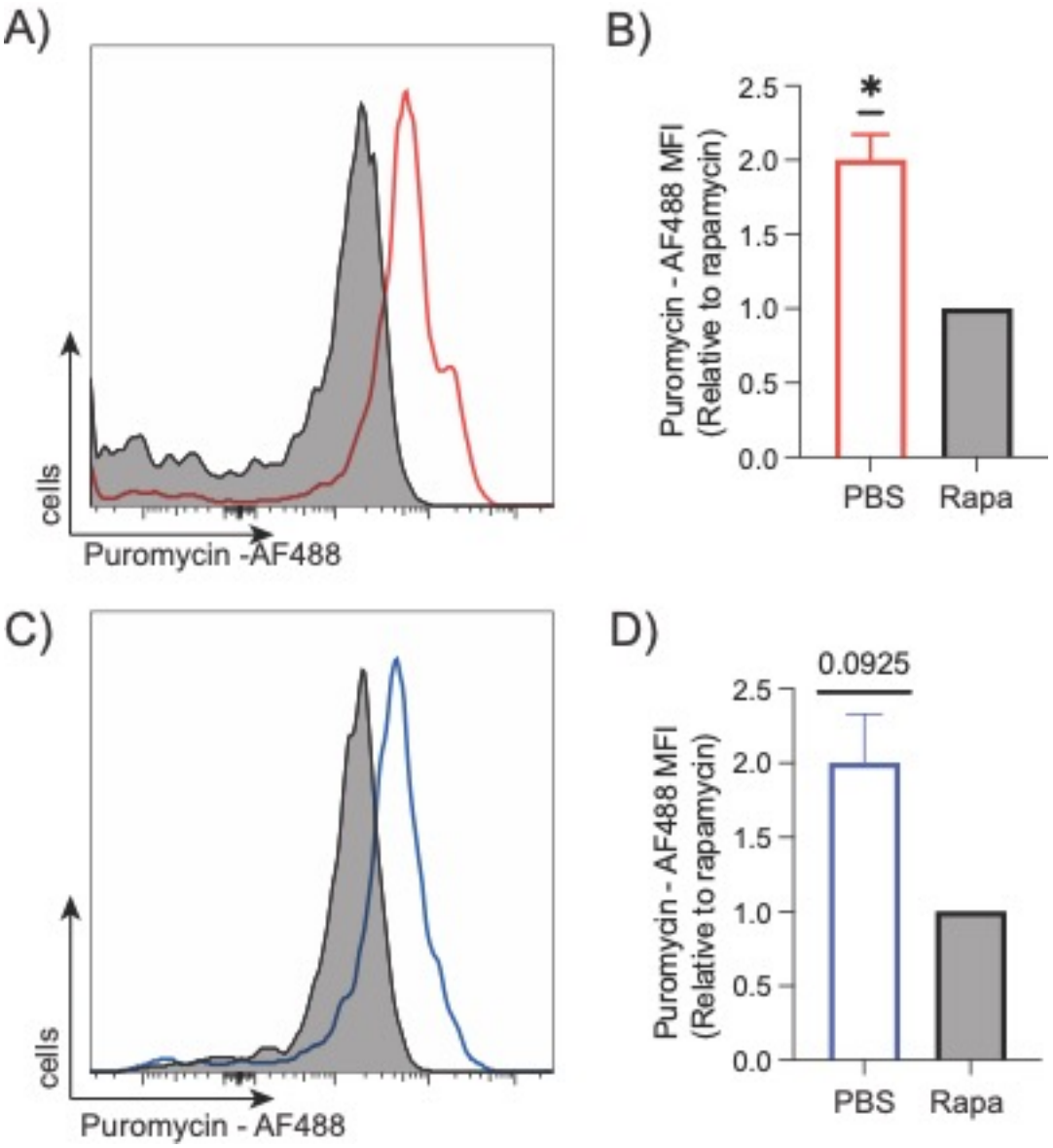

Figure 4.11 – mTORC1 signalling controls protein synthesis in cDCs in the steady-state

(A-D) Flow cytometry analysis of splenocytes from C57Bl/6 mice inoculated with B16-Flt3l cells analysing protein translation rate by measuring the incorporation of puromycin into nascent peptide chains in **(A,B)** cDC1s and **(C,D)** cDC2s. Splenocytes were treated with PBS (vehicle control) or 20nM rapamycin for 1 hour, and protein synthesis was measured. Data are representative **(A,C)** or mean +/- SEM **(B,D)** of three independent experiments. Data were analysed using a one-sample t-test against a theoretical value of 1. (*$p<0.05$)

4.4 mTORC1 regulates protein synthesis in response to TLR9 stimulation in cDC1s and cDC2s

The literature has reported that GMDCs alter their translation rate in two phases following LPS stimulation (Lelouard et al., 2007). The first phase involves increased protein synthesis peaking after 4 hours of stimulation, which is proposed to support the increased biosynthetic demands associated with DC maturation, including cytokine production and the upregulation of co-stimulatory markers. The second phase involves a gradual decrease in protein synthesis, which falls below steady-state rates after 18 hours post-stimulation and is thought to support DC longevity (Lelouard et al., 2007). As shown in Chapter 3, cDCs stimulated *in vivo* with the TLR9 agonist CpG-B have reduced protein synthesis rates relative to the steady state. As mTORC1 signalling was shown to control the rate of protein synthesis in steady-state DCs, I next investigated the induction of mTORC1 signalling in response to stimulation **(Fig. 4.12)**. Splenocytes were stimulated *in vitro* with CpG-B for 1h, and mTORC1 activity was determined by the phosphorylation of the mTORC1 targets S6. Both cDC1s **(Fig. 4.12 A,B)** and cDC2s **(Fig. 4.12 C,D)** significantly increase the phosphorylation of S6 in a mTORC1-dependent manner, indicating enhanced mTORC1 signalling in response to stimulation. To investigate whether mTORC1 signalling regulates protein synthesis in response to acute stimulation, splenocytes were stimulated with CpG-B for 1h in the presence or absence of rapamycin. The protein synthesis rate was determined by puromycin incorporation into nascent peptide chains by flow cytometry **(Fig. 4.13)**. CpG-B stimulation significantly increased the protein translation rate **(Fig. 4.13 A-D)**, which was reduced with rapamycin treatment in cDC1s **(Fig. 4.13 A,B)** and cDC2s **(Fig. 4.13 C,D).** These data indicate that acute activation is associated with increased mTORC1 signalling, which promotes enhanced protein translation in cDC1s and cDC2s.

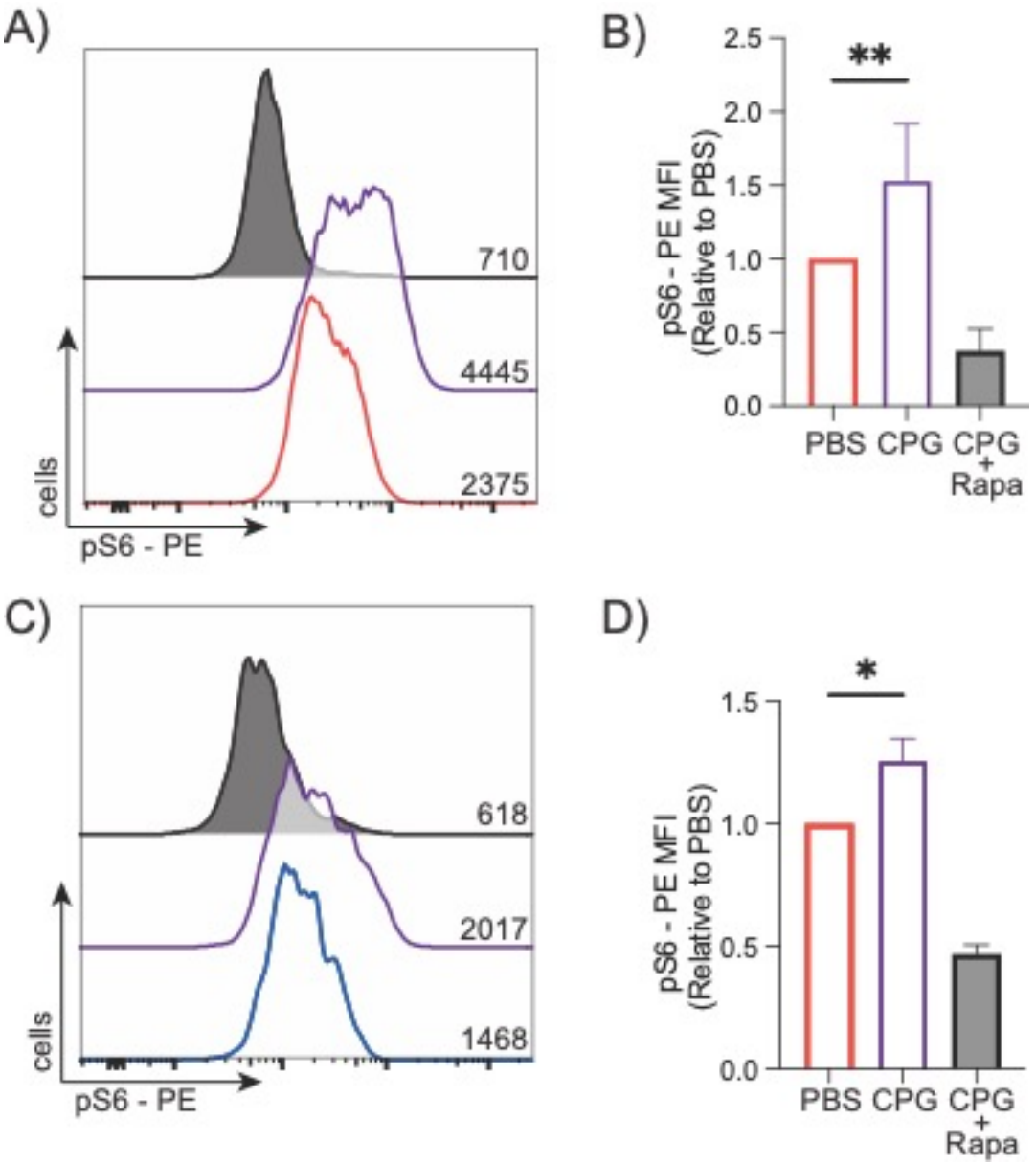

Figure 4.12 – CpG-B stimulation induces mTORC1 signalling in cDCs
(A-D) Flow cytometry analysis of splenocytes from C57Bl/6 mice inoculated with B16-Flt3l cells analysing the phosphorylation of the mTORC1 target S6 **in** cDC1s **(A,B)** and cDC2s **(C,D)**. Splenocytes were treated with PBS (vehicle control) or 4 μg/ml CpG-B for 1 hour in the presence or absence of 20 nM rapamycin. Data are representative **(A,C)** or mean +/- SEM **(B,D)** of three independent experiments. Data were analysed using a one-sample t-test against a theoretical value of 1. (*p<0.05, **p<0.01)

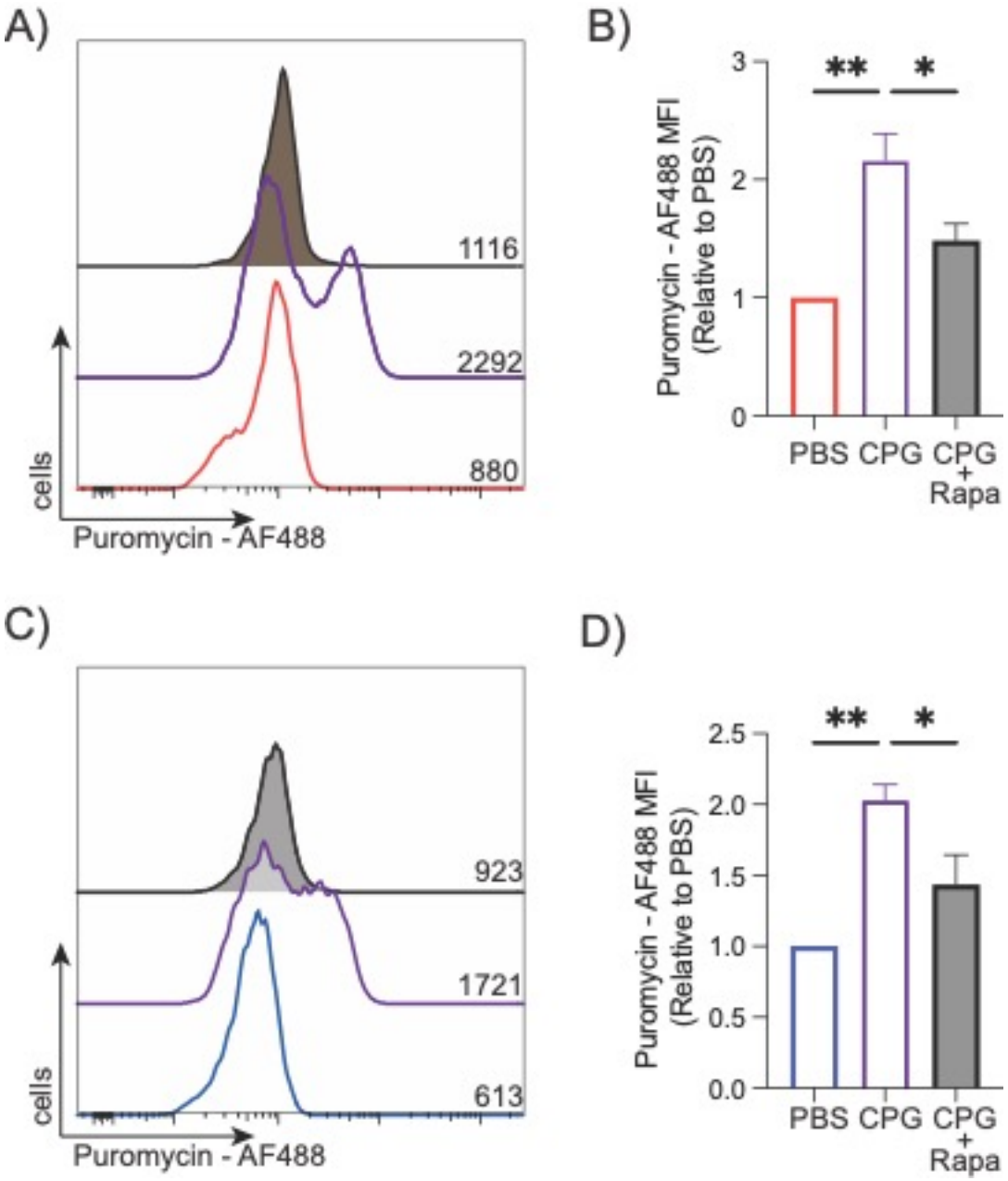

Figure 4.13 – mTORC1 signalling controls protein synthesis in cDCs in response to CpG-B stimulation

(A-D) Flow cytometry analysis of splenocytes from C57Bl/6 mice inoculated with B16-Flt3l cells analysing protein translation rate by measuring the incorporation of puromycin into nascent peptide chains in **(A,B)** cDC1s and **(C,D)** cDC2s. Splenocytes were treated with PBS (vehicle control) or 4μg/ml CpG-B in the presence or absence of 20nM rapamycin for 1 hour, and protein synthesis was measured. Data are representative **(A,C)** or mean +/- SEM **(B,D)** of three independent experiments. Data were analysed using a one-sample t-test against a theoretical value of 1. (*$p<0.05$)

4.5 SLC7A5 amino acid transport is a more potent regulator of mTORC1 activity than glutamine availability

In contrast to mTORC2, mTORC1 activity is tightly controlled by intracellular amino acid levels (Saxton & Sabatini, 2017). In particular, the amino acids leucine and arginine are indispensable for active mTORC1 signalling (Chantranupong et al., 2016; Saxton et al., 2016). In addition, numerous studies demonstrate that glutamine can control mTORC1 activity (Bodineau et al., 2021; Jewell et al., 2015). Considering the enrichment of Slc1a5 and Slc7a5 expression and the differential mTORC1 activity observed in cDC1s and cDC2s, I next investigated the control of mTORC1 signalling by these transporters. Slc1a5 is the primary glutamine transporter expressed in immune cells. As Slc1a5 is significantly more abundant than other glutamine transporters in cDC1s and cDC2s and the current lack of specific Slc1a5 pharmacological inhibitors, I used glutamine deprivation to proxy for Slc1a5 activity. Flow cytometry analysis of splenocytes stimulated with CpG-B for 1h in glutamine-free media or the presence of the Slc7a5 inhibitor BCH inhibits mTORC1 signalling in response to CpG-B stimulation **(Fig. 4.14)**. The extent of inhibition is more pronounced in response to BCH when compared to glutamine deprivation, indicating that Slc7a5 exerts greater control over mTORC1 signalling than Slc1a5. Indeed, Slc7a5 inhibition rapidly leads to the dephosphorylation of both S6 and EIF4BP1/2 in cDC1s **(Fig. 4.15 A-C)** and cDC2s **(Fig. 4.15 D-F)**. As glutamine availability, in a recent publication, has been reported to selectively control cDC1 function, this chapter will further investigate the functional implications of Slc7a5 mediated mTORC1 activity on cDC function.

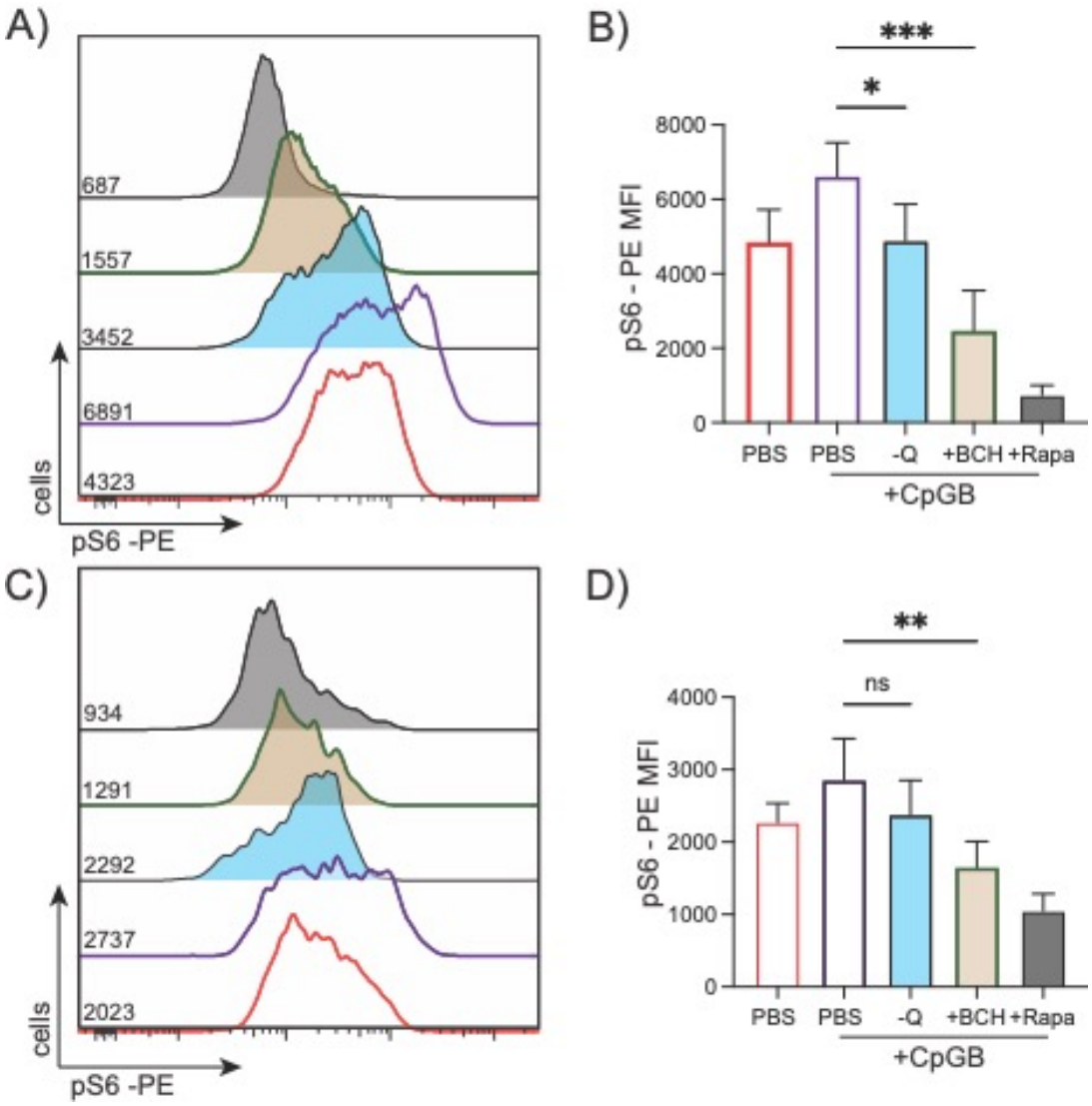

Figure 4.14 – Slc7a5 transport inhibition is a more potent inhibitor of mTORC1 signalling than glutamine availability

(A-D) Flow cytometry analysis of splenocytes from C57Bl/6 mice inoculated with B16-Flt3l cells analysing mTORC1 signalling in cDC1s **(A,B)** and cDC2s **(C,D)** by measuring the phosphorylation of mTORC1 targets S6. Splenocytes were stimulated with 4μg/ml CpG-B with BCH (25mM), rapamycin (20nM) or in glutamine-free media as indicated. Data are representative **(A,C)** or mean +/- SEM of three independent experiments **(B,D)**. Data were analysed using one-way ANOVA with Tukey's post-test. (*p<0.05, **p<0.01,***p<0.001, ns = not significant)

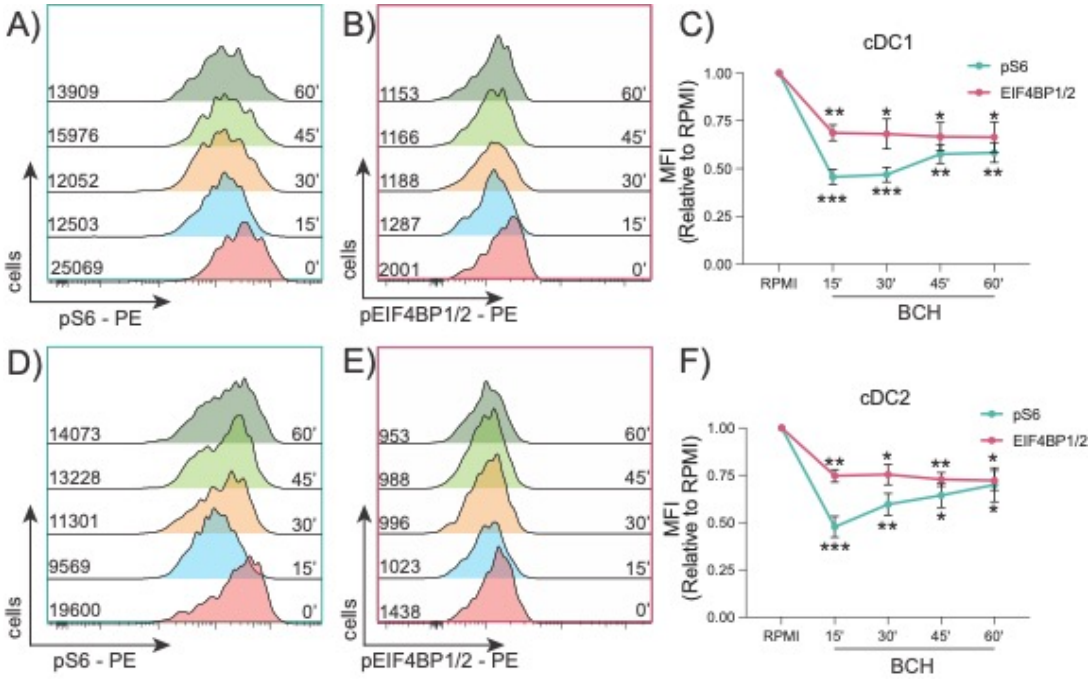

Figure 4.15 – SLC7A5 transport inhibition rapidly blocks mTORC1 signalling in cDC1s and cDC2s

(A-F) Flow cytometry analysis of splenocytes from C57Bl/6 mice inoculated with B16-Flt3l cells analysing mTORC1 signalling by measuring the phosphorylation of mTORC1 targets S6 **(A,D)** and EIF4BP1/2 **(B,E)** in cDC1s **(A-C)** and cDC2s **(E-F)**. Splenocytes were treated with BCH (25mM) for the indicated times before flow cytometry analysis. Pooled data is relative to RPMI (no BCH) condition. Data are representative **(A,B,D,E)** or mean +/- SEM **(C,F)** of four biological replicates. Data were analysed using multiple one-sample t-tests against a theoretical value of 1. (*p<0.05, **p<0.01, ***p<0.001)

4.6 – cDCs do not increase SLC7A5 transport activity after acute CpG-B stimulation

Many immune cells, particularly lymphocytes, have been shown to significantly upregulate SLC7A5 expression and activity during activation (Howden et al., 2019; Loftus et al., 2018). I next investigated whether 6 hours of CpG-B stimulation induces SLC7A5 amino acid uptake in cDC1s **(Fig. 4.16 A,B)** and cDC2s **(Fig. 4.16 C,D).** Six hours of CpG-B stimulation does not affect SLC7A5 amino acid transport.

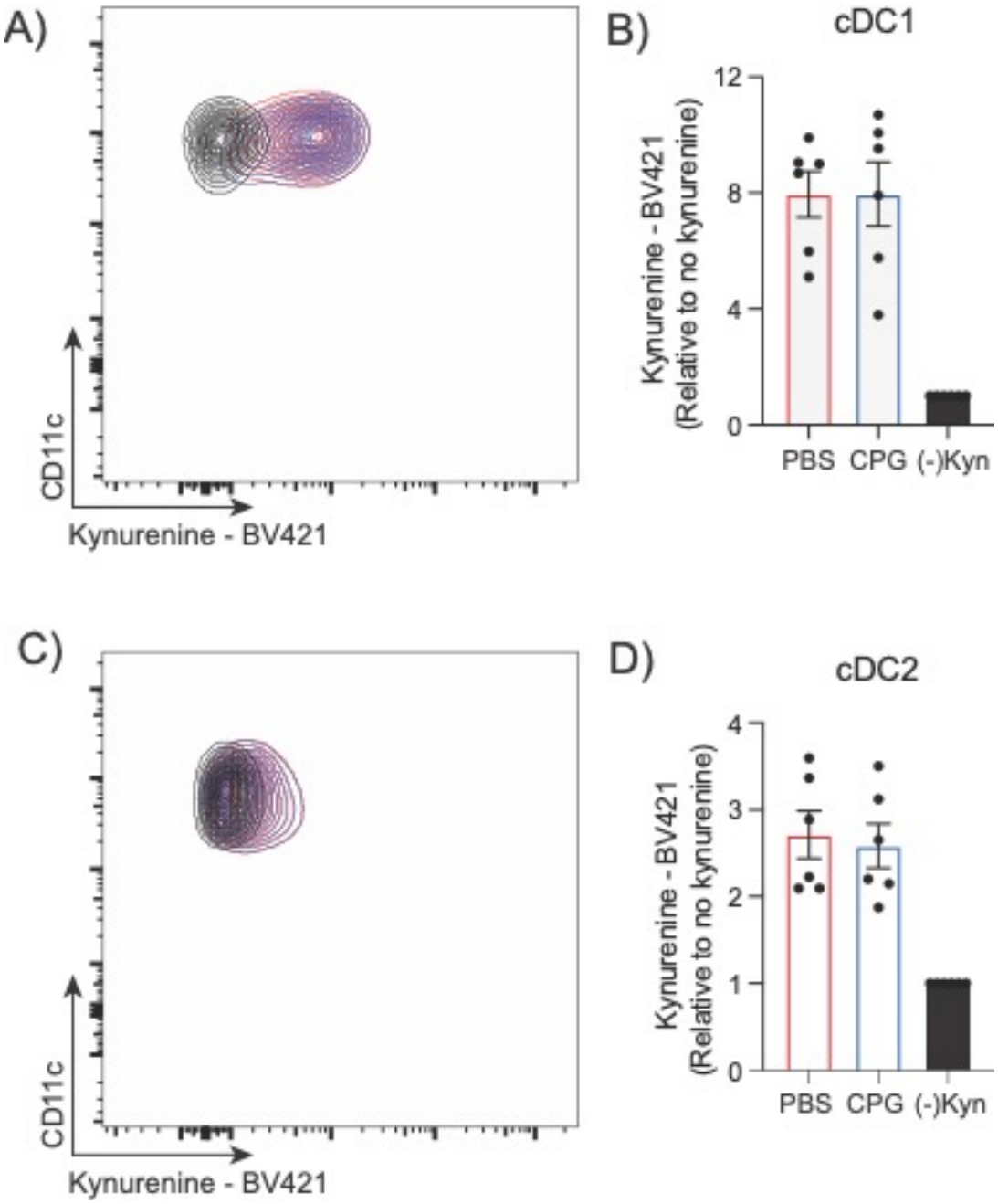

Figure 4.16 – cDCs do not increase SLC7A5 amino acid transport in response to CpG-B stimulation

(A-D) Flow cytometry analysis of splenocytes from C57Bl/6 mice inoculated with B16-Flt3l cells analysing SLC7A5 amino acid transport by monitoring kynurenine uptake in cDC1s **(A,B)** and cDC2s **(C,D)**. Splenocytes were stimulated with PBS (vehicle control) or 4μg/ml CpG-B for 6 hours before flow cytometry analysis. Pooled data is relative to no kynurenine control **(B,D)**. Data are representative **(A,C)** or mean +/- SEM **(B,D)** of six biological replicates.

4.7 SLC7A5 inhibition does not affect cDC proinflammatory outputs in response to CpG-B stimulation

Numerous studies have investigated the role of mTORC1 signalling on the proinflammatory cytokine production of DCs (Haidinger et al., 2010; Ohtani et al., 2012; Pelgrom et al., 2022). These studies show conflicting results depending on the DC model used and the method to modulate mTORC1 activity. For example, human moDCs, stimulated with an inflammatory cytokine cocktail in the presence of rapamycin, have enhanced IL12p70 production relative to the no rapamycin control. The enhanced IL12p70 production depended on reduced IL10 production in the rapamycin-treated group (Haidinger et al., 2010). On the other hand, a recent report by Pelgrom et al. utilises a CD11c-creRaptorfl/fl genetic model, which has deficient mTORC1 signalling in cDCs. This study shows that deficient mTORC1 signalling does not affect splenic cDC1 and cDC2 proinflammatory cytokine production in a model of Listeria infection (Pelgrom et al., 2022). Considering the control exerted on mTORC1 signalling by SLC7A5 amino acid transport, I investigated whether SLC7A5 transport inhibition affects proinflammatory cytokine production in cDC1s **(Fig. 4.17 A-F)** and cDC2s **(Fig. 4.18 A-F)**. Splenocytes were stimulated with CpG-B in the presence or absence of BCH for 6 hours, and proinflammatory cytokine production was measured by flow cytometry. BCH treatment in response to CPG-B stimulation does not alter proinflammatory cytokine production in either cDC1s **(Fig. 4.17 A-F)** or cDC2s **(Fig. 4.18 A-F)**.

DCs in the steady state have low expression of costimulatory markers, including CD40, CD80 and CD86, to limit the inappropriate activation of adaptive immune cells to maintain immune tolerance. DCs upregulate these markers upon immunogenic stimulation to effectively promote adaptive immune responses. I next investigated the effect of SLC7A5 transport inhibition on the induction of costimulatory marker expression in cDC1s **(Fig. 4.19 A,B)** and cDC2s **(Fig. 4.20 A,B).** Splenocytes were stimulated with CpG-B in the presence or absence of BCH, and costimulatory marker expression was quantified by flow cytometry. BCH treatment significantly reduced CD40 and CD86 expression in cDC1s **(Fig. 4.19 A,B)** and cDC2s **(Fig. 4.20 A,B).**

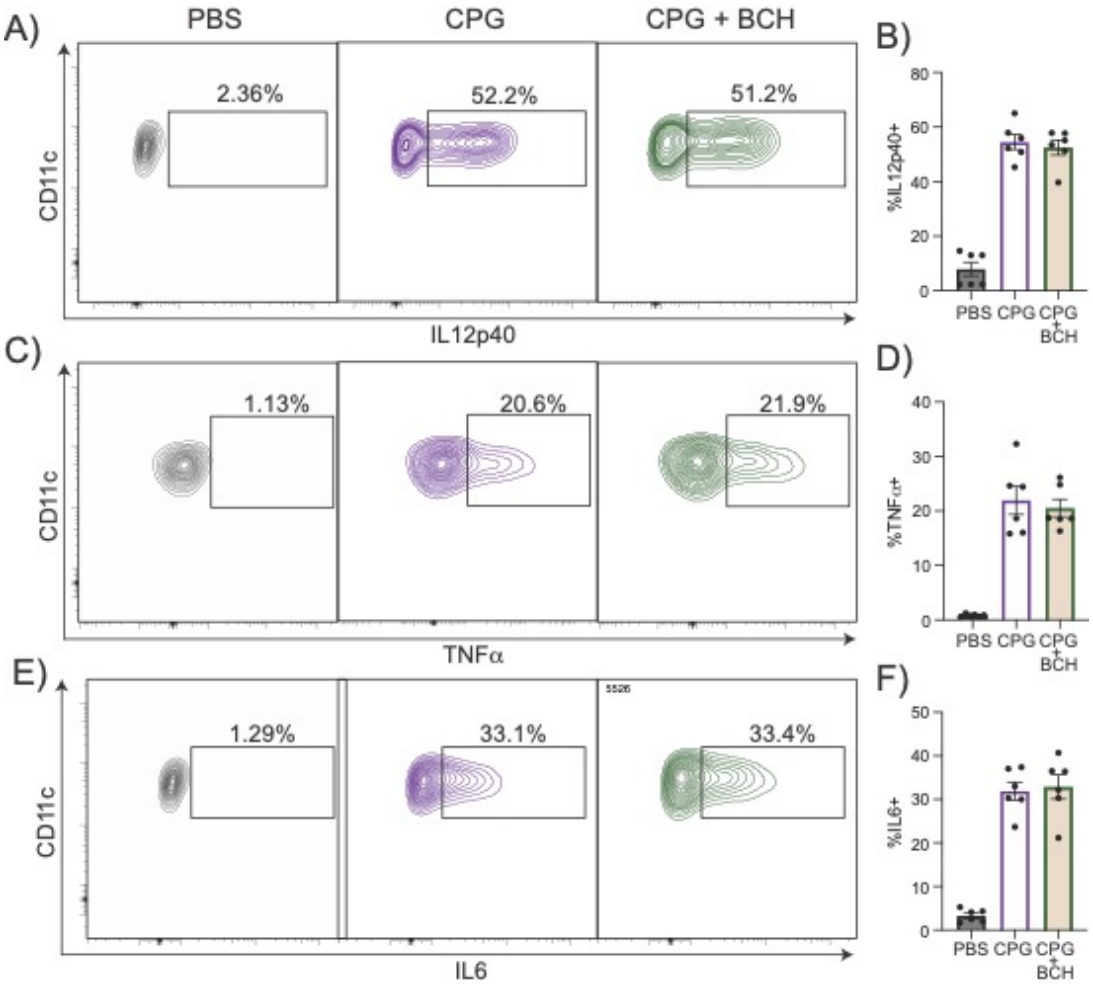

Figure 4.17 – SLC7A5 transport inhibition does not affect cDC proinflammatory cytokine production in cDC1s

(A-F) Flow cytometry analysis of splenocytes from C57Bl/6 mice inoculated with B16-Flt3l cells analysing proinflammatory cytokine production in cDC1s. Splenocytes were treated with PBS (vehicle control) or 4μg/ml CpG-B in the presence or absence of BCH (25mM) before flow cytometry analysis. Brefeldin A was added during the last 4 hours of stimulation to prevent cytokine release. Data are representative **(A,C,E)** or mean +/- SEM **(B,D,F)** of six biological replicates. Data were analysed using one-way ANOVA with Tukey's post-test.

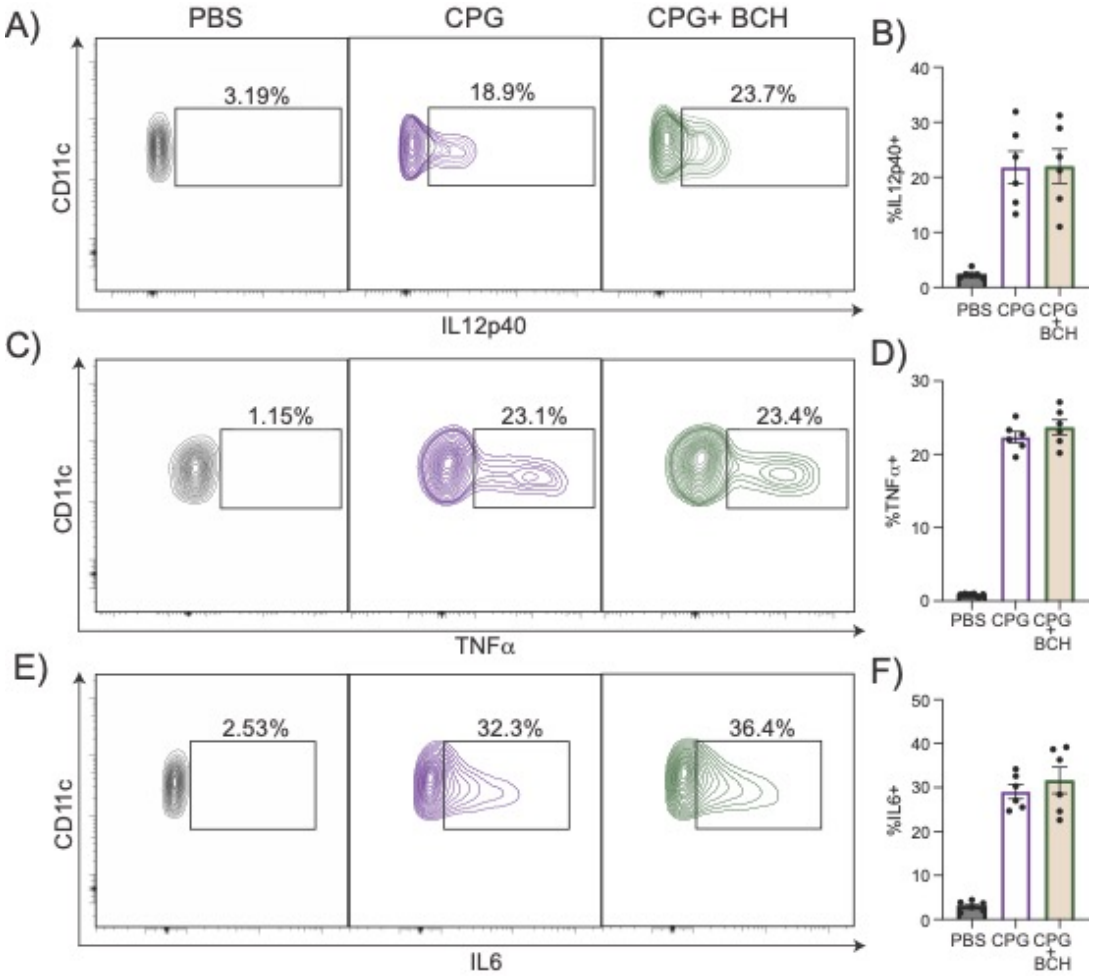

Figure 4.18 – SLC7A5 transport inhibition does not affect cDC proinflammatory cytokine production in cDC2s

(A-F) Flow cytometry analysis of splenocytes from C57Bl/6 mice inoculated with B16-Flt3l cells analysing proinflammatory cytokine production in cDC2s. Splenocytes were treated with PBS (vehicle control) or 4μg/ml CpG-B in the presence or absence of BCH (25mM) before flow cytometry analysis. Brefeldin A was added during the last 4 hours of stimulation to prevent cytokine release. Data are representative **(A,C,E)** or mean +/- SEM **(B,D,F)** of six biological replicates. Data were analysed using one-way ANOVA with Tukey's post-test.

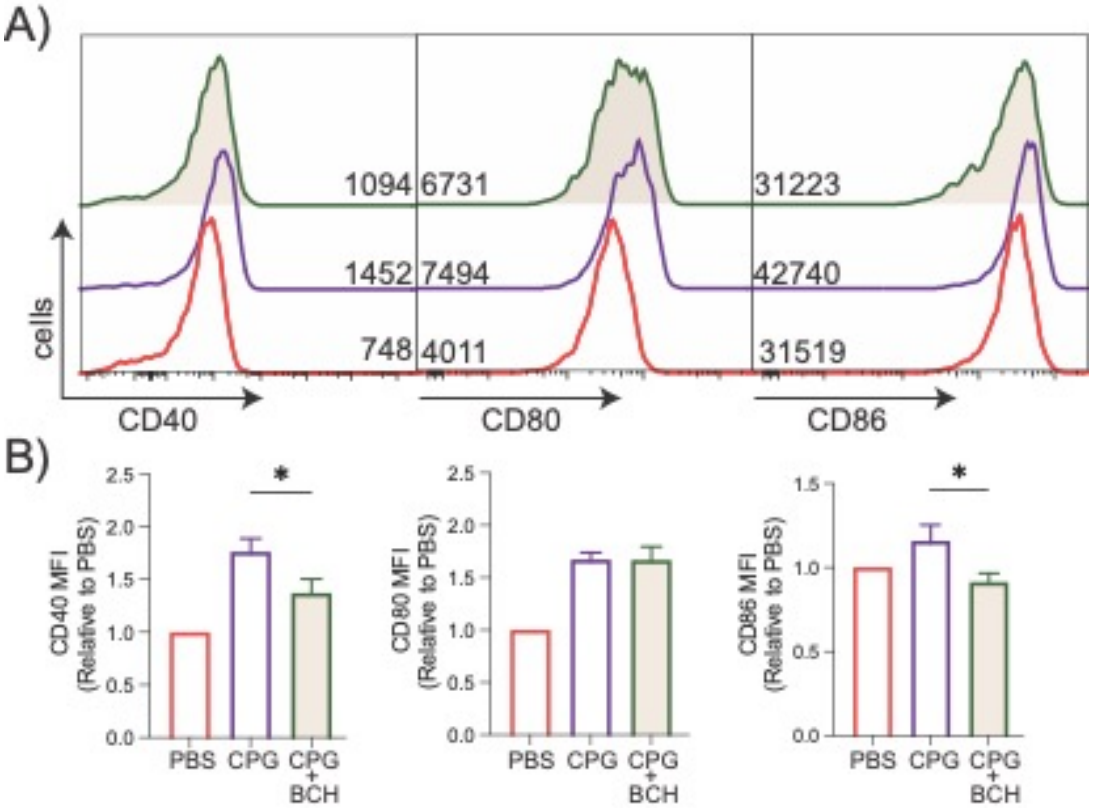

Figure 4.19 – SLC7A5 transport inhibition reduces costimulatory marker expression in response to CpG-B stimulation in cDC1s

(A,B) Flow cytometry analysis of splenocytes from C57Bl/6 mice inoculated with B16-Flt3l cells analysing costimulatory marker expression in cDC1s. Splenocytes were treated with PBS (vehicle control) or 4μg/ml CpG-B in the presence or absence of BCH (25mM) before flow cytometry analysis. Pooled data is relative to PBS control **(B)**. Data are representative **(A)** or mean +/- SEM **(B)** of six biological replicates. Data were analysed using one-way ANOVA with Tukey's post-test. (*p<0.05)

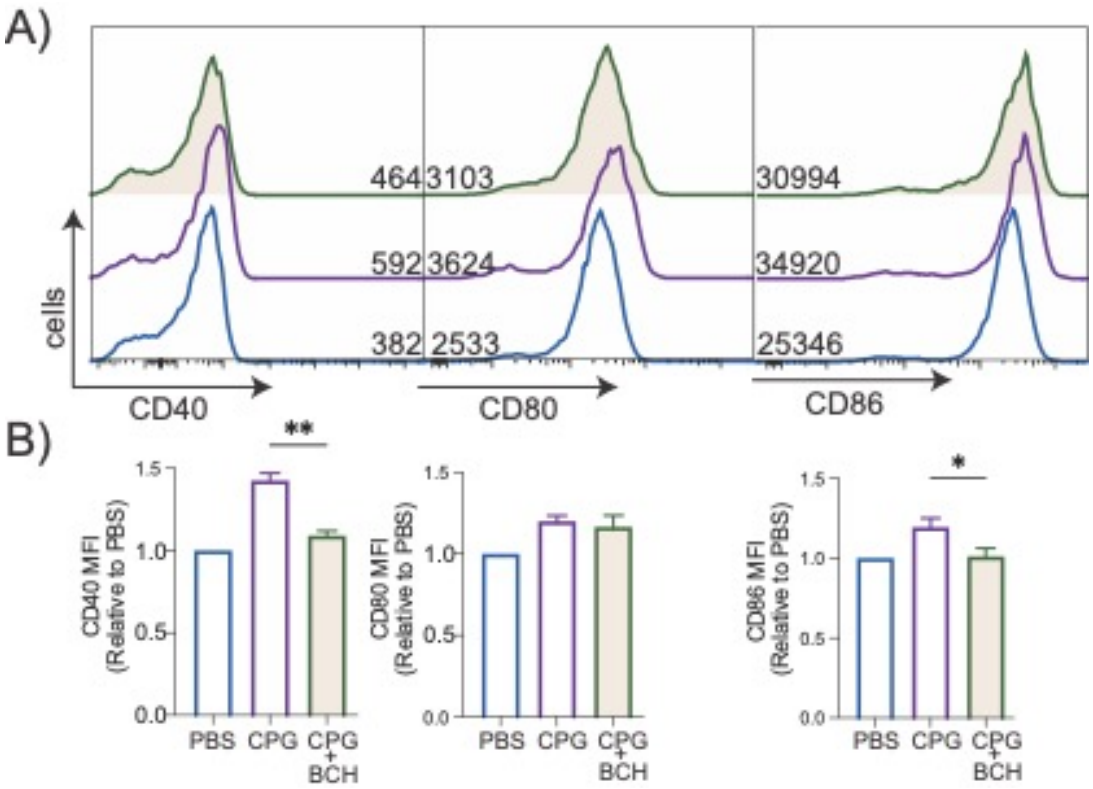

Figure 4.20 – SLC7A5 transport inhibition reduces costimulatory marker expression in response to CpG-B stimulation in cDC2s

(A,B) Flow cytometry analysis of splenocytes from C57Bl/6 mice inoculated with B16-Flt3l cells analysing costimulatory marker expression in cDC1s. Splenocytes were treated with PBS (vehicle control) or 4μg/ml CpG-B in the presence or absence of BCH (25mM) before flow cytometry analysis. Pooled data is relative to PBS control **(B)**. Data are representative **(A)** or mean +/- SEM **(B)** of six biological replicates. Data were analysed using one-way ANOVA with Tukey's post-test. (*$p<0.05$)

4.8 The cDC1 proteome is specialised for antigen cross-presentation

All nucleated cells express MHCI molecules ubiquitously and present protein fragments of cytosolic and nuclear origin at the cell surface (Neefjes et al., 2011). Presentation of self-antigens on MHCI is essential to prevent NK cell-mediated killing of healthy cells (Bix et al., 1991). On the other hand, once cells become malignant or virally infected, MHCI presents non-self-antigens for targeting by cytotoxic CD8 T cells. As cDCs are specialised in antigen presentation, I first determined the expression of MHCI in cDC1s and cDC2s **(Fig. 4.21 A)**. In line with the reported ability of cDC1s to specialise in MHCI presentation, they have significantly higher expression of MHCI than cDC2s. The proteasome primarily generates peptides for MHCI loading, and the resulting peptides are translocated to the ER by transporter associated with antigen presentation (TAP) to access MHCI molecules (Neefjes et al., 2011). The MHCI binding groove typically favours peptides between 8 and 11 amino acids in length (Momburg et al., 1994). Thus, TAP-transported peptides, which are between 8 and 16 amino acids, are usually trimmed by ER aminopeptidases (ERAP1 and ERAP2) before loading onto MHCI by the MHCI peptide loading complex (PLC) (TAPBP, CALR, ERP57) (Serwold et al., 2002). Thus, I next determined the expression of the ER amino peptidases and MHCI PLC components in cDC1s and cDC2s **(Fig. 4.21 B)**. In accordance with previously reported mRNA microarray data, cDC1s have higher expression of the MHCI presentation machinery than cDC2s (Dudziak et al., 2007a). As the rate of peptide generation is proportional to the rate of protein synthesis, it has been suggested that protein synthesis is a rate-limiting factor in MHCI presentation (Neefjes et al., 2011). Indeed, ionising radiation has increased MHCI antigen presentation by activating mTORC1 signalling and increasing the protein synthesis rate in MC38 tumour cells (Reits et al., 2006). Thus, it is conceivable that the enhanced mTORC1-dependent protein synthesis rate observed in cDC1s is favourable in supporting efficient MHCI presentation.

To activate cytotoxic CD8 T cell responses against virally infected and malignant cells, APCs must present exogenous antigens on MHCI through antigen cross-presentation (Embgenbroich & Burgdorf, 2018). Antigen cross-

presentation primarily occurs through two main pathways: the vacuolar pathway, which involves the endolysosomal degradation of antigens and the endosome-to-cytosol pathway, which involves the transfer of antigens from endolysosomes to the cytosol for proteasomal degradation. cDC1s excel in the cross-presentation of antigens to CD8 T cells (Embgenbroich & Burgdorf, 2018). Several studies suggest that delayed endolysosomal antigen degradation is an important regulator of cross-presentation (Delamarre et al., 2005; Samie & Cresswell, 2015; Savina et al., 2006). Rapid antigen degradation is generally assumed to quickly destroy epitopes before they can be processed and loaded onto MHCI molecules. It was demonstrated that DCs express lower levels of pH-sensitive lysosomal proteases and display reduced velocity of endosome maturation compared to macrophages (Delamarre et al., 2005). This property of DC lysosomes was shown to prolong antigen stability after internalisation by DCs. In addition, RNA microarray data shows that cDC2s have higher expression of lysosomal cathepsins than cDC1s (Dudziak et al., 2007a). Thus, it is possible that cDC subsets have different rates of endo-lysosomal degradation. Therefore, I next investigated the lysosomal proteomes of cDC1s and cDC2s **(Fig. 4.22)**. cDC1s have a higher lysosomal protein content as a percentage of total protein content relative to cDC2s **(Fig. 4.22 A)**. However, despite having a general enrichment of lysosomal proteins, cDC1s have lower expression of lysosomal proteases than cDC2s **(Fig. 4.22 B)** with the notable exception of cathepsin S **(Fig. 4.22 C)**. Interestingly, cathepsin S has been reported to be required for antigen cross-presentation as mice whose APCs lack cathepsin S have reduced cross-presentation to particulate and cell-associated antigens (Shen et al., 2004).

I next investigated whether the proteomics findings in **(Fig. 4.22)** reflect differences in the rate of antigen degradation in cDC1s and cDC2s. I first measure the rate of antigen capture in cDCs using a fluorescent uptake reporter (BSA-AF647). Splenocytes were treated with 10μg/ml BSA-AF647 for 1 hour, and uptake was measured by flow cytometry. cDC1s have significantly higher BSA-AF647 uptake than cDC2s **(Fig. 4.23 A,B)**. To

measure antigen degradation, I treated splenocytes with DQ-OVA, a fluorescent reporter that increases fluorescence upon proteolytic degradation. A pulse-chase experiment was performed. Splenocytes were treated with 10μg/ml DQ-OVA for 1 hour (pulse), after which all extracellular DQ-OVA was washed away, and the cells were replated for a 1 hour chase period in cRPMI **(Fig. 4.24)**. This analysis shows that although a similar percentage of cDC1s and cDC2s degrade DQ-OVA **(Fig. 4.24 A-C),** the DQ-OVA signal is significantly higher in cDC1s **(Fig. 4.24 D,E)**. However, the extent of DQ-OVA degradation is also a function of the rate of antigen capture. As cDC1s have higher rates of antigen uptake than cDC2s, this would lead to higher DQ-OVA. Normalisation of the DQ-OVA signal by the rate of antigen uptake shows that cDC2s have significantly higher rates of antigen degradation than cDC1s **(Fig. 4.24 F)**.

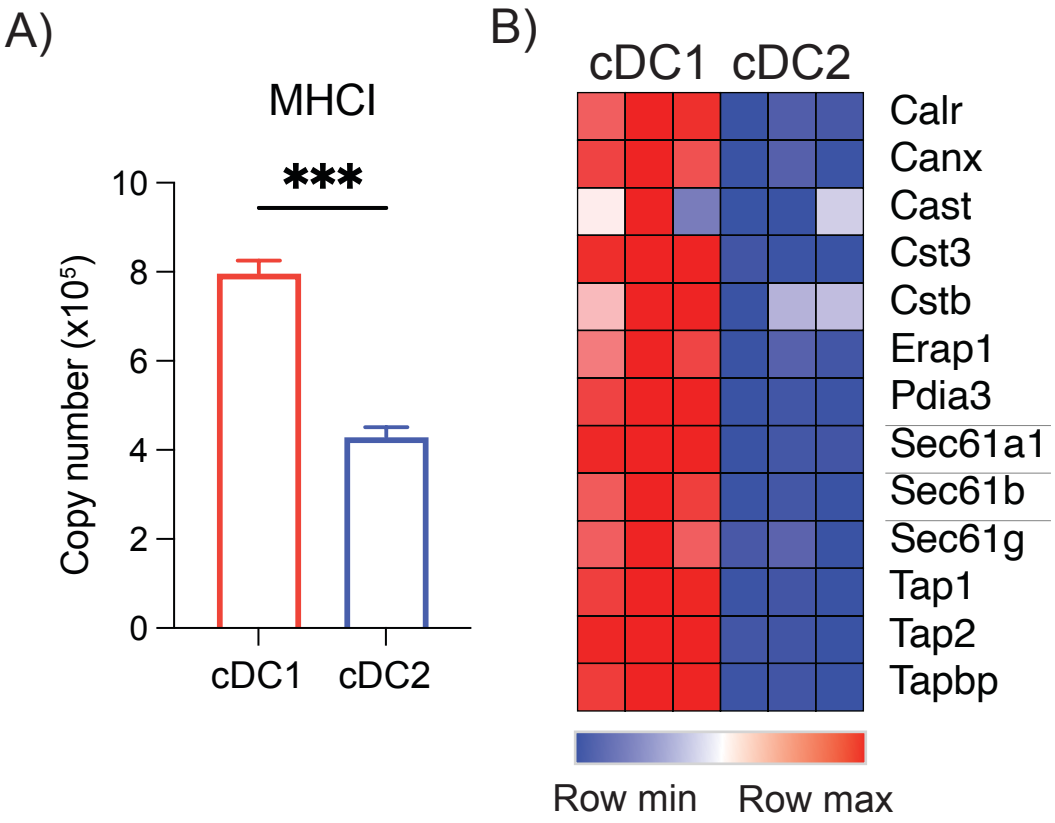

Figure 4.21 – The cDC1 proteome is enriched for proteins in the MHI presentation pathway

(A,B) Quantitative proteomic analysis was performed on splenic cDC1s and cDC2s from C57Bl/6 mice inoculated with B16-Flt3l cells, analysing the expression of proteins involved in MHCI presentation. **(A)** Copy number per cell of H2-K1 (MHC-I) in cDC1s and cDC2s determined by quantitative proteomics. **(B)** Heatmap representing the log_2 copy number per cell of proteins involved in MHCI presentation. Protein expression is graded from blue (low) to red (high) per row. Quantitative proteomics was performed on three biological replicates. Data were analysed using paired students' t-tests. (***p<0.001)

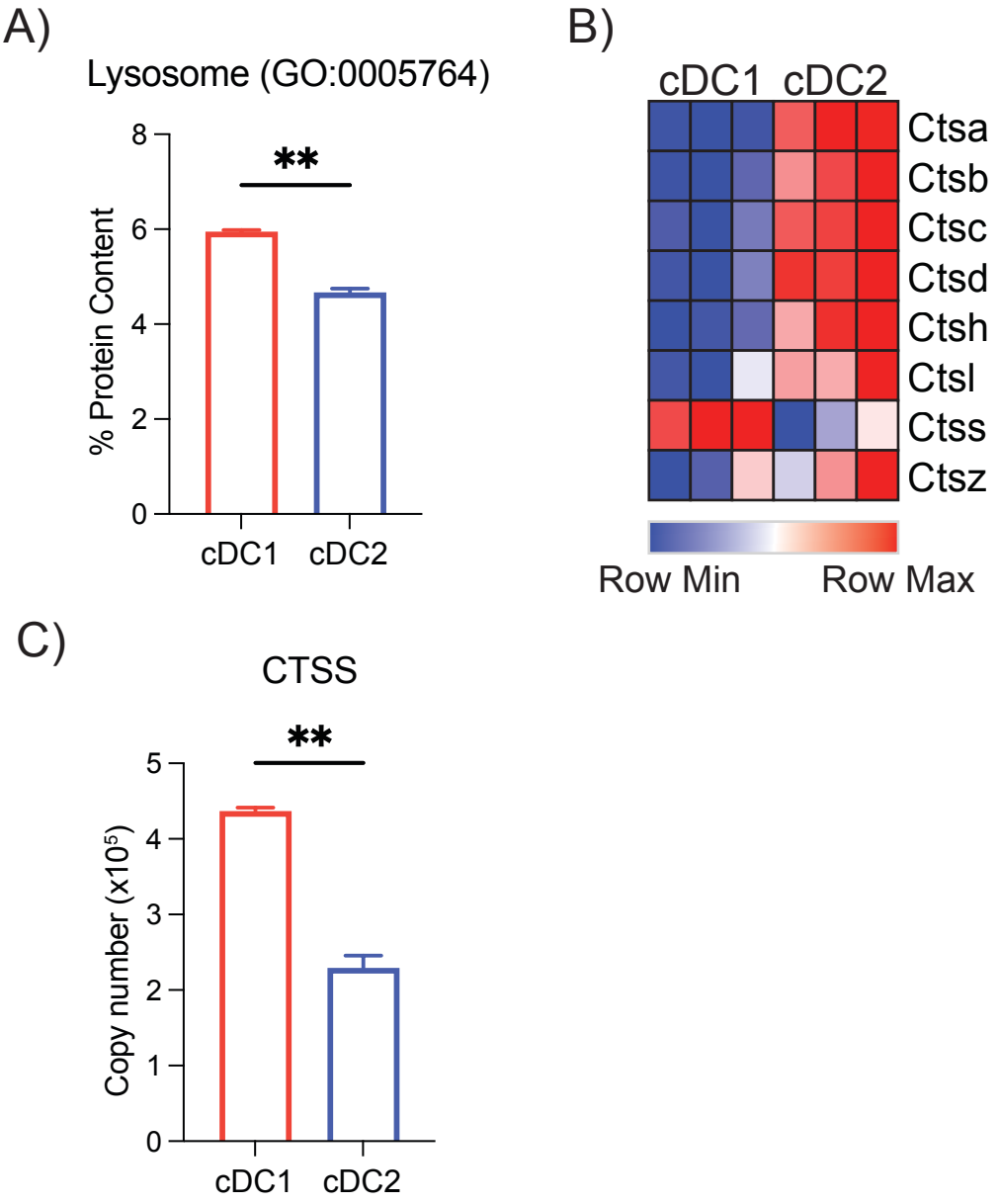

Figure 4.22 – cDC1s have lower expression of lysosomal proteases than cDC2s

(A-C) Quantitative proteomic analysis was performed on splenic cDC1s and cDC2s from C57Bl/6 mice inoculated with B16-Flt3l cells, analysing the abundance of lysosomal proteins. **(A)** Lysosomal proteins (GO:0005764) were quantified as a percentage of total cellular protein content in cDC1s and cDC2s. **(B)** Heatmap representing the $\log_2$ copy number per cell of lysosomal cathepsins in cDC1s and cDC2s. Protein expression is graded from blue (low) to red (high) per row. **(C)** Copy number per cell of CTSS in cDC1s and cDC2s. Quantitative proteomics was performed on three biological replicates. Data was analysed using paired students' t-tests. (**p<0.01)

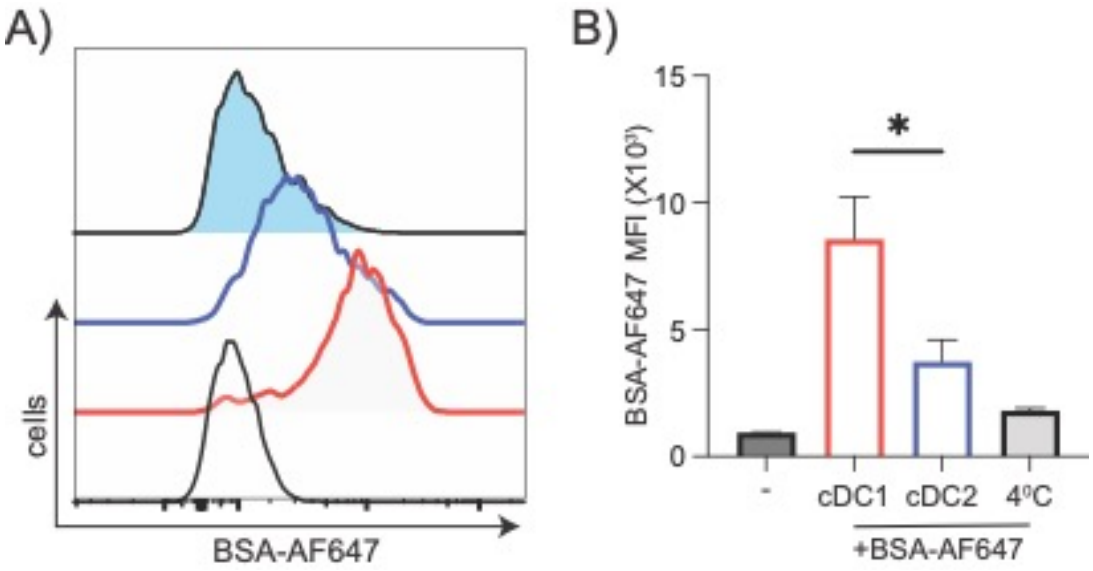

Figure 4.23 – cDC1s have a higher rate of antigen uptake than cDC2s
(A,B) Flow cytometry analysis of splenocytes from C57Bl/6 mice inoculated with B16-Flt3l cells analysing the rate of antigen uptake in cDCs. Splenocytes were treated with 10μg/ml of a fluorescent BSA conjugate (BSA-AF647) for 1 hour before flow cytometry analysis. Data are representative **(A)** or mean +/- SEM **(B)** of six biological replicates. Data were analysed using one-way ANOVA with Tukey's post-test. (*$p<0.05$)

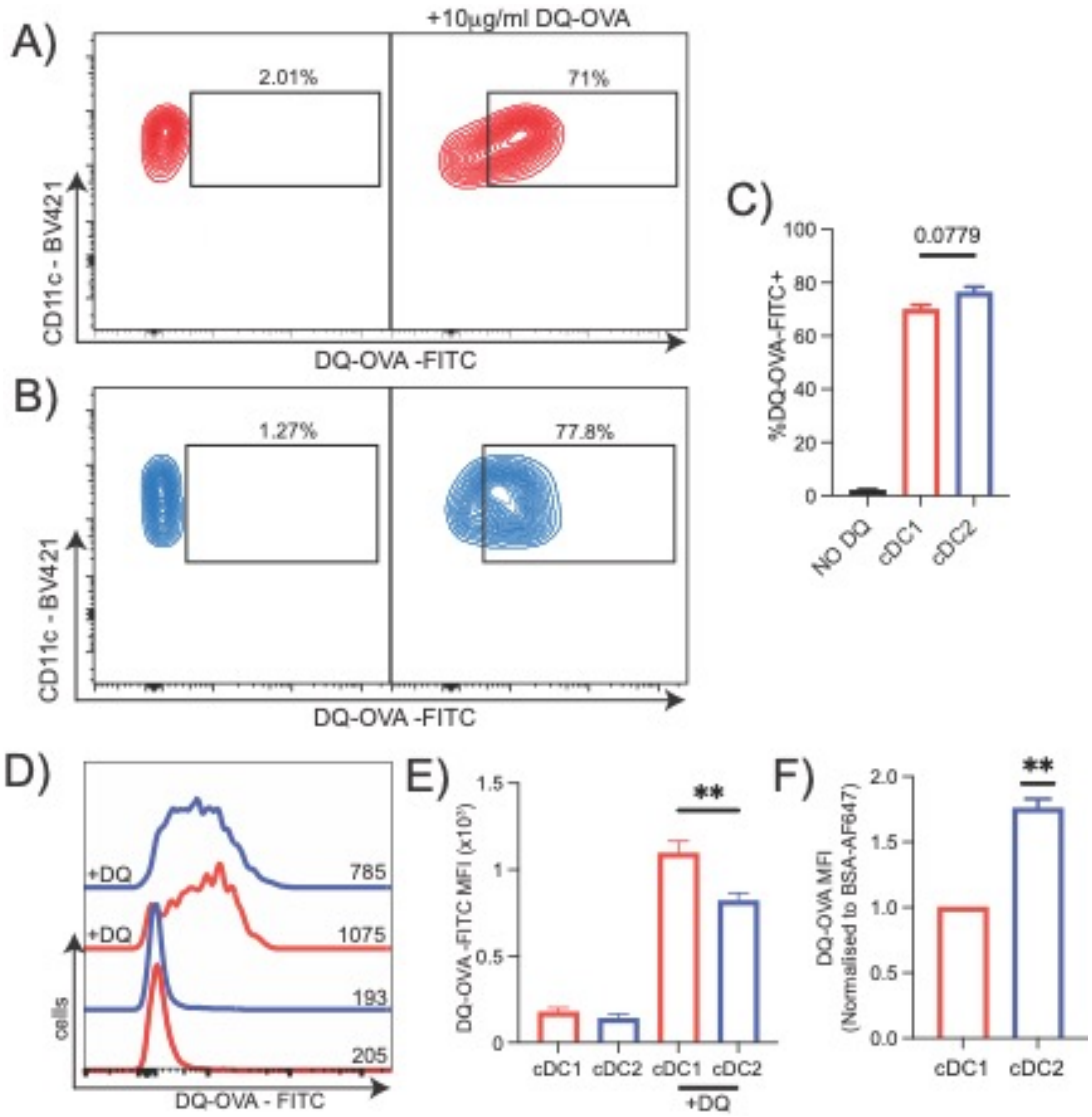

Figure 4.24 – cDC2s have higher rates of antigen degradation than cDC1s

(A-F) Flow cytometry analysis of splenocytes from C57Bl/6 mice inoculated with B16-Flt3l cells analysing the rate of antigen degradation in cDC1s **(A)** and cDC2s **(B).** DQ-OVA is a fluorescently quenched OVA conjugate whose fluorescence increases upon proteolytic degradation. Splenocytes were treated with 10μg/ml DQ-OVA for 1h (pulse), after which all extracellular OVA was washed off. Cells were further incubated for 1h (chase), and DQ-OVA fluorescence was determined by flow cytometry. Pooled data **(F)** is normalised to BSA-AF647 uptake. Data are representative **(A,B,D)** or mean +/- SEM **(C,E,F)** of four biological replicates. Data were analysed using one-way ANOVA with Tukey's post-test. (**p<0.01)

4.9 SLC7A5 transport inhibition increases antigen degradation in cDC1s

mTORC1 activity has been described to limit lysosomal catabolism, inhibiting the V-ATPase complex assembly that controls lysosomal acidification (Ratto et al., 2022). As enhanced lysosomal acidification increases the rate of antigen degradation, I next investigated whether SLC7A5 transport activity regulates the OVA degradation in cDC1s and cDC2s **(Fig. 4.25)**. As in **(Fig. 4.24),** a pulse-chase experiment of DQ-OVA was performed in the presence or absence of BCH. BCH treatment significantly enhanced DQ-OVA fluorescence in cDC1s **(Fig. 4.25 A,B).** SLC7A5 inhibition did not affect cDC2 antigen degradation **(Fig. 4.25 C,D)**. mTORC1 inhibition induces increased lysosomal catabolism to regenerate amino acids in the absence of sufficient extracellular amino acids. It has been described in cancer cells that the degradation of proteins acquired by macropinocytosis can restore mTORC1 signalling in the absence of adequate amino acids (Palm et al., 2015). Considering the high rates of macropinocytosis in cDC1s and the increase in antigen degradation in response to mTORC1 inhibition, I next investigated whether cDC1s catabolise extracellular proteins in the absence of amino acids. Chloroquine is a weak base commonly used to inhibit autophagy that can also lead to an increase in the pH of endolysosomes, which would prevent protein degradation. Indeed, DQ-OVA degradation is inhibited by 50μM chloroquine, which suggests that maintaining high endolysosomal pH prevents protein degradation **(Fig. 4.26 A,B)**. To investigate whether cDC1s can utilise extracellular protein to restore mTORC1 activity, splenocytes were deprived of amino acids and treated with increasing concentrations of BSA **(Fig. 4.27 A,B).** BSA treatment resulted in a partial rescue in mTORC1 signalling in a dose-dependent manner, indicating that cDC1s can degrade extracellular proteins to support mTORC1 activity. Importantly, when chloroquine, which inhibits protein degradation, was added, the increase in mTORC1 signalling in response to BSA treatment was lost **(Fig. 4.27 C,D)**.

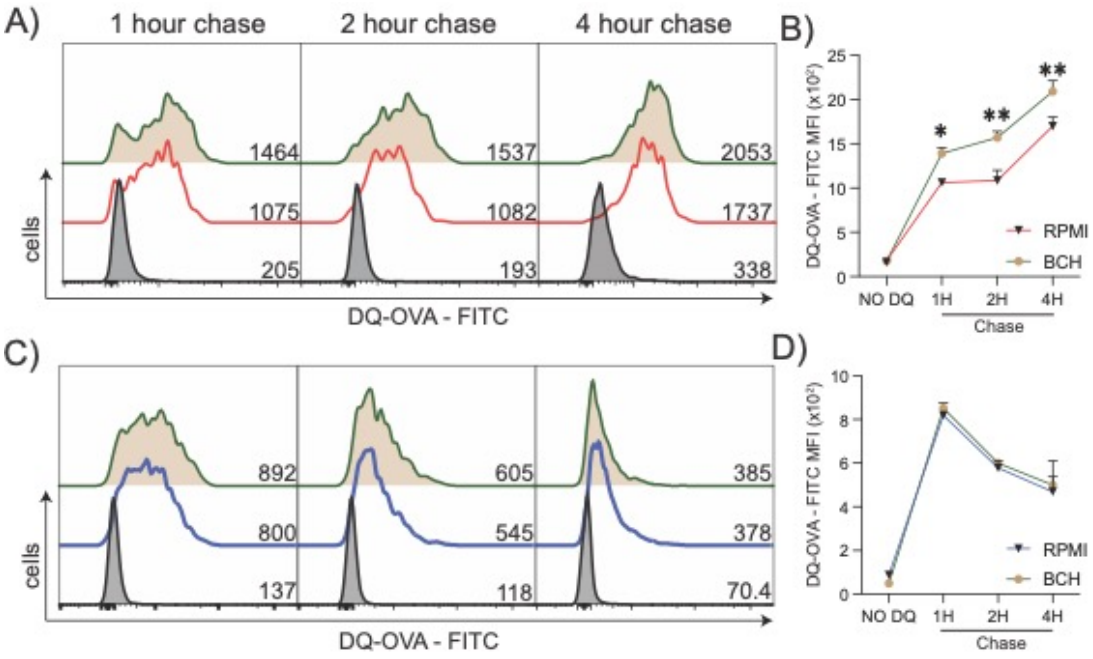

Figure 4.25 – SLC7A5 transport inhibition increases the rate of antigen degradation in cDC1s

(A-D) Flow cytometry analysis of splenocytes from C57Bl/6 mice inoculated with B16-Flt3l cells analysing the rate of antigen degradation in cDC1s **(A,B)** and cDC2s **(C,D).** DQ-OVA is a fluorescently quenched OVA conjugate whose fluorescence increases upon proteolytic degradation. Splenocytes were treated with 10μg/ml DQ-OVA for 1h (pulse), after which all extracellular OVA was washed off. Cells were further incubated for the indicated chase periods in the presence or absence of BCH (25mM) before flow cytometry analysis. Data are representative **(A,C)** or mean +/- SEM **(C,D)** of three independent experiments. Data were analysed using multiple unpaired t-tests. (*p<0.05, **p<0.01)

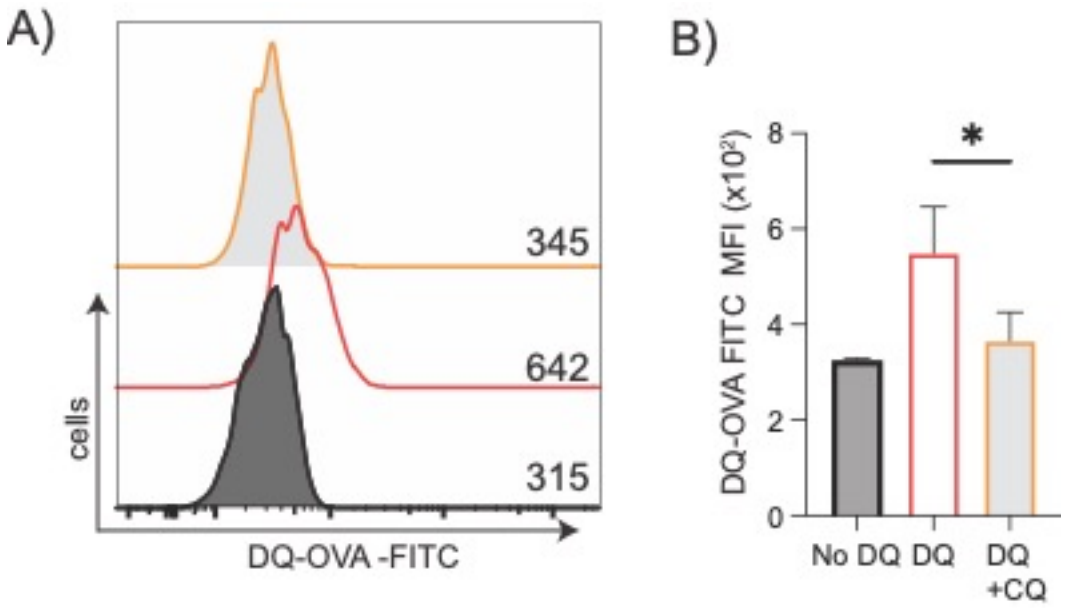

Figure 4.26 – Chloroquine treatment reduces antigen degradation in cDC1s

(A,B) Flow cytometry analysis of splenocytes from C57Bl/6 mice inoculated with B16-Flt3l cells analysing the rate of antigen degradation in cDC1s **(A,B).** Chloroquine is a lysosomotropic weak base that diffuses into lysosomes, increasing pH and reducing lysosomal protein degradation. Splenocytes were treated with 10μg/ml DQ-OVA for 1h (pulse), after which all extracellular OVA was washed off. Cells were further incubated for 1h (chase) in the presence or absence of chloroquine (50μM), and DQ-OVA fluorescence was determined by flow cytometry. Data are representative **(A)** or mean +/- SEM **(B)** of four biological replicates. Data were analysed using one-way ANOVA with Tukey's post-test. (*$p<0.05$)

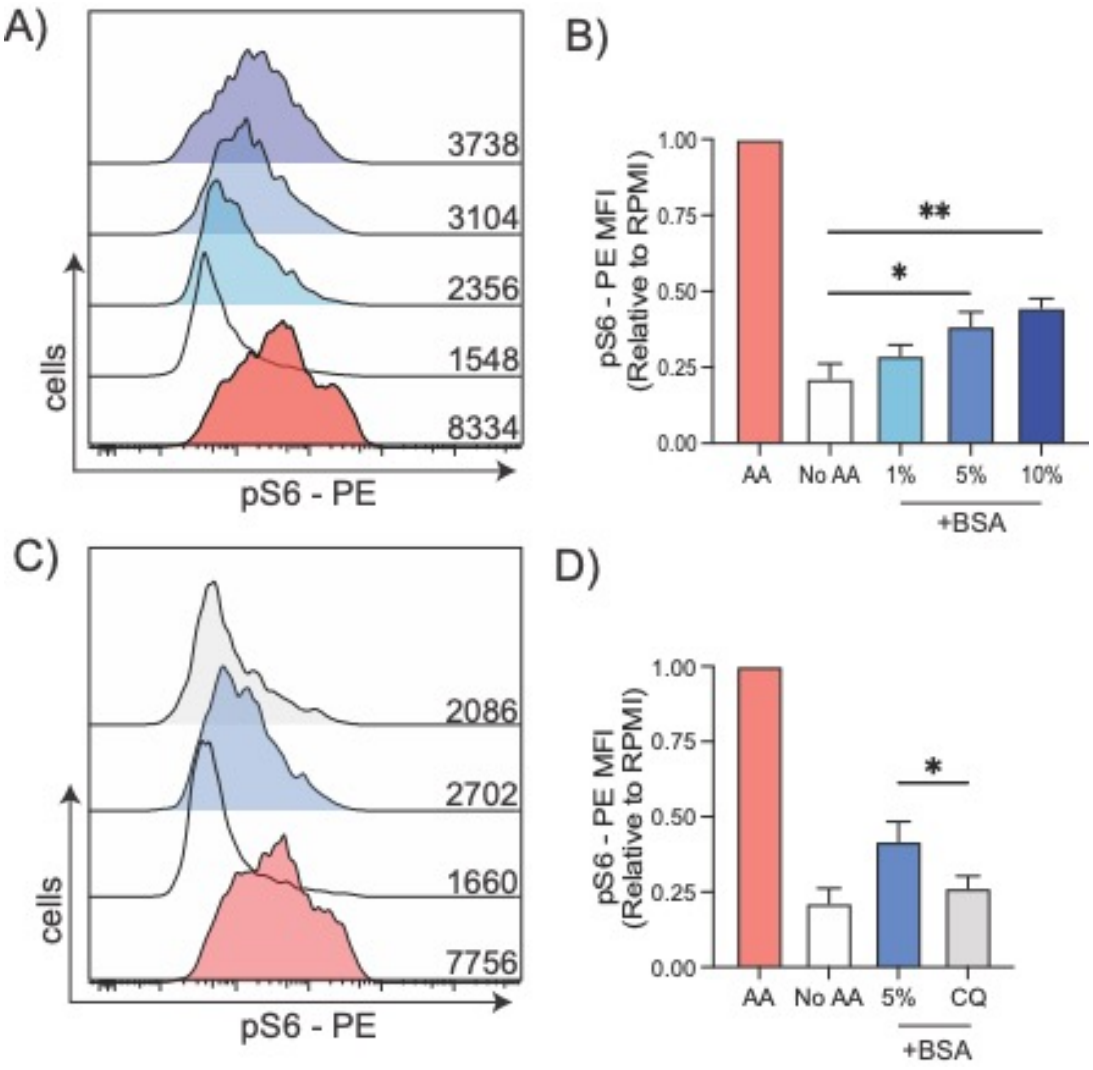

Figure 4.27 – Lysosomal protein catabolism recovers mTORC1 signalling during amino acid deprivation

(A-D) Flow cytometry analysis of splenocytes from C57Bl/6 mice inoculated with B16-Flt3l cells analysing mTORC1 signalling by phosphorylation of the mTORC1 target S6 in cDC1s. **(A,B)** Splenocytes were cultured in HBSS + EAA/NEAA cocktail or HBSS (No AA) for 30 mins, followed by the addition of the indicated concentrations of BSA (w/v) for 2h before flow cytometry analysis. **(C,D)** Splenocytes were cultured in HBSS + EAA/NEAA cocktail or HBSS (No AA) for 30 mins followed by the addition of 5% (w/v) BSA in the presence or absence of chloroquine (50μM) for 2h. Pooled data is relative to the AA condition. Data are representative **(A,C)** or mean +/- SD **(B,D)** of three biological replicates. Data were analysed using one-way ANOVA with Tukey's post-test. (*p<0.05, **p<0.01)

4.10 SLC7A5 transport regulates cross-presentation in cDC1s

To investigate whether enhanced OVA degradation is due to changes in endolysosomal acidification, I measured endolysosomal acidification rates in response to SLC7A5 transport inhibition. cDC1s were treated with BCH or HBSS (Vehicle control) for the indicated times, and endolysosomal acidification was determined by pHrodo green dextran and lysotracker red staining by flow cytometry **(Fig 4.28)**. pHrodo green is a rhodamine-derived fluorogenic probe whose fluorescence increases as pH decreases. The dextran conjugation targets the pHrodo dye to the endolysosomal compartment, thus offering a measure of endolysosomal pH. First, the dextran uptake rate was determined using a pH-insensitive dextran conjugate (dextran-AF647) **(Fig 4.28 A)**. BCH treatment significantly reduces dextran uptake relative to vehicle control. In line with the enhanced antigen degradation observed in response to SLC7A5 inhibition, BCH significantly increases lysosomal acidification in cDC1s **(Fig 4.28 B)**. This observation was confirmed using lysotracker red staining, which increases fluorescence as lysosomal pH decreases **(Fig 4.28 C)**. These data suggest that SLC7A5 transport inhibition increases the rate of antigen degradation by increasing the rate of lysosomal acidification.

As lysosomal acidification has been reported to regulate cross-presentation in DCs, I investigated whether SLC7A5 transport inhibition affects cross-presentation in cDC1s (Delamarre et al., 2005). Splenocytes were stimulated with CpG-B in the presence or absence of 20μg/ml soluble OVA protein. After 6 hours, extracellular OVA was washed off, and splenocytes were cultured for 12 hours in cRPMI. Cross-presentation was determined using the H2-KB-SIINFEKL antibody by flow cytometry, which is specific for OVA peptide MHCI complexes. In accordance with the literature, cDC1s more effectively cross-present soluble OVA than cDC2s **(Fig 4.29).** To test whether SLC7A5 inhibition influences cross-presentation, I measured H2KB activity at an early **(Fig 4.30)** and late time point **(Fig 4.31)**. Interestingly, BCH treatment of cDC1s increases cross-presentation after 3 hours of stimulation **(Fig 4.30 A-C).** cDC1s treated with the SIINFEKL peptide, which has a high affinity for

MHCI molecules and does not require antigen processing, are not affected by BCH treatment, indicating that BCH is increasing the rate of antigen processing in cDC1s **(Fig. 4.30 D-F)**. This supports findings that DC maturation induces lysosomal acidification by promoting V-ATPase complex assembly, which supports antigen processing (Liberman et al., 2014). Thus, increased lysosomal acidification due to BCH treatment would be expected to increase cross-presentation at earlier times. However, many studies have shown that enhanced lysosomal acidification is detrimental to cross-presentation. It has been reported that delayed antigen degradation supports the sustained cross-presentation of antigens by preserving antigen epitopes (Van Montfoort et al., 2009). In line with these reports, the percentage of cDC1s cross-presenting the H2-kB peptide is trending downwards ($P<0.08$) when treated with OVA protein in the presence of BCH for 18 hours **(Fig. 4.31 A,B)**. Additionally, the MFI of H2-kB expression of cDC1s is significantly reduced in the BCH treated group relative to RPMI **(Fig 4.31 C,D)**. As BCH treatment decreased the rate of dextran uptake, I investigated whether effects on OVA uptake may account for the reduced cross-presentation in response to BCH treatment **(Fig. 4.32 A,B)**. cDC1s were treated with a fluorescently conjugated OVA protein (OVA-647) in the presence or absence of BCH for the indicated times. BCH treatment does not affect the rate of OVA uptake in cDC1s.

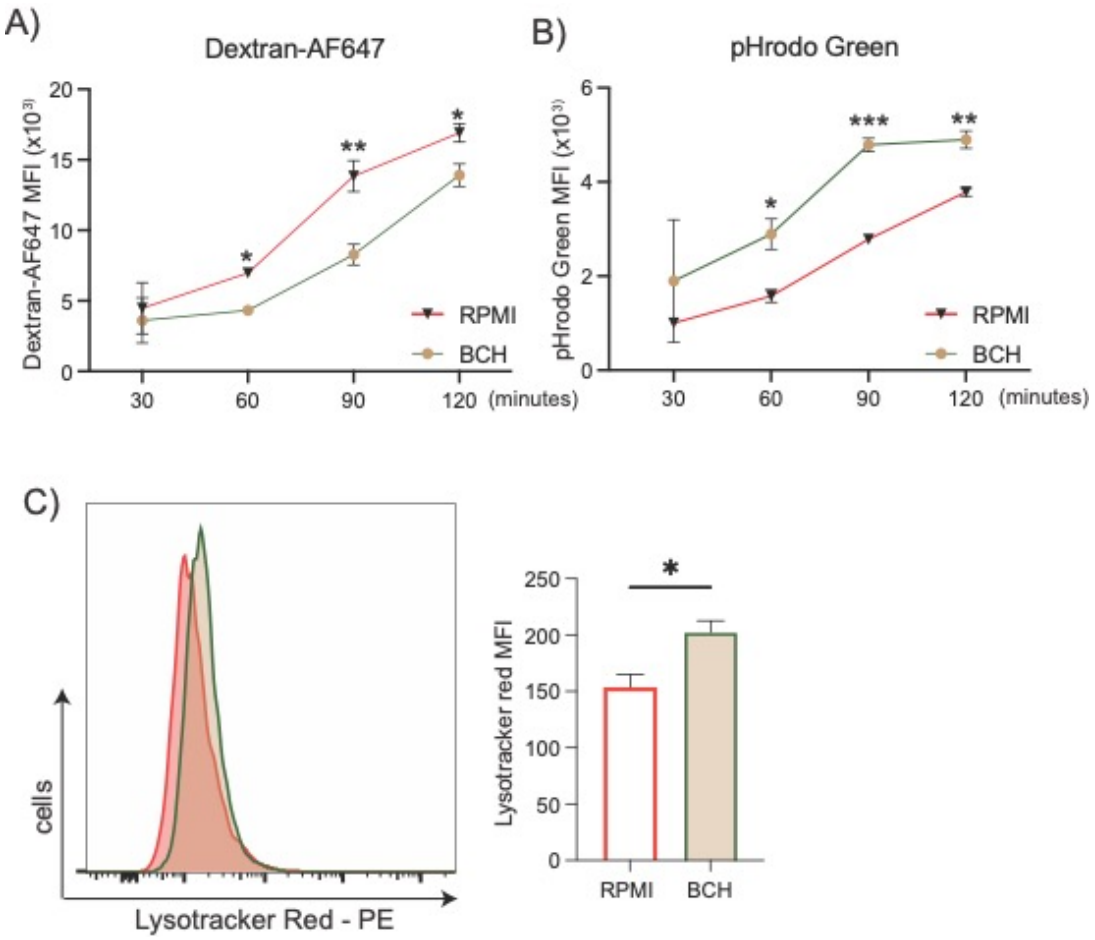

Figure 4.28 – SLC7A5 transport inhibition induces lysosomal acidification in cDC1s

(A-D) Flow cytometry analysis of magnetic bead sorted XCR1⁺ cDC1s from C57Bl/6 mice inoculated with B16-Flt3l cells analysing lysosomal acidification. **(A,B)** cDC1s were treated with **(A)** dextran-AF647 or **(B)** pHrodo green dextran (20ng/ml) for the indicated times in the presence or absence of BCH (25mM) before flow cytometry analysis. **(C)** cDC1s were treated with PBS (vehicle control) or BCH (25mM) for three hours before lysotracker red analysis. Data are representative **(C)** or mean +/- SEM **(A,B,D)** of four biological replicates. Data were analysed using a two-way ANOVA with Dunnett's post-test **(A,B)** or unpaired students' t-test **(C) (A-D)** (*p<0.05, **p<0.01, ***p<0.001)

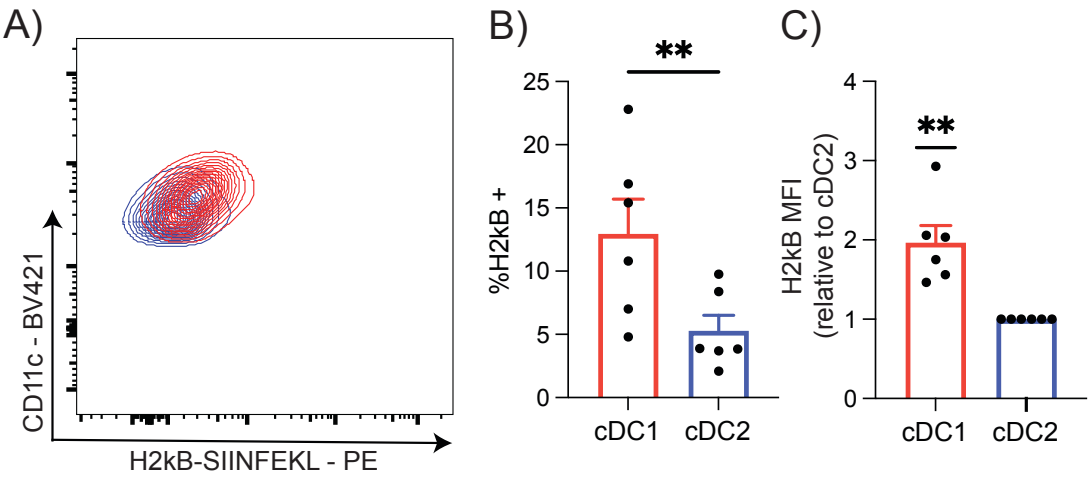

Figure 4.29 – cDC1s are superior at antigen cross-presentation than cDC2s

(A-C) Flow cytometry analysis of splenocytes from C57Bl/6 mice inoculated with B16-Flt3l cells analysing the cross-presentation of soluble OVA protein by H2kB-OVA staining. H2kB-SIINFEKL (25-D1.16) recognises MHCI molecules that present the OVA peptide SIINFEKL (OVA 257-264). Splenocytes were stimulated with 4μg/ml CpG-B and treated with soluble OVA protein (20μg/ml) for 6 hours, after which all extracellular OVA was washed off. Splenocytes were cultured for a further 12 hours in cRPMI before flow cytometry analysis. Data are representative **(A)** or mean +/- SEM **(B,C)** of six independent experiments. Data were analysed using paired students' t-tests. (**p<0.01)

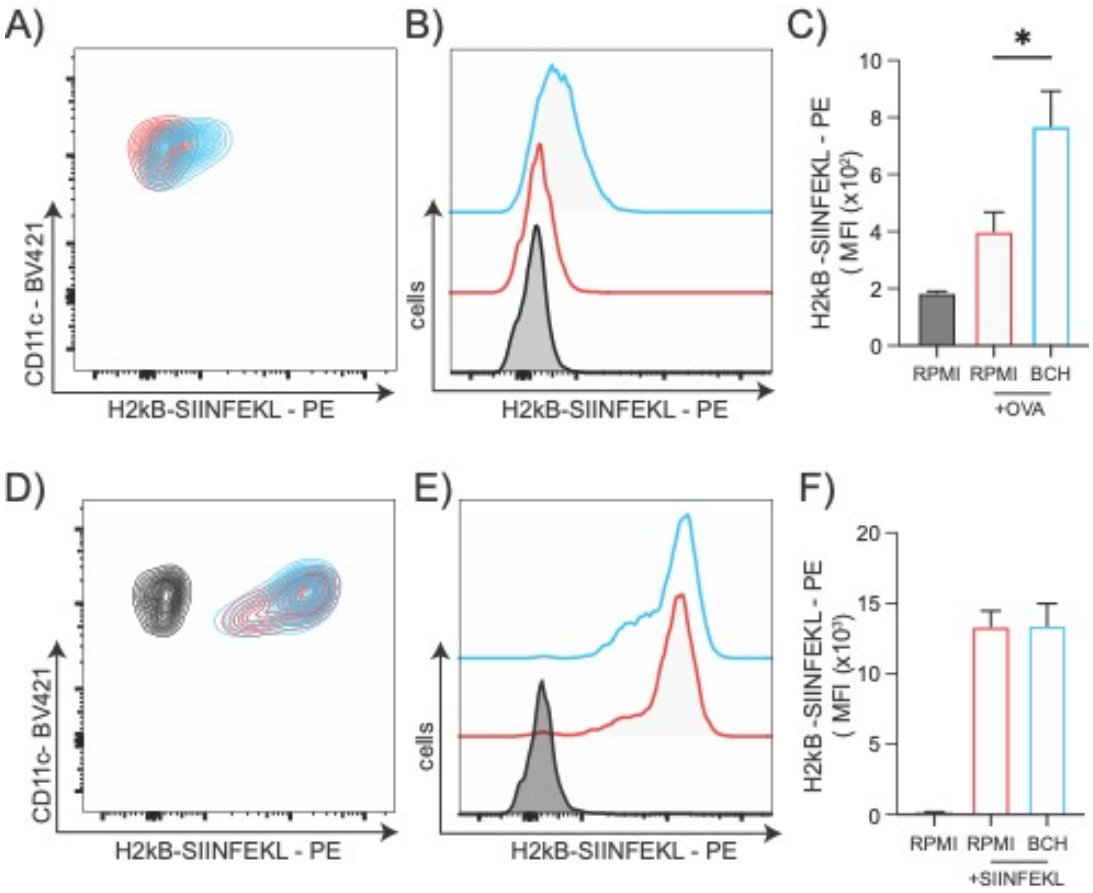

Figure 4.30 – SLC7A5 inhibition enhances early cross-presentation in cDC1s

(A-F) Flow cytometry analysis of magnetically sorted XCR1$^+$ cDC1s from C57Bl/6 mice inoculated with B16-Flt3l cells analysing the cross-presentation of soluble OVA protein by H2kB-SIINFEKL staining. H2KB-OVA recognises MHCI molecules that present the OVA peptide SIINFEKL. Splenocytes were stimulated with 4μg/ml CpG-B and treated with **(A-C)** soluble OVA protein (20μg/ml) or **(D-F)** SIINFEKL peptide (1μg/ml) for 3 hours before flow cytometry analysis. Data are representative **(A,B,D,E)** or mean +/- SEM **(C,F)** of four biological replicates. Data were analysed using one-way ANOVA with Tukey's post-test. (*p<0.05)

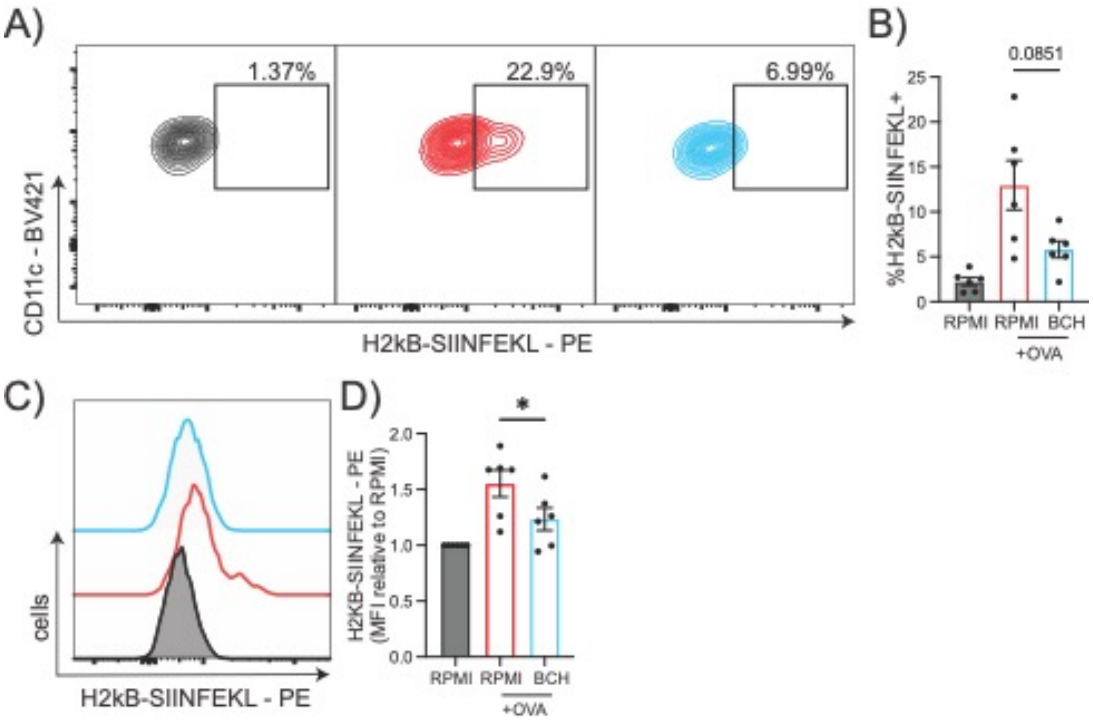

Figure 4.31 – SLC7A5 inhibition reduces sustained cross-presentation in cDC1s

(A-D) Flow cytometry analysis of splenocytes from C57Bl/6 mice inoculated with B16-Flt3l cells analysing the cross-presentation of soluble OVA protein by H2kB-SIINFEKL staining in cDC1s. H2KB-SIINFEKL recognises MHCI molecules that present the OVA peptide SIINFEKL. Splenocytes were stimulated with 4μg/ml CpG-B and treated with soluble OVA (20μg/ml) for 6 hours, after which all extracellular OVA was washed off. Splenocytes were cultured for a further 12 hours in cRPMI before flow cytometry analysis. Data are representative **(A,C)** or mean +/- SEM **(B,D)** of six biological replicates. Data were analysed using one-way ANOVA with Tukey's post-test. (*p<0.05)

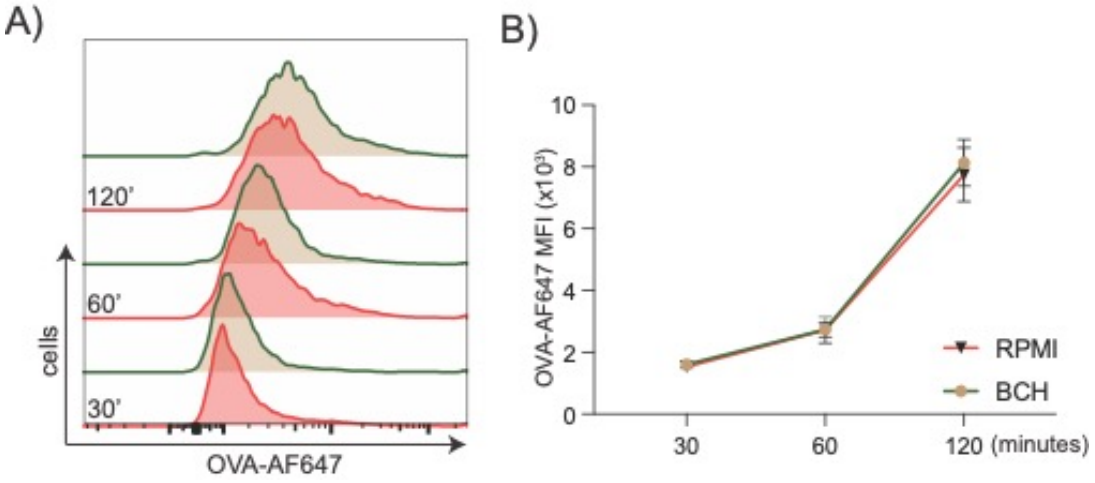

Figure 4.32 – SLC7A5 transport inhibition does not affect the rate of OVA uptake in cDC1s

(A,B) Flow cytometry analysis of magnetically sorted XCR1^{+} cDC1s from C57Bl/6 mice inoculated with B16-Flt3l cells analysing the rate of OVA uptake in cDC1s. cDC1s were treated with 1μg/ml of the fluorescent OVA conjugate (OVA-AF647) for the indicated times in the presence or absence of BCH (25mM) before flow cytometry analysis. Data are representative **(A)** or mean +/- SEM **(B)** of four biological replicates.

4.11 SLC7A5 regulates DC-mediated CD8 T cell responses in cDC1s

As SLC7A5 transport inhibition reduced co-stimulatory marker expression and cross-presentation capacity of cDC1s, I next investigated if pharmacological inhibition of SLC7A5 affects cDC1 mediated CD8 T cell responses. Purified cDC1s were stimulated with CpG-B in the presence or absence of BCH, with or without OVA protein, for 6 hours, after which cDC1s were co-cultured with OT-1 T cells at a ratio of 1:1 in cRPMI **(Fig. 4.33)**. OT-1 T cells have a transgenic TCR specific to the SIINFEKL peptide presented on MHCI. cDC1s and OT-1 T cells were co-cultured for 24 **(Fig 4.33 A,B)**, 48 **(Fig 4.33 C,D)** and 72 hours **(Fig 4.33 E,F)** and OT-1 T cell viability was determined by flow cytometry. As expected, OT-1 T cells co-cultured with cDC1s in the absence of OVA and thus lacking TCR stimulation have low viability at all time points tested **(Fig 4.33 A-F)**. BCH treated cDC1s promote similar OT-1 T cell viability after 24 hours of co-culture **(Fig 4.33 A-B);** however, OT-1 T cell viability is significantly reduced at 48 hours **(Fig 4.33 C,D)** and 72 hours **(Fig 4.33 E,F)** of co-culture. This data aligns with the ability of SLC7A5 transport inhibition to enhance early cross-presentation **(Fig 4.30)** but abrogate prolonged cross-presentation in cDC1s **(Fig 4.31)**. I next assessed whether cDC1 SLC7A5 transport inhibition affects OT-1 T cell activation after 24 hours **(Fig 4.34)** and 48 hours **(Fig 4.35)** of co-culture. OT-1 T cell activation was determined by measuring the expression of the T cell activation marker CD69 by flow cytometry. Co-culture of OT-1 T cells in the presence of OVA protein or SIINFEKL short peptide induces CD69 expression at 24 and 48 hours of coculture, indicating T cell activation. In line with OT-1 T cell viability after 24 hours of co-culture, BCH treated cDC1s induce similar OT-1 T cell activation with both OVA **(Fig 4.34 A,C,D,E)** and SIINFEKL treatment **(Fig 4.34 B,C,D,E)**. After 48 hours of co-culture, OT-1 T cell CD69 expression is significantly reduced when co-cultured with BCH and OVA-treated cDC1s **(Fig 4.35 A,C,D,E)**, indicating a reduction in cDC1 mediated T cell activation. Interestingly, BCH treatment does not affect OT-1 T cell activation in the presence of the SIINFEKL short peptide. This suggests that the BCH-mediated reduction in OT-1 T cell activation with OVA protein is due to differences in antigen processing.

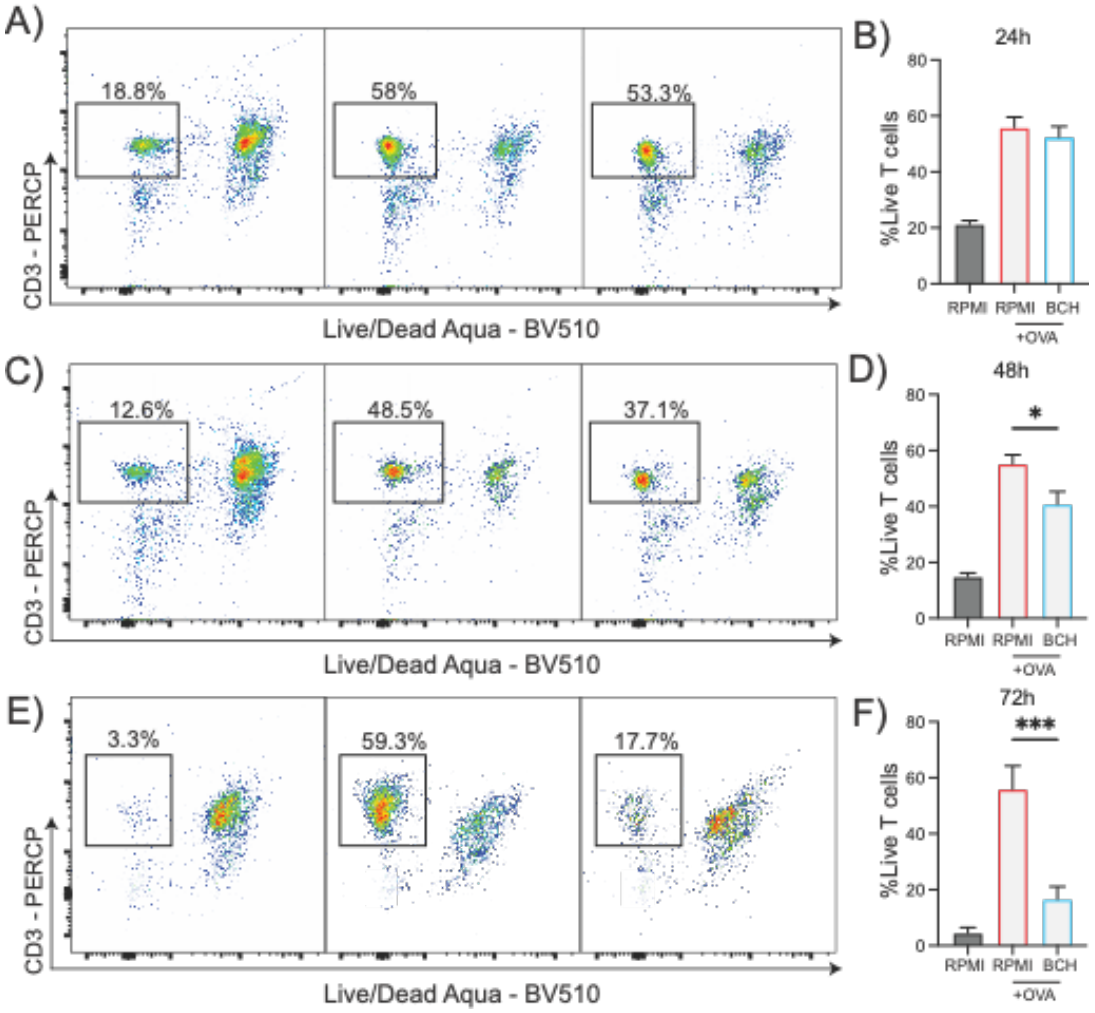

Figure 4.33 – SLC7A5 transport inhibition reduces OT-1 T cell survival *in vitro*

(A-F) Flow cytometry analysis of magnetically sorted XCR1$^+$ cDC1s from C57Bl/6 mice inoculated with B16-Flt3l cells co-cultured with OT-1$^+$ T cells in vitro. OT-1$^+$ T cells have a transgenic TCR specific for MHC-I, presenting the SIINFEKL peptide. cDC1s were stimulated with 4μg/ml ODN1826 in the presence or absence of BCH (25mM), with or without soluble OVA protein (20μg/ml) for 6 hours, after which all extracellular OVA was washed away. cDC1s were co-cultured with OT-I CD8 T cells at a ratio of 1:1 for the indicated times in cRPMI before flow cytometry analysis. Data are representative **(A,C,E)** or mean +/- SEM **(B,D,F)** of three biological replicates. Data were analysed using one-way ANOVA with Tukey's post-test. (*p<0.05)

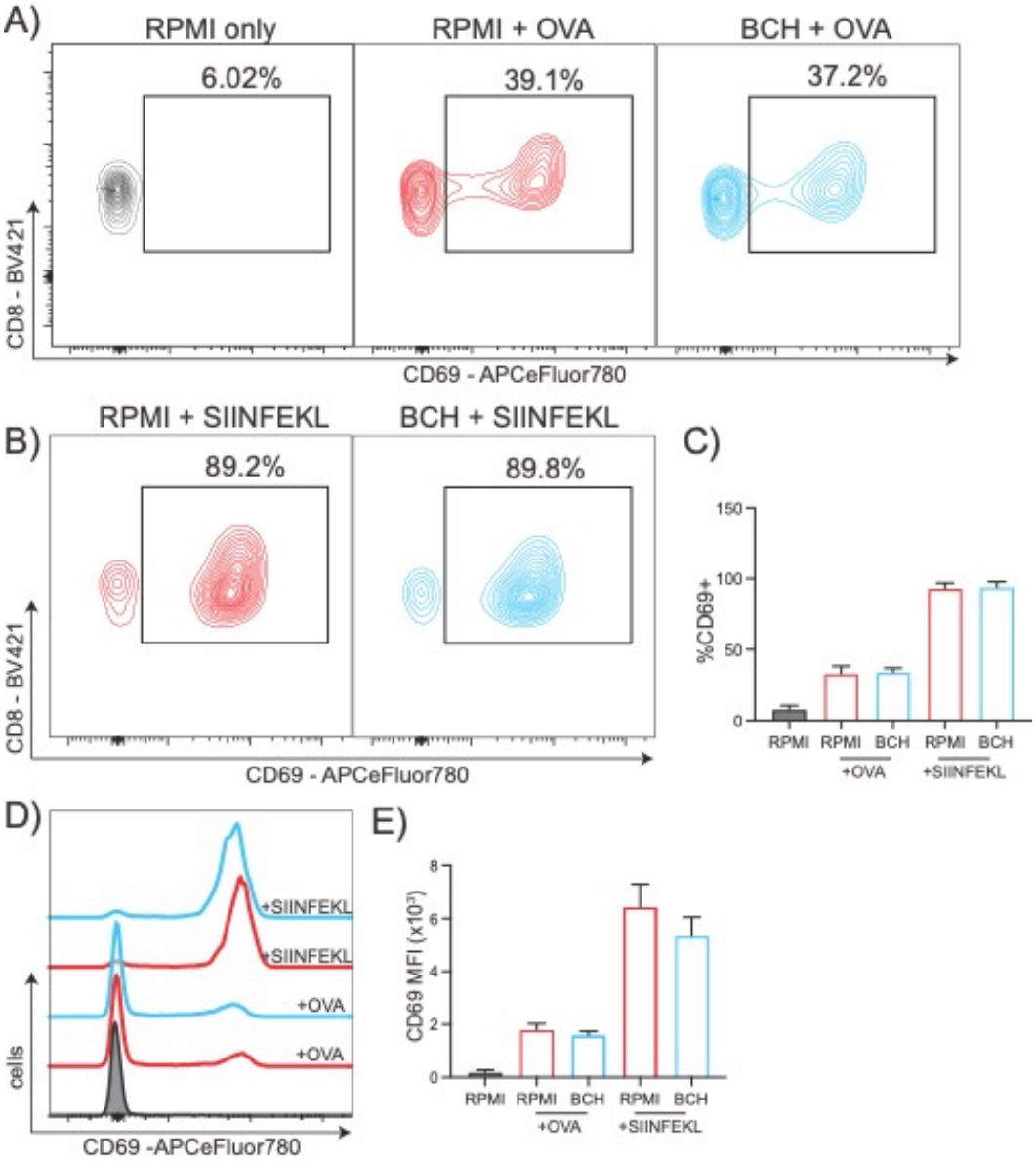

Figure 4.34 – SLC7A5 transport inhibition in cDC1s does not affect OT-I activation after 24h of co-culture

(A-E) Flow cytometry analysis of magnetically sorted XCR1$^+$ cDC1s from C57Bl/6 mice inoculated with B16-Flt3l cells co-cultured with OT-1$^+$ T cells in vitro. OT-1$^+$ T cells have a transgenic TCR specific for MCHI, presenting the SIINFEKL peptide. cDC1s were stimulated with 4μg/ml CpG-B in the presence or absence of BCH (25mM), with or without **(A)** soluble OVA protein (20μg/ml) or **(B)** SIINFEKL (1μg/ml) peptide for 6 hours, after which all extracellular OVA was washed away. cDC1s were co-cultured with OT-I CD8 T cells at a ratio of 1:1 for 24 hours in cRPMI before flow cytometry analysis. OT-1 T cell activation was measured by the induction of CD69 expression. Data are representative **(A,B,D)** or mean +/- SEM **(C,E)** of three biological replicates. Data were analysed using one-way ANOVA with Tukey's post-test. (*p<0.05)

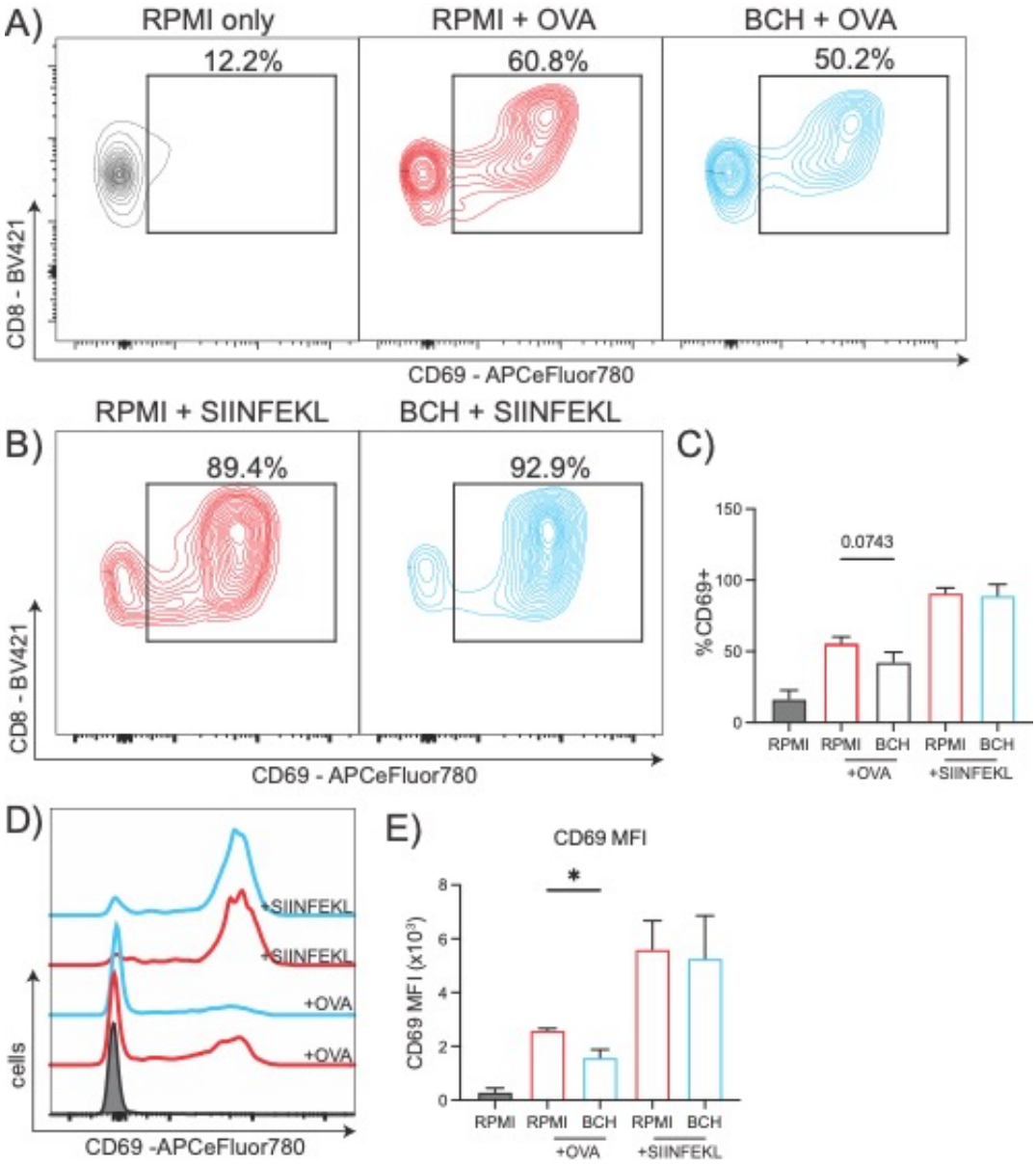

Figure 4.35 - SLC7A5 transport inhibition in cDC1s reduces OT-I activation after 48h of co-culture

(A-E) Flow cytometry analysis of magnetically sorted XCR1$^+$ cDC1s from C57Bl/6 mice inoculated with B16-Flt3l cells co-cultured with OT-1$^+$ T cells in vitro. OT-1$^+$ T cells have a transgenic TCR specific for MCHI, presenting the SIINFEKL peptide. cDC1s were stimulated with 4μg/ml CpG-B in the presence or absence of BCH (25mM), with or without **(A)** soluble OVA protein (20μg/ml) or **(B)** SIINFEKL (1μg/ml) peptide for 6 hours, after which all extracellular OVA was washed away. cDC1s were co-cultured with OT-I CD8 T cells at a ratio of 1:1 for 48 hours in cRPMI before flow cytometry analysis. OT-1 T cell activation was measured by the induction of CD69 expression. Data are representative **(A,B,D)** or mean +/- SEM **(C,E)** of three biological replicates. Data were analysed using one-way ANOVA with Tukey's post-test. (*p<0.05)

4.12 Discussion

Chapter 4 investigated the role of SLC7A5-mediated amino acid transport on splenic cDC function. SLC7A5 is a large neutral amino acid transporter whose activity has been described to play a critical role in modulating immune cell function and the proliferation of malignant cells (CRUK Rosetta Grand Challenge Consortium et al., 2021; Nachef et al., 2021; O'Brien & Finlay, 2019). In proliferating lymphocytes, SLC7A5 controls anabolic processes by regulating the activity and stability of anabolic regulators, including mTORC1 and cMYC (Loftus et al., 2018; Marchingo et al., 2020; L. V. Sinclair et al., 2013). As cMYC was shown to be repressed during the development of cDCs (Anderson et al., 2022; Kc et al., 2014), I decided to investigate the control of mTORC1 signalling by SLC7A5-mediated amino acid transport. The role of mTORC1 on DC biology has been studied extensively and seems context- and species-dependent (Snyder & Amiel, 2019). For example, while some studies report that mTORC1 inhibition can augment DC activation (Cheng et al., 2016; Haidinger et al., 2010; Raïch-Regué et al., 2015), others have shown a negative impact on DC maturation (Amiel et al., 2012, 2014). The source of this disparity across studies may be attributed to using different DC models, including bone marrow-derived DCs (BMDCs), monocyte-derived DCs and tissue-resident DC subsets. A recent report from Pelgrom et al. brought clarity to the role of mTORC1 signalling in splenic cDC subsets by using a CD11c-creRaptor$^{fl/fl}$ transgenic approach, which generated DCs that lack the mTORC1 complex subunit Raptor and have deficient mTORC1 signalling (Pelgrom et al., 2022). This study found that loss of Raptor alters their metabolic properties and compromises DC maturation, particularly in cDC1s. In agreement with the more pronounced effect of Raptor deletion on cDC1 maturation reported in Pelgrom et al., cDC1s were found to have a higher abundance of mTORC1 complex components, including Raptor, than cDC2s in the steady state. In addition, cDC1s have higher mTORC1 activity than cDC2s, as determined by the phosphorylation of the mTORC1 targets S6 and EIF4BP1/2. This observation aligns with the proteomic findings in Chapter 3 that cDC1s have higher protein translation rates than cDC2s, as both S6 and EIF4BP1/2 regulate translation initiation. Indeed, inhibition of

mTORC1 signalling with rapamycin reduces the rate of protein synthesis in cDC1s and cDC2s. Upon acute CpG-B stimulation, both cDC1s and cDC2s increase mTORC1 activity, which is required for the upregulation of translation associated with DC maturation. This early increase in protein biosynthesis has been previously reported in BMDCs and proposed to facilitate the synthesis of costimulatory markers and cytokines associated with DC maturation (Lelouard et al., 2007).

In contrast to mTORC2, mTORC1 activity is acutely sensitive to amino acid availability, particularly leucine and arginine (Chantranupong et al., 2016; Geiger et al., 2016; Jewell et al., 2015; Saxton et al., 2016). mTORC1 senses amino acid availability at the lysosome through a complex mechanism mediated by Rag GTPases (Saxton & Sabatini, 2017). Extracellular leucine uptake in immune cells is primarily mediated by the L-type amino acid transporters (LATs), while arginine uptake is mediated by cationic amino acid transporters (CATs). Analysis of amino acid transporter expression in cDC1s and cDC2s identifies that SLC7A5 (LAT1) is the only LAT expressed in both subsets. While SLC7A1 (CAT1) is the only CAT expressed, it is lowly abundant relative to SLC7A5. This suggests that SLC7A5 may be the primary amino acid transporter regulating mTORC1 activity in cDCs. SLC7A5 forms a heterodimer with CD98 (SLC3A2) to facilitate amino acid transport. In line with the higher mTORC1 activity observed, cDC1s have significantly higher expression of both SLC7A5 and CD98 compared to cDC2s. The anti-inflammatory metabolite kynurenine has been identified as a substrate of LATs (L. V. Sinclair et al., 2018). Considering SLC7A5 is the only LAT expressed in cDCs, kynurenine uptake is proportional to the rate of SLC7A5 transport. Indeed, in line with the higher SLC7A5:CD98 heterodimer expression, cDC1s have significantly higher rates of kynurenine uptake than cDC2s.

To investigate whether SLC7A5 transport activity controls mTORC1 signalling in cDCs, I used the SLC7A5 transport inhibitor BCH. As previously described in lymphocytes, BCH treatment rapidly inhibited mTORC1 signalling in cDC1s and cDC2s (Loftus et al., 2018; L. V. Sinclair et al., 2013). This suggests that

the higher expression and activity of SLC7A5 in cDC1s supports the enhanced mTORC1 signalling and protein biosynthesis observed. Interestingly, despite increased mTORC1 signalling and puromycin incorporation in response to CpG-B stimulation, there is no increase in kynurenine uptake. This result contrasts with what is observed in activated lymphocytes, which profoundly increase SLC7A5 expression and transport activity upon activation (Howden et al., 2019). For example, while naïve CD8 T cells have <10,000 copies per cell of SLC7A5, cytotoxic T lymphocytes (CTLs) have approximately 300,000 copies, representing a 30-fold increase in expression(Howden et al., 2019). It is important to consider that in contrast to cDCs, T-cell activation is associated with extremely high rates of proliferation and biosynthesis required for clonal expansion.

Despite no increase in SLC7A5 activity upon immunogenic stimulation, BCH treatment abrogated the increase in mTORC1 signalling in response to CpG-B stimulation. This indicates that homeostatic SLC7A5 activity is sufficient to sustain anabolic signalling in cDCs. As briefly mentioned above, the role of mTORC1 signalling during DC maturation has been studied extensively (Snyder & Amiel, 2019; Sukhbaatar et al., 2016). However, how the control of mTORC1 activity by amino acid availability regulates DC maturation needs to be clarified. Thus, I next investigated whether SLC7A5-mediated transport activity plays a role in DC maturation. SLC7A5 inhibition with BCH did not affect proinflammatory cytokine production in both cDC1s and cDC2s in response to CpG-B stimulation. This agrees with the observation from Pelgrom et al. that attenuated mTORC1 signalling does not affect cytokine production in cDC1s and cDC2s (Pelgrom et al., 2022). On the other hand, analysis of costimulatory marker expression reveals that SLC7A5 inhibition significantly reduces the expression of CD40 and CD86 in both cDC1s and cDC2s. This finding contrasts with those of Pelgrom et al., who show no impact on costimulatory marker expression when mTORC1 is repressed. Considering that enhanced protein synthesis during the early phase of DC maturation is proposed to support the requirement for cytokine and costimulatory marker production (Lelouard et al., 2007), it is interesting to consider how a global reduction in protein translation in response to BCH

leads to a reduction in the expression of some proteins but not others. For example, despite global translational reduction, mTORC1 inhibition has been described as promoting the selective translation of specific mRNAs by regulating eIF3D-mediated mRNA translation (Shin et al., 2023). This mechanism is akin to the expression of ATF4 target proteins during global translation inhibition associated with the ER stress response (Mendes et al., 2021). In addition to its effect on protein synthesis, mTORC1 inhibition can also regulate gene transcription through the regulation of transcription factors. Thus, further research is required to understand the complex regulation of protein translation by mTORC1 in DCs. Further, it is important to note that while SLC7A5 transport regulates mTORC1 signalling, its effects may not phenocopy that of pharmacological mTORC1 inhibitors. During amino acid deprivation, mTORC1 inhibition upregulates cellular catabolic processes such as autophagy to restore nutrient homeostasis. While autophagy facilitates adaptation to low extracellular nutrient concentrations, it does not overcome pharmacological mTORC1 inhibition. Additionally, SLC7A5 is a prominent methionine transporter in immune cells (L. V. Sinclair et al., 2019). Methionine is an essential amino acid which serves as a critical source of methyl groups required for the fundamental cellular processes, including histone and DNA methylation, protein methylation and polyamine synthesis.

cDC1s have a superior ability to prime CD8 T cell and Th1 polarised CD4 T cell responses while cDC2s are more efficient in priming Th2 and Th17 CD4 T cell immunity (Cabeza-Cabrerizo et al., 2021). Numerous mechanisms have been proposed to mediate this functional partition, including cellular localisation within lymphatic organs, antigen presentation machinery expression and differential antigen degradation rates (Eisenbarth, 2019; Embgenbroich & Burgdorf, 2018). In agreement with previously reported mRNA microarray data, cDC1s have higher expression of the MHCI presentation machinery than cDC2s (Dudziak et al., 2007b). Antigen cross-presentation involves capturing, processing and presenting exogenous antigens on MHCI to induce CTL activation required for anti-viral and anti-tumour immunity (Embgenbroich & Burgdorf, 2018). Numerous studies have revealed that delayed endolysosomal antigen degradation correlates with

efficient cross-presentation (Accapezzato et al., 2005; Belizaire & Unanue, 2009; Cebrian et al., 2011; Delamarre et al., 2005; Jancic et al., 2007; Mantegazza et al., 2008; Savina et al., 2006). It is generally assumed that delayed degradation allows antigens time to escape the endolysosomal system for MHCI loading before complete antigen destruction. A pioneering study from Delamarre et al. revealed that BMDCs have lower expression of lysosomal proteases and slower protein degradation rates than BMDMs, favouring antigen presentation in dendritic cells (Delamarre et al., 2005). A limitation of this study is the use of BMDCs. Thus, I next investigated the expression of lysosomal proteases in cDC1s and cDC2s. Interestingly, despite having lower overall lysosomal protein content, cDC2s have higher expression of lysosomal cathepsins than cDC1s, with the notable exception of cathepsin S. While cathepsin S has been implicated in mediating MHCII presentation, it has also been identified as a key regulator of antigen generation for the vacuolar pathway of cross-presentation (Shen et al., 2004). Overall, the higher cathepsin expression in cDC2s indicates a more degrative endolysosomal environment than cDC1s, which is predicted not to favour cross-presentation. Indeed, as exogenous antigens are also targeted for MHCII presentation in the endolysosomal system, it has been proposed that more extensive lysosomal proteolysis favours MHCII presentation (Samie & Cresswell, 2015).

Lysosomal proteases are zymogens that are poorly active under alkaline pH. As antigen-laden endosomes fuse with acidic lysosomes, lysosomal proteolysis occurs, leading to antigen degradation. It has been revealed that cDC1s maintain a more alkaline endolysosomal pH than cDC2s, limiting lysosomal protease activity and allowing efficient cross-presentation (Jancic et al., 2007; Savina et al., 2006). A publication from the Amigorena lab revealed that in DCs, the small GTPase Rab27a induced the recruitment of NADPH oxidase (NOX2) to endolysosomes, which limits phagosomal acidification by scavenging protons for the generation of reactive oxygen species (Jancic et al., 2007). Genetic ablation of Rab27a expression was shown to delay NOX2 recruitment to phagosomes by 2-3h, which was sufficient to impair the cross-presentation of the model antigen ovalbumin. A

subsequent study from the same group revealed that cDC1s but not cDC2s effectively recruit NOX2 to phagosomes in a process mediated by the differential localisation of the Rho family small GTPase Rac2 (Savina et al., 2009) . Thus, cDC1s maintain a more alkaline phagosomal pH, favouring antigen cross-presentation. Indeed, analysis of lysosomal degradation in cDC1s and cDC2s using the fluorescent probe, DQ-Ovalbumin (DQ-OVA), reveals that cDC2s have higher rates of endolysosomal OVA degradation than cDC1s.

In subsequent years, additional mechanisms have been identified to regulate endolysosomal acidification in DCs. For example, the lysosomal regulator transcription factor EB (TFEB) has been shown to regulate the balance of MHCI and MHCII presentation of exogenous antigens (Samie & Cresswell, 2015). Activation and nuclear translocation of TFEB enhance lysosomal protease expression and antigen degradation, limiting antigen cross-presentation and promoting MHCII presentation. Notably, it was identified that $CD4^+$ DCs (cDC2s) and $CD11b^+$ macrophages have higher TFEB expression than $CD8^+$ cDC1s, which is proposed to be a contributing factor in their superior cross-presentation capacity. The mechanism underpinning TFEB activity in DCs is still undetermined. Interestingly, TFEB is a target of mTORC1, which phosphorylates a serine residue (Ser211) within its nuclear localisation signal, preventing TFEB translocation to the nucleus (Martina et al., 2012). Under nutrient deprivation, mTORC1 signalling is lost, allowing TFEB-mediated gene expression associated with lysosomal biogenesis and autophagy. Thus, the elevated mTORC1 signalling observed in cDC1s may be limiting TFEB nuclear activity, creating a more favourable environment for antigen cross-presentation.

In addition to regulating TFEB, mTORC1 has been shown to modulate lysosomal acidification directly by controlling the assembly and activity of the V-ATPase complex. Ratto et al. revealed that mTORC1 signalling is inhibited under nutrient deprivation, which induces V-ATPase assembly and enhanced endolysosomal degradation (Ratto et al., 2022). By increasing catabolic activity within the endolysosomal compartment, cells initiate the degradation

of proteins to restore intracellular nutrient homeostasis. This work supports previous findings from this group, showing that cancer cells sustain proliferation by the degradation of extracellular proteins in the absence of sufficient extracellular amino acids (Palm et al., 2015). Indeed, in the absence of extracellular amino acids, increasing concentrations of extracellular BSA lead to the restoration of mTORC1 signalling in cDC1s, suggesting that extracellular protein catabolism is a source of intracellular amino acids. Considering that cDCs have high rates of extracellular protein acquisition associated with immune surveillance and that SLC7A5 activity controls mTORC1 signalling, I investigated whether SLC7A5 amino acid transport controls endolysosomal degradation in cDCs. Using DQ-OVA to determine lysosomal degradation, SLC7A5 inhibition significantly increases OVA degradation in cDC1s but not cDC2s. To investigate whether this effect is mediated through the inhibition of mTORC1 signalling, I tested the rate of OVA degradation in the presence of rapamycin. Rapamycin significantly increased DQ-OVA fluorescence, similar to BCH treatment, which indicates that SLC7A5 controls endolysosomal degradation through mTORC1 signalling. Notably, inhibition of lysosomal catabolism using the lysosomotropic weak base chloroquine prevents the restoration of mTORC1 signalling in the absence of extracellular amino acids. Chloroquine has been shown to enhance antigen cross-presentation to $CD8^+$ T cells in a murine vaccination influenza model by modulating the rate of antigen degradation in DCs (Accapezzato et al., 2005). These data suggest a balance between extracellular amino acid availability and endolysosomal protein degradation through a mTORC1-mediated mechanism.

I next investigated whether the enhanced lysosomal degradation in response to SLC7A5 transport inhibition relates to changes in endolysosomal pH. pHrodo green is a fluorescent probe whose fluorescence increases in acidic environments. I used pHrodo green conjugated to dextran beads, which target the fluorescent dye to the endolysosomal compartment. To control for differential rates of dextran uptake across conditions, I measure the uptake of dextran conjugated to the pH-insensitive fluorophore Alexa-fluor 647 (AF647). BCH treatment significantly reduced the rate of dextran uptake relative to the

RPMI control. This data aligns with a previous report that mTORC1 inhibition with rapamycin abrogates macropinocytosis and mannose receptor-mediated endocytosis in BMDCs (Hackstein et al., 2002). After normalisation for differential rates of dextran uptake, BCH treatment was found to significantly and rapidly increase endolysosomal acidification.

Considering the effect of SLC7A5 inhibition on lysosomal acidification and lysosomal degradation, I next investigated the effect of BCH on antigen cross-presentation in cDC1s. Cross-presentation was determined by measuring the generation of MHCI-SIINFEKL complexes on the cell surface by flow cytometry in response to OVA. Interestingly, BCH treatment enhanced the rate of cross-presentation after 3h of OVA incubation. Notably, there was no change in response with incubation of the SIINFEKL short peptide, which bypasses the need for antigen degradation, indicating that the effect of BCH is associated with intracellular antigen processing. On the other hand, cross-presentation after 18h of BCH treatment significantly reduced the number of MCHI-SIINFEKL complexes in cDC1s. The enhanced cross-presentation observed after 3h of OVA incubation in response to BCH treatment suggests that enhanced lysosomal degradation increases the rate of antigen generation. This aligns with the observation that DC maturation transiently increases lysosomal acidification to promote the generation of antigens for both MHCII presentation and MHCI cross-presentation (Trombetta et al., 2003). However, as discussed above, rapid antigen degradation is proposed to reduce the efficiency of DCs to cross-present antigens to CD8 T cells. The reduction in MHCI-SIINFEKL complexes after 18h of BCH treatment suggests that at this later time point, OVA is fully degraded, which reduces sustained antigen cross-presentation. In agreement with this hypothesis, BCH treatment did not affect the survival of OT-I T cells after 24h of coculture with OVA-treated cDC1s in vitro. However, there is a significant reduction in the number of live CD8 T cells after 48 and 72h of culture. Furthermore, BCH only reduced T cell activation after 48h of co-culture but not at 24h. This effect on T-cell activation only occurred when cDC1s were treated with the OVA-full protein but not the SIINFEKL short peptide, indicating that the deficit was not due to changes in MHCI expression. Further experiments are required to determine

the effect of BCH treatment on cDC1-mediated T cell proliferation and cytokine production. While difficult to directly compare in vitro and in vivo systems, the enhanced OT-I T cell survival observed at later time points aligns with the findings of Garulli et al., who show that inhibition of lysosomal degradation using chloroquine moderately reduced OT-I T cell proliferation after 2 days but led to significant inhibition of T cell proliferation after 4 days. Overall, these data suggest that delayed antigen degradation permits prolonged DC-mediated T cell responses.

Chapter 5 – Quantitative proteomics reveals conserved expression of the transferrin receptor in pDCs

5.1 Introduction

Plasmacytoid dendritic cells (pDCs) are a unique subset of dendritic cells that are specialised in detecting viral ligands and the rapid production of large quantities of type-I interferon upon activation (Reizis, 2019). In the steady state, pDCs differ from classical DCs, showing a smooth round lymphoid morphology, low expression of co-stimulatory markers and weak stimulators of T cell proliferation. Upon activation, pDCs acquire a dendritic morphology, upregulated MHCII expression and co-stimulatory markers and activate T cells, although less efficiently than classical DCs (Reizis et al., 2011). A unifying feature of pDCs and cDCs is their reliance on the cytokine Fltl3 for their development (Cueto & Sancho, 2021). Unlike cDCs, pDCs have both “myeloid” and “lymphoid” features, which may be attributed to their complex developmental origin. Both myeloid and lymphoid hematopoietic precursors have been described to have the potential to generate pDCs in the bone marrow (Rodrigues & Tussiwand, 2020). For these reasons, despite being a member of the DC family, pDCs have distinct metabolic and functional properties (Guo & Chi, 2023; Møller et al., 2022; Wculek et al., 2019).

Despite extensive research in recent years, our knowledge of the phenotypic and metabolic drivers of pDC function are limited. In particular, it has emerged that the integration of both antigenic and environmental signals is a critical determinant in directing immune cell function (Guo & Chi, 2023). Environmental cues, including nutrient availability and oxygen tension, provide additional context at the site of infection or malignancy, promoting potentially beneficial or detrimental immune responses. For example, iron is a key element required for bacterial proliferation and immune cell function (Cronin et al., 2019). During bacterial infection, the host employs several strategies to sequester iron to limit bacterial growth and survival. However, limited iron availability has also been shown to negatively impact immune cell effector function (Frost et al., 2021; Littwitz-Salomon et al., 2021). Thus, there

is a complex interplay of environmental regulation between host and pathogen.

Chapter 6 will characterise the pDC proteome, identifying the relationship between mRNA and protein abundance and the conservation between murine and human pDCs. In particular, I examine the pDC antigen and environment-sensing machinery in murine and human pDCs and across splenic DC subsets to identify novel regulators of pDC function.

5.2 – Applying proteomic analysis to pDCs

Splenic pDCs are a rare immune cell population accounting for < 1% of total splenic immune cells (Reizis, 2019). pDCs were identified by flow cytometry as Lin^- (CD3, CD19, F4/80, LY6G) $CD11c^{int}CD317^+$ cells **(Fig. 5.1 A).** To generate enough pDCs to perform quantitative proteomics, C57/BL6 mice were inoculated with B16-Flt3l tumour cells for 10 days to induce expansion of the splenic DC compartment. pDC expansion in response to B16-Flt3l inoculation was quantified, showing significant enrichment of the pDC compartment **(Fig. 5.1 B,C)**. Quantitative proteomics was performed on splenic pDCs in the steady state, and the protein copy number per cell was determined using the proteomic histone ruler method (Wiśniewski et al., 2014). This analysis identified the expression of approximately 6700 proteins (BR1=6709, BR2=6696, BR3=6694) in each biological replicate (BR), of which 6631 proteins were co-expressed in all three replicates **(Fig. 5.2 A)**.

To confirm the reliability of this analysis, the quantification accuracy was determined by enumerating the number of unique peptides used to identify each protein. Proteins with high accuracy had more than eight unique and razor peptides; proteins with medium accuracy had between eight and three peptides; and any proteins below three unique peptides were characterised as low accuracy (Howden et al., 2019). Notably, most of the detected proteins exhibit a high accuracy in quantification, with approximately 52% classified as high accuracy, 30% as medium accuracy, and 18% as low

accuracy **(Fig. 5.2 B).** Furthermore, the total protein content per cell was determined, yielding an average of approximately 60pg/cell, consistent across three biological replicates **(Fig. 5.2 C)**. Indeed, linear regression analysis of protein copy number in the three biological replicates **(Fig. 5.3 A-C)** shows a high degree of similarity with an R^2 value (Pearson's correlation coefficient) of at least 0.96. Approximately 98% of proteins were detected in all three biological replicates, and a small percentage of outliers were found to be expressed in individual replicates (BR1 = 0.26%, BR2 = 0.19%, BR3 = 0.28%) **(Fig. 5.3 D)**.

Finally, as the proteomic analysis was performed on pDCs, cDC1s and cDC2s, I confirmed the specificity of the cell purification by identifying the abundance of cDC and pDC phenotype markers **(Fig. 5.4)**. In agreement with the flow cytometry analysis **(Fig. 5.1 A)**, pDCs have an intermediate abundance of CD11c and a low abundance of MHCII relative to cDCs **(Fig. 5.4 A)**. Further, pDCs do not express the cDC1 marker XCR1 and have low expression of the cDC2 marker, SIRPα **(Fig. 5.4 B)**. Analysis of pDC-specific phenotype markers, including the cell surface markers CD317 and B220 **(Fig. 5.4 C)** and pDC lineage transcription factors E2-2 and SPIB **(Fig. 5.4 D),** are enriched in pDCs as expected.

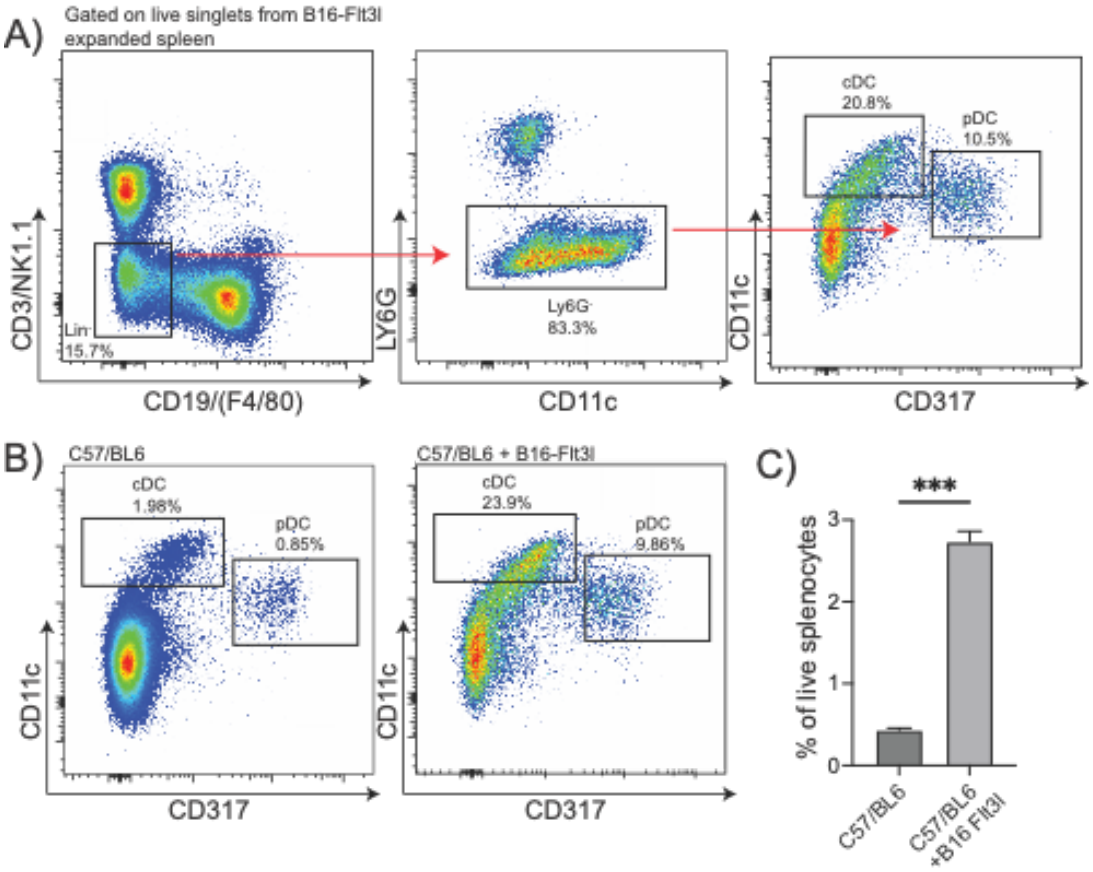

Figure 5.1 – Gating strategy used to identify splenic pDCs
(A-C) Flow cytometry analysis of splenocytes from C57Bl/6 mice or C57Bl/6 mice inoculated with B16-Flt3l cells for 10 days identifying splenic pDC. Splenic pDCs were identified as Lin^- (CD3, CD19, NK1.1, F4/80) $LY6G^-$, $CD11c^{int}CD317^+$ cells as shown in **(A) (B)** A comparison of the frequency of pDCs within splenocytes from untreated mice (left) and those inoculated B16-Flt3l cells (right). **(C)** Bar plot indicating the % of pDCs of live splenocytes from C57Bl/6 mice or C57Bl/6 mice inoculated with B16-Flt3l cells. Data are representative **(A,B)** or mean +/- SEM of three independent experiments **(C)**. Data are analysed using student's t-test (***p<0.001)

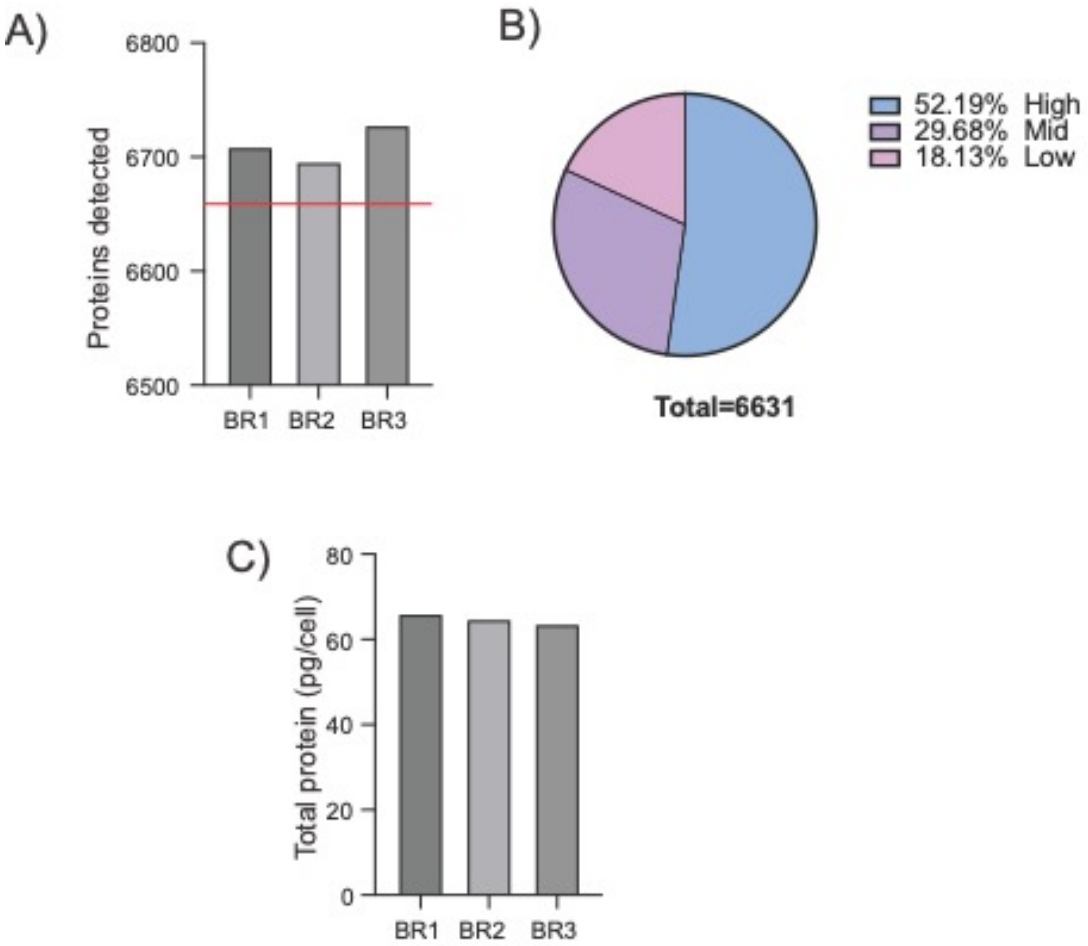

Figure 5.2 – Total protein content of splenic pDCs
(A-C) Quantitative proteomic analysis was performed on splenic pDCs from C57Bl/6 mice inoculated with B16-Flt3l cells, analysing the total number of proteins identified. **(A)** Total number of proteins identified in each biological replicate. The red line indicates the number of proteins shared in all three biological replicates. **(B)** Pie chart displaying the average percentage of proteins identified with high, medium and low confidence in three biological replicates. Proteins characterised as high confidence had more than eight unique and razor peptides; proteins characterised as medium confidence had between eight and three peptides; and any proteins below three unique peptides were characterised as low confidence. **(C)** Total protein content in each biological replicate. Total protein content was calculated as (copy number/cell x protein molecular weight)/Avogadro's constant. Quantitative proteomics was performed on three biological replicates.

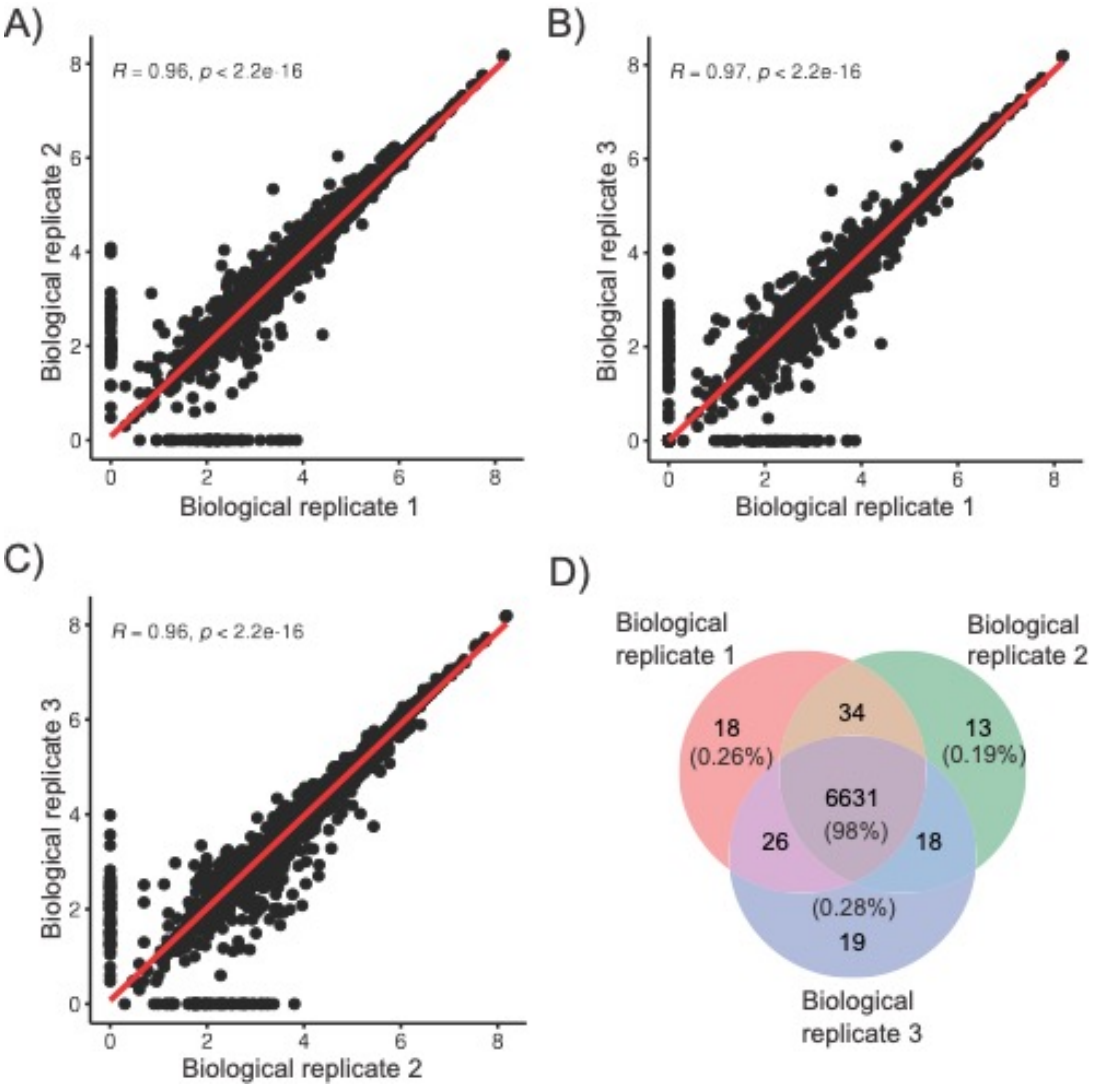

Figure 5.3 – Biological replicates of pDC proteomics are highly correlated

(A-D) Quantitative proteomic analysis was performed on three biological replicates of splenic pDCs from C57Bl/6 mice inoculated with B16-Flt3l cells, analysing the linear correlation between the copy numbers of each biological replicate. **(A-C)** Linear correlation of $\log_{10}$ copy number of proteins identified in three biological replicates. **(D)** Venn diagram of the number of shared and uniquely expressed proteins in pDC biological replicates. Data were analysed **(A-C)** using linear regression and Pearson's correlation—R^2 = Pearson's correlation coefficient.

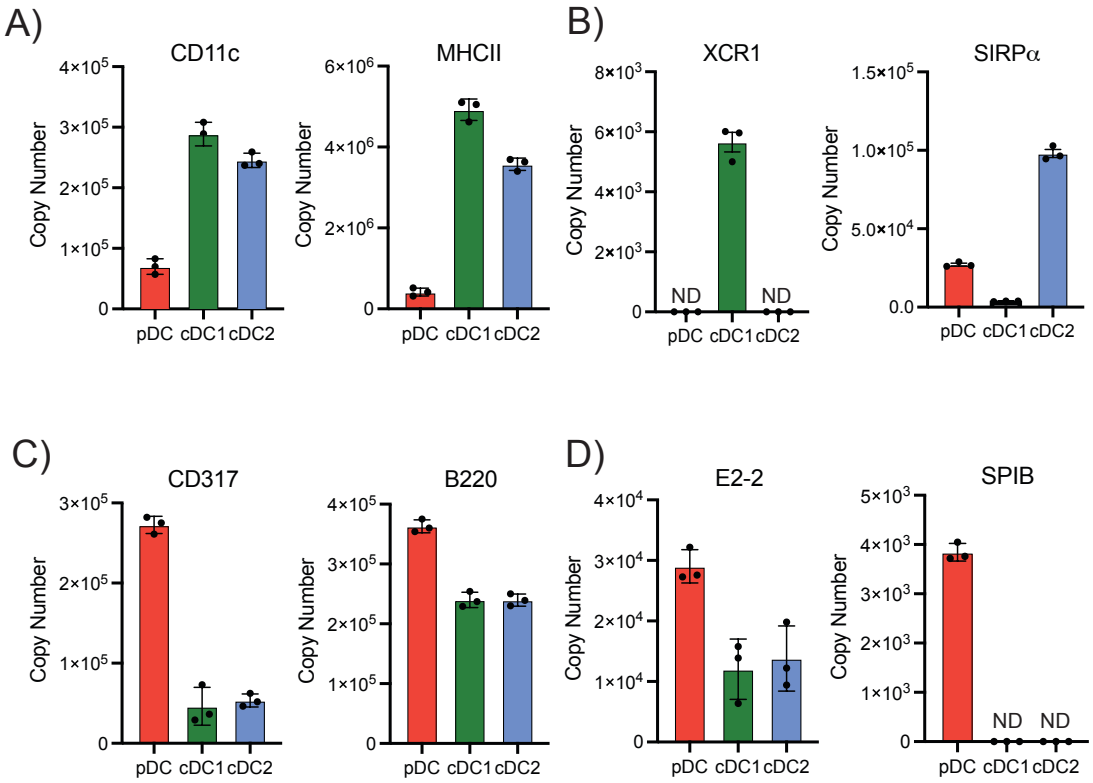

Figure 5.4 – Expression of pDC phenotype markers in quantitative proteomic analysis

(A-D) Quantitative proteomic analysis was performed on splenic DC subsets from C57Bl/6 mice inoculated with B16-Flt3l cells, specifically cDC1s ($CD11^{+}MHCII^{+}XCR1^{+}SIRPa^{-}$), cDC2s ($CD11^{+}MHCII^{+}SIRPa^{+}XCR1^{-}$) and pDCs ($CD11c^{int}MHCII^{lo}CD317^{+}$) analysing the expression of cell surface phenotype marker and lineage transcription factors. Copy number per cell (determined by the proteomic histone ruler) of **(A)** general DC markers, **(B)** cDC cell surface phenotype markers, **(C)** pDC cell surface phenotype markers and **(D)** pDC lineage transcription factors. Quantitative proteomics was performed on three biological replicates **(A-D)**. Pooled data is mean +/- SEM **(A-D)**. ND = Not detected

5.3 – General features of the pDC proteome

Understanding the proteome of a cell is useful for unveiling cellular mechanisms and identifying the underlying machinery of cellular metabolism and function (Howden et al., 2019; Marchingo et al., 2020). The proteome, comprising the complete set of proteins expressed by a cell, reflects its biological state. By characterising the proteome at both the level of individual protein abundance and, more broadly, at the level of global proteome architecture, valuable insights into cellular function can be revealed. Analysis of protein abundance in pDCs shows that a small number of highly abundant proteins account for the majority of the total protein copies identified in the pDC proteome **(Fig. 5.5 A)**. Strikingly, despite identifying approximately 6700 unique proteins, only 23 proteins (0.34% of all proteins) account for over 50% of the total protein copies identified in the cell. This observation underscores the concept of protein abundance heterogeneity within cellular systems, highlighting the magnitude of expression of specific protein groups and their contribution to the total cellular proteome. The high expression of these proteins is reflected in their roles in fundamental cellular processes, including DNA packaging, cell shape maintenance and protein synthesis **(Table. 5.1)**.

To better understand the architecture of the pDC proteome, I next investigated the distribution of proteins into different cellular compartments **(Fig. 5.5 B)**. This distribution provides information about cellular organisation and can be used to infer the functional properties of a cell. For example, as discussed in Chapter 3, cDC1s were found to have an enrichment of ribosomal proteins relative to cDC2s, which supports the observed enhanced rates of protein translation. Proteins were assigned to different cellular compartments based on their designated gene ontology (GO) identifiers using the mouse genome informatics resource (MGI) (https://www.informatics.jax.org). The distribution of proteins into the membrane (GO:0005886), nuclear envelope (GO:0005635), mitochondria (GO:0005739), ribosome (GO:0005840) and lysosome (GO:0005764) were identified. This analysis shows that approximately 25% of total protein

copies are associated with plasma membrane proteins, while approximately 16% are related to proteins in the mitochondria **(Fig. 5.5 B)**. On the other hand, only approximately 5% of proteins are associated with the lysosome and ribosome.

To approximate the functional landscape of the pDC proteome, I next performed gene set enrichment analysis (GSEA) of pDC proteins based on their abundance in the pDC proteome **(Fig. 5.6 A)**. Protein copy numbers per cell were ranked in order of abundance (log_{10} copy number) and separated into intensity quartiles (colours) showing KEGG pathways enriched in that quartile relative to the entire dataset. Categorising functional pathways based on their abundance in the proteome allows us to discern the predominant biological processes associated with different abundance levels of proteins in pDCs. The analysis reveals that highly abundant proteins identified in the upper quartile are enriched for pathways related to cellular metabolism and protein synthesis **(Fig. 5.6 A)**. Notably, pathways such as glycolysis, the TCA cycle and oxidative phosphorylation are associated with highly abundant proteins. On the other hand, lower abundance proteins are enriched for pathways related to immune cell function (PRR signalling, TNFα signalling) and basal transcription factors **(Fig. 5.6 A)**. Due to the cooperative nature of signalling proteins and transcription factors, a small number of proteins can propagate extensive functional responses. Thus, it is important to consider the functional context when examining protein abundance in isolation.

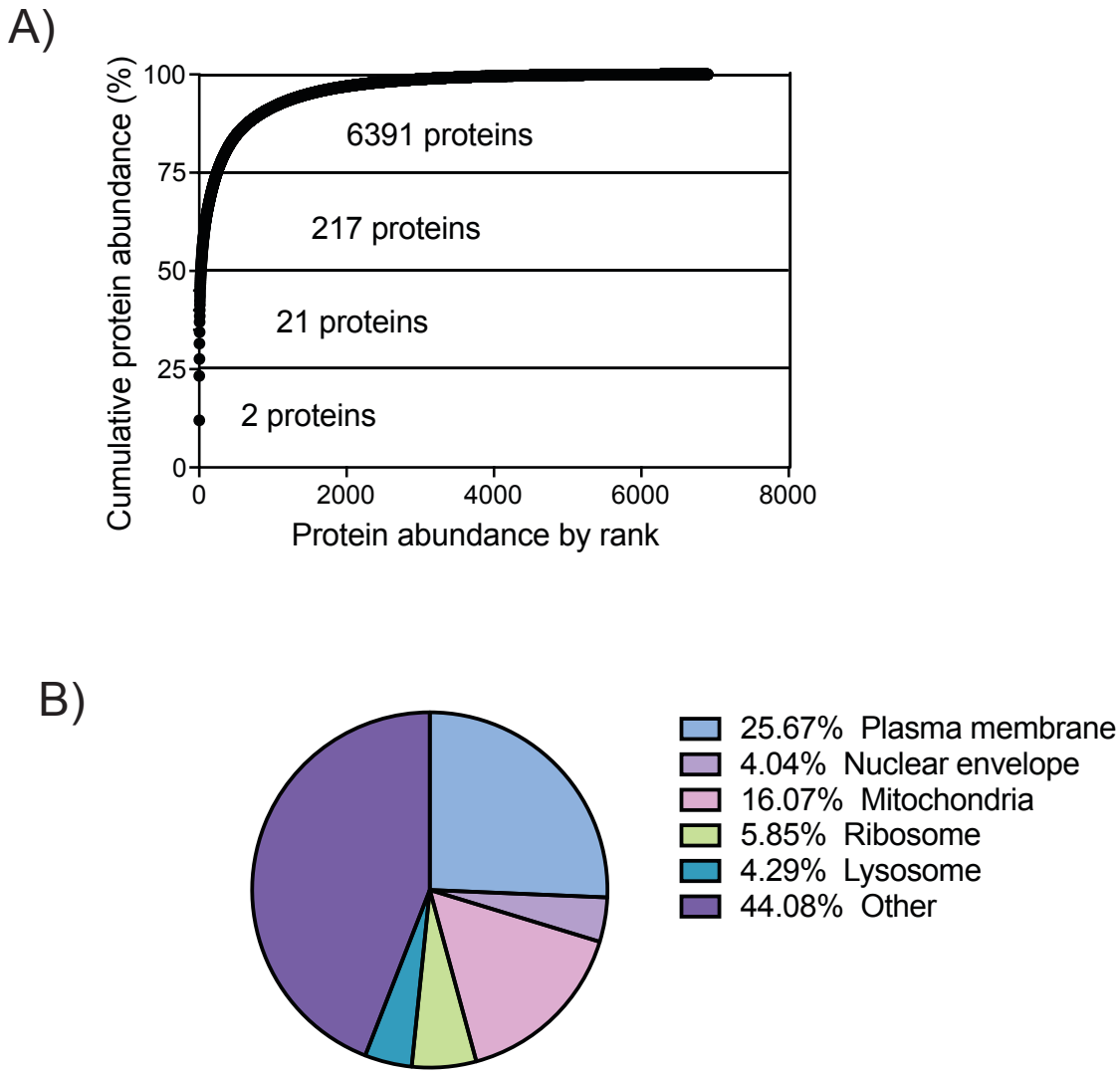

Figure 5.5 – Distribution of proteins in the pDC proteome
(A,B) Quantitative proteomic analysis was performed on splenic pDCs from C57Bl/6 mice inoculated with B16-Flt3l cells analysing the distribution of proteins in the pDC proteome. **(A)** Proteins were ranked in order of abundance (X-axis) and plotted against cumulative protein abundance (Y-axis). Horizontal lines represent quartiles of cumulative abundance with the number of proteins in each quartile. **(B)** Pie chart of cellular compartments (Plasma membrane: GO: 0005886, Nuclear envelope: GO:0005635, Mitochondria: GO:0005739, Ribosome: GO:0005840, Lysosome: GO:0005764) as a mean percentage of total protein abundance per cell. Quantitative proteomics was performed on three biological replicates.

A)

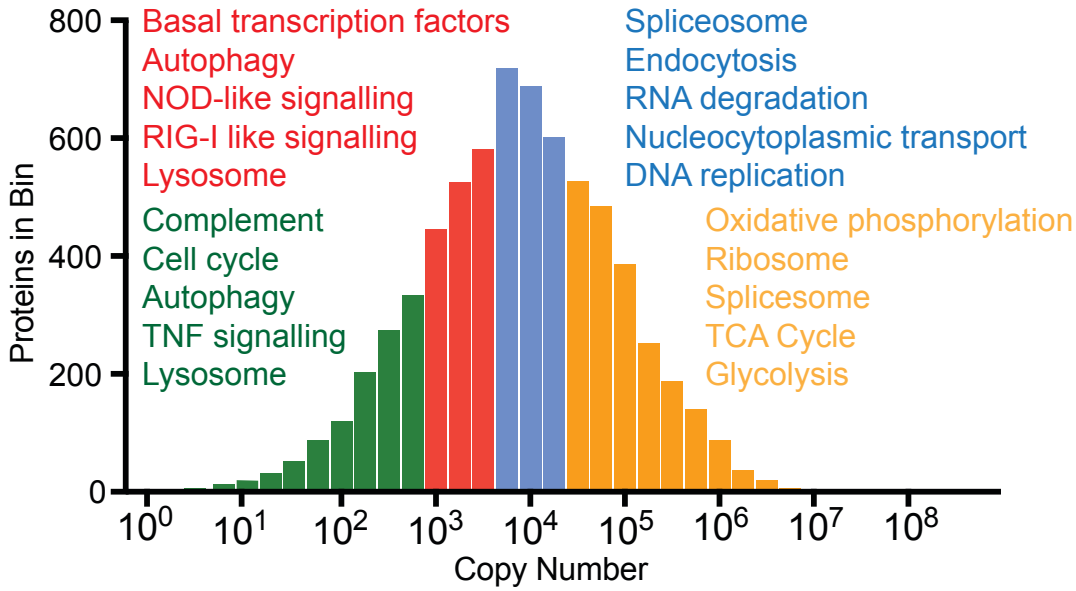

Figure 5.6 – Functional distribution of proteins in the pDC proteome
Quantitative proteomic analysis was performed on splenic pDCs from C57Bl/6 mice inoculated with B16-Flt3l cells analysing the enrichment of functional pathways by protein abundance in the pDC proteome. **(A)** Protein copy numbers per cell were ranked in order of abundance (log_{10} copy number) and separated into intensity quartiles (colours) showing KEGG pathways enriched in that quartile relative to the entire dataset. Quantitative proteomics was performed on three biological replicates.

Rank	Gene Name	Protein Name	Cellular Process	Average copy number	Cumulative Abundance (%)
1	H4c1	Histone H4c1	Chromatin remodeling	1.54E+08	11.99%
2	H2bc7	Histone H2bc7	Chromatin remodeling	1.46E+08	23.31%
3	Hist1h2af	Histone H2af	Chromatin remodeling	5.54E+07	27.61%
4	Actc1	Actin, alpha cardiac muscle 1	Cytoskeleton organization	5.04E+07	31.52%
5	H1-3	Histone H1-3	Chromatin remodeling	3.73E+07	34.42%
6	H3c2	Histone H3c2	Chromatin remodeling	3.33E+07	37.01%
7	Ppia	Peptidyl-prolyl cis-trans isomerase A	Protein folding	1.98E+07	38.54%
8	Actb	Actin, cytoplasmic 1	Cytoskeleton organization	1.95E+07	40.05%
9	Pfn1	Profilin-1	Actin polymerization	1.72E+07	41.39%
10	Lgals1	Galectin-1	Cell adhesion	1.36E+07	42.44%
11	Tmsb4x	Thymosin beta-4	Actin polymerization	1.22E+07	43.39%
12	H1-5	Histone H1-5	Chromatin remodeling	1.10E+07	44.24%
13	Rps27a	Ubiquitin-40S ribosomal protein S27a	Protein synthesis	9.53E+06	45.05%
14	Cfl1	Cofilin-1	Actin depolymerization	1.04E+07	45.79%
15	H1-4	Histone H1-4	Chromatin remodeling	6.21E+06	46.34%
16	H1-2	Histone H1-2	Chromatin remodeling	6.80E+06	46.87%
17	Tagln2	Transgelin-2	Actin-binding	7.13E+06	47.37%
18	Gapdh	Glyceraldehyde-3-phosphate dehydrogenase	Glycolysis	6.42E+06	47.85%
19	Actbl2	Beta-actin-like protein 2	Cytoskeleton organization	5.77E+06	48.30%
20	Ube2d3	Ubiquitin-conjugating enzyme E2 D3	Protein ubiquitination	5.32E+06	48.71%

Table 5.1 – List of the Top 20 most abundant proteins in murine pDCs in the steady-state

Proteins are ranked in order of copy number per cell and cumulative abundance as a percentage of their contribution to the total copy number of all cellular proteins.

5.4 The pDC transcriptome and proteome have a weak correlation

Transcriptomic analysis provides insight into the gene expression profile of a cell by measuring mRNA abundance, while proteomic analysis reveals the actual proteins present in a cell. To date, due to the smaller amount of cellular material required, transcriptomic analysis has been used extensively to investigate pDC phenotype and function (Robbins et al., 2008). However, the relationship between mRNA abundance and protein abundance is not always linear due to post-transcriptional regulation of gene expression, including alternative splicing, mRNA stability, and microRNA-mediated regulation. Furthermore, post-translational modifications can influence protein stability and turnover, which also influence the relationship between the transcriptome and proteome (Marchingo & Cantrell, 2022). Having characterised the pDC proteome, I next investigated the relationship between the pDC transcriptome and proteome **(Fig. 5.7)**.

Microarray gene transcript abundance of splenic pDCs was acquired from the Immunological Genome Project (Immgen) (GSE15907) and aligned with protein abundance from the quantitative proteomic dataset. Correlation analysis between gene transcript abundance and protein abundance shows a correlation of R^2=0.4 (Pearson's correlation coefficient) **(Fig. 5.7 A)**. For example, mRNA transcripts are enriched relative to protein expression of inflammatory transcription factors, including IRF8, STAT2, IRF4 and IRF3 **(Fig. 5.7 B)**. On the contrary, there is no apparent bias in the expression of PRRs as some receptors are enriched at the mRNA level (TLR7, TLR9) and others enriched at the protein level (RIG-I, TLR3) **(Fig. 5.7 C)**. Overall, as protein abundance directly influences cellular function, the observation of a weak correlation between the pDC transcriptome and proteome emphasises the importance of complementary analysis when performing transcriptomic studies.

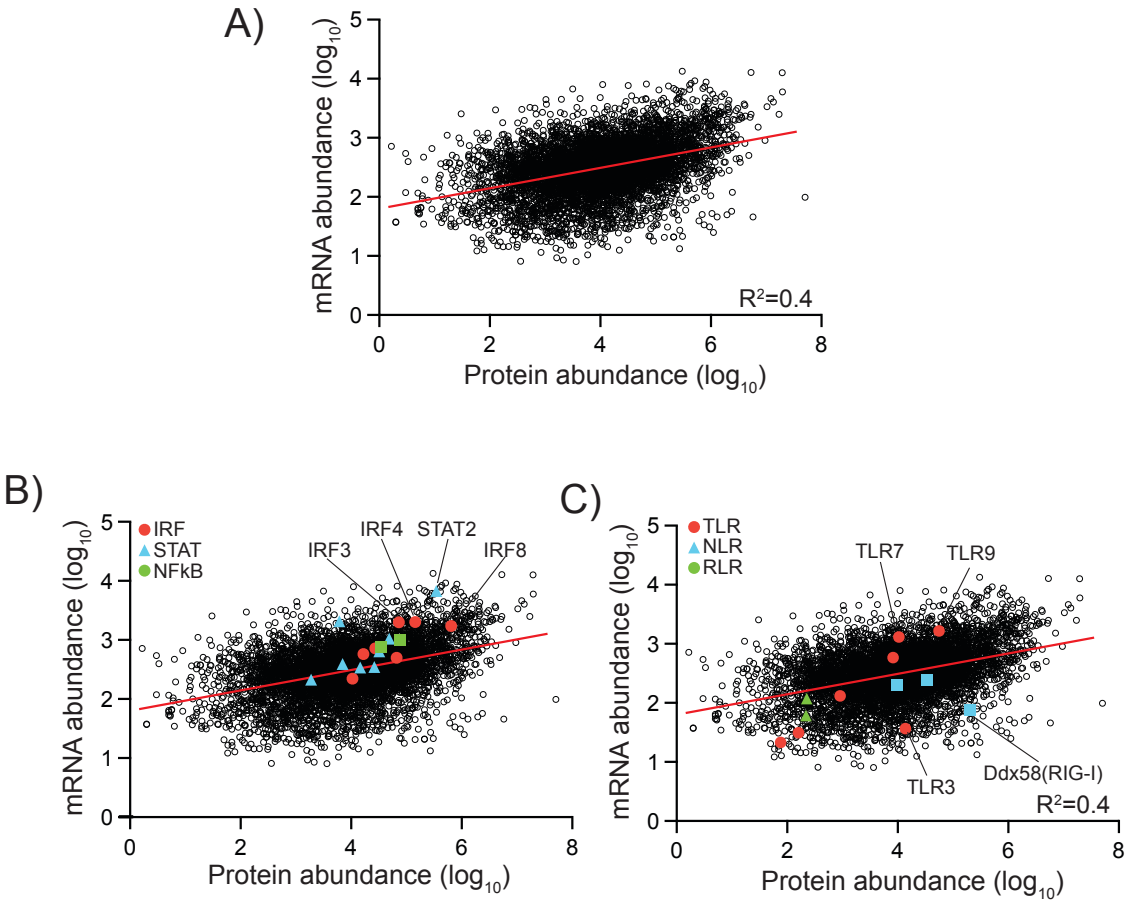

Figure 5.7 – Weak correlation between pDC transcriptome and proteome **(A)** mRNA abundance (Log_{10} mean value, Affymetrix microarray) plotted against the protein copy number per cell (Log_{10} protein abundance) identified by quantitative proteomics. Microarray data was acquired from the Immgen dataset (GSE15907) and analysed by converting mRNA transcripts gene identifiers into protein identifiers aligned to proteins in the quantitative proteomics dataset. **(B,C)** Comparison as in **(A)** highlighting the expression of immune response transcription factors **(B)** and PRRs **(C)** expressed in splenic pDCs. Quantitative proteomics was performed on three biological replicates. Microarray array data was reanalysed using three biological replicates. Data were analysed using linear regression analysis. R^2 = Pearson's correlation coefficient

5.5 Correlation between murine and human pDCs

The level of functional and phenotypical conservation between mice and man determines the value of murine models in studying immunology. A landmark study in 2016 by Guilliams et al. demonstrated elegantly, using a combination of flow and mass cytometry, that DC subsets are conserved across tissues and species (Guilliams et al., 2016). In addition, earlier work from the Dalod group shows that pDCs are highly conserved at the transcriptional level (Robbins et al., 2008). Considering the observations in **(Fig. 5.7)** showing the weak correlation between the pDC transcriptome and proteome, I next investigated the relationship between the proteomes of murine and human pDCs.

Human pDC proteomic data was acquired from ProteomeXchange Consortium (https://www.proteomexchange.org) (PXD004352). Human protein identifiers were converted into murine protein identifiers and aligned with the murine pDC proteomic dataset. Protein copy numbers per cell were normalised, and a linear correlation analysis was performed **(Fig. 5.8 A)**. 5546 proteins were identified in human and mouse datasets with a correlation coefficient of R^2=0.83. Phenotypically, human pDCs express significantly lower levels of the DC-specific integrin CD11c than murine pDCs, as previously described (Swiecki & Colonna, 2015). In contrast, human pDCs rely on IL-3 signalling through IL-3Ra to promote survival and activation (Cella et al., 2000). Indeed, IL3Ra is significantly more abundant in human pDCs **(Fig. 5.8 A)**. Interestingly, proteins associated with aerobic glycolysis, including the glucose transporter SLC2A1, the lactate-producing enzyme LDHB and the lactate transporter SLC16A3, are enriched in human pDCs **(Fig. 5.8 A)**. This finding aligns with the observation that human pDCs rely more on aerobic glycolysis than murine pDCs during early activation (Bajwa et al., 2016; Fekete et al., 2018). In contrast, murine pDCs have been described to rely more on mitochondrial metabolism fueled by beta-oxidation (Wu et al., 2016). On the other hand, proteins involved in cytoplasmic viral nucleic acid sensing, including PYHIN1 and members of the RIG-I sensing machinery (DDX58, DHX58, IFIH1) are enriched in

murine pDCs **(Fig. 5.8 A)**. Thus, despite a positive correlation between murine and human pDC proteomes, indicating that most proteins share a similar expression pattern across species, analysis of differentially enriched proteins may indicate species-specific functional and metabolic adaptations.

To understand the proteomic architecture of human pDCs, I performed a cumulative protein analysis **(Fig. 5.8 B)** and investigated the distribution of proteins into subcellular compartments **(Fig. 5.8 C)**. This analysis shows that 195 highly abundant proteins account for 50% of the total protein copy number in the human pDC proteome. Like murine pDCs, the top twenty most highly abundant proteins in human pDCs are highly populated by histone proteins, cytoskeletal proteins, and metabolic proteins, including GAPDH **(Table. 6.2)**. Notably, these highly abundant proteins compose a smaller proportion of the human pDC proteome relative to murine pDCs **(Fig. 5.8 B)**. The distribution of proteins into different subcellular compartments also differs between human and murine pDCs **(Fig. 5.8 C)**. Murine pDCs have a higher proportion of proteins associated with the plasma membrane and lysosome than human pDCs **(Fig. 5.5 B) (Fig. 5.8 C)**. On the other hand, human pDCs have more ribosomal proteins than murine pDCs. Proteins associated with the mitochondrial and nuclear envelope are similarly expressed in both human and murine pDCs. Thus, although overall, there is a strong correlation between human and mouse pDC proteomes, there are significant differences in the distribution of proteins between mice and men.

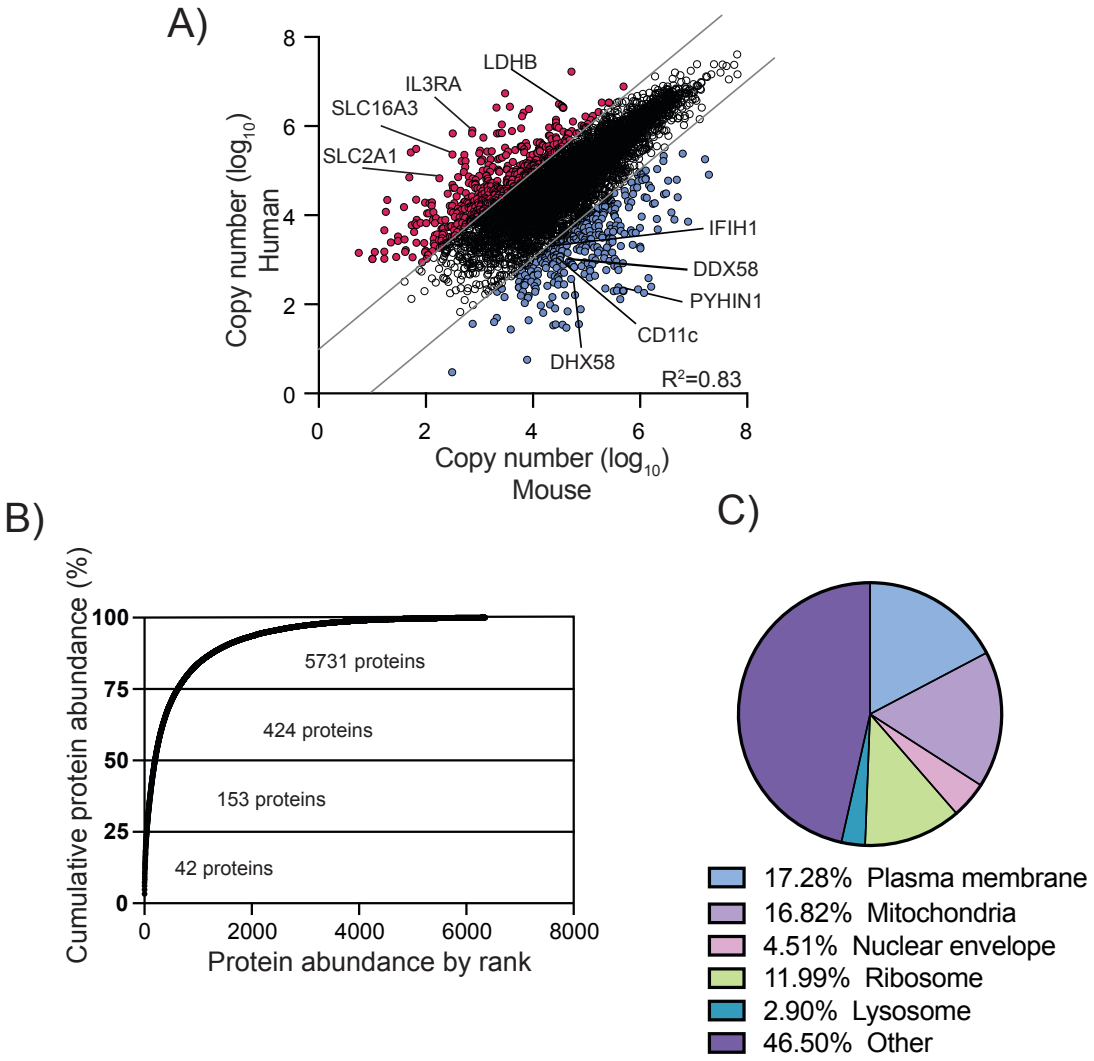

Figure 5.8 – Conservation between murine and human pDC proteomes
(A) Linear regression analysis of log_{10} normalised copy number per cell of proteins identified in murine and human pDCs. Human copy number data was acquired from the ProteomeXchange database (PXD004352) and aligned with proteins identified in the murine dataset. Diagonal lines indicate proteins with a log_{10}=1 higher abundance in murine (blue) or human (red) pDCs. Selected proteins are labelled on the graph. **(B)** Rank-ordered plot of protein copy numbers from the human pDC dataset by abundance (X-axis) plotted against cumulative protein abundance (Y-axis). Horizontal lines represent quartiles of cumulative abundance, with the number of proteins in each quartile indicated. **(C)** Pie chart illustrating the mean percentage of total protein abundance per cell in human pDCs across different cellular compartments: Plasma membrane (GO: 0005886), Nuclear envelope (GO: 0005635), Mitochondria (GO: 0005739), Ribosome (GO: 0005840), and Lysosome (GO: 0005764). Murine quantitative proteomics was performed on three biological replicates. Human quantitative proteomics was analysed from four biological replicates. Data were analysed by linear regression analysis **(A)**. R^2 = Pearson's correlation coefficient

Rank	Gene Name	Protein Name	Cellular Process	Average copy number	Cumulative Abundance (%)
1	HIST1H4A	Histone H4	Chromatin remodeling	8.23E+07	3.29%
2	ACTB	Actin, cytoplasmic 1	Cytoskeleton organization	4.09E+07	4.80%
3	HIST1H2BC	Histone H2B	Chromatin remodeling	3.77E+07	6.11%
4	HIST2H3A	Histone H3.2	Chromatin remodeling	3.28E+07	7.27%
5	HIST2H2AC	Histone H2A	Chromatin remodeling	2.90E+07	8.26%
6	VIM	Vimentin	Intermediate filament organization	2.47E+07	9.23%
7	HIST1H1E	Histone H1.4	Chromatin remodeling	2.46E+07	10.22%
8	TAGLN2	Transgelin-2	Actin-binding	2.45E+07	10.96%
9	CFL1	Cofilin-1	Actin depolymerization	2.43E+07	11.85%
10	PFN1	Profilin-1	Actin polymerization	2.38E+07	12.43%
11	TMSB4X	Thymosin beta-4	Actin polymerization	2.23E+07	13.07%
12	HIST1H1B	Histone H1.2	Chromatin remodeling	1.85E+07	13.65%
13	YWHAZ	14-3-3 protein zeta/delta	Cell signaling	1.75E+07	14.18%
14	APOA1	Apolipoprotein A-I	Lipid transport	1.67E+07	14.81%
15	RPS27A	Ubiquitin-40S ribosomal protein S27a	Protein synthesis	1.60E+07	15.32%
16	TXN	Thioredoxin	Redox regulation	1.59E+07	15.85%
17	GAPDH	Glyceraldehyde-3-phosphate dehydrogenase	Glycolysis	1.45E+07	16.41%
18	PPIA	Peptidyl-prolyl cis-trans isomerase A	Protein folding	1.45E+07	16.85%
19	PPIB	Peptidyl-prolyl cis-trans isomerase B	Protein folding	1.40E+07	17.27%
20	SAMHD1	SAM domain and HD domain-containing protein 1	Nucleotide metabolism regulation	1.32E+07	17.74%

Table 5.2 – List of the Top 20 most abundant proteins in human pDCs in the steady-state

Proteins are ranked in order of copy number per cell and cumulative abundance as a percentage of their contribution to the total copy number of all cellular proteins.

5.6 Analysis of pathogen sensing machinery in the pDC proteome

Steady-state pDCs are specialised in antigen capture and detection. Antigen detection is mediated by pathogen recognition receptors (PRRs) that recognise conserved pathogen-associated molecular patterns (PAMPs) present in bacteria, viruses, fungi, and parasites (Li & Wu, 2021). PRRs can be categorised into several families, including toll-like receptors (TLRs), C-type lectin receptors (CLRs), NOD-like receptors (NLRs), RIG-I-like receptors (RLRs) and DNA sensors (cGAS-STING). The repertoire of PRRs a cell expresses dictates its ability to respond to different pathogens. In **(Fig. 5.8 A),** I identified that murine pDCs are enriched for expression of the viral nucleic acid sensors RIG-I (DDX58) and MDA5 (IFIH1) compared to human pDCs. Analysing differences in PRR expression between mice and humans is crucial to better understand immune response variations, optimising therapies and vaccines, elucidating disease pathogenesis and gaining insights into immune system evolution. Thus, I next investigated the expression of different PRR families in murine **(Fig. 5.9 A)** and human pDCs **(Fig. 5.9 B) (Table. 5.3)**.

Protein copy numbers per cell were ranked in order of abundance (log_{10} copy number), and TLR (green), CLR (yellow), NLR (red), RLR (blue) and cytosolic DNA sensors of the cGAS-STING pathway (pink) were plotted according to their abundance **(Fig. 5.9 A,B)**. In line with the ability of pDCs to respond to viral infection, viral RNA (TLR7/TLR9, RIG-I/MDA5) and DNA sensors (cGAS-STING) are among the most abundant PRRs detected in both murine and human pDCs. Conversely, CLRs, specialising in detecting PAMPs associated with bacterial and fungal expression, are lowly abundant in murine and human pDCs. Although numerous studies have shown that pDCs can respond to bacterial and fungal infection (Maldonado et al., 2022; Parcina et al., 2008; Pepper et al., 2008; Preite et al., 2018), this suggests that it is not a primary function of pDCs. In accordance with this statement, the NLR proteins, nucleotide-binding oligomerisation domain-containing proteins 1/2 (NOD1, NOD2), which detect peptidoglycan found in the cell wall of bacteria, are lowly expressed (mouse) or absent (human) in pDCs. Thus, broadly speaking, the PRR repertoire of mouse and human pDCs reflects their reported specialisation in anti-viral immunity.

Overall, these data show that although murine and human pDCs share a similar expression profile for certain PRRs, species-specific differences should be considered when modelling human pDC function in the murine model.

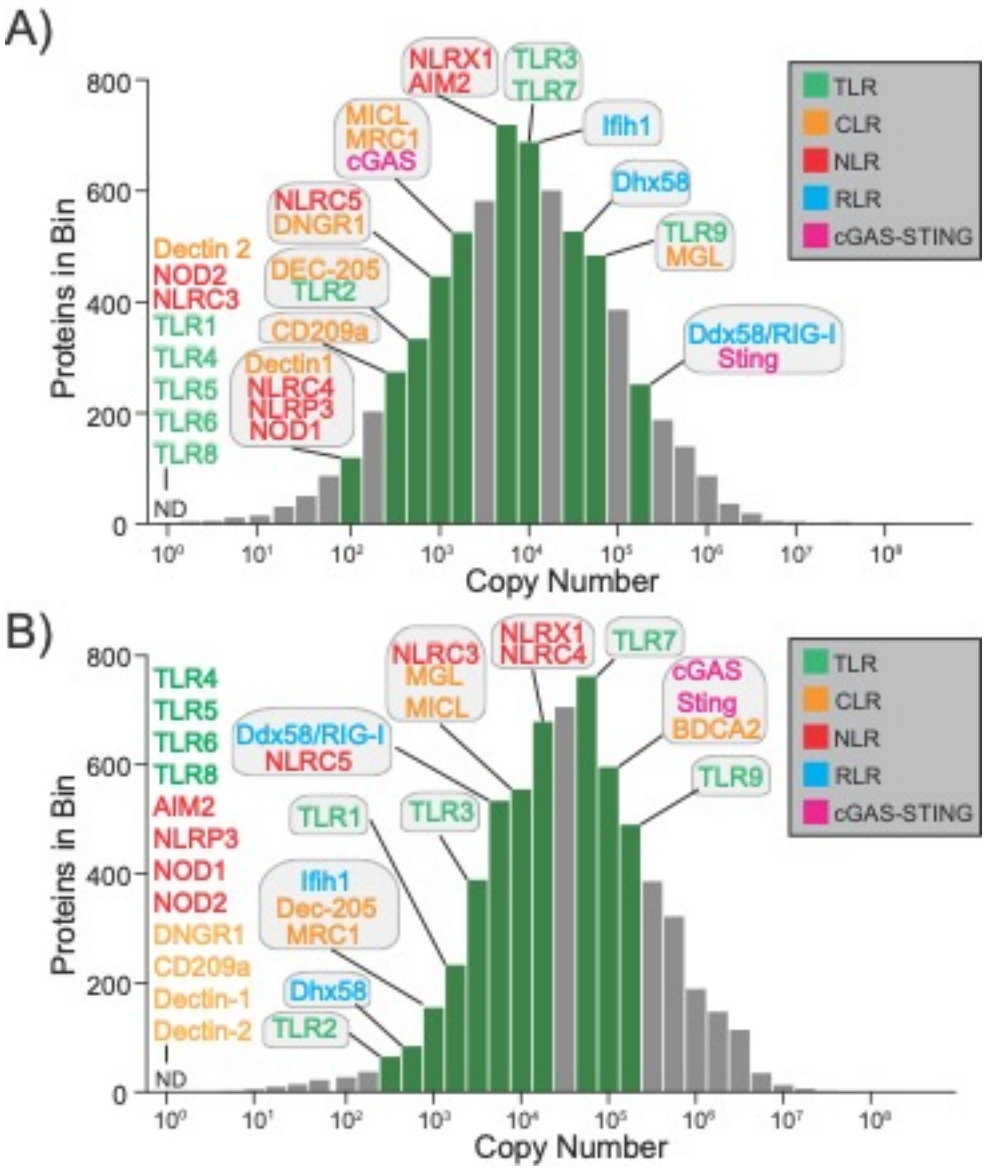

Figure 5.9 – Analysis of antigen sensing machinery in murine and human pDCs

(A,B) Analysis of the protein copy number per cell of PRRs in murine and human pDCs by quantitative proteomics. Protein copy numbers per cell in the murine **(A)** and human **(B)** pDC proteomes were ranked in order of abundance (log_{10} copy number) (x-axis) and plotted against the number of proteins in that intensity band (proteins in bin) (y-axis). TLR proteins (red), CLR proteins (yellow), NLR proteins (red), RLR (blue) and cytosolic DNA sensor cGAS-STING (pink) were assigned to intensity bands by their copy number per cell (green bars). **(A)** Murine quantitative proteomics was performed on three biological replicates. **(B)** Human quantitative proteomics was analysed from a publicly available dataset from the ProteomeXchange consortium (PXD004352) on four biological replicates. ND = not detected

Protein Name	Gene Name	PRR Family	Ligands	Subcellular Localization	Murine pDC	Human pDC
TLR1	TLR1	TLR	Bacterial lipopeptides	Plasma membrane	ND	+
TLR2	TLR2	TLR	Lipoteichoic acid, lipoproteins, peptidog	Plasma membrane	+	+
TLR3	TLR3	TLR	Viral double-stranded RNA	Endosome	++	+
TLR7	TLR7	TLR	Viral single-stranded RNA	Endosome	++	++
TLR9	TLR9	TLR	Unmethylated CpG DNA motifs	Endosome	+++	+++
BDCA2	CLEC4C	CLR	Unknown	Plasma membrane	ND	+++
CD209	CD209	CLR	Various pathogens including viruses an	Plasma membrane	+	ND
MGL	CLEC10A	CLR	Pathogens and tumor cells	Plasma membrane	+++	+
MICL	CLEC12A	CLR	Unknown	Cell surface	+	+
MRC1	MRC1	CLR	Mannose, fucose, N-acetylglucosamine	Endosome, Plasma membr	+	+
DNGR1	CLEC9A	CLR	F-Actin	Endosome	+	ND
DEC-205	LY75	CLR	Antigen uptake and presentation	Endosome	+	+
Dectin 1	CLEC7A	CLR	β-glucans found in fungal cell walls	Plasma membrane	+	ND
Dectin 2	CLEC6A	CLR	Fungal components	Cell surface	ND	ND
NOD1	NOD1	NLR	Bacterial peptidoglycan fragments	Cytoplasmic	+	+
NOD2	NOD2	NLR	Bacterial peptidoglycan fragments	Cytoplasmic	ND	ND
NLRP3	NLRP3	NLR	Various danger signals	Cytoplasmic	+	ND
AIM2	AIM2	NLR	Double-stranded DNA	Cytoplasmic	++	ND
RIG-I	DDX58	RLR	Viral RNA	Cytoplasmic	+++	+
MDA5	IFIH1	RLR	Viral RNA	Cytoplasmic	+++	+
LGP2	DHX58	RLR	Viral RNA	Cytoplasmic	++	+
cGAS	MB21D1	Other	Cytosolic DNA	Cytoplasmic	+	+++
STING	TMEM173	Other	Activation by cGAS	ER membrane	+++	+++

Table 5.3 – Expression of PRRs in murine and human pDCs
Table summarising the expression of PRRs in murine and human pDCs identified in **(Fig. 5.9 A,B)**. Columns include protein name, gene name, PRR ligands, subcellular PRR localisation and abundance in the murine and human pDC proteomes. Expression intensity was determined as relative abundance in the murine and human pDC proteomes using the following parameters: ND= not detected, Low = bottom intensity quartile (<25%), + = Lower middle-intensity quartile (25%-50%), ++ = Upper middle-intensity quartile (50%-75%) and +++ = Upper-intensity quartile (>75%).

5.7– Analysis of environment-sensing machinery in murine and human pDCs

Environmental sensing of nutrients, encompassing a diverse array from glucose and amino acids to metals like iron and zinc, plays a pivotal role in immune cell function. Beyond serving as fuel for cellular metabolism, these nutrients act as signalling molecules, influencing critical cellular processes (O'Neill et al., 2016; Pearce et al., 2013). Glucose, for instance, serves as a key energy source, while amino acids are indispensable for protein synthesis and immune regulation. Metals such as iron and zinc are essential cofactors in enzymatic reactions, modulating immune responses. Additionally, sensing lactate and adenosine, metabolic by-products, can profoundly impact immune cell function, influencing immune tolerance and inflammation. By integrating signals from nutrient availability alongside pathogen detection through pattern recognition receptors (PRRs), DCs orchestrate tailored immune responses, ensuring efficient pathogen clearance while maintaining immune homeostasis.

Thus, understanding the complex interplay between nutrient sensing and immune surveillance in DCs holds the potential for developing strategies to combat infections and autoimmune diseases. The importance of metabolic sensors in other immune cells, including T cells and NK cells, is emerging (Howden et al., 2019; Littwitz-Salomon et al., 2021; L. V. Sinclair et al., 2013). However, the characterisation of the environmental sensing machinery in pDCs is still lacking. As the nutrient transporter repertoire of a cell reflects its nutrient requirements, I next investigated the abundance of nutrient transporters, including glucose (orange), amino acid (blue), fatty acid (green), metal (red), lactate (black) and adenosine (brown) transporters in murine **(Fig. 5.10 A)** and human **(Fig. 5.10 B)** pDCs.

Analysis of glucose transporter (SLC2A family, also called GLUTs) expression in pDCs identifies the expression of both SLC2A1 and SLC2A3 in murine and human pDCs **(Fig. 5.10 A, B) (Table 5.4)**. While SLC2A1 has been identified as an important protein involved in the immunometabolic reprogramming of DCs, the role of SLC2A3 in DC biology is less characterised

(Everts et al., 2014; Thwe et al., 2017). Interestingly, in murine pDCs, SLC2A3 is enriched relative to SLC2A1 (~8000 and ~250 copies, respectively). By contrast, GLUT1 is the most abundant glucose transporter expressed in human pDCs (GLUT1 ~100000 copies, GLUT3 ~5000 copies). Notably, there is a striking difference in GLUT1 expression between murine and human pDCs, which may indicate a higher requirement for glucose uptake in human pDCs.

Analysis of amino acid transporter expression in pDCs identifies the co-expression of a similar repertoire of transporters, including SLC1A5, SLC7A5, SLC7A1, SLC38A1 and SLC38A2. Despite expressing the same repertoire of amino acid transporters, the abundance of these transporters varies between mice and human pDCs **(Fig. 5.10 A, B) (Table 5.4)**. In particular, the System L transporter SLC7A5 is highly expressed in human pDCs relative to mice (~100000 and ~10000 copies, respectively). As discussed in **Chapter 4,** SLC7A5 has been identified as a critical regulatory factor in the function of many immune cells. Indeed, a recent publication has shown that SLC7A5 transport activity primes human pDCs for type-I interferon production in an IL3RA- and mTORC1-dependent manner (Grzes et al., 2021).

Due to their hydrophobicity, short-chain fatty acids can passively diffuse across the plasma membrane along a concentration gradient. However, long-chain fatty acids are actively transported by cell surface transporters, including the transmembrane glycoprotein CD36 and members of the fatty acid transport proteins (FATP) (SLC27A1-4). Both CD36 and FATP proteins are abundant in both murine and human pDCs. In particular, SLC27A1 (FATP1) is highly abundant.

Micronutrients, including iron, zinc, and copper, have been identified as important regulators of immune cell function (G. Weiss, 2015). The uptake of extracellular iron is primarily mediated by two plasma membrane transporters, TFRC and DMT1, in immune cells (Cronin et al., 2019). TFRC catalyses the endocytosis of transferrin-bound iron, while DMT1 has a high affinity for non-transferrin-bound iron. While DMT1 expression was not detected in both

mouse and human pDCs, TFRC is highly expressed, indicating this is the primary mode of iron uptake in pDCs. Notably, TFRC is the most highly expressed nutrient transporter detected in both murine and human pDCs. Zinc transport across the plasma membrane is mediated by the ZRT/IRT-like protein family (ZIP) (SLC39A1-13), of which SLC39A7 and SLC39A11 are expressed similarly in both murine and human pDCs. Extracellular copper uptake is catalysed by two transporters, CTR1 and CTR2, neither of which were detected in the proteomic datasets.

It is now emerging that by-products of metabolism, including lactate and adenosine, play crucial roles in immune cell metabolism and function (Caslin et al., 2021; Pasquini et al., 2021). Lactate transport is catalysed by the monocarboxylate transporters (MCT), MCT1 (SLC16A1) and MCT4 (SLC16A3) in immune cells. MCT4 is specialised for the efflux of lactate in glycolytic cells, while MCT1 has a higher affinity for lactate than MCT4, allowing the acquisition of extracellular lactate across the plasma membrane. MCT4 is expressed in both murine and human pDCs; however, its abundance is enriched in human pDCs (Human ~1000 copies, Mouse ~50 copies) **(Fig. 5.10 A,B)**. This aligns with the observation that human pDCs have higher glucose transporter expression and may suggest a higher capacity to perform aerobic glycolysis. Indeed, human pDCs have a significantly higher abundance of the enzyme lactate dehydrogenase B (LDHB) (Human ~ 8000000 copies, Mouse ~ 150000 copies), which catalyses the conversion of pyruvate to lactate. Adenosine is a purine nucleoside that can accumulate in the extracellular space under conditions of inflammation, hypoxia, or tissue damage(Feng et al., 2020). Adenosine acts upon specific adenosine receptors and can be transported into the cell by SLC28A1, SLC28A2 and SLC29A1-4. SLC29A1 is detected in murine and human pDCs, and SLC28A2 is detected only in murine pDCs. However, the abundance of these transporters is low, suggesting that adenosine uptake is not prioritised in pDCs **(Fig. 5.10 A,B)**.

Overall, these data reveal that while the expression of many nutrient transporters is conserved (high TFRC and SLC27A1 expression, for

example), there are differences in nutrient transporter expression between murine and human pDCs **(Fig. 5.10 A, B) (Table 5.4)**. This may indicate species-specific differences in metabolic fuel preferences and regulation by extracellular nutrient levels. This has important implications for modelling human pDC metabolism in the murine system.

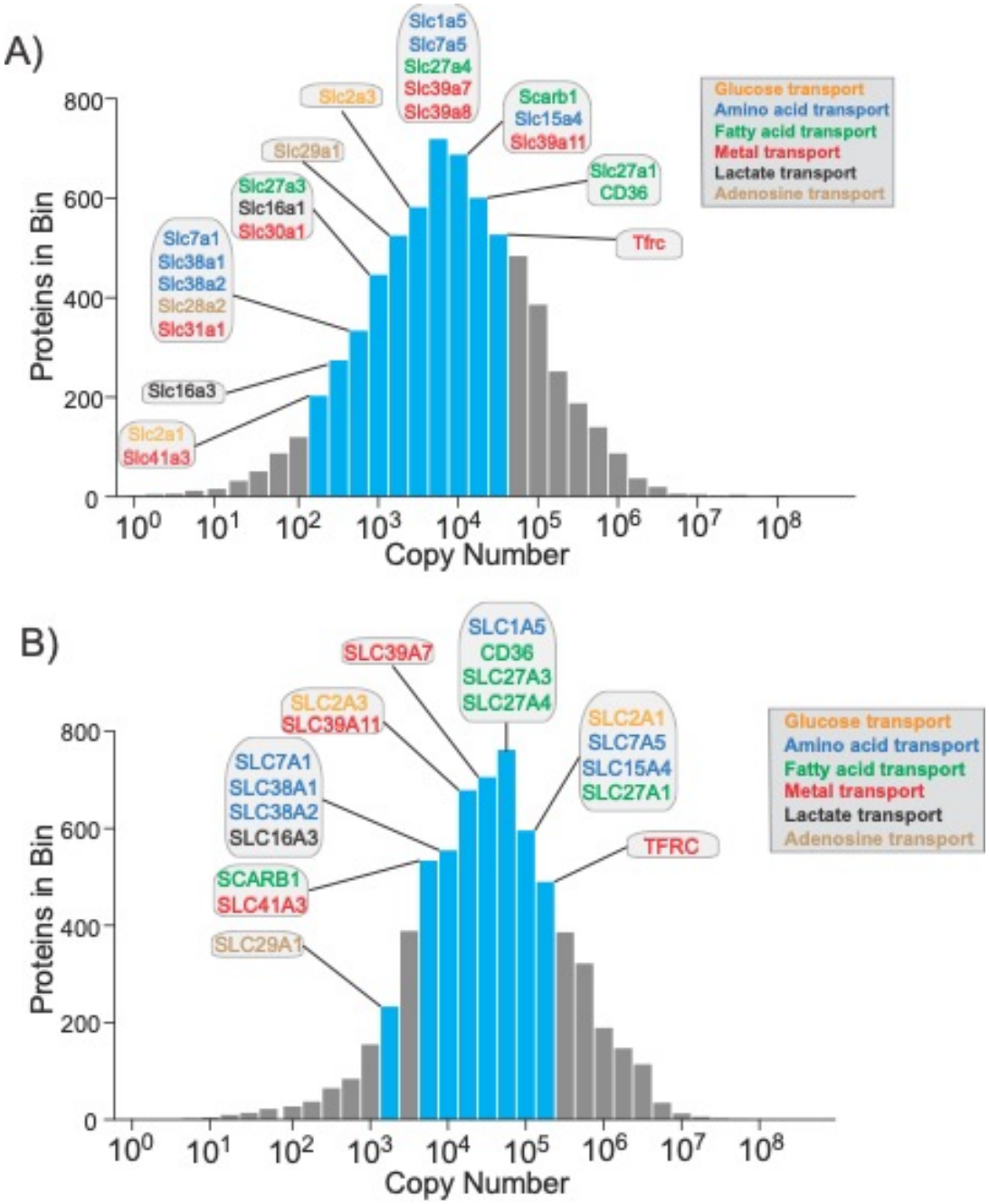

Figure 5.10 – Analysis of environment-sensing machinery in murine and human pDCs

(A,B) Analysis of the protein copy number per cell of nutrient transporters in murine and human pDCs by quantitative proteomics. Protein copy numbers per cell in the murine **(A)** and human **(B)** pDC proteomes were ranked in order of abundance (log_{10} copy number) (x-axis) and plotted against the number of proteins in that intensity band (proteins in bin) (y-axis). Glucose transporters (yellow), amino acid transporters (blue), fatty acid transporters (green), metal transporters (red), lactate transporters (black) and adenosine transporters (brown) were assigned to intensity bands by their copy number per cell (blue bars). **(A)** Murine quantitative proteomics was performed on three biological replicates. **(B)** Human quantitative proteomics was analysed from a publicly available dataset from the ProteomeXchange consortium (PXD004352) on four biological replicates.

Gene	Protein	Group	Subcellular localisation	Substrate(s)	Murine pDC	Human pDC
SLC2A1	GLUT1	Glucose transport	Plasma membrane	Glucose	+	+++
SLC2A3	GLUT3	Glucose transport	Plasma membrane	Glucose	+	+
SLC1A5	ASCT2	Amino acid transport	Plasma membrane	Neutral amino acids	++	++
SLC7A1	CAT1	Amino acid transport	Plasma membrane	Cationic amino acids	low	+
SLC7A5	LAT1	Amino acid transport	Plasma membrane	Neutral amino acids	++	+++
SLC38A1	SNAT1	Amino acid transport	Plasma membrane	Neutral amino acids	low	+
SLC38A2	SNAT2	Amino acid transport	Plasma membrane	Neutral amino acids	low	+
CD36	CD36	Fatty acid transport	Plasma membrane	LCFAs, lipoproteins	+++	++
SLC27A1	FATP1	Fatty acid transport	Plasma membrane, ER	LCFAs	+++	+++
SLC27A3	FATP3	Fatty acid transport	Plasma membrane, mitochondrion	LCFAs	+	++
SLC27A4	FATP4	Fatty acid transport	Plasma membrane, ER	LCFAs	++	++
SCARB1	SRB1	Fatty acid transport	Plasma membrane	Lipoproteins,cholesterol	++	low
TFRC	TFRC	Metal transport	Plasma membrane, Endosome	Transferrin bound iron	+++	+++
SLC30A1	ZNT1	Metal transport	Plasma membrane, ER, Golgi	Zinc ions	low	low
SLC31A1	CTR1	Metal transport	Plasma membrane	Copper ions	low	low
SLC39A7	ZIP7	Metal transport	Plasma membrane, ER, Golgi	Zinc ions	++	++
SLC39A11	ZIP11	Metal transport	Plasma membrane, ER, Golgi	Zinc ions	++	+
SLC16A1	MCT1	Lactate transport	Plasma membrane	Monocarboxylates	+	ND
SLC16A3	MCT4	Lactate transport	Plasma membrane	Monocarboxylates	low	+
SLC28A2	CNT2	Adenosine transport	Plasma membrane	Nucleosides	low	ND
SLC29A2	ENT1	Adenosine transport	Plasma membrane	Nucleosides	+	low

Table 5.4 – Expression of nutrient transporters in murine and human pDCs

Table summarising the expression of nutrient transporters in murine and human pDCs identified in **(Fig 10 A,B)**. Columns include protein name, gene name, transporter group, subcellular PRR localisation, transporter substrate and abundance in the murine and human pDC proteomes. Expression intensity was determined as relative abundance in the murine and human pDC proteomes using the following parameters: ND= not detected, Low = bottom intensity quartile (<25%), + = Lower middle-intensity quartile (25%-50%), ++ = Upper middle-intensity quartile (50%-75%) and +++ = Upper-intensity quartile (>75%).

5.8 – Comparison of nutrient transport machinery between pDCs and cDCs

Having identified the environment-sensing machinery in murine and human pDCs, I investigated whether these transporters are enriched in pDCs relative to cDCs. I performed a differential expression analysis comparing the expression of nutrient transporters between pDCs, cDC1s **(Fig. 5.11 A)** and cDC2s **(Fig. 5.11 B)**. This analysis identifies two transporters, the iron transporter Tfrc and the fatty acid transporter (Slc27a1), which are significantly upregulated in pDCs compared to cDC1s and cDC2 **(Fig. 5.11 A,B).** This finding, in combination with the observation that Tfrc is the most highly expressed environmental sensor in both murine **(Fig. 5.10 A)** and human **(Fig. 5.10 B)** pDC, suggests that iron availability may play a role in pDC function.

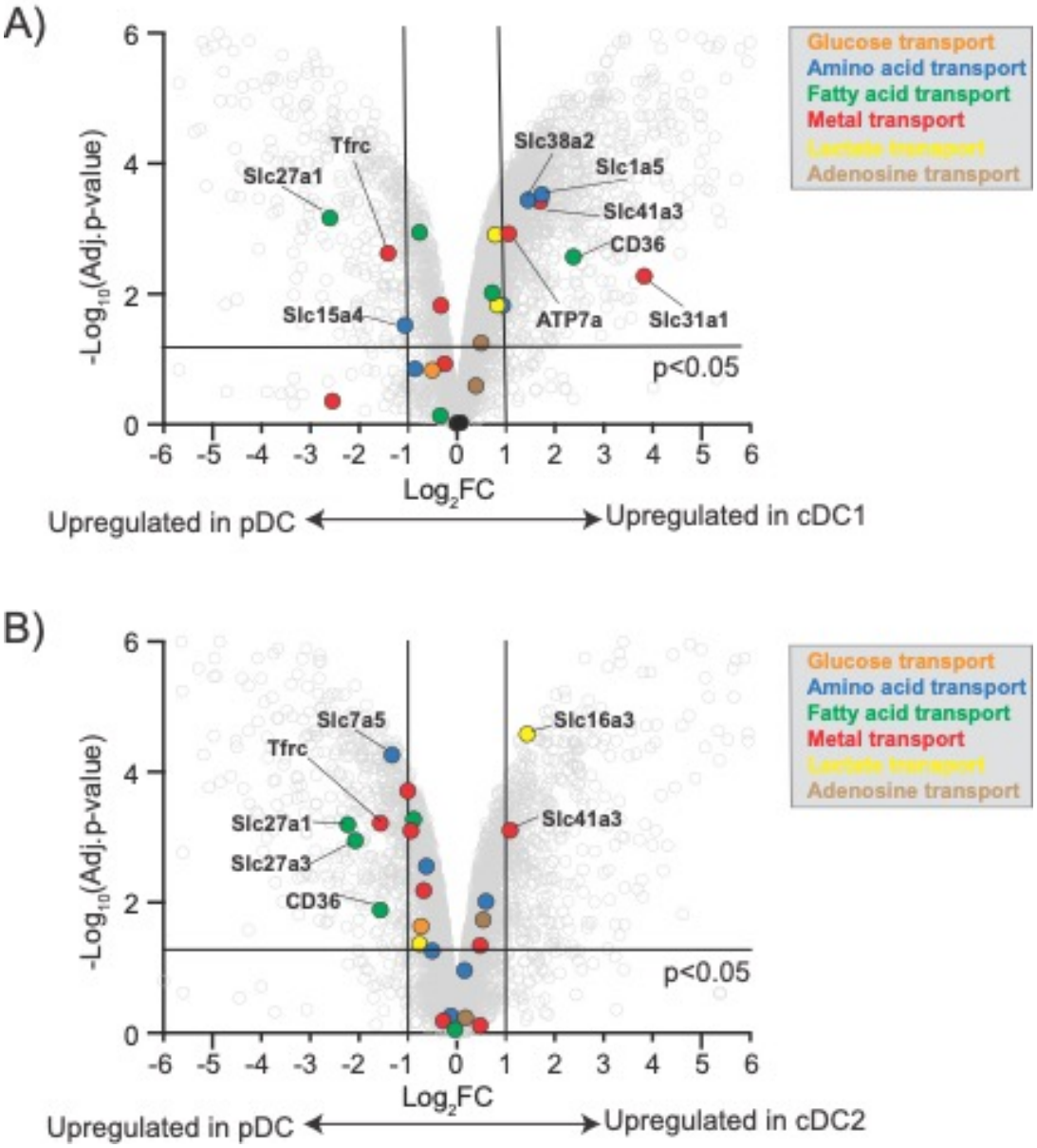

Figure 5.11 – Differential expression analysis of environment-sensing machinery between pDC and splenic cDCs

(A,B) Differential expression analysis of nutrient transporters comparing pDCs with **(A)** cDC1s and **(B)** cDC2s. Volcano plots represent the log_2 fold change (x-axis) versus the $-log_{10}$ adjusted p-value identified by the differential expression analysis. Vertical lines represent a log_2 fold change >1 or <-1. The horizontal line represents an adjusted p-value of less than <0.05. Coloured dots represent glucose transporters (yellow), amino acid transporters (blue), fatty acid transporters (green), metal transporters (red), lactate transporters (black) and adenosine transporters (brown) identified in both pDC and cDC subsets. Quantitative proteomics was performed on three biological replicates.

5.9 Steady-state pDCs are characterised by high expression and activity of the iron transporter Tfrc

The differential expression analysis of nutrient transporters between pDCs and cDCs indicated that the iron transporter Tfrc (CD71) is enriched in pDCs relative to cDCs. Indeed, pDCs have significantly higher Tfrc copies per cell than cDC1s and cDC2s **(Fig. 5.12 A)**. Flow cytometry analysis of Tfrc expression in steady-state pDCs and cDCs confirms the quantitative proteomic data **(Fig. 5.12 B, C)**. Further, analysis of Tfrc expression in splenocytes by flow cytometry using T-SNE dimension reduction analysis shows that high Tfrc expression is a distinctive feature of pDC **(Fig 5.13 A)**. This is further supported by Tfrc microarray expression data analysed from the Immunological Genome Project (Immgen), which shows that pDCs have an enrichment of Tfrc expression at the transcriptional level relative to other immune cells in the steady state **(Fig. 5.13 B)**. This enrichment of Tfrc expression is also conserved in human pDCs relative to other immune cells in the steady state as determined by quantitative proteomics of human immune cells **(Fig. 5.13 C)**. To investigate the activity of Tfrc in pDCs, I measured the uptake of transferrin conjugated to an APC-fluorophore by flow cytometry **(Fig. 5.14 A-C).** In line with the high Tfrc expression identified in pDCs, most pDCs are positive for transferrin uptake **(Fig. 5.14 A)**. This uptake is specific to transferrin as competition with unlabelled holo transferrin effectively competes with fluorescent transferrin uptake. In addition, transferrin uptake was performed at 4°C to inhibit endocytosis, effectively reducing the uptake of fluorescent transferrin in pDCs. To determine whether the enriched expression of Tfrc in pDCs relative to other immune cells reflects the differential rate of transferrin uptake, I next compared the rate of fluorescent transferrin uptake in different immune cells by flow cytometry **(Fig. 5.15 A, B)**. In accordance with the higher expression of Tfrc observed in pDCs, pDCs have significantly higher rates of transferrin uptake relative to other immune cells in the steady state.

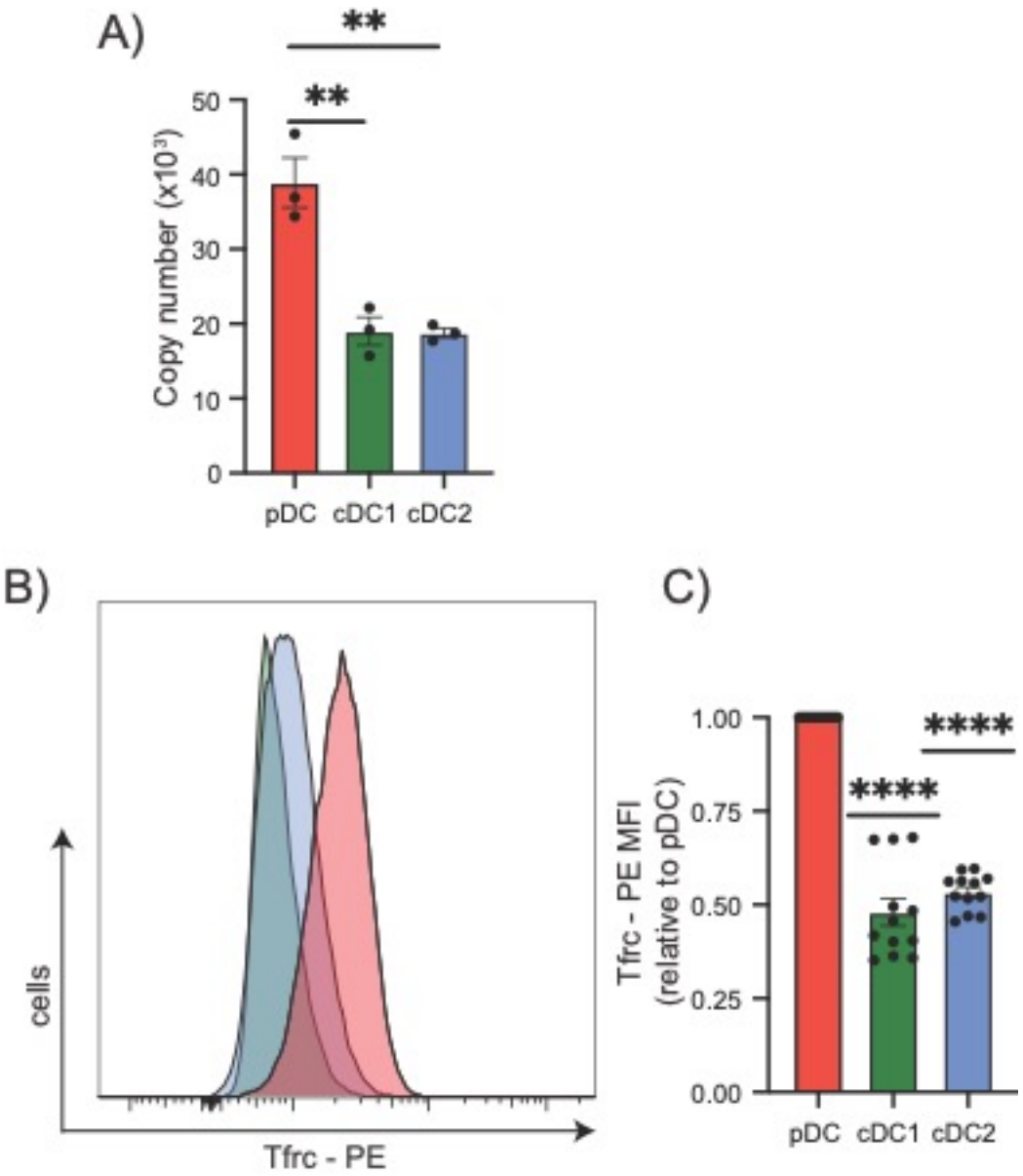

Figure 5.12 – Enrichment of Tfrc in pDCs relative to cDCs
(A) Quantitative proteomic analysis was performed on splenic DC subsets from C57Bl/6 mice inoculated with B16-Flt3l cells, including cDC1s, cDC2s and pDCs analysing copy number per cell of the iron transporter Tfrc. **(B,C)** Flow cytometry analysis of splenocytes from C57Bl/6 mice inoculated with B16-Flt3l cells analysing the expression of Tfrc in pDCs, cDC1s and cDC2s. Data are representative **(B)** or mean +/- SEM of three independent experiments **(A,C)**. Data were analysed using a one-sample t-test against a theoretical value of 1. (****p<0.0001)

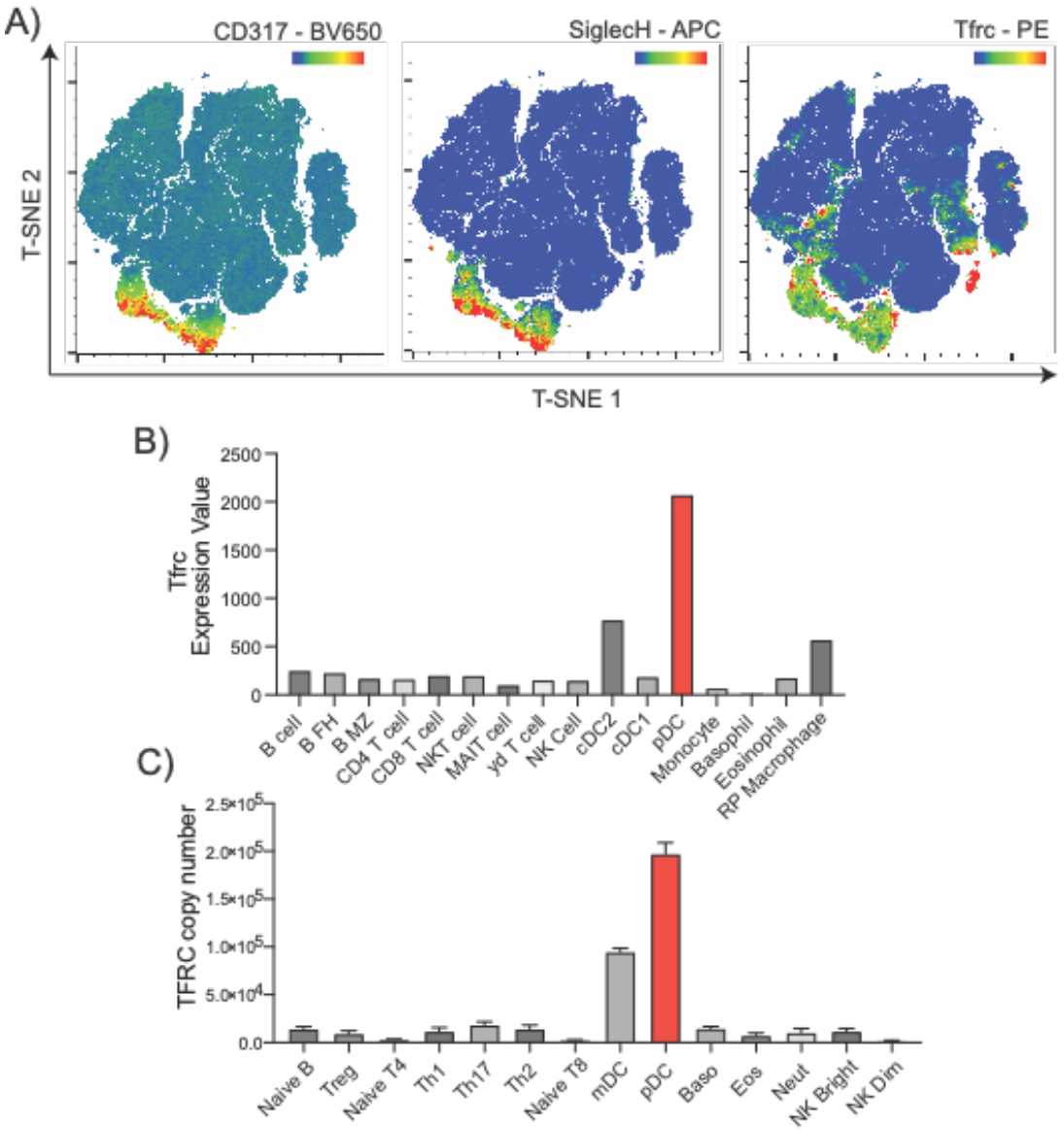

Figure 5.13 – Steady-state pDCs exhibit high expression of Tfrc, which is conserved in murine and human pDCs

(A) Flow cytometry analysis of splenic immune cells from C57Bl/6 mice inoculated with B16-Flt3l cells analysing the expression of Tfrc. T-SNE dimensional reduction analysis was performed on singlet, live/dead negative splenocytes, identifying the co-expression of CD317^{hi}, Siglech^{hi} Tfrc^{hi} cells. The left panel displays the CD317 expression; the middle panel shows the expression of Siglec-H, and the right panel shows the Tfrc expression. **(B)** Quantification of mRNA expression analysed from the Immgen microarray dataset (GSE15907) comparing the expression of Tfrc in the indicated immune cells in the steady state. **(C)** Quantification of the copy number per cell of Tfrc in the indicated human immune cells analysed from publicly available quantitative proteomics data acquired from the ProeomeXchange consortium (PXD004352). Data are representative **(A)** or mean **(B)** or mean +/- SEM **(C)** of six **(A)** or at least 3 **(B,C)** independent experiments.

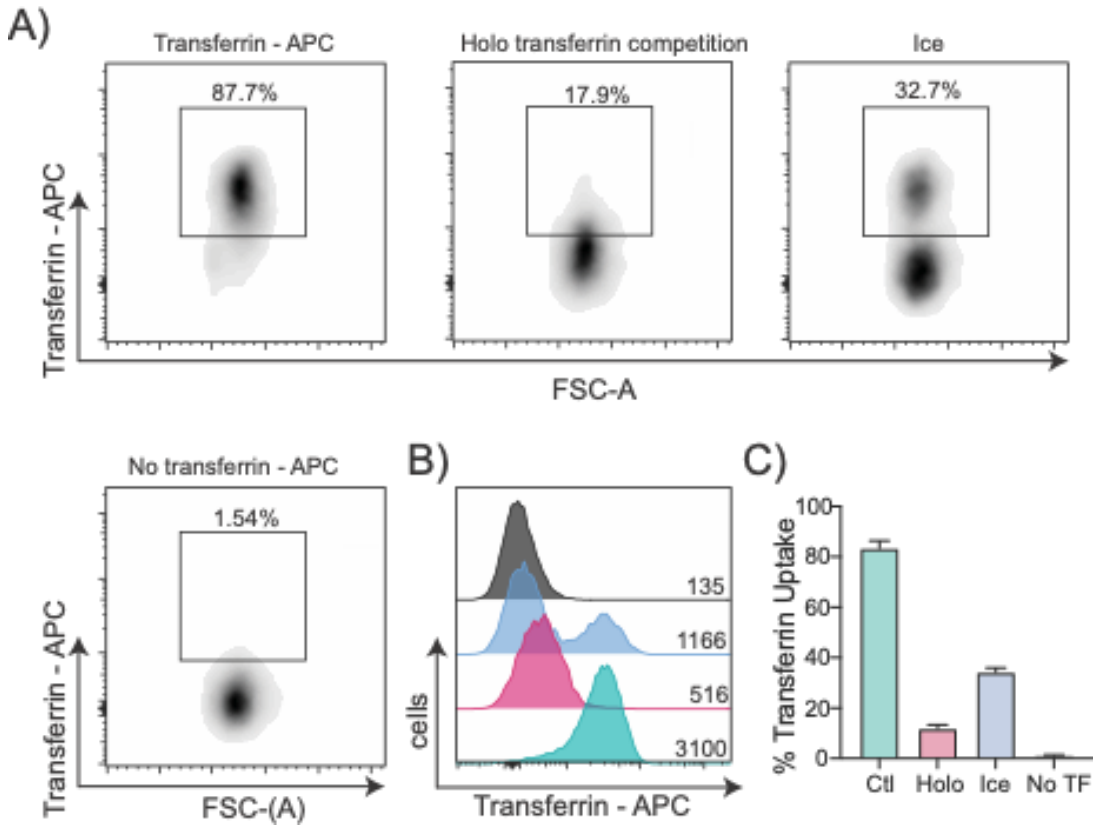

Figure 5.14 – pDCs actively uptake transferrin in the steady state
(A-C) Flow cytometry analysis of splenocytes from C57Bl/6 mice inoculated with B16-Flt3l cells analysing the uptake of fluorescently conjugated transferrin (transferrin – APC) in pDCs. Splenocytes were treated with transferrin-APC at 37ºC in the presence or absence of holo transferrin (competition control) or on ice to inhibit active transport. Transferrin uptake was determined by fluorescence in the APC channel. **(A)** Representative density plots indicating transferrin uptake in pDCs at 37C (upper left panel), in the presence of holo transferrin competition control (upper middle panel), on ice (upper right panel) or in the absence of fluorescent transferrin (lower right panel). **(B)** Representative histogram of the intensity of transferrin uptake. **(C)** Quantification of transferrin uptake is presented as the percentage of pDCs positive for transferrin-APC. Data are representative **(A,B)** or mean +/- SEM of three independent experiments **(C)**. **Experiments performed with Ms Carrie Corkish.**

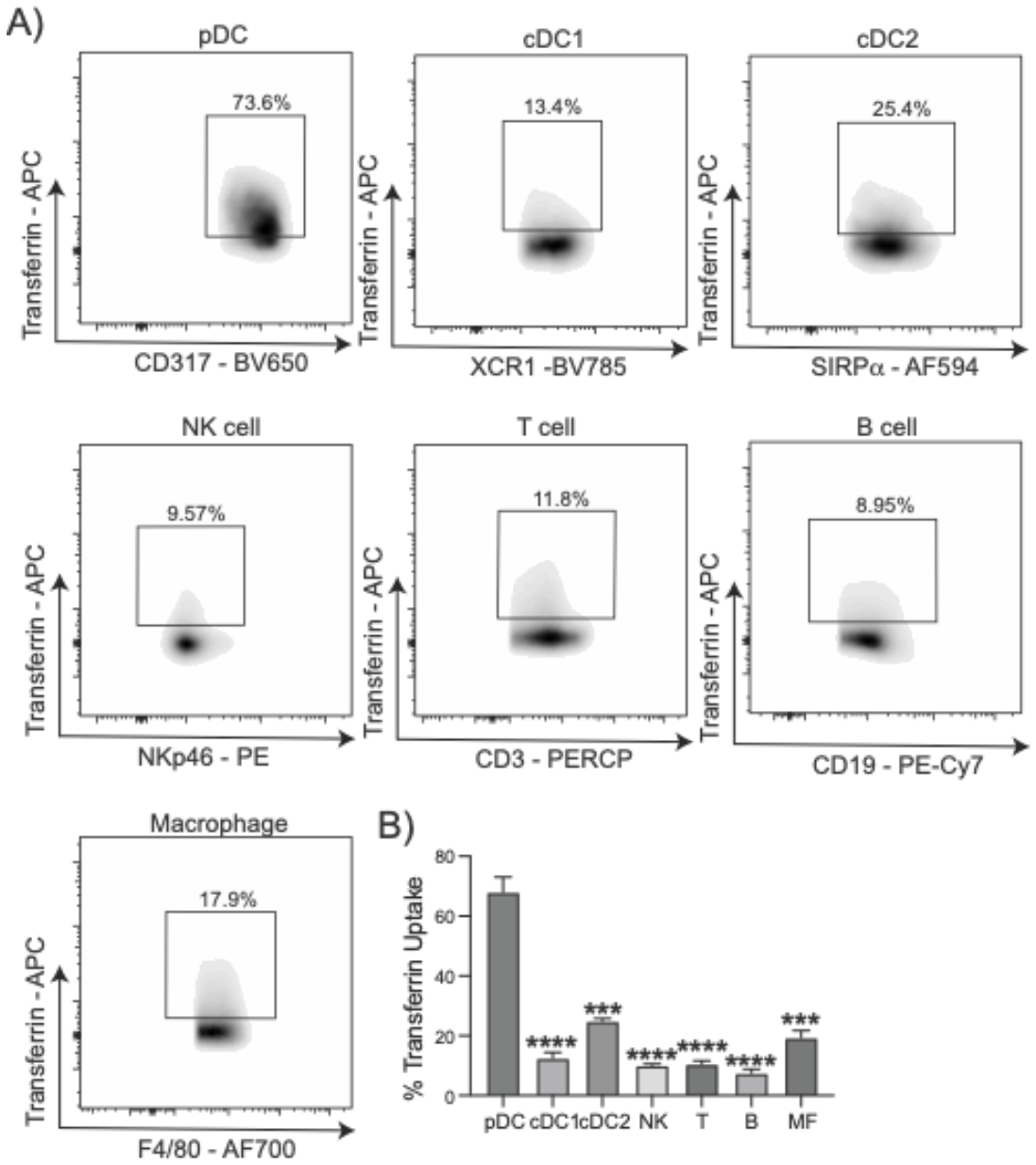

Figure 5.15 – pDCs have high transferrin uptake in the steady-state relative to other immune cells

(A,B) Flow cytometry analysis of splenocytes from C57Bl/6 mice inoculated with B16-Flt3l cells analysing the uptake of fluorescently conjugated transferrin in splenic pDCs ($CD11c^{int}CD317^{+}$), cDC1s ($CD11c^{+}MHCII^{+}XCR1^{+}$), cDC2s ($CD11c^{+}MHCII^{+}SIRP\alpha^{+}$), NK cells ($NKp46^{+}$), T cells ($CD3^{+}$), B cells ($CD19^{+}$) and macrophages ($CD11b^{+}F4/80^{+}$). **(A)** Representative density plots illustrating transferrin uptake in splenic immune cells. **(B)** Quantification of transferrin uptake is presented as the percentage of cells positive for transferrin-APC in splenic immune cells. Data are representative **(A)** or mean +/- three biological replicates **(B)**. Data were analysed using one-way ANOVA and Tukey's post-test comparing the % transferrin uptake to pDCs. (***p<0.001, ****p<0.0001) **Experiments performed with Ms Carrie Corkish.**

5.10 Characterisation of the pDC ironome

Iron's ability to act as an electron donor and acceptor is a characteristic utilised by cellular proteins for catalysis of reduction-oxidation (redox) reactions and oxygen binding. The fate of intracellular iron is highly regulated, as excess unbound iron leads to the generation of reactive oxygen species by the Fenton reaction. Thus, to prevent iron toxicity, iron is rapidly coordinated with iron-binding proteins, stored in the iron storage ferritin complex, or transported out of the cell by the iron transporter ferroportin. In light of the observation that pDCs have constitutively high transferrin uptake in the steady state, I investigated the fate of intracellular iron in pDCs.

To achieve this, I utilised an *in silico* approach to determine the set of iron-binding proteins in pDCs **(Fig. 5.17)**. This analysis is adapted from a recent publication by Teh et al., comparing the role of iron-dependent proteins in $CD4^+$ and $CD8^+$ cells (Teh et al., 2021). A list of iron-binding proteins was derived from a study by Andreini et al., who identified 398 human genes whose protein products interact with iron (Andreini et al., 2018). This human gene set was cross-referenced with murine genes, and most homologues were identified (349/398, 88%). This analysis identified 153 iron-binding in the pDC proteome **(Fig. 5.17 A)**. To place this finding in the context of other immune cells, I performed this *in silico* analysis on publicly available proteomic datasets (CD4 T, CD8 T, B cell, BMDM) from the Immunological proteome resource (Immpres) and proteomics data generated by the Finlay lab (cDC1, cDC2, NK). Similar numbers of iron-dependent proteins were observed in cDC1s, cDC2s and BMDMs (151, 148, and 150, respectively), with lower numbers in splenic lymphocytes (CD4T 140, CD8T 125, B cell 129 and NK cell 117). The analysis by (Andreini et al., 2018) predicts that approximately 2% of the human proteome comprises iron-binding proteins. In line with this prediction, iron-interacting proteins compose ~2% of the proteins identified in the tested splenic immune cells **(Fig. 5.17 B)**.

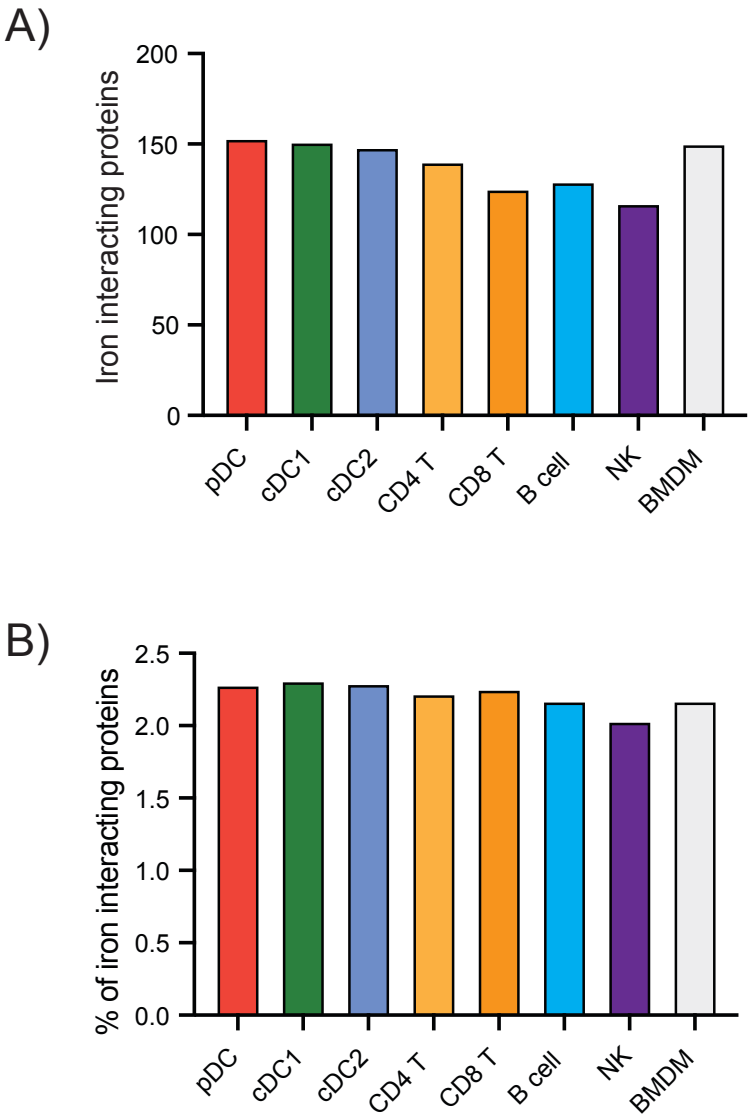

Figure 5.16 – *In silico* analysis of iron-dependent proteins in steady-state immune cells

Iron is an essential cofactor required for the function of many proteins, termed iron-dependent proteins, which are involved in various cellular processes, including DNA replication, antioxidation and cellular metabolism. **(A-B)** Identification and quantification of iron-dependent proteins as **(A)** total number of iron-dependent proteins and **(B)** iron-dependent proteins as a percentage of total proteins identified in steady-state immune cells by quantitative proteomics. An iron-interacting protein list derived from Andreini et al. was cross-compared against proteomic datasets of pDCs, cDC1s, cDC2s, $CD4^+$ T cells, $CD8^+$ T cells, B cells, NK cells and bone marrow-derived macrophage (BMDMs). pDC, cDC1, cDC2 and NK cell datasets were generated by the Finlay lab, and each represents three independent experiments. CD4 T cell, CD8 T cell, B cell and BMDM datasets were analysed from publicly available data acquired from the Immpres database from at least three biological replicates per dataset. Data is presented as mean values.

5.10.1 – Composition and distribution of iron-binding proteins in steady-state immune cells

Protein interactions with iron can occur directly with iron ions or via heme or iron-sulfur (FE-S) cluster prosthetic groups (Andreini et al., 2018). Approximately 55% of iron-binding proteins are bound via FE-S prosthetic groups, 25% are bound via heme and 20% are directly coordinated to iron ions in pDCs **(Fig. 5.17 A)**. This distribution is comparable to splenic cDC subsets, while lymphocytes, including B cells, CD4 T cells and CD8 T cells, have a higher proportion of FE-S bound iron than pDCs. I performed gene set enrichment analysis on the identified iron-binding proteins to understand if specific pathways may particularly rely on iron-dependent proteins **(Fig. 5.17 B)**. This analysis identifies pathways associated with oxidative metabolism, DNA replication, and, unsurprisingly, iron ion homeostasis, which is enriched among the iron-binding proteins. Notably, most iron-interacting proteins are related to oxidative metabolism in all cells tested. The enrichment of these pathways with iron interacting proteins suggests that iron scarcity may disproportionately disrupt these processes.

To better understand how alterations in iron availability may impact pDC function, I estimated the cellular iron requirements relative to cDC1s and cDC2s **(Fig. 5.18 A)**. Using the copy numbers of iron-binding proteins and known values of iron atoms per protein species, I determined the cellular iron requirements of pDCs, cDC1s and cDC2s. In cases where exact values were not available, the estimation of 1 iron atom for heme or iron ion interactions or two atoms for FE-S cluster interactions was used as described in Teh et al. pDCs are estimated to have an average of $2x10^7$ iron atoms coordinated to proteins. This value is similar to cDC2s but significantly less than cDC1s, which have approximately $2.7x10^7$ iron atoms. To identify protein species which may collectively bind high amounts of iron due to a combination of high copy number and/or high iron interacting protein: iron atom stoichiometry, I ranked iron interacting proteins by the predicted iron atoms bound by each protein species. Among the proteins predicted to bind the most iron are components of the electron transport chain Sdhb, Ndufs1, the TCA cycle enzyme Aco2 and the iron storage protein Ftl1. These proteins were highly

expressed across all three DC subsets. Strikingly, the top 10 proteins in each cell type are predicted to account for ~60% of all cellular iron **(Table. 5.5)**.

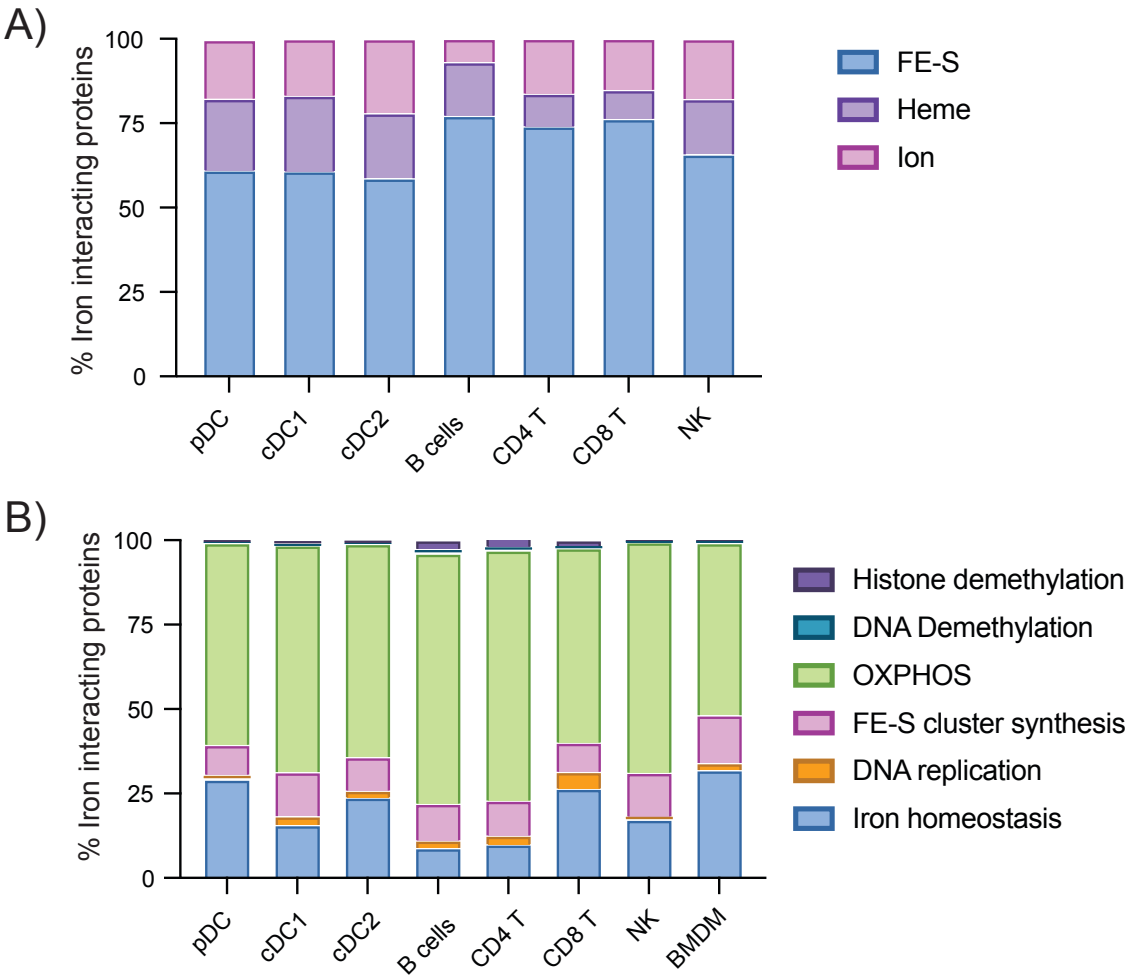

Figure 5.17 – *In silico* functional analysis of iron-dependent proteins
(A) Iron interacts with iron-dependent proteins via iron-sulfur (Fe-S) or heme prosthetic groups or by direct interaction with iron ions. The analysis shows the proportion of iron interaction with iron-dependent proteins as a percentage of the total number of iron-interacting proteins identified in each immune cell. **(B)** Gene Ontology (GO) term analysis of iron-dependent proteins presented as a percentage of the number of iron-interacting proteins identified in each immune cell. GO terms include Histone demethylation (GO:0016577), DNA demethylation (GO:0080111), Oxidative phosphorylation (OXPHOS) (GO:0006119), Fe-S cluster synthesis (GO:0016226), DNA replication (GO:0006260), and Iron homeostasis (GO:0055072). Data represent the percentage of total proteins from at least three independent experiments **(A,B).**

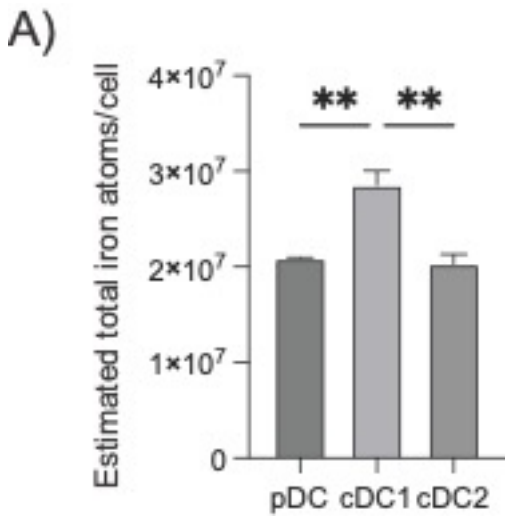

Figure 5.18 – pDCs do not have a higher requirement of iron to saturate iron-dependent proteins relative to cDCs
Cellular iron content was estimated by assuming complete saturation of all iron binding sites by iron-interacting proteins. Where possible, known values of iron atom:protein stoichiometry were used, with values assumed to be 2 for FE-S clusters, 1 for heme groups and 1 for iron ions of unknown. Estimated cellular iron content was calculated as the product of protein copy number of iron-dependent proteins and the number of iron ions predicted to bind that protein. **(A)** Predicted iron atoms per cell of pDCs, cDC1s and cDC2s in the steady state. Data represent the mean +/- SEM of three independent experiments. Statistical analysis was performed using one-way ANOVA followed by Tukey's post-test. (**p<0.01)

Rank	pDC	Cumulative	cDC1	Cumulative	cDC2	Cumulative
1	Sdhb	12.17%	Ndufs1	10.47%	Ndufs1	12.13%
2	Ndufs1	22.88%	Sdhb	20.64%	Sdhb	22.40%
3	Aco2	31.18%	Ftl1	27.46%	Ftl1	29.25%
4	Ftl1	37.14%	Aco2	33.30%	Aco2	35.93%
5	Cycs	41.21%	Cycs	39.09%	Cycs	40.46%
6	Fth1	45.15%	Cyb5a	43.20%	Ndufs8	43.45%
7	Ndufs8	48.52%	Nubp2	46.37%	Nubp2	46.15%
8	Cox5a	51.37%	Ndufs8	49.11%	Cox5a	48.52%
9	Gstp1	54.10%	Cox5a	51.32%	Fth1	50.86%
10	Ndufs2	56.58%	Ndufs2	53.33%	Gstp1	53.05%
11	Ndufv1	58.90%	Cisd1	55.33%	Ndufs2	55.20%
12	Nubp2	61.15%	Nubp1	57.26%	Cisd1	57.19%
13	Cisd1	63.27%	Ndufv1	59.18%	Ndufv1	59.16%
14	Uqcrfs1	65.39%	Cat	60.96%	Cyb5a	61.01%
15	Cyb561a3	67.47%	Uqcrfs1	62.73%	Uqcrfs1	62.85%

Table 5.5 – List of the top 15 iron-dependent proteins predicted to bind the most iron ions in splenic DC subsets

Table summarising the top 15 iron-dependent proteins predicted to bind the most iron ions in splenic DC subsets. The proteins are ranked in order of the number of predicted iron-binding sites. Columns include rank, protein name and cumulative abundance of iron-binding sites as a percentage of the total number of iron-binding sites in each proteome.

5.10.2 – Expression of iron storage and export machinery ferritin in steady-state immune cells

The data presented above shows that pDCs are not enriched for iron-interacting proteins (**Fig. 5.17,5.18**) despite the increased Tfrc expression (**Fig. 5.12, 5.13**) and capacity for transferrin-iron uptake (**Fig. 5.14, 5.15**). Indeed, closer analysis showed that pDCs do not store or export iron. During the transferrin uptake cycle, iron is released from transferrin in early endosomes due to the acidic pH in these vesicles. Ferric iron ($Fe3^{+}$) is reduced to the bioavailable ferrous ($Fe2^{+}$) oxidation state and transported into the cytosol by DMT1. Excess intracellular iron has two fates: storage in the protein complex ferritin (FTH1, FTL1) or export by the transporter ferroportin (FPN). The ferritin complex comprises 24 subunits of light (FTL1) and heavy chains (FTH1) that form a nano-cage complex. Iron is stored in ferritin in the non-toxic Fe3+ oxidation state maintained by the ferroxidase activity of FTH1. Analysis of ferritin expression in immune cells shows that myeloid cells generally have higher ferritin expression than lymphocytes, but FTH1 and FHL1 are not enriched in pDC **(Fig. 5.19 A,B)**. Ferroportin (FPN) is the only known iron exporter expressed in mammalian cells (Ward & Kaplan, 2012). FPN is similarly expressed in the proteomes of pDCs, cDC1s and cDC2s **(Fig. 5.20 A)**.

These data indicate that despite constitutively high Tfrc expression and transferrin uptake, pDCs do not have an apparent phenotype for iron sensing, storage or export. Therefore, the pDC proteome does not appear to explain why pDCs express high Tfrc levels and have constitutive transferrin-iron uptake.

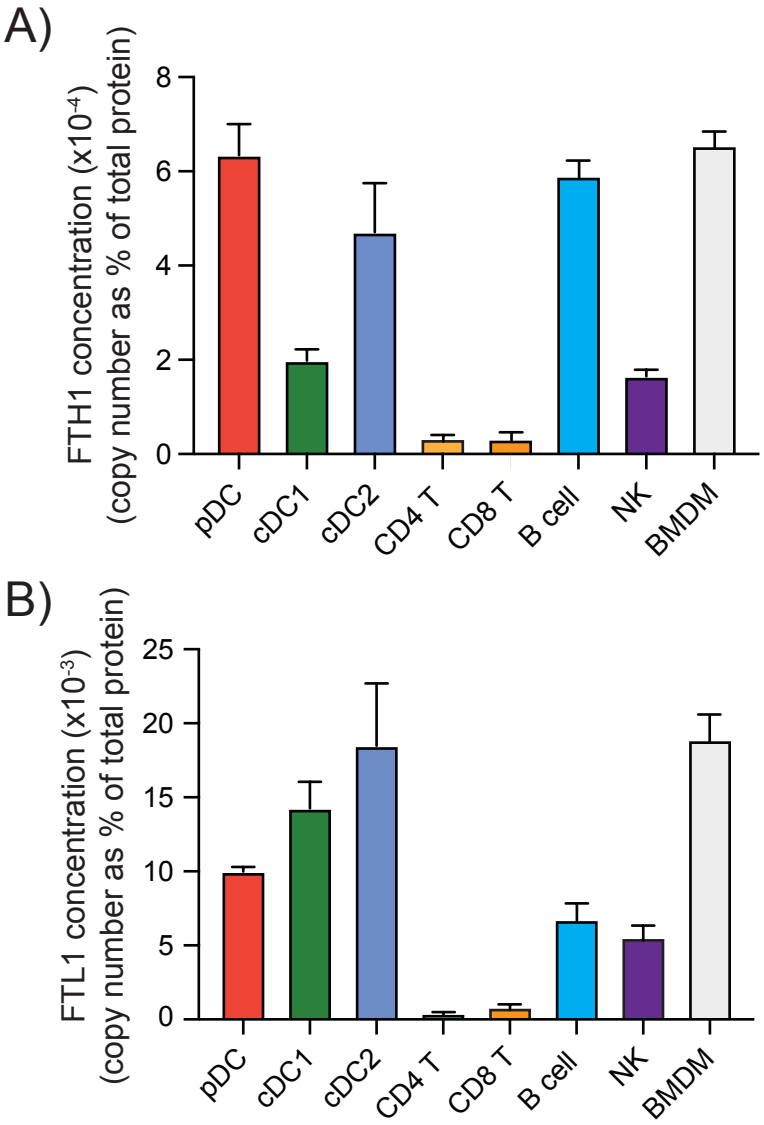

Figure 5.19 – Expression of iron storage proteins ferritin in steady-state immune cells

(A,B) Analysis of the abundance of the iron storage ferritin proteins Fth1 and Ftl1 in splenic pDCs, cDC1s, cDC2s, CD4 T cells, CD8 T cells, B cells, NK cells and bone marrow-derived macrophages (BMDM) in the steady state by quantitative proteomics. **(A,B)** The abundance of **(A)** Fth1 and **(B)** Ftl1 is presented as protein concentration, calculated as the mean protein copy number per cell divided by the copy number of all proteins identified in that cell (% of total copy number). pDC, cDC1, cDC2 and NK cell datasets were generated by the Finlay lab, and each represents three independent experiments. CD4 T cell, CD8 T cell, B cell and BMDM datasets were analysed from publicly available data acquired from the Immpres database from at least three biological replicates per dataset. Data is presented as mean +/- SD.

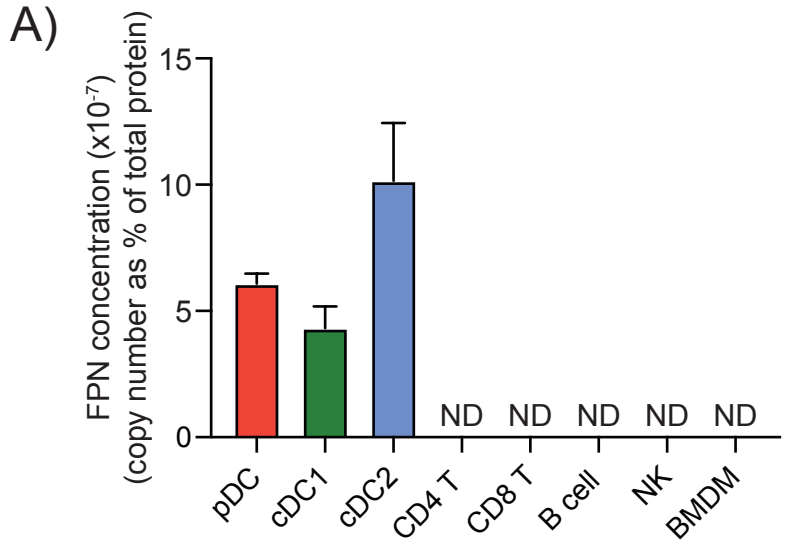

Figure 5.20 – Analysis of iron exporter ferroportin
(A) Analysis of the abundance of the iron export protein ferroportin (Fpn) in splenic pDCs, cDC1s, cDC2s, CD4 T cells, CD8 T cells, B cells, NK cells and bone marrow-derived macrophages (BMDM) in the steady state by quantitative proteomics. The data are presented as protein concentration, calculated as the mean protein copy number per cell divided by the copy number of all proteins identified in that cell (% of total copy number). pDC, cDC1, cDC2 and NK cell datasets were generated by the Finlay lab, and each represents three independent experiments. CD4 T cell, CD8 T cell, B cell and BMDM datasets were analysed from publicly available data acquired from the Immpres database from at least three biological replicates per dataset. Data are presented as mean +/- SD. ND = Not detected

5.11 – Iron availability does not affect pDC IFNα production

Next, I considered whether iron is important for pDC cytokine production. Limiting iron availability has been reported to inhibit immune cell effector function, including T cells, NK cells and macrophages (Frost et al., 2021; Littwitz-Salomon et al., 2021; Pereira et al., 2019). As pDCs have such striking levels of transferrin uptake, I next investigated whether limiting iron availability impacts Type-I interferon production in response to TLR9 stimulation. First, I confirmed that CD317^{+} pDCs are the primary producers of INFα among splenocytes in response to CpG-A-mediated TLR9 activation **(Fig. 5.21 A,B)**. Splenocytes from C57/BL6 mice inoculated with Flt3L-secreting B16 melanoma were stimulated with 4μg/ml CpG-A for 6 hours, and IFNα production was determined by flow cytometry. Indeed, CD317^{+} splenocytes account for the majority of cells that are positive for IFNα production **(Fig. 5.21 A, B)**. Notably, in response to CpG-A stimulation alone, the number of IFN-positive cells is low. This aligns with reports that few pDCs nucleate the type-I IFN response, leading to subsequent IFN production via IFNAR1 signalling (Wimmers et al., 2018). Indeed, CpG-A stimulation in combination with IFNα treatment significantly increases the number of IFN-positive cells.

To investigate the impact of iron availability on pDC cytokine production, I stimulated splenocytes from Flt3L-B16 expanded mice with CpG-A in the presence of 20μg/ml of the iron chelator deferoxamine (DFO) and measured IFNα **(Fig. 5.22 A, C)** and TNFα **(Fig. 5.22 B, D)** production by flow cytometry. DFO treatment did not affect pDC IFNα and TNFα production, indicating that iron availability does not regulate pDC proinflammatory cytokine production.

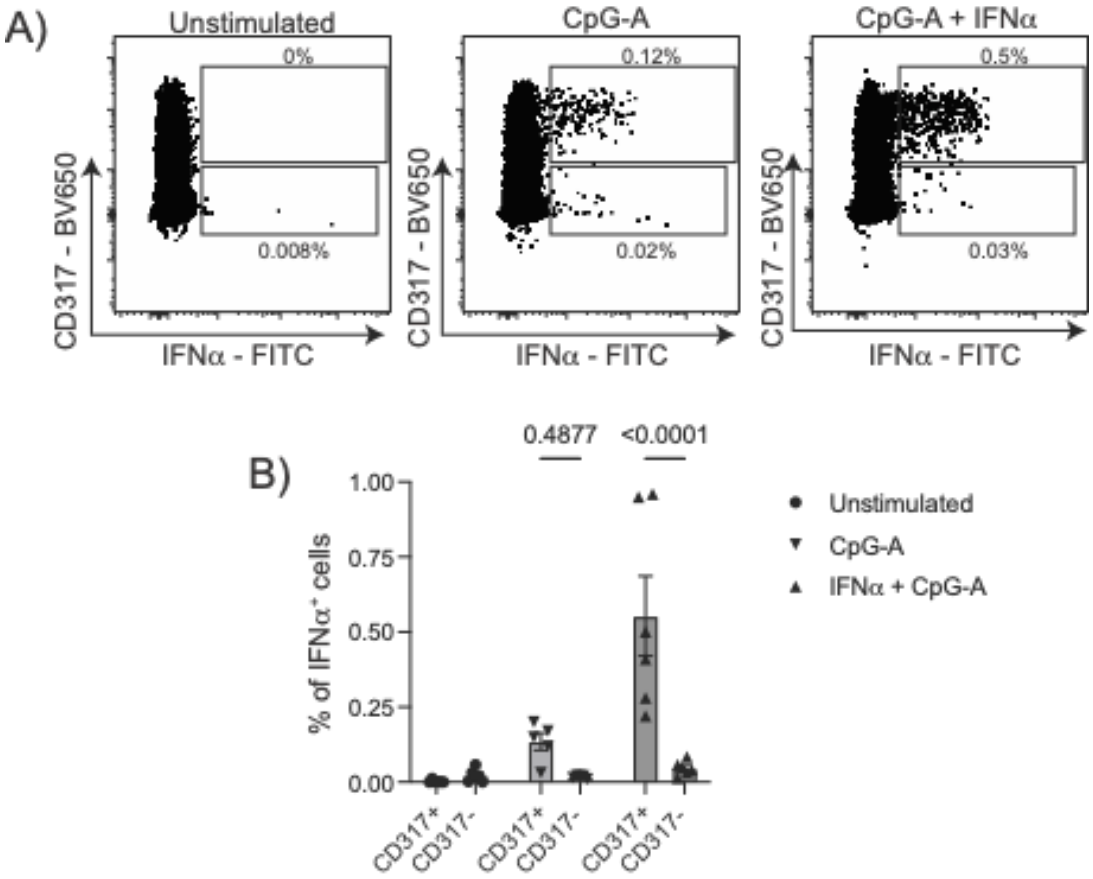

Figure 5.21 – CD317$^+$ pDCs are the primary producers of INFα in splenocytes in response to TLR9 activation

(A-C) Flow cytometry analysis was performed on splenocytes isolated from C57Bl/6 mice injected with B16-Flt3l cells to investigate interferon-alpha (IFNα) production in response to TLR9 activation. Splenocytes were treated with 4 μg/ml CpG-A in the presence or absence of 1 μg/ml IFNα for six hours, and intracellular IFNα production was assessed. **(A)** Representative gating strategy comparing IFNα production in CD317$^+$ and CD317$^-$ splenocytes following treatment with PBS (left panel), CpG-A (middle panel), or a combination of CpG-A and IFNα (right panel). **(B)** Pooled data comparing the percentage of IFNα producing cells in CD317$^+$ and CD317$^-$ splenocytes in response to PBS, CPG-A, or a combination of CPG-A and IFNα. Data are representative **(A)** or mean +/- SEM of six biological replicates. Statistical analysis was performed using two-way ANOVA followed by Sidak's post-test.

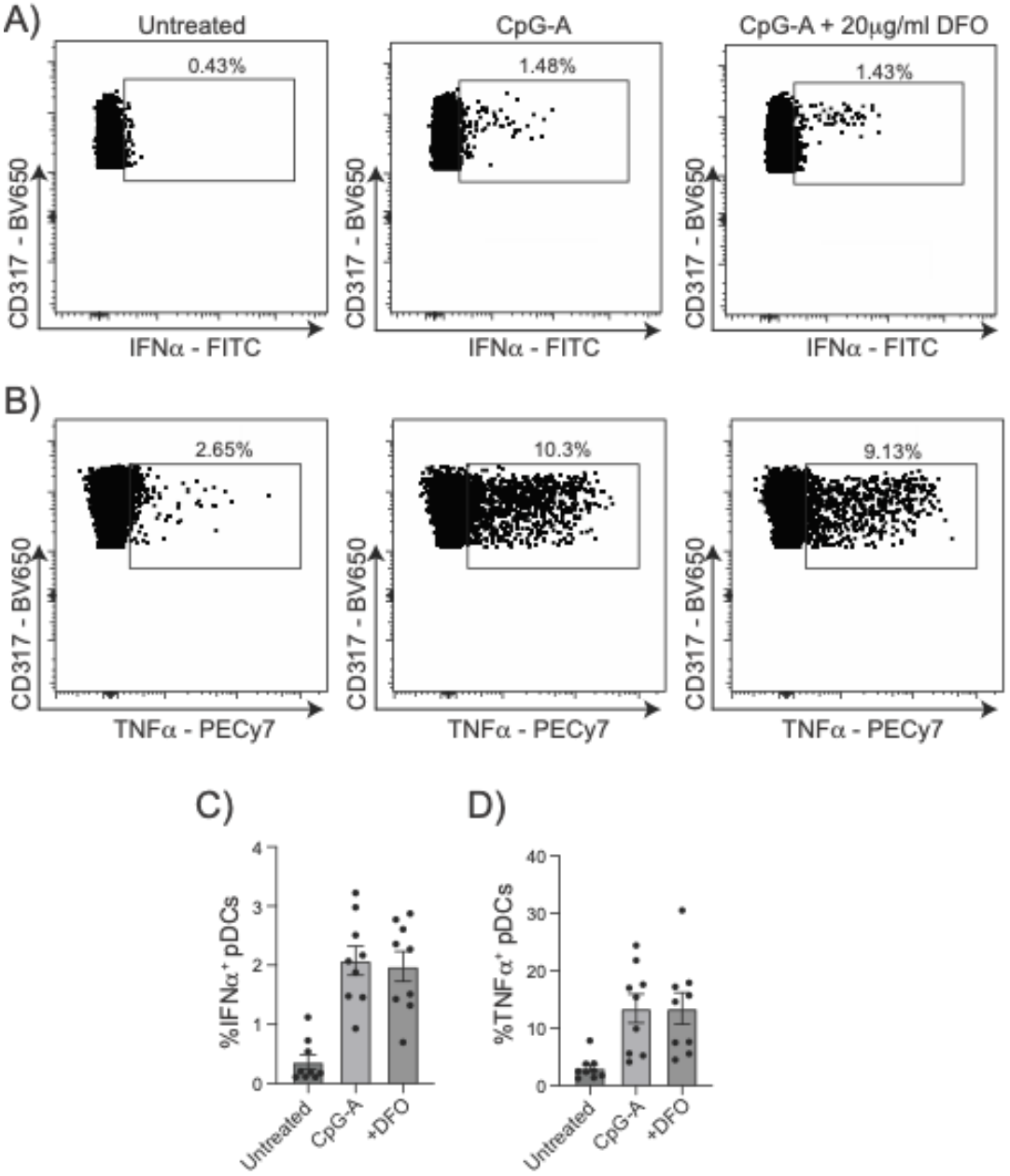

Figure 5.22 – Iron chelation with deferoxamine does not affect pDC cytokine production

(A-D) Flow cytometry analysis was performed on splenocytes isolated from C57Bl/6 mice injected with B16-Flt3l cells to investigate the effect of iron chelation on proinflammatory cytokine production. Splenocytes were stimulated for 6 hours with CPG-A in the presence or absence of the iron chelating agent deferoxamine (DFO) (20μg/ml), and proinflammatory cytokine production was assessed. **(A,B)** Representative dot plots of **(A)** interferon-alpha (IFNα) and **(B)** tumour necrosis factor-alpha (TNFα) production in untreated (left panel), CPG-A treated (middle panel) and CpG-A and DFO treated (right panel) pDCs. **(C,D)** Pooled data indicating the percentage of pDCs positive for **(C)** IFNα and **(D)** TNFα production. Data are representative **(A,B)** or mean +/- SEM of nine biological replicates.

Figure 5.12 – Iron limitation disproportionately inhibits pDC differentiation

Iron is essential for immune cell haematopoiesis as it acts as a cofactor for enzymes involved in DNA replication and cell division. Numerous studies have investigated the role of hypoferremia on immune cell development. These studies indicate that the development of specific immune cells is particularly sensitive to limited iron availability. For example, a recent publication from Frost et al. identified that neutrophils have high iron requirements associated with the oxidative burst machinery, and their development is particularly sensitive to iron deprivation. On the other hand, this study showed enhanced monocyte generation under low iron conditions. Considering the high baseline expression of Tfrc in pDCs and the observation that iron availability does not impact pDC effector function, I investigated whether iron availability is essential for pDC differentiation.

pDCs can arise from both myeloid and lymphoid progenitors in the bone marrow. Myeloid pDCs share a common developmental origin with cDCs, which develop from the common dendritic cell precursor (CDP). To investigate the role of iron availability on pDC development, I first measured the expression of Tfrc in myeloid DC progenitors using the publicly available Immgen microarray dataset (GSE15907) **(Fig. 5.23 A)**. There is a stepwise increase in Tfrc expression in DC progenitors (CMP = Common myeloid progenitor, MDP = Myeloid dendritic cell precursor, CDP = Common dendritic cell precursor), which is maintained in mature pDCs but lost in cDC1s and cDC2s **(Fig. 5.23 A)**. To investigate the effect of iron availability on DC differentiation, I generated in vitro Flt3L cultured DCs in the presence or absence of the iron chelator DFO **(Fig. 5.24 A-C)**. Bone marrow was cultured with 100ng/ml Flt3l for seven days to generate FL-DCs. 20μg/ml DFO was added on day 0, day three or day 5 of the culture, and the number of live DCs was measured. DFO treatment reduces the percentage of live DCs depending on when it was added to the culture **(Fig. 5.24 B)**. DFO treatment on all days significantly reduces the number of DCs generated **(Fig. 5.24 C)**. As adding DFO on day 5 had the mildest effect on DC viability, I next investigated the

impact of DFO treatment on cDC and pDC development **(Fig. 5.25 A-C)**. This analysis shows that pDCs the percentage of pDCs **(Fig. 5.25 A)** and cDC1s **(Fig. 5.25 B)** among live cells post-DFO treatment are significantly reduced when compared to RPMI alone. Indeed, analysis of the total number of live DCs generated shows that pDCs are significantly depleted in response to iron deprivation **(Fig. 5.25 C)**.

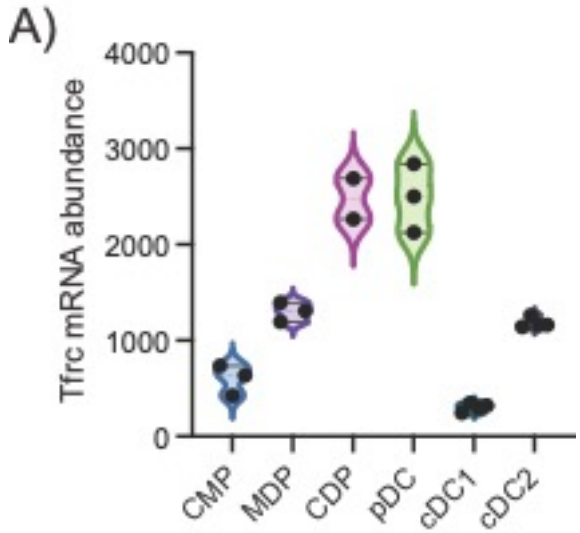

Figure 5.23: Divergent Tfrc Expression Downstream of the Common Dendritic Cell Precursor (CDP) in pDCs and cDCs
(A) Microarray data depicting the expression levels of transferrin receptor (Tfrc) analysed from the Immgen dataset (GSE15907) across various bone marrow dendritic cell precursors and splenic dendritic cell subsets. The Abbreviations used are CMP = Common myeloid progenitor, MDP = Macrophage/Dendritic cell precursor, and CDP = Common dendritic cell precursor.

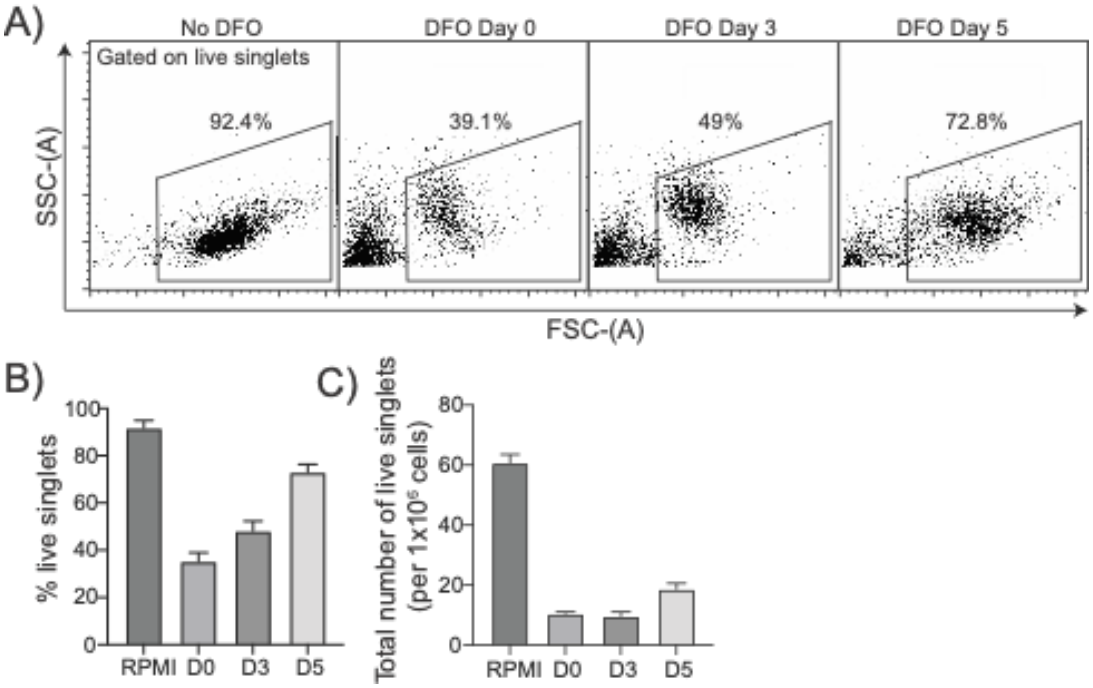

Figure 5.24 – Iron chelation inhibits the development of dendritic cells *in vitro*

(A-C) Flow cytometry analysis was conducted on *in vitro* Flt3l bone marrow cultures to examine the impact of DFO treatment on the viability of Flt3 ligand-induced dendritic cells (FL-DCs). Bone marrow cells were treated with 100 ng/ml Flt3l for seven days in the presence or absence of 20 µg/ml DFO. DFO was added at different time points: day 0, day 3, or day 5 of the culture. **(A)** Representative dot plots and **(B)** pooled data depicting the percentage of FL-DCs identified among live, single cells in response to DFO treatment. **(C)** Quantification of the absolute number of total live FL-DCs per $1x10^6$ bone marrow cells cultured in response to DFO treatment. Data are representative **(A)** or mean +/- SEM of three independent experiments **(B,C)**.

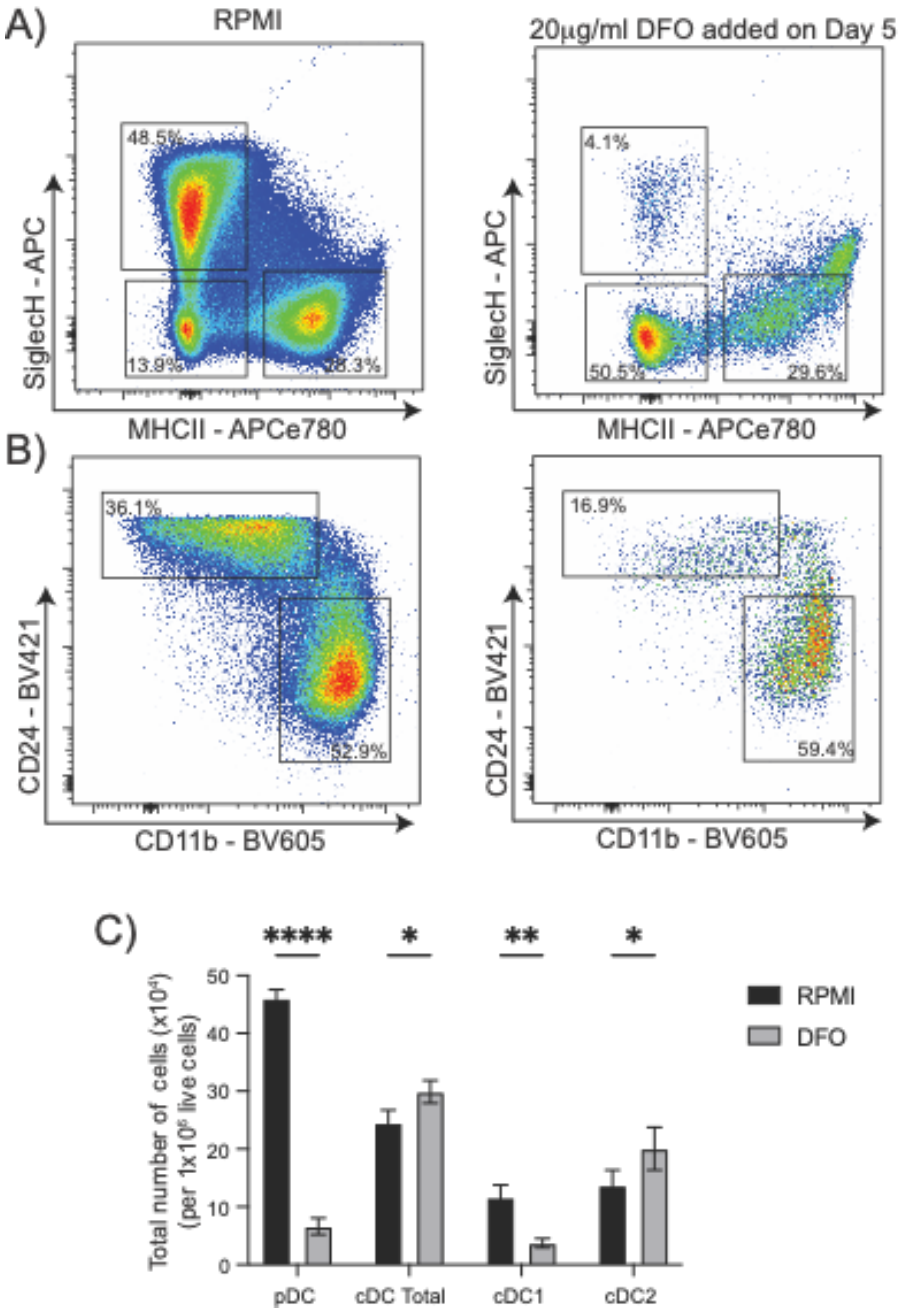

Figure 5.25 – Iron chelation with DFO disproportionately inhibits pDC development

(A-C) Flow cytometry analysis was conducted on *in vitro* Flt3l bone marrow cultures to examine the impact of deferoxamine (DFO) treatment on the generation of pDCs (Siglec-H$^+$), cDC1s (MHCII$^+$,CD24$^+$,CD11b$^-$) and cDC2s (MHCII$^+$,CD24$^-$,CD11b$^+$). DFO (20µg/ml) was added on day 5 of the culture, and DC generation was quantified. **(A,B)** Representative dot plots indicating the percentage of **(A)** pDCs and cDCs and **(B)** cDC1s and cDC2s in response to RPMI (vehicle control) (left panels) and DFO treatment (right panels) on day 5 of the culture. **(C)** Quantification of the number of pDCs, total cDCs, cDC1s and cDC2s generated per 1x10^6 live cells in response to RPMI and DFO treatment. Data are representative **(A,B)** or mean +/- SEM of three independent experiments **(C)**. Data were analysed using two-way ANOVA and Sidak's post-test. (*p<0.05, **p<0.01, ****p<0.0001)

5.13 Discussion

pDCs are a unique dendritic cell subset that shares both myeloid and lymphoid characteristics and are specialised in producing type-I interferons in response to viral infection (Reizis, 2019). While substantial progress has been made in understanding the molecular mechanisms underpinning pDC function, the research on pDCs is comparatively limited relative to other immune cells. To date, no studies have been reported in the literature that have detailed the murine pDC proteome. As discussed in Chapter 3, quantitative proteomics is a valuable approach to identify novel metabolic and functional drivers of cellular function. This study investigates the splenic pDC proteome in the steady state at the level of individual protein expression and global proteome architecture. It compares the relationship between the pDC transcriptome and proteome and the conservation of the proteome between mouse and human pDCs. This analysis reveals that the iron-transporting transferrin receptor (Tfrc) is highly enriched in murine and human pDCs. As iron availability is now recognised as a critical requirement for immune cell function, I investigated the utilisation of iron within the pDC proteome and the impact of iron availability on pDC development and function.

A key benefit of this study is the use of primary splenic pDCs analysed directly *ex vivo*. Given the scarcity of pDCs *in vivo*, many studies utilise *in vitro*-generated bone marrow-derived DCs for phenotypic and metabolic studies. While these *in vitro* models have proven valuable for studying pDC biology, they may not accurately reflect the phenotype of natural DCs (Helft et al., 2015; Mayer et al., 2014). In particular, the recognition that the supraphysiological nutrient concentrations present in standard cell culture media directly influence the cellular metabolism of immune cells emphasises the need to exercise caution in interpreting these studies (Kaymak et al., 2022). Thus, to acquire enough cells for mass-spectrometry proteomics analysis, I expanded the pDC compartment *in vivo* by inoculating mice with B16-Flt3L-secreting melanoma cells.

Proteomics was performed on three biological replicates, identifying approximately 6700 proteins in each replicate. Analysis of the number of

peptides used to identify each protein revealed that the majority of proteins were quantified with medium or high confidence. Furthermore, linear correlation analysis of each biological replicate shows a high degree of correlation and a small number of outliers expressed in each replicate. These data emphasise the reproducibility of the proteomic analysis, providing confidence for subsequent analysis.

Quantitative proteomics offers several advantages over transcriptomics. The primary benefit is the direct measurement of protein levels rather than mRNA, providing a more accurate reflection of cellular activity. In addition, this study utilised the proteomic histone ruler methodology, which allows absolute protein quantification rather than relative expression values (Wiśniewski et al., 2014). This facilitates the investigation of global proteome features, including abundance analysis and the distribution of proteins into different subcellular compartments. Cumulative protein abundance analysis reveals that, similarly to cDCs, a small number of highly abundant proteins account for the majority of the total protein content of pDCs. Strikingly, 23 proteins (0.3% of all proteins identified) account for over 50 per cent of the total protein content of pDCs. The high abundance of these proteins reflects their roles in fundamental cellular processes, including DNA packaging, cellular organisation and intermediary metabolism. While analysis of the mRNA abundance of these highly abundant proteins reveals that they are also enriched at the transcriptional level, the scale of enrichment does not accurately reflect protein levels. For example, the cytoskeletal protein Actin B (Actb) accounts for 1.5% of the total protein content in pDCs. In comparison, it only accounts for 0.2% of the total transcript abundance identified from the Immgen dataset (GSE15907). Additionally, absolute protein quantification allows the analysis of protein distribution into different subcellular compartments. For example, approximately 16 per cent of proteins in the pDC proteome are associated with the mitochondria. This finding reflects the enrichment of metabolic pathways, including the TCA cycle and OXPHOS among the upper quartile of proteins expressed in the pDC proteome.

Linear correlation analysis between the pDC proteome and transcriptome reveals a weak correlation, indicating that mRNA abundance is a poor surrogate marker for protein abundance. This finding suggests substantial post-transcriptional and post-translational regulation of gene expression. Examples of discordance include the expression of inflammatory transcription factors and pathogen recognition receptors. Notably, the endosomal TLRs, TLR7 and TLR9, are enriched at the mRNA level, while the cytoplasmic RNA sensor, RIG-I, is enriched at the protein level. These data emphasise the need for further research on the control of gene expression in pDCs. Indeed, a study by Colina et al. shows that IRF7, the primary transcription factor involved in type-I interferon production in pDCs, is translationally regulated by the translational repressors 4E-BP1 and 4E-BP2 (Colina et al., 2008). Genetic ablation of these proteins increased the translation of Irf7 mRNA and conferred resistance to viral replication.

Murine pDCs are the preferred biological system to model human pDC metabolism and function. The phenotypic conservation between species dictates the value of this model. Transcriptional approaches have revealed that pDCs are highly conserved in mice and humans (Guilliams et al., 2016; Robbins et al., 2008). However, considering the discordance between the murine pDC transcriptome and proteome, comparing protein abundance across species is favourable. To compare murine and human pDCs, I performed a linear regression analysis between the murine pDC proteome and human pDC proteomics data generated by (Rieckmann et al., 2017). This analysis reveals a strong positive correlation with a Pearson's correlation coefficient of 0.83, indicating a high degree of conservation of protein expression between mice and humans. A potential limitation of this comparison is that the human dataset is generated from circulating pDCs in the blood, while the murine set is derived from splenic pDCs. However, it is generally accepted that murine pDCs continuously recirculate between the bloodstream and lymphoid organs (Reizis, 2019). This analysis confirms the species-specific reliance on IL3 signalling in human pDCs as they have an enrichment of the IL3 receptor (IL3RA) (Swiecki & Colonna, 2015). Notably, the human pDC proteome was enriched for proteins involved in glucose

metabolism, including the glucose transporter GLUT1 (Slc2a1), the lactate-producing protein LDHB and the lactate transporter MCT4 (Slc16a3). While no studies have directly compared the metabolic profiles of murine and human pDCs, studies indicate that glycolytic metabolism is important for human pDC function (Bajwa et al., 2016; Fekete et al., 2018). By contrast, murine pDCs derived from the Flt3l *in vitro* stimulated bone marrow cultures show no increase in glycolytic flux in response to CpG-A stimulation (Wu et al., 2016). Rather, these cells rely on enhanced FAO and mitochondrial OXPHOS to support IFNα production. The proteomic data may suggest that this disparity is not just a consequence of the source (sorted from peripheral blood mononuclear cells versus sorted from Flt3L bone marrow cultures) of pDCs but rather species-specific differences in immunometabolic fuel preference.

It is now recognised that in addition to the sensing of PAMPs by PRRs, the availability of nutrients at the site of infection can influence the subsequent immune response (Newsholme, 2021). The nutrient requirements of a cell are closely related to the expression of nutrient transporters (H. J. Weiss & Angiari, 2020). Thus, considering the enrichment of glucose and lactate transporters from the linear correlation analysis, I investigated the expression of nutrient transporters in murine and human pDCs. This analysis reveals conserved expression of specific transporters, including the transferrin receptor (Tfrc) and the fatty acid transporter SLC27A1. Conversely, there is a discordance in the expression of various transporters, including the large neutral amino acid transporter SLC7A5 and, as previously mentioned, the glucose transporter SLC2A1. The enrichment of SLC7A5 in human pDCs supports a recent publication from Grzes et al., who demonstrated that SLC7A5 amino acid transport is essential for type-I interferon production in human pDCs by regulating the activity of mTORC1 (Grzes et al., 2021). Notably, the expression of SLC7A5 was shown to be controlled by IL3 signalling, which is specific to human pDCs. Of particular interest is the observation that Tfrc is the most abundant nutrient transporter across both species. Indeed, Tfrc expression is also significantly enriched in murine pDCs

compared to both cDC1s and cDC2s. Iron availability has recently been identified as a crucial mediator of immune cell function (Cronin et al., 2019). While the role of iron in numerous immune cells, including T cells, B cells, macrophages and neutrophils, has been demonstrated, the reliance of pDC function on iron availability is still undetermined (Frost et al., 2021, 2022; Jabara et al., 2016; Sindrilaru et al., 2011).

Iron is essential for cellular function by acting as a cofactor for proteins involved in fundamental cellular processes, including DNA replication, control of oxidative stress and cellular metabolism (Andreini et al., 2018; Cronin et al., 2019). The importance of iron availability on immune cell function was demonstrated by a study that investigated children bearing a mutation in the transferrin receptor, which impaired cellular iron uptake, leading to severe combined immunodeficiency, including hypogammaglobulinemia and defective lymphocyte proliferation (Jabara et al., 2016). While it is now established that iron availability is important for immune cell responses, the underlying mechanisms why iron is needed are unclear. As free iron is toxic, it must be rapidly coordinated to iron-dependent proteins upon uptake. Iron in excess of these proteins is stored in nanocage structures composed of ferritin or exported from the cell by the iron exporter ferroportin. Iron uptake for the purpose of storage can have two primary biological functions. As iron is an essential nutrient for bacterial and viral replication, infection can lead to iron deprivation at the site of infection. Thus, ferritin provides an iron buffer to sustain immune cell function during disease. Conversely, immune cells, particularly macrophages, have been reported to sequester iron into ferritin storage depots during infection to limit the availability of iron to siderophilic pathogens (Parrow et al., 2013). Analysis of ferritin expression in murine immune cells does not indicate that pDCs have elevated iron storage. Further, since pDCs are a rare immune cell population, they are unlikely to contribute to systemic iron homeostasis. Similarly, while ferroportin is detected in pDCs, its expression is highly limited relative to Tfrc, suggesting that pDCs have a weak capacity to recycle iron. Indeed, it is generally accepted that ferroportin expression is limited to professional iron-handling cells, including enterocytes, which mediate dietary iron uptake from the gut and macrophages, facilitating

systemic iron recycling of erythrocytes (Drakesmith et al., 2015). These data indicate that the transferrin-mediated iron uptake in pDCs is likely linked to utilisation by iron-dependent proteins rather than for generating storage depots or iron recycling by ferroportin.

To investigate the cellular usage of iron by pDCs, I performed an in-*silico* analysis of iron-dependent proteins within the pDC proteome. A study by Andreini et al. highlighted the central role of iron in cellular biochemistry by revealing that approximately 2% of human proteins interact with iron (Andreini et al., 2018). This study derived, for the first time, a comprehensive list of iron-dependent proteins in human cells. Teh et al. utilised this list to reveal the cellular iron proteome of $CD4^+$ and $CD8^+$ T cells during immunogenic activation (Teh et al., 2021). Using the approach outlined in Teh et al., I identified ~150 iron-binding proteins in the pDC proteome, which accounts for 2.2% of all proteins identified, as predicted by (Andreini et al., 2018). A comparison of the number of iron-dependent proteins across different immune systems reveals that myeloid cells, including cDCs and BMDMs, have a comparable number of iron-dependent proteins to pDCs. Protein interactions with iron can occur directly with iron ions or via heme or iron-sulfur cluster prosthetic groups. While iron ions that bind proteins directly are predominantly involved in catalysis, FE-S-mediated iron-protein interactions play an important role in mitochondrial respiration and DNA synthesis (Andreini et al., 2018; Johnson et al., 2005). In pDCs, iron is predominantly coordinated to proteins via FE-S clusters, accounting for approximately 55% of total protein-iron interaction. The preferential binding of iron via FE-S clusters is similar across different immune cells; however, lymphocytes appear to have a higher proportion of FE-S clusters relative to DC subsets. Gene set enrichment analysis of iron-dependent proteins in immune cells shows that the majority of iron-dependent proteins are associated with oxidative phosphorylation. This aligns with the enrichment of FE-S clusters, which play an essential role in electron transfer reactions within the electron transport chain. Overall, however, no iron-dependent pathway is significantly enriched in pDCs versus other immune cells. These data reveal that despite

pDCs having enriched Tfrc expression and transferrin uptake, there is no clear signature for iron utilisation within the pDC proteome.

To understand the iron requirements of these proteins, I estimated the total iron atoms per cell in pDCs and cDC subsets. This analysis reveals that despite a similar number of iron-dependent proteins across DC subsets, cDC1s have a significantly higher total iron requirement than pDCs and cDC2s. Strikingly, the 15 proteins predicted to bind the most iron in the pDC proteome account for ~67% of the total predicted iron atoms in the pDC proteome. These proteins, outlined in Table 3, relate to processes including iron storage, the TCA cycle and the electron transport chain. Thus, it is predicted that these processes would be disproportionately affected by limited iron availability. Overall, *in silico* analysis of iron utilisation within pDCs does not indicate that they have enrichment for iron storage or iron-binding proteins despite constitutive Tfrc recycling.

Considering there is no apparent enrichment of iron utilisation within the pDC proteome, this suggests that Tfrc activity in pDCs may have immunological functions independent of iron acquisition. As discussed above, steady-state pDCs specialise in detecting viral antigens to induce Type-I interferon responses. Several viruses, including New World hemorrhagic fever virus, Influenza A and SARS-CoV-2, have been shown to co-opt Tfrc as a cell entry receptor (Liao et al., 2024; Mazel-Sanchez et al., 2023; Radoshitzky et al., 2007). Furthermore, IgA1 has also been described as binding to Tfrc, possibly indicating a role in the uptake of opsonised pathogens into the endocytic compartment (Mkaddem et al., 2014). Since the transferrin receptor provides entry to early endosomes, which colocalise with TLR7 and TLR9, it is plausible that the high rates of transferrin endocytosis observed in pDCs act to sequester microbial nucleic acids to trigger inflammation. Importantly, it has been shown that TLR9 ligation in early endosomes induces IRF7 phosphorylation and Type-I interferon production (Guiducci et al., 2006; Honda et al., 2005). In contrast, TLR9 triggering in late endosomes is associated with pDC maturation driven by NfκB signalling but weak type-I IFN

responses (Guiducci et al., 2006). Thus, further research is required to determine the role of Tfrc endocytosis in pDC microbial detection.

Despite no clear consensus on pDC iron utilisation from the proteomic analysis, I next investigated the impact of iron availability on pDC cytokine production. Flow cytometry analysis shows that pDCs are the primary producers of IFNα among splenocytes stimulated with CpG-A. In agreement with the absence of an iron-dependent signature in pDCs, treatment with the iron chelator deferoxamine has no effect on IFNα and TNFα production in response to CpG-A stimulation. While Tfrc is typically lowly expressed in immature immune cells, it is generally recognised as a maturation marker of lymphocytes, including T cells, B cells and NK cells. Indeed, proteomic analysis of $CD8^+$ T cells shows that Tfrc expression increases by greater than 500-fold upon immunogenic stimulation (Howden et al., 2019). While the increased iron demand associated with proliferation is apparent, it has also been shown that iron scarcity limits cytokine production by OT-I $CD8^+$ T cells in an *in vivo* iron deprivation model (Frost et al., 2021). Notably, while pDCs have an unusually high abundance of Tfrc in the steady state, this abundance is profoundly less than that observed in activated lymphocytes. While the absence of proliferative capacity of pDCs may partially explain this deficit, the observation that iron chelation does not influence cytokine production indicates that Tfrc may be more important for steady-state rather than mature pDC function.

Systemic iron availability is tightly linked to haematopoiesis. In particular, iron is essential for erythrocyte development by controlling haemoglobin synthesis required for oxygen transport (Sinha et al., 2021). The role of iron availability on leukocyte development is less well characterised. A recent report by Frost et al. addressed this question using a murine model of iron deficiency (Frost et al., 2022). This study revealed that cells of the monocytic lineage are refractory to the effects of iron deficiency, while granulocytes, including neutrophils and eosinophils production, are highly sensitive to iron scarcity. Considering the high steady-state expression of Tfrc in pDCs, I investigated

whether iron availability is important for pDC development. Analysis of Tfrc mRNA abundance during myeloid DC development shows that Tfrc expression diverges downstream of the common dendritic cell precursor, maintained in pDCs but lost in cDCs. To investigate the influence of iron availability on DC differentiation, I generated FL-DCs *in vitro* in the presence or absence of deferoxamine. This data reveals that, although iron limitation reduces the overall production of DC subsets, pDCs are particularly sensitive to iron limitation. This observation closely reflects the findings of Weigert et al., who demonstrated that hypoxia-induced HIF1α activity is a negative regulator of pDC development (Weigert et al., 2012). This study showed that HIF1α activity represses the pDC developmental transcription factor E2-2 by enforcing ID2 expression, reducing pDC differentiation. Iron availability regulates HIF1α stability by acting as a cofactor for prolyl hydroxylase 1 (PHD1). Therefore, when iron levels are low, PHD1 activity is repressed, promoting HIF1α.

Overall, proteomic analysis of the steady-state pDC proteome identified the transferrin receptor's uniquely high and conserved expression in mice and humans. As Tfrc is the primary iron import mechanism in immune cells, this suggested a role for iron in pDC function. A combination of in silico and functional analysis revealed that the pDC proteome is not enriched with iron-dependent proteins, nor is iron required for type-I interferon production in response to immunogenic stimulation. While not directly explored in this study, together, these data indicate an iron-independent role of Tfrc in steady-state pDCs.

Chapter 6 - General Discussion

The data presented in this thesis examine the molecular basis of metabolic heterogeneity between natural splenic DC subsets. Quantitative proteomic analysis of cDC1s and cDC2s reveals substantial differences in the expression of proteins that govern cellular metabolism, including nutrient transporters, intermediary metabolic pathways, anabolic regulators, and protein biosynthesis machinery, which translates ATP availability into functional outcomes. The abundance of amino acid transporters is examined in greater detail, identifying SLC7A5-mediated amino acid uptake as a potent regulator of mTORC1 signalling in cDCs. In particular, pharmacological targeting of SLC7A5 amino acid transport modulates antigen processing in cDC1s, which impacts the kinetics of cross-presentation. Finally, analysis of nutrient transporter expression in pDCs reveals that the transferrin receptor is highly enriched in the steady state, a feature that is conserved in mice and humans. Despite the described role of TFRC in facilitating iron availability to immune cells (Cronin et al., 2019; Jabara et al., 2016), *in silico* and functional analysis suggests an iron-independent role of TFRC in pDCs.

Immunometabolism research aims to uncover the metabolic processes that govern immune cell function. Basic research on the metabolic features of immune function and dysfunction opens the possibility of new therapeutic interventions to direct immunity, both to temper pathologic inflammation and bolster responses during infection and malignancy. As immune cells have different metabolic demands associated with their function, fundamental discoveries in the metabolism of each cell type and their subsets in different contexts are essential first steps to meet the primary research aim of translating basic research from bench to bedside. To achieve this, collaboration is paramount, combining expertise and different methodologies to piece together the immunometabolic puzzle. In the past 20 years, technological advancements in immunometabolic research have accelerated the pace of discovery.

Extracellular flux analysis using platforms such as Seahorse revolutionised the study of immunometabolism. It allowed the determination of glycolytic and oxidative metabolism in live cells by measuring extracellular acidification and oxygen consumption in response to metabolic inhibitors. While useful in studying abundant cells, the requirement for a large population of homogenous cells is prohibitive in studying rare populations, including DCs. More recently, single-cell approaches to investigate immunometabolism at the transcriptional (scRNA-seq) and protein level (mass cytometry (CyToF), Flow cytometry) have allowed the interrogation of rare cells and the identification of metabolic heterogeneity within populations (Artyomov & Van Den Bossche, 2020; Purohit et al., 2022). Novel approaches have leveraged the flow cytometer to measure metabolic protein expression (MetFlow), metabolic flux (SCENITH) and nutrient uptake (QuasR) (Ahl et al., 2020; Argüello et al., 2020; Pelgrom et al., 2023). Mass-spectrometry analysis applied to proteomics and metabolomics has allowed the broad characterisation of metabolic networks and flux in different cell types and contexts. Finally, the generation of genetic approaches to specifically target metabolism facilitates the translation of *in vitro/ex vivo* analyses to *in vivo* contexts. Through combining these approaches (among others) across different studies, meaningful breakthroughs can be made.

It is now clear that metabolic rewiring is a feature of all aspects of DC biology, including differentiation, maturation, and disease response (Guo & Chi, 2023; Møller et al., 2022; Wculek et al., 2019). Additionally, methods to genetically deplete DC subsets *in vivo* are clarifying their subset-specific roles in immunity (Arnold et al., 2019; T.-T. Liu et al., 2022). However, the characterisation of the metabolic profiles of cDC subsets is still in its infancy. Studies in recent years have begun to reveal cDC subset specific metabolic programmes that underlie their functional partitioning, including distinct metabolic drivers (X. Du et al., 2018), divergent reliance on metabolic regulators such as mTORC1 and AMPK (Pelgrom et al., 2019, 2022; Wang et al., 2019) and different sensitivity to amino acid availability (Guo et al., 2023). Chapter 3 of this thesis aims to contribute to this knowledge by analysing the proteomic features associated with immunometabolism in

cDC1s and cDC2s. Through a combination of proteomic and flow cytometry analysis, data presented in Chapter 3 reveals that cDC1s maintain a higher rate of protein synthesis than cDC2s in the steady state, which is reflected in their proteome. cDC1s have a significantly higher abundance of ribosomes, which facilitate the synthesis of polypeptide chains and the expression of proteins that mediate the initiation of translation. In addition, cDC1s have a higher abundance of ER proteins, which aligns with previous reports that constitutive ER stress regulates cDC1 function (Mendes et al., 2021; Osorio et al., 2014; Tavernier et al., 2017). Indeed, genetic knockout of the ER stress regulator XBP1 disrupts ER architecture in cDC1s, abrogating their ability to cross-present antigens (Osorio et al., 2014). The ER is the site of folding for proteins destined for secretion or the plasma membrane. Thus, ER function and protein translation are intricately linked. The induction of the ER stress response is mediated by three sensors: IRE1, PERK and ATF6. Accordingly, the accumulation of unfolded proteins in the ER activates the ER stress response, which involves the coordinated inhibition of global protein synthesis while allowing the specific translation of proteins to restore ER homeostasis, including protein-folding chaperones and amino acid transporters. Importantly, Mendes and colleagues revealed that despite having constitutive PERK signalling and EIF2a phosphorylation in the steady-state, cDCs are resistant to translation inhibition (Mendes et al., 2021). Importantly, they show that cDC1s have higher EIF2a phosphorylation than cDC2s but maintain higher protein synthesis.

Proteomic analysis also reveals that cDC1s are enriched for mitochondrial proteins, reflected in higher mitochondrial mass and membrane potential, as observed previously (X. Du et al., 2018; Pelgrom et al., 2019, 2022). A study from Du and colleagues shows that mitochondrial metabolism in cDC1s is regulated by the Hippo kinases Mst1/2 (X. Du et al., 2018). Indeed, protein translation in cDC1s is highly dependent on mitochondrial ATP for its maintenance. Additionally, cDC1s were shown to have a higher abundance of amino acid transporters than cDC2s, which would facilitate the amino acid uptake required for translation. Interestingly, amino acid transporter expression is regulated downstream of PERK-ATF4 signalling (Torrence et

al., 2021). Thus, it is conceivable that constitutive PERK-ATF4 signalling promotes amino acid transporter expression in cDC1s. Finally, Chapter 4 showed that cDC1s have higher mTORC1 activity in the steady-state mediated by amino acid uptake. Overall, this work reveals a metabolic circuit within cDC1s characterised by protein translation regulated by mTORC1 signalling, mitochondrial metabolism, and amino acid transport encoded within the proteome. While the functional implications of this circuit are not yet clear, the identification that constitutive ER stress regulates cDC1 function provides the basis for future research on the interplay between these processes **(Fig. 6.1)**

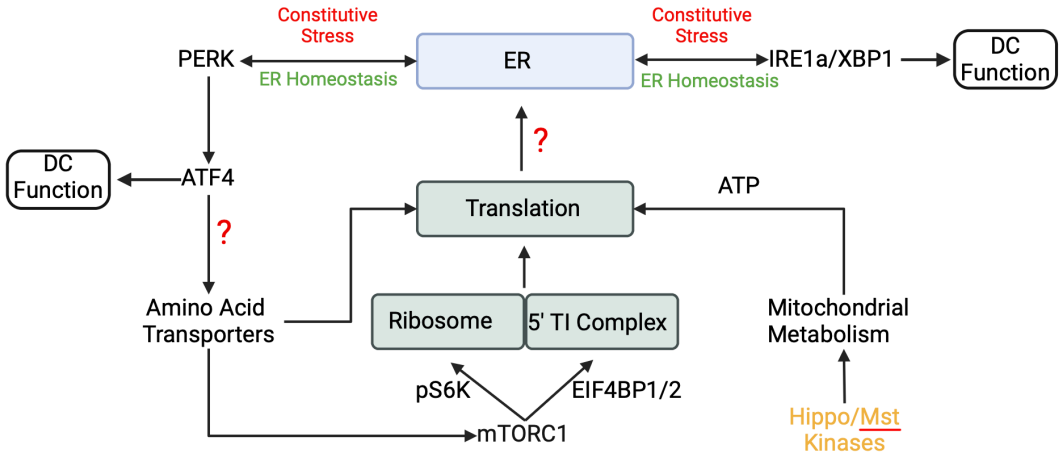

Figure 6.1 – Schematic illustration of the hypothetical interplay of the cDC1 metabolic circuit and ER stress signalling
cDC1s maintain elevated protein translation, facilitated by the enrichment of ribosomal proteins and the 5' translation initiation complex. This is supported energetically by enhanced mitochondrial metabolism, which may be driven by the Hippo/Mst kinase axis (X. Du et al., 2018). cDC1s have active mTORC1 signalling, which is maintained by amino acid transport and is required for protein translation by regulating the activity of the translational regulators pS6K and EIF4BP1/2. cDC1s maintain constitutive ER stress signalling, which supports functional outputs (Mendes et al., 2021; Osorio et al., 2014; Tavernier et al., 2017). It is unknown whether protein translation influences ER stress in cDC1s and if ER stress regulators such as ATF4 promote the expression of elevated amino acid transporters in cDC1s.

Chapter 4 investigates the amino acid transporter repertoire expressed in cDC1s and cDC2s, revealing that SLC7A5-mediated amino acid uptake regulates mTORC1 activity in both subsets. In accordance with the observed biosynthetic phenotype described in Chapter 3, cDC1s have higher mTORC1 activity relative to cDC2s, which is supported by amino acid uptake via SLC7A5. SLC7A5 has been reported to control anabolic signalling and metabolic reprogramming in highly proliferative cells, including T cells, NK cells and tumour cells (Chapman & Chi, 2022; Mossmann et al., 2018; O'Brien & Finlay, 2019). In contrast to the aforementioned cells, DCs, after leaving the bone marrow, are not proliferative and do not increase Slc7a5 amino acid

transport upon activation, indicating a novel role for Slc7a5 amino acid uptake in DCs. Data presented in Chapter 4 reveals that Slc7a5-mediated amino acid transport directs antigen cross-presentation by modulating the rate of endolysosomal antigen degradation in cDC1s. Numerous studies have reported that the regulation of endolysosomal acidification is an important factor in the efficiency of antigen cross-presentation (Delamarre et al., 2005; Jancic et al., 2007; Mantegazza et al., 2008; Savina et al., 2006, 2009). In particular, cDC1s have been shown to maintain a more alkaline endolysosomal compartment than cDC2s, which has been suggested to delay the degradation of captured antigens and preserve epitopes for MHCI cross-presentation (Savina et al., 2009). mTORC1 senses cytoplasmic amino acid sufficiency at the lysosomal membrane and has been described to modulate lysosome function by controlling the assembly of the V-ATPase complex, which controls lysosomal acidification and the activity of the transcription factor TFEB which is a crucial regulator of lysosomal biogenesis and function (Ratto et al., 2022; Samie & Cresswell, 2015). When extracellular amino acid levels are low, mTORC1 is inhibited, inducing cellular mechanisms to restore nutrient homeostasis, including lysosomal acidification, which contributes to autophagy. This study proposes that amino acid uptake through Slc7a5, which exerts substantial control over mTORC1 signalling, modulates lysosomal activity regulating cross-presentation in cDC1s.

Fine control of endolysosomal degradative activity is required to modulate cross-presentation in DCs (Embgenbroich & Burgdorf, 2018). There is a delicate balance between inadequate digestion, which prevents the generation of presentable epitopes, and excessive degradation, which leads to rapid peptide destruction. DC maturation, which transitions DCs from a “pro-sensing” to a “pro-presenting” phenotype, has been shown to induce lysosomal acidification, which is required for effective MHCII antigen presentation. Interestingly, TFEB has been reported to control the balance between MHCI cross-presentation and MHCII presentation in DCs (Samie & Cresswell, 2015). This study shows that upon GMDC maturation with LPS, TFEB is activated and translocates to the nucleus, resulting in decreased lysosomal pH and increased expression of lysosomal proteases. This

phenotype supports MHCII antigen presentation while limiting antigen cross-presentation of OVA. In contrast, genetic silencing of TFEB limits lysosomal acidification and enhances antigen cross-presentation *in vitro* and *in vivo*. Notably, it was reported that cDC1s, which specialise in cross-presentation, have lower expression of TFEB than cDC2s in the steady state, suggesting that TFEB expression contributes to the enhanced cross-presentation capacity in cDC1s (Samie & Cresswell, 2015). TFEB activity is regulated by mTORC1 in the context of nutrient stress (Martina et al., 2012). It has been shown that when mTORC1 is inhibited, either by nutrient deprivation or pharmacologically, TFEB accumulates in the nucleus, inducing lysosomal activity to restore nutrient homeostasis. In addition, mTORC1 has been shown to regulate lysosomal acidification by regulating the activity of the V-ATPase complex (Ratto et al., 2022). In this study, pharmacological inhibition of mTORC1 activates V-ATPase, increasing lysosomal acidification and catabolism of lysosomal protein. Further research is required to determine the role of mTORC1 signalling in mediating TFEB and V-ATPase activity in cDC subsets and how this influences cross-presentation. Additional work is ongoing to investigate whether Slc7a5 mediated control of mTORC1 signalling and lysosomal activity is mediated through the mTORC1-TFEB axis and whether this controls the balance of antigen cross-presentation in cDC1s and cDC2s.

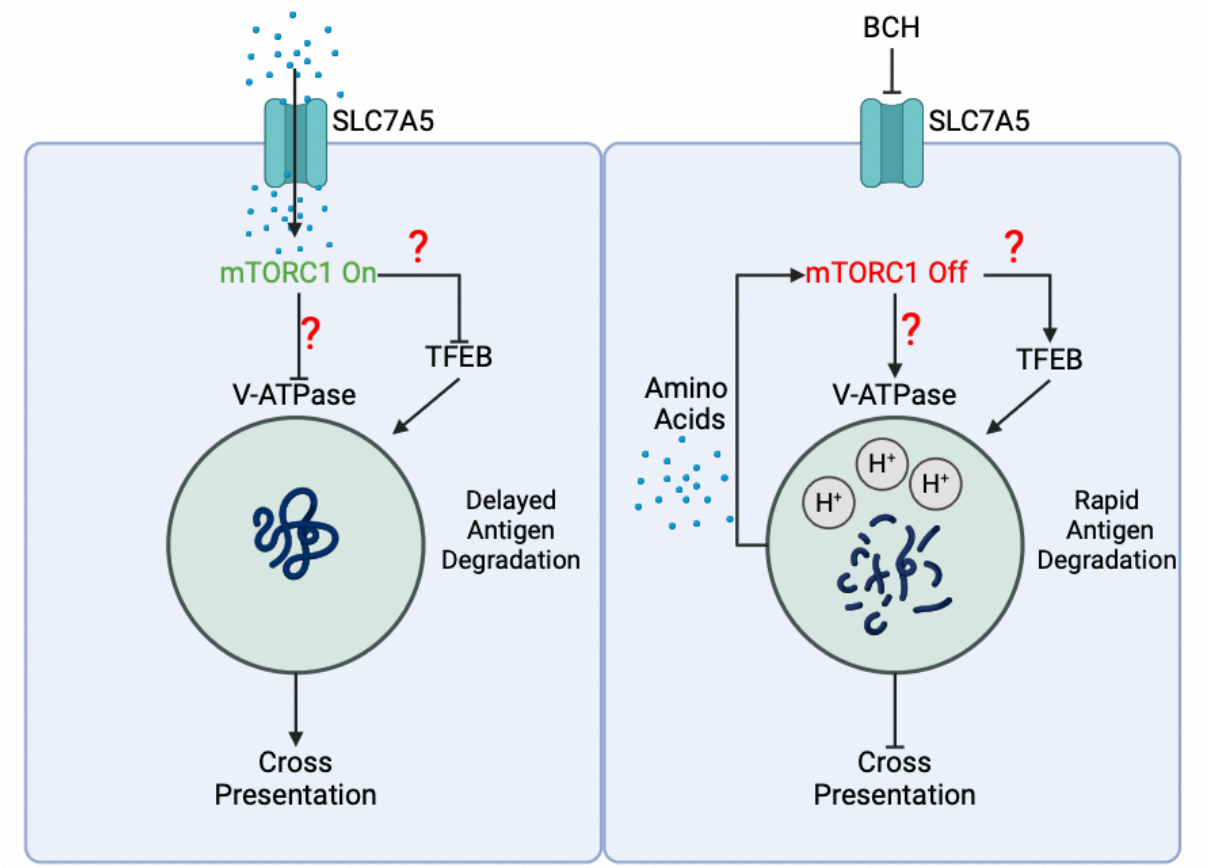

Figure 6.2 – Illustration of a hypothetical mechanism linking SLC7A5 amino acid transport to antigen cross-presentation
SLC7A5 amino acid transport is required for mTORC1 signalling in cDC1s, which limits lysosomal catabolism, delaying the rate of antigen degradation and supporting cross-presentation (left panel). Pharmacological inhibition of SLC7A5 transport with BCH inhibits mTORC1 signalling, promoting lysosomal catabolism and rapidly degrading proteins to generate amino acids to restore amino acid homeostasis and reactivate mTORC1. Enhanced lysosomal catabolism abrogates sustained antigen cross-presentation in cDC1s (right panel). The mechanism linking mTORC1 and lysosomal catabolism in cDC1s has not been investigated; however, evidence suggests that it may be through direct modulation of the V-ATPase activity or by promoting TFEB activation.

In the context of infection, previous work from the Finlay lab showed that activated T cells outcompete GMDCs for glucose, inhibiting mTORC1 signalling in DCs and enhancing the induction of CD8 T cell responses (Lawless et al., 2017). Quantitative proteomic analysis of CD8 T cells reveals that amino acid transporters dramatically increase upon activation, including Slc1a5 and Slc7a5 (Howden et al., 2019). Thus, in addition to glucose competition, it is likely that DCs become locally deprived of amino acids under inflammatory conditions. It is interesting to speculate whether this local and temporal amino acid deprivation influences cDC mTORC1 signalling and the kinetics of peptide-MHCI complexes for cross-presentation. A potential hypothesis requiring further investigation is that as cDC1s migrate from the site of antigen acquisition, mTORC1 signalling is sustained by amino acids present in the circulation, limiting the rate of antigen degradation. Within the lymph node, antigen-specific T-cell activation promotes local amino acid deprivation, increasing the rate of cDC1 antigen degradation and temporally enhancing the generation of peptide-MHCI complexes for presentation. In the context of cancer, imaging of tumours using positron emission tomography (PET) revealed that cancer cells have the greatest capacity to acquire glutamine compared to T cells and myeloid cells in the TME, indicating that glutamine uptake by tumours may limit the availability of glutamine to immune cells (Reinfeld et al., 2021). A recent study revealed that glutamine competition within the TME influences cDC1 anti-tumour responses via the FLCN-TFEB axis via glutamine competition mediated through the glutamine transporter Slc38a2 (Guo et al., 2023). Studies have shown that Slc7a5 is upregulated in many types of cancer and is a putative metabolic checkpoint currently under investigation (CRUK Rosetta Grand Challenge Consortium et al., 2021; Nachef et al., 2021). For example, Nanvuranlat (JPH-203), a selective Slc7a5 inhibitor, has been used in a phase 1 clinical trial against solid tumours (UMIN000016546) and a phase 2 trial against refractory biliary tract cancer (UMIN000034080). Further research is required to understand the role of cDC Slc7a5 expression in the TME and the implications of its pharmacological inhibition in cancer treatment.

Chapter 5 investigated the nutrient transporter expression of pDCs using quantitative proteomics. This work revealed that the iron transporter Tfrc is highly enriched in pDCs, which is conserved in mice and men. As of 2023, it is estimated that approximately one-fourth (2 billion people) of the world's population is anaemic, of which the primary cause is iron deficiency (Gardner et al., 2023). The importance of iron availability on immune cell function was demonstrated by a study that investigated children bearing a mutation in the transferrin receptor, which impaired cellular iron uptake, leading to severe combined immunodeficiency, including hypogammaglobulinemia and defective lymphocyte proliferation (Jabara et al., 2016). As iron is required as a co-factor for proteins involved in many core cellular processes, including cellular metabolism, the implications of iron deficiency on immune cell metabolism and function is a growing area of interest. Data presented in Chapter 5 shows that despite enrichment of Tfrc expression and transferrin uptake, *in silico* analysis of iron-dependent proteins does not indicate that pDCs have enhanced utilisation of iron within the proteome. This is reflected in the finding that iron deprivation does not influence proinflammatory cytokine production in response to TLR ligation. This suggests an iron-independent role of Tfrc in pDCs. As steady-state pDCs are specialised in the immunosurveillance of viruses, particularly through endosomal detection of viral PAMPs by TLR7 and TLR9, the acquisition of viruses through Tfrc may represent a currently unexplored avenue of antigen detection in pDCs.

6.1 – Limitations of this study

A key aim of this study was to apply quantitative proteomics to natural DC subsets directly *ex vivo* to limit metabolic artefacts associated with cell culture. Due to the rarity of DCs *in vivo*, this study required the enrichment of DCs using B16-Flt3l melanoma cells. For consistency with the proteomic data, subsequent experiments were performed using DCs isolated from mice inoculated with B16-Flt3l tumours. While the functional analysis was performed, indicating the tumour treatment does not induce DC maturation, further validation experiments are required to determine the impact on the metabolic phenotype of DCs. An intrinsic limitation associated with quantitative proteomics in this study is the requirement for a homogenous cell

population. In particular, the cDC2 population has been described to be heterogeneous. Thus, this study does not provide insight into the proteome of cDC2 subsets but rather an average of all cDC2s. Therefore, the relative contribution of each subset is unknown.

Chapter 4 investigates the control of cDC mTORC1 activity by Slc7a5 and its implications on cDC function. While this study characterises the impact of Slc7a5-mediated lysosomal activity and antigen degradation on cDC1s without a maturation stimulus, further investigation is required to determine its role during maturation. This study relies on the pharmacological inhibition of Slc7a5 transport using BCH. Although BCH is a specific inhibitor of LAT-mediated amino acid transport, genetic knockdown of Slc7a5 is required to determine the specific role of Slc7a5 amino acid transport *in vitro* and *in vivo*. Similarly, due to the lack of reliable Slc1a5 pharmacological inhibitors, glutamine deprivation was used to proxy Slc1a5 activity. However, glutamine is not the sole substrate transported by this transporter, and thus, the specific control of mTORC1 signalling by Slc1a5 could not be determined.

6.2 Final Conclusions

In conclusion, the data presented in this thesis provide new insights into the molecular basis of metabolic heterogeneity in cDC1s, cDC2s, and pDCs. This work highlights the strength of using quantitative proteomics in the investigation of immunometabolism, identifying currently undescribed regulators of cDC1 and pDC biology. Harnessing the findings in this study will inform future investigations of DC immunometabolism and function.

Chapter 7 - Bibliography

Accapezzato, D., Visco, V., Francavilla, V., Molette, C., Donato, T., Paroli, M., Mondelli, M. U., Doria, M., Torrisi, M. R., & Barnaba, V. (2005). Chloroquine enhances human CD8+ T cell responses against soluble antigens in vivo. *The Journal of Experimental Medicine*, *202*(6), 817–828. https://doi.org/10.1084/jem.20051106

Ahl, P. J., Hopkins, R. A., Xiang, W. W., Au, B., Kaliaperumal, N., Fairhurst, A.-M., & Connolly, J. E. (2020). Met-Flow, a strategy for single-cell metabolic analysis highlights dynamic changes in immune subpopulations. *Communications Biology*, *3*(1), 305. https://doi.org/10.1038/s42003-020-1027-9

Alcántara-Hernández, M., Leylek, R., Wagar, L. E., Engleman, E. G., Keler, T., Marinkovich, M. P., Davis, M. M., Nolan, G. P., & Idoyaga, J. (2017). High-Dimensional Phenotypic Mapping of Human Dendritic Cells Reveals Interindividual Variation and Tissue Specialization. *Immunity*, *47*(6), 1037-1050.e6. https://doi.org/10.1016/j.immuni.2017.11.001

Amiel, E., Everts, B., Freitas, T. C., King, I. L., Curtis, J. D., Pearce, E. L., & Pearce, E. J. (2012). Inhibition of Mechanistic Target of Rapamycin Promotes Dendritic Cell Activation and Enhances Therapeutic Autologous Vaccination in Mice. *The Journal of Immunology*, *189*(5), 2151–2158. https://doi.org/10.4049/jimmunol.1103741

Amiel, E., Everts, B., Fritz, D., Beauchamp, S., Ge, B., Pearce, E. L., & Pearce, E. J. (2014). Mechanistic Target of Rapamycin Inhibition Extends Cellular Lifespan in Dendritic Cells by Preserving Mitochondrial Function. *The Journal of Immunology*, *193*(6), 2821–2830. https://doi.org/10.4049/jimmunol.1302498

Amunugama, R., Jones, R., Ford, M., & Allen, D. (2013). Bottom-Up Mass Spectrometry-Based Proteomics as an Investigative Analytical Tool for Discovery and Quantification of Proteins in Biological Samples. *Advances in Wound Care*, *2*(9), 549–557. https://doi.org/10.1089/wound.2012.0384

Anderson, D. A., Ou, F., Kim, S., Murphy, T. L., & Murphy, K. M. (2022). Transition from cMyc to L-Myc during dendritic cell development coordinated by rising levels of IRF8. *The Journal of Experimental Medicine*, *219*(2), e20211483. https://doi.org/10.1084/jem.20211483

Andreini, C., Putignano, V., Rosato, A., & Banci, L. (2018). The human iron-proteome†. *Metallomics*, *10*(9), 1223–1231. https://doi.org/10.1039/c8mt00146d

Argüello, R. J., Combes, A. J., Char, R., Gigan, J.-P., Baaziz, A. I., Bousiquot, E., Camosseto, V., Samad, B., Tsui, J., Yan, P., Boissonneau, S., Figarella-Branger, D., Gatti, E., Tabouret, E., Krummel, M. F., & Pierre, P. (2020). SCENITH: A Flow Cytometry-

Based Method to Functionally Profile Energy Metabolism with Single-Cell Resolution. *Cell Metabolism*, *32*(6), 1063-1075.e7. https://doi.org/10.1016/j.cmet.2020.11.007

Arnold, I. C., Zhang, X., Artola-Boran, M., Fallegger, A., Sander, P., Johansen, P., & Müller, A. (2019). BATF3-dependent dendritic cells drive both effector and regulatory T-cell responses in bacterially infected tissues. *PLOS Pathogens*, *15*(6), e1007866. https://doi.org/10.1371/journal.ppat.1007866

Artyomov, M. N., & Van Den Bossche, J. (2020). Immunometabolism in the Single-Cell Era. *Cell Metabolism*, *32*(5), 710–725. https://doi.org/10.1016/j.cmet.2020.09.013

Arya, S., Wiatrek-Moumoulidis, D., Synowsky, S. A., Shirran, S. L., Botting, C. H., Powis, S. J., & Stewart, A. J. (2019). Quantitative proteomic changes in LPS-activated monocyte-derived dendritic cells: A SWATH-MS study. *Scientific Reports*, *9*(1), 4343. https://doi.org/10.1038/s41598-019-40773-6

Asselin-Paturel, C., Brizard, G., Chemin, K., Boonstra, A., O'Garra, A., Vicari, A., & Trinchieri, G. (2005). Type I interferon dependence of plasmacytoid dendritic cell activation and migration. *The Journal of Experimental Medicine*, *201*(7), 1157–1167. https://doi.org/10.1084/jem.20041930

Bagadia, P., Huang, X., Liu, T.-T., Durai, V., Grajales-Reyes, G. E., Nitschké, M., Modrusan, Z., Granja, J. M., Satpathy, A. T., Briseño, C. G., Gargaro, M., Iwata, A., Kim, S., Chang, H. Y., Shaw, A. S., Murphy, T. L., & Murphy, K. M. (2019). An Nfil3-Zeb2-Id2 pathway imposes Irf8 enhancer switching during cDC1 development. *Nature Immunology*, *20*(9), 1174–1185. https://doi.org/10.1038/s41590-019-0449-3

Bajwa, G., DeBerardinis, R. J., Shao, B., Hall, B., Farrar, J. D., & Gill, M. A. (2016). Cutting Edge: Critical Role of Glycolysis in Human Plasmacytoid Dendritic Cell Antiviral Responses. *The Journal of Immunology*, *196*(5), 2004–2009. https://doi.org/10.4049/jimmunol.1501557

Basit, F., Mathan, T., Sancho, D., & De Vries, I. J. M. (2018). Human Dendritic Cell Subsets Undergo Distinct Metabolic Reprogramming for Immune Response. *Frontiers in Immunology*, *9*, 2489. https://doi.org/10.3389/fimmu.2018.02489

Bassing, C. H., Swat, W., & Alt, F. W. (2002). The mechanism and regulation of chromosomal V(D)J recombination. *Cell*, *109 Suppl*, S45-55. https://doi.org/10.1016/s0092-8674(02)00675-x

Belizaire, R., & Unanue, E. R. (2009). Targeting proteins to distinct subcellular compartments reveals unique requirements for MHC class I and II presentation. *Proceedings of the National Academy of Sciences of the United States of America*, *106*(41), 17463–17468. https://doi.org/10.1073/pnas.0908583106

Bix, M., Liao, N.-S., Zijlstra, M., Loring, J., Jaenisch, R., & Raulet, D. (1991). Rejection of class I MHC-deficient haemopoietic cells by irradiated MHC-matched mice. *Nature*, *349*(6307), 329–331. https://doi.org/10.1038/349329a0

Bodineau, C., Tomé, M., Courtois, S., Costa, A. S. H., Sciacovelli, M., Rousseau, B., Richard, E., Vacher, P., Parejo-Pérez, C., Bessede, E., Varon, C., Soubeyran, P., Frezza, C., Murdoch, P. D. S., Villar, V. H., & Durán, R. V. (2021). Two parallel pathways connect glutamine metabolism and mTORC1 activity to regulate glutamoptosis. *Nature Communications*, *12*(1), 4814. https://doi.org/10.1038/s41467-021-25079-4

Bougnères, L., Helft, J., Tiwari, S., Vargas, P., Chang, B. H.-J., Chan, L., Campisi, L., Lauvau, G., Hugues, S., Kumar, P., Kamphorst, A. O., Dumenil, A.-M. L., Nussenzweig, M., MacMicking, J. D., Amigorena, S., & Guermonprez, P. (2009). A Role for Lipid Bodies in the Cross-presentation of Phagocytosed Antigens by MHC Class I in Dendritic Cells. *Immunity*, *31*(2), 232–244. https://doi.org/10.1016/j.immuni.2009.06.022

Bourdely, P., Anselmi, G., Vaivode, K., Ramos, R. N., Missolo-Koussou, Y., Hidalgo, S., Tosselo, J., Nuñez, N., Richer, W., Vincent-Salomon, A., Saxena, A., Wood, K., Lladser, A., Piaggio, E., Helft, J., & Guermonprez, P. (2020). Transcriptional and Functional Analysis of CD1c+ Human Dendritic Cells Identifies a CD163+ Subset Priming CD8+CD103+ T Cells. *Immunity*, *53*(2), 335-352.e8. https://doi.org/10.1016/j.immuni.2020.06.002

Brenes, A. J., Lamond, A. I., & Cantrell, D. A. (2023). The Immunological Proteome Resource. *Nature Immunology*, *24*(5), 731–731. https://doi.org/10.1038/s41590-023-01483-4

Briseño, C. G., Haldar, M., Kretzer, N. M., Wu, X., Theisen, D. J., Kc, W., Durai, V., Grajales-Reyes, G. E., Iwata, A., Bagadia, P., Murphy, T. L., & Murphy, K. M. (2016). Distinct Transcriptional Programs Control Cross-Priming in Classical and Monocyte-Derived Dendritic Cells. *Cell Reports*, *15*(11), 2462–2474. https://doi.org/10.1016/j.celrep.2016.05.025

Brown, C. C., Gudjonson, H., Pritykin, Y., Deep, D., Lavallée, V.-P., Mendoza, A., Fromme, R., Mazutis, L., Ariyan, C., Leslie, C., Pe'er, D., & Rudensky, A. Y. (2019). Transcriptional Basis of Mouse and Human Dendritic Cell Heterogeneity. *Cell*, *179*(4), 846-863.e24. https://doi.org/10.1016/j.cell.2019.09.035

Buttgereit, F., & Brand, M. D. (1995a). A hierarchy of ATP-consuming processes in mammalian cells. *The Biochemical Journal*, *312 (Pt 1)*(Pt 1), 163–167. https://doi.org/10.1042/bj3120163

Buttgereit, F., & Brand, M. D. (1995b). A hierarchy of ATP-consuming processes in mammalian cells. *The Biochemical Journal*, *312 (Pt 1)*(Pt 1), 163–167. https://doi.org/10.1042/bj3120163

Cabeza-Cabrerizo, M., Cardoso, A., Minutti, C. M., Pereira Da Costa, M., & Reis E Sousa, C. (2021). Dendritic Cells Revisited. *Annual Review of Immunology*, *39*(1), 131–166. https://doi.org/10.1146/annurev-immunol-061020-053707

Cantor, J. R., Abu-Remaileh, M., Kanarek, N., Freinkman, E., Gao, X., Louissaint, A., Lewis, C. A., & Sabatini, D. M. (2017). Physiologic Medium Rewires Cellular Metabolism and Reveals Uric Acid as an Endogenous Inhibitor of UMP Synthase. *Cell*, *169*(2), 258-272.e17. https://doi.org/10.1016/j.cell.2017.03.023

Cao, W., Manicassamy, S., Tang, H., Kasturi, S. P., Pirani, A., Murthy, N., & Pulendran, B. (2008). Toll-like receptor–mediated induction of type I interferon in plasmacytoid dendritic cells requires the rapamycin-sensitive PI(3)K-mTOR-p70S6K pathway. *Nature Immunology*, *9*(10), 1157–1164. https://doi.org/10.1038/ni.1645

Caslin, H. L., Abebayehu, D., Pinette, J. A., & Ryan, J. J. (2021). Lactate Is a Metabolic Mediator That Shapes Immune Cell Fate and Function. *Frontiers in Physiology*, *12*, 688485. https://doi.org/10.3389/fphys.2021.688485

Cebrian, I., Visentin, G., Blanchard, N., Jouve, M., Bobard, A., Moita, C., Enninga, J., Moita, L. F., Amigorena, S., & Savina, A. (2011). Sec22b Regulates Phagosomal Maturation and Antigen Crosspresentation by Dendritic Cells. *Cell*, *147*(6), 1355–1368. https://doi.org/10.1016/j.cell.2011.11.021

Cella, M., Facchetti, F., Lanzavecchia, A., & Colonna, M. (2000). Plasmacytoid dendritic cells activated by influenza virus and CD40L drive a potent TH1 polarization. *Nature Immunology*, *1*(4), 305–310. https://doi.org/10.1038/79747

Chantranupong, L., Scaria, S. M., Saxton, R. A., Gygi, M. P., Shen, K., Wyant, G. A., Wang, T., Harper, J. W., Gygi, S. P., & Sabatini, D. M. (2016). The CASTOR Proteins Are Arginine Sensors for the mTORC1 Pathway. *Cell*, *165*(1), 153–164. https://doi.org/10.1016/j.cell.2016.02.035

Chapman, N. M., & Chi, H. (2022). Metabolic adaptation of lymphocytes in immunity and disease. *Immunity*, *55*(1), 14–30. https://doi.org/10.1016/j.immuni.2021.12.012

Chen, X., Sun, Y., Zhang, T., Shu, L., Roepstorff, P., & Yang, F. (2021). Quantitative Proteomics Using Isobaric Labeling: A Practical Guide. *Genomics, Proteomics & Bioinformatics*, *19*(5), 689–706. https://doi.org/10.1016/j.gpb.2021.08.012

Cheng, M., Hu, S., Wang, Z., Pei, Y., Fan, R., Liu, X., Wang, L., Zhou, J., Zheng, S., Zhang, T., Lin, Y., Zhang, M., Tao, R., & Zhong, J. (2016).

Inhibition of neddylation regulates dendritic cell functions via Deptor accumulation driven mTOR inactivation. *Oncotarget*, *7*(24), 35643–35654. https://doi.org/10.18632/oncotarget.9543

Cheong, C., Matos, I., Choi, J.-H., Dandamudi, D. B., Shrestha, E., Longhi, M. P., Jeffrey, K. L., Anthony, R. M., Kluger, C., Nchinda, G., Koh, H., Rodriguez, A., Idoyaga, J., Pack, M., Velinzon, K., Park, C. G., & Steinman, R. M. (2010). Microbial stimulation fully differentiates monocytes to DC-SIGN/CD209(+) dendritic cells for immune T cell areas. *Cell*, *143*(3), 416–429. https://doi.org/10.1016/j.cell.2010.09.039

Chougnet, C. A., Thacker, R. I., Shehata, H. M., Hennies, C. M., Lehn, M. A., Lages, C. S., & Janssen, E. M. (2015). Loss of Phagocytic and Antigen Cross-Presenting Capacity in Aging Dendritic Cells Is Associated with Mitochondrial Dysfunction. *The Journal of Immunology*, *195*(6), 2624–2632. https://doi.org/10.4049/jimmunol.1501006

Cisse, B., Caton, M. L., Lehner, M., Maeda, T., Scheu, S., Locksley, R., Holmberg, D., Zweier, C., den Hollander, N. S., Kant, S. G., Holter, W., Rauch, A., Zhuang, Y., & Reizis, B. (2008). Transcription factor E2-2 is an essential and specific regulator of plasmacytoid dendritic cell development. *Cell*, *135*(1), 37–48. https://doi.org/10.1016/j.cell.2008.09.016

Colina, R., Costa-Mattioli, M., Dowling, R. J. O., Jaramillo, M., Tai, L.-H., Breitbach, C. J., Martineau, Y., Larsson, O., Rong, L., Svitkin, Y. V., Makrigiannis, A. P., Bell, J. C., & Sonenberg, N. (2008). Translational control of the innate immune response through IRF-7. *Nature*, *452*(7185), 323–328. https://doi.org/10.1038/nature06730

Collin, M., & Milne, P. (2016). Langerhans cell origin and regulation. *Current Opinion in Hematology*, *23*(1), 28–35. https://doi.org/10.1097/MOH.0000000000000202

Cronin, S. J. F., Woolf, C. J., Weiss, G., & Penninger, J. M. (2019). The Role of Iron Regulation in Immunometabolism and Immune-Related Disease. *Frontiers in Molecular Biosciences*, *6*, 116. https://doi.org/10.3389/fmolb.2019.00116

Croxford, A. L., Lanzinger, M., Hartmann, F. J., Schreiner, B., Mair, F., Pelczar, P., Clausen, B. E., Jung, S., Greter, M., & Becher, B. (2015). The Cytokine GM-CSF Drives the Inflammatory Signature of CCR2+ Monocytes and Licenses Autoimmunity. *Immunity*, *43*(3), 502–514. https://doi.org/10.1016/j.immuni.2015.08.010

Crozat, K., Guiton, R., Contreras, V., Feuillet, V., Dutertre, C.-A., Ventre, E., Vu Manh, T.-P., Baranek, T., Storset, A. K., Marvel, J., Boudinot, P., Hosmalin, A., Schwartz-Cornil, I., & Dalod, M. (2010). The XC chemokine receptor 1 is a conserved selective marker of mammalian cells homologous to mouse CD8alpha+ dendritic cells. *The Journal of*

Experimental Medicine, *207*(6), 1283–1292. https://doi.org/10.1084/jem.20100223

Crozat, K., Tamoutounour, S., Vu Manh, T.-P., Fossum, E., Luche, H., Ardouin, L., Guilliams, M., Azukizawa, H., Bogen, B., Malissen, B., Henri, S., & Dalod, M. (2011). Cutting edge: Expression of XCR1 defines mouse lymphoid-tissue resident and migratory dendritic cells of the CD8α+ type. *Journal of Immunology (Baltimore, Md.: 1950)*, *187*(9), 4411–4415. https://doi.org/10.4049/jimmunol.1101717

CRUK Rosetta Grand Challenge Consortium, Najumudeen, A. K., Ceteci, F., Fey, S. K., Hamm, G., Steven, R. T., Hall, H., Nikula, C. J., Dexter, A., Murta, T., Race, A. M., Sumpton, D., Vlahov, N., Gay, D. M., Knight, J. R. P., Jackstadt, R., Leach, J. D. G., Ridgway, R. A., Johnson, E. R., … Sansom, O. J. (2021). The amino acid transporter SLC7A5 is required for efficient growth of KRAS-mutant colorectal cancer. *Nature Genetics*, *53*(1), 16–26. https://doi.org/10.1038/s41588-020-00753-3

Cruzat, V., Macedo Rogero, M., Noel Keane, K., Curi, R., & Newsholme, P. (2018). Glutamine: Metabolism and Immune Function, Supplementation and Clinical Translation. *Nutrients*, *10*(11), 1564. https://doi.org/10.3390/nu10111564

Cueto, F. J., & Sancho, D. (2021). The Flt3L/Flt3 Axis in Dendritic Cell Biology and Cancer Immunotherapy. *Cancers*, *13*(7), 1525. https://doi.org/10.3390/cancers13071525

Davies, V., Wandy, J., Weidt, S., Van Der Hooft, J. J. J., Miller, A., Daly, R., & Rogers, S. (2021). Rapid Development of Improved Data-Dependent Acquisition Strategies. *Analytical Chemistry*, *93*(14), 5676–5683. https://doi.org/10.1021/acs.analchem.0c03895

Delamarre, L., Pack, M., Chang, H., Mellman, I., & Trombetta, E. S. (2005). Differential Lysosomal Proteolysis in Antigen-Presenting Cells Determines Antigen Fate. *Science*, *307*(5715), 1630–1634. https://doi.org/10.1126/science.1108003

Den Brok, M. H., Büll, C., Wassink, M., De Graaf, A. M., Wagenaars, J. A., Minderman, M., Thakur, M., Amigorena, S., Rijke, E. O., Schrier, C. C., & Adema, G. J. (2016). Saponin-based adjuvants induce cross-presentation in dendritic cells by intracellular lipid body formation. *Nature Communications*, *7*(1), 13324. https://doi.org/10.1038/ncomms13324

Den Haan, J. M. M., Lehar, S. M., & Bevan, M. J. (2000). Cd8+ but Not Cd8− Dendritic Cells Cross-Prime Cytotoxic T Cells in Vivo. *The Journal of Experimental Medicine*, *192*(12), 1685–1696. https://doi.org/10.1084/jem.192.12.1685

Dowell, J. A., Wright, L. J., Armstrong, E. A., & Denu, J. M. (2021). Benchmarking Quantitative Performance in Label-Free Proteomics.

ACS Omega, *6*(4), 2494–2504. https://doi.org/10.1021/acsomega.0c04030

Drakesmith, H., Nemeth, E., & Ganz, T. (2015). Ironing out Ferroportin. *Cell Metabolism*, *22*(5), 777–787. https://doi.org/10.1016/j.cmet.2015.09.006

Dress, R. J., Dutertre, C.-A., Giladi, A., Schlitzer, A., Low, I., Shadan, N. B., Tay, A., Lum, J., Kairi, M. F. B. M., Hwang, Y. Y., Becht, E., Cheng, Y., Chevrier, M., Larbi, A., Newell, E. W., Amit, I., Chen, J., & Ginhoux, F. (2019). Plasmacytoid dendritic cells develop from Ly6D+ lymphoid progenitors distinct from the myeloid lineage. *Nature Immunology*, *20*(7), 852–864. https://doi.org/10.1038/s41590-019-0420-3

Du, X., Wen, J., Wang, Y., Karmaus, P. W. F., Khatamian, A., Tan, H., Li, Y., Guy, C., Nguyen, T.-L. M., Dhungana, Y., Neale, G., Peng, J., Yu, J., & Chi, H. (2018). Hippo/Mst signalling couples metabolic state and immune function of CD8α+ dendritic cells. *Nature*, *558*(7708), 141–145. https://doi.org/10.1038/s41586-018-0177-0

Du, Y., Wang, Y., Xu, Q., Zhu, J., & Lin, Y. (2021). TMT-based quantitative proteomics analysis reveals the key proteins related with the differentiation process of goat intramuscular adipocytes. *BMC Genomics*, *22*(1), 417. https://doi.org/10.1186/s12864-021-07730-y

Dudziak, D., Kamphorst, A. O., Heidkamp, G. F., Buchholz, V. R., Trumpfheller, C., Yamazaki, S., Cheong, C., Liu, K., Lee, H.-W., Park, C. G., Steinman, R. M., & Nussenzweig, M. C. (2007a). Differential antigen processing by dendritic cell subsets in vivo. *Science (New York, N.Y.)*, *315*(5808), 107–111. https://doi.org/10.1126/science.1136080

Dudziak, D., Kamphorst, A. O., Heidkamp, G. F., Buchholz, V. R., Trumpfheller, C., Yamazaki, S., Cheong, C., Liu, K., Lee, H.-W., Park, C. G., Steinman, R. M., & Nussenzweig, M. C. (2007b). Differential Antigen Processing by Dendritic Cell Subsets in Vivo. *Science*, *315*(5808), 107–111. https://doi.org/10.1126/science.1136080

Dutertre, C.-A., Becht, E., Irac, S. E., Khalilnezhad, A., Narang, V., Khalilnezhad, S., Ng, P. Y., van den Hoogen, L. L., Leong, J. Y., Lee, B., Chevrier, M., Zhang, X. M., Yong, P. J. A., Koh, G., Lum, J., Howland, S. W., Mok, E., Chen, J., Larbi, A., … Ginhoux, F. (2019). Single-Cell Analysis of Human Mononuclear Phagocytes Reveals Subset-Defining Markers and Identifies Circulating Inflammatory Dendritic Cells. *Immunity*, *51*(3), 573-589.e8. https://doi.org/10.1016/j.immuni.2019.08.008

Eisenbarth, S. C. (2019). Dendritic cell subsets in T cell programming: Location dictates function. *Nature Reviews Immunology*, *19*(2), 89–103. https://doi.org/10.1038/s41577-018-0088-1

Embgenbroich, M., & Burgdorf, S. (2018). Current Concepts of Antigen Cross-Presentation. *Frontiers in Immunology*, *9*, 1643. https://doi.org/10.3389/fimmu.2018.01643

Everts, B., Amiel, E., Huang, S. C.-C., Smith, A. M., Chang, C.-H., Lam, W. Y., Redmann, V., Freitas, T. C., Blagih, J., Van Der Windt, G. J. W., Artyomov, M. N., Jones, R. G., Pearce, E. L., & Pearce, E. J. (2014). TLR-driven early glycolytic reprogramming via the kinases TBK1-IKKε supports the anabolic demands of dendritic cell activation. *Nature Immunology*, *15*(4), 323–332. https://doi.org/10.1038/ni.2833

Everts, B., Amiel, E., van der Windt, G. J. W., Freitas, T. C., Chott, R., Yarasheski, K. E., Pearce, E. L., & Pearce, E. J. (2012). Commitment to glycolysis sustains survival of NO-producing inflammatory dendritic cells. *Blood*, *120*(7), 1422–1431. https://doi.org/10.1182/blood-2012-03-419747

Fekete, T., Sütö, M. I., Bencze, D., Mázló, A., Szabo, A., Biro, T., Bacsi, A., & Pazmandi, K. (2018). Human Plasmacytoid and Monocyte-Derived Dendritic Cells Display Distinct Metabolic Profile Upon RIG-I Activation. *Frontiers in Immunology*, *9*, 3070. https://doi.org/10.3389/fimmu.2018.03070

Feng, L., Cai, Y., Zhu, M., Xing, L., & Wang, X. (2020). The yin and yang functions of extracellular ATP and adenosine in tumor immunity. *Cancer Cell International*, *20*(1), 110. https://doi.org/10.1186/s12935-020-01195-x

Flajnik, M. F., & Kasahara, M. (2010). Origin and evolution of the adaptive immune system: Genetic events and selective pressures. *Nature Reviews Genetics*, *11*(1), 47–59. https://doi.org/10.1038/nrg2703

Frost, J. N., Tan, T. K., Abbas, M., Wideman, S. K., Bonadonna, M., Stoffel, N. U., Wray, K., Kronsteiner, B., Smits, G., Campagna, D. R., Duarte, T. L., Lopes, J. M., Shah, A., Armitage, A. E., Arezes, J., Lim, P. J., Preston, A. E., Ahern, D., Teh, M., … Drakesmith, H. (2021). Hepcidin-Mediated Hypoferremia Disrupts Immune Responses to Vaccination and Infection. *Med (New York, N.Y.)*, *2*(2), 164-179.e12. https://doi.org/10.1016/j.medj.2020.10.004

Frost, J. N., Wideman, S. K., Preston, A. E., Teh, M. R., Ai, Z., Wang, L., Cross, A., White, N., Yazicioglu, Y., Bonadonna, M., Clarke, A. J., Armitage, A. E., Galy, B., Udalova, I. A., & Drakesmith, H. (2022). Plasma iron controls neutrophil production and function. *Science Advances*, *8*(40), eabq5384. https://doi.org/10.1126/sciadv.abq5384

Gao, Y., Nish, S. A., Jiang, R., Hou, L., Licona-Limón, P., Weinstein, J. S., Zhao, H., & Medzhitov, R. (2013). Control of T helper 2 responses by transcription factor IRF4-dependent dendritic cells. *Immunity*, *39*(4), 722–732. https://doi.org/10.1016/j.immuni.2013.08.028

Gardner, W. M., Razo, C., McHugh, T. A., Hagins, H., Vilchis-Tella, V. M., Hennessy, C., Taylor, H. J., Perumal, N., Fuller, K., Cercy, K. M.,

Zoeckler, L. Z., Chen, C. S., Lim, S. S., Aali, A., Abate, K. H., Abd-Elsalam, S., Abdurehman, A. M., Abebe, G., Abidi, H., … Kassebaum, N. J. (2023). Prevalence, years lived with disability, and trends in anaemia burden by severity and cause, 1990–2021: Findings from the Global Burden of Disease Study 2021. *The Lancet Haematology*, *10*(9), e713–e734. https://doi.org/10.1016/S2352-3026(23)00160-6

Gauthier-Coles, G., Vennitti, J., Zhang, Z., Comb, W. C., Xing, S., Javed, K., Bröer, A., & Bröer, S. (2021). Quantitative modelling of amino acid transport and homeostasis in mammalian cells. *Nature Communications*, *12*(1), 5282. https://doi.org/10.1038/s41467-021-25563-x

Geiger, R., Rieckmann, J. C., Wolf, T., Basso, C., Feng, Y., Fuhrer, T., Kogadeeva, M., Picotti, P., Meissner, F., Mann, M., Zamboni, N., Sallusto, F., & Lanzavecchia, A. (2016). L-Arginine Modulates T Cell Metabolism and Enhances Survival and Anti-tumor Activity. *Cell*, *167*(3), 829-842.e13. https://doi.org/10.1016/j.cell.2016.09.031

Ghazalpour, A., Bennett, B., Petyuk, V. A., Orozco, L., Hagopian, R., Mungrue, I. N., Farber, C. R., Sinsheimer, J., Kang, H. M., Furlotte, N., Park, C. C., Wen, P.-Z., Brewer, H., Weitz, K., Camp, D. G., Pan, C., Yordanova, R., Neuhaus, I., Tilford, C., … Lusis, A. J. (2011). Comparative analysis of proteome and transcriptome variation in mouse. *PLoS Genetics*, *7*(6), e1001393. https://doi.org/10.1371/journal.pgen.1001393

Gillet, L. C., Navarro, P., Tate, S., Röst, H., Selevsek, N., Reiter, L., Bonner, R., & Aebersold, R. (2012). Targeted data extraction of the MS/MS spectra generated by data-independent acquisition: A new concept for consistent and accurate proteome analysis. *Molecular & Cellular Proteomics: MCP*, *11*(6), O111.016717. https://doi.org/10.1074/mcp.O111.016717

Ginhoux, F., Liu, K., Helft, J., Bogunovic, M., Greter, M., Hashimoto, D., Price, J., Yin, N., Bromberg, J., Lira, S. A., Stanley, E. R., Nussenzweig, M., & Merad, M. (2009). The origin and development of nonlymphoid tissue CD103+ DCs. *The Journal of Experimental Medicine*, *206*(13), 3115–3130. https://doi.org/10.1084/jem.20091756

Giuffrè, A., Sarti, P., D'Itri, E., Buse, G., Soulimane, T., & Brunori, M. (1996). On the mechanism of inhibition of cytochrome c oxidase by nitric oxide. *The Journal of Biological Chemistry*, *271*(52), 33404–33408. https://doi.org/10.1074/jbc.271.52.33404

Gouw, J. W., Krijgsveld, J., & Heck, A. J. R. (2010). Quantitative proteomics by metabolic labeling of model organisms. *Molecular & Cellular Proteomics: MCP*, *9*(1), 11–24. https://doi.org/10.1074/mcp.R900001-MCP200

Grajales-Reyes, G. E., Iwata, A., Albring, J., Wu, X., Tussiwand, R., Kc, W., Kretzer, N. M., Briseño, C. G., Durai, V., Bagadia, P., Haldar, M.,

Schönheit, J., Rosenbauer, F., Murphy, T. L., & Murphy, K. M. (2015). Batf3 maintains autoactivation of Irf8 for commitment of a CD8α(+) conventional DC clonogenic progenitor. *Nature Immunology*, *16*(7), 708–717. https://doi.org/10.1038/ni.3197

Greter, M., Lelios, I., Pelczar, P., Hoeffel, G., Price, J., Leboeuf, M., Kündig, T. M., Frei, K., Ginhoux, F., Merad, M., & Becher, B. (2012). Stroma-derived interleukin-34 controls the development and maintenance of langerhans cells and the maintenance of microglia. *Immunity*, *37*(6), 1050–1060. https://doi.org/10.1016/j.immuni.2012.11.001

Grzes, K. M., Sanin, D. E., Kabat, A. M., Stanczak, M. A., Edwards-Hicks, J., Matsushita, M., Hackl, A., Hässler, F., Knoke, K., Zahalka, S., Villa, M., Kofler, D. M., Voll, R. E., Zigrino, P., Fabri, M., Pearce, E. L., & Pearce, E. J. (2021). Plasmacytoid dendritic cell activation is dependent on coordinated expression of distinct amino acid transporters. *Immunity*, *54*(11), 2514-2530.e7. https://doi.org/10.1016/j.immuni.2021.10.009

Guiducci, C., Ott, G., Chan, J. H., Damon, E., Calacsan, C., Matray, T., Lee, K.-D., Coffman, R. L., & Barrat, F. J. (2006). Properties regulating the nature of the plasmacytoid dendritic cell response to Toll-like receptor 9 activation. *The Journal of Experimental Medicine*, *203*(8), 1999–2008. https://doi.org/10.1084/jem.20060401

Guilliams, M., Dutertre, C.-A., Scott, C. L., McGovern, N., Sichien, D., Chakarov, S., Van Gassen, S., Chen, J., Poidinger, M., De Prijck, S., Tavernier, S. J., Low, I., Irac, S. E., Mattar, C. N., Sumatoh, H. R., Low, G. H. L., Chung, T. J. K., Chan, D. K. H., Tan, K. K., … Ginhoux, F. (2016). Unsupervised High-Dimensional Analysis Aligns Dendritic Cells across Tissues and Species. *Immunity*, *45*(3), 669–684. https://doi.org/10.1016/j.immuni.2016.08.015

Guilliams, M., Ginhoux, F., Jakubzick, C., Naik, S. H., Onai, N., Schraml, B. U., Segura, E., Tussiwand, R., & Yona, S. (2014). Dendritic cells, monocytes and macrophages: A unified nomenclature based on ontogeny. *Nature Reviews. Immunology*, *14*(8), 571–578. https://doi.org/10.1038/nri3712

Gunawardana, Y., & Niranjan, M. (2013). Bridging the gap between transcriptome and proteome measurements identifies post-translationally regulated genes. *Bioinformatics*, *29*(23), 3060–3066. https://doi.org/10.1093/bioinformatics/btt537

Guo, C., & Chi, H. (2023). Immunometabolism of dendritic cells in health and disease. In *Advances in Immunology* (Vol. 160, pp. 83–116). Elsevier. https://doi.org/10.1016/bs.ai.2023.10.002

Guo, C., You, Z., Shi, H., Sun, Y., Du, X., Palacios, G., Guy, C., Yuan, S., Chapman, N. M., Lim, S. A., Sun, X., Saravia, J., Rankin, S., Dhungana, Y., & Chi, H. (2023). SLC38A2 and glutamine signalling in

cDC1s dictate anti-tumour immunity. *Nature*, *620*(7972), 200–208. https://doi.org/10.1038/s41586-023-06299-8

Hackstein, H., Taner, T., Logar, A. J., & Thomson, A. W. (2002). Rapamycin inhibits macropinocytosis and mannose receptor–mediated endocytosis by bone marrow–derived dendritic cells. *Blood*, *100*(3), 1084–1087. https://doi.org/10.1182/blood.V100.3.1084

Hackstein, H., Taner, T., Zahorchak, A. F., Morelli, A. E., Logar, A. J., Gessner, A., & Thomson, A. W. (2003). Rapamycin inhibits IL-4—Induced dendritic cell maturation in vitro and dendritic cell mobilization and function in vivo. *Blood*, *101*(11), 4457–4463. https://doi.org/10.1182/blood-2002-11-3370

Haidinger, M., Poglitsch, M., Geyeregger, R., Kasturi, S., Zeyda, M., Zlabinger, G. J., Pulendran, B., Hörl, W. H., Säemann, M. D., & Weichhart, T. (2010). A Versatile Role of Mammalian Target of Rapamycin in Human Dendritic Cell Function and Differentiation. *The Journal of Immunology*, *185*(7), 3919–3931. https://doi.org/10.4049/jimmunol.1000296

Halestrap, A. P. (2013). The SLC16 gene family – Structure, role and regulation in health and disease. *Molecular Aspects of Medicine*, *34*(2–3), 337–349. https://doi.org/10.1016/j.mam.2012.05.003

Hammer, G. E., & Ma, A. (2013). Molecular Control of Steady-State Dendritic Cell Maturation and Immune Homeostasis. *Annual Review of Immunology*, *31*(1), 743–791. https://doi.org/10.1146/annurev-immunol-020711-074929

Harpur, C. M., Kato, Y., Dewi, S. T., Stankovic, S., Johnson, D. N., Bedoui, S., Whitney, P. G., Lahoud, M. H., Caminschi, I., Heath, W. R., Brooks, A. G., & Gebhardt, T. (2019). Classical Type 1 Dendritic Cells Dominate Priming of Th1 Responses to Herpes Simplex Virus Type 1 Skin Infection. *Journal of Immunology (Baltimore, Md.: 1950)*, *202*(3), 653–663. https://doi.org/10.4049/jimmunol.1800218

Hasegawa, H., & Matsumoto, T. (2018). Mechanisms of Tolerance Induction by Dendritic Cells In Vivo. *Frontiers in Immunology*, *9*, 350. https://doi.org/10.3389/fimmu.2018.00350

Helft, J., Böttcher, J., Chakravarty, P., Zelenay, S., Huotari, J., Schraml, B. U., Goubau, D., & Reis e Sousa, C. (2015). GM-CSF Mouse Bone Marrow Cultures Comprise a Heterogeneous Population of CD11c(+)MHCII(+) Macrophages and Dendritic Cells. *Immunity*, *42*(6), 1197–1211. https://doi.org/10.1016/j.immuni.2015.05.018

Heras-Murillo, I., Adán-Barrientos, I., Galán, M., Wculek, S. K., & Sancho, D. (2024). Dendritic cells as orchestrators of anticancer immunity and immunotherapy. *Nature Reviews. Clinical Oncology*, *21*(4), 257–277. https://doi.org/10.1038/s41571-024-00859-1

Herber, D. L., Cao, W., Nefedova, Y., Novitskiy, S. V., Nagaraj, S., Tyurin, V. A., Corzo, A., Cho, H.-I., Celis, E., Lennox, B., Knight, S. C., Padhya,

T., McCaffrey, T. V., McCaffrey, J. C., Antonia, S., Fishman, M., Ferris, R. L., Kagan, V. E., & Gabrilovich, D. I. (2010). Lipid accumulation and dendritic cell dysfunction in cancer. *Nature Medicine*, *16*(8), 880–886. https://doi.org/10.1038/nm.2172

Herman, J. S., Sagar, null, & Grün, D. (2018). FateID infers cell fate bias in multipotent progenitors from single-cell RNA-seq data. *Nature Methods*, *15*(5), 379–386. https://doi.org/10.1038/nmeth.4662

Herzig, S., & Shaw, R. J. (2018). AMPK: Guardian of metabolism and mitochondrial homeostasis. *Nature Reviews Molecular Cell Biology*, *19*(2), 121–135. https://doi.org/10.1038/nrm.2017.95

Hildner, K., Edelson, B. T., Purtha, W. E., Diamond, M., Matsushita, H., Kohyama, M., Calderon, B., Schraml, B. U., Unanue, E. R., Diamond, M. S., Schreiber, R. D., Murphy, T. L., & Murphy, K. M. (2008). *Batf3* Deficiency Reveals a Critical Role for CD8α $^{+}$ Dendritic Cells in Cytotoxic T Cell Immunity. *Science*, *322*(5904), 1097–1100. https://doi.org/10.1126/science.1164206

Ho, C. S., Lam, C. W. K., Chan, M. H. M., Cheung, R. C. K., Law, L. K., Lit, L. C. W., Ng, K. F., Suen, M. W. M., & Tai, H. L. (2003). Electrospray ionisation mass spectrometry: Principles and clinical applications. *The Clinical Biochemist. Reviews*, *24*(1), 3–12.

Honda, K., Ohba, Y., Yanai, H., Negishi, H., Mizutani, T., Takaoka, A., Taya, C., & Taniguchi, T. (2005). Spatiotemporal regulation of MyD88–IRF-7 signalling for robust type-I interferon induction. *Nature*, *434*(7036), 1035–1040. https://doi.org/10.1038/nature03547

Hotamisligil, G. S., Shargill, N. S., & Spiegelman, B. M. (1993). Adipose Expression of Tumor Necrosis Factor-α: Direct Role in Obesity-Linked Insulin Resistance. *Science*, *259*(5091), 87–91. https://doi.org/10.1126/science.7678183

Howden, A. J. M., Hukelmann, J. L., Brenes, A., Spinelli, L., Sinclair, L. V., Lamond, A. I., & Cantrell, D. A. (2019). Quantitative analysis of T cell proteomes and environmental sensors during T cell differentiation. *Nature Immunology*, *20*(11), 1542–1554. https://doi.org/10.1038/s41590-019-0495-x

Hukelmann, J. L., Anderson, K. E., Sinclair, L. V., Grzes, K. M., Murillo, A. B., Hawkins, P. T., Stephens, L. R., Lamond, A. I., & Cantrell, D. A. (2016). The cytotoxic T cell proteome and its shaping by the kinase mTOR. *Nature Immunology*, *17*(1), 104–112. https://doi.org/10.1038/ni.3314

Iwakoshi, N. N., Pypaert, M., & Glimcher, L. H. (2007). The transcription factor XBP-1 is essential for the development and survival of dendritic cells. *The Journal of Experimental Medicine*, *204*(10), 2267–2275. https://doi.org/10.1084/jem.20070525

Jabara, H. H., Boyden, S. E., Chou, J., Ramesh, N., Massaad, M. J., Benson, H., Bainter, W., Fraulino, D., Rahimov, F., Sieff, C., Liu, Z.-J.,

Alshemmari, S. H., Al-Ramadi, B. K., Al-Dhekri, H., Arnaout, R., Abu-Shukair, M., Vatsayan, A., Silver, E., Ahuja, S., … Geha, R. S. (2016). A missense mutation in TFRC, encoding transferrin receptor 1, causes combined immunodeficiency. *Nature Genetics*, *48*(1), 74–78. https://doi.org/10.1038/ng.3465

Jancic, C., Savina, A., Wasmeier, C., Tolmachova, T., El-Benna, J., Dang, P. M.-C., Pascolo, S., Gougerot-Pocidalo, M.-A., Raposo, G., Seabra, M. C., & Amigorena, S. (2007). Rab27a regulates phagosomal pH and NADPH oxidase recruitment to dendritic cell phagosomes. *Nature Cell Biology*, *9*(4), 367–378. https://doi.org/10.1038/ncb1552

Janeway, C. A., & Medzhitov, R. (2002). Innate Immune Recognition. *Annual Review of Immunology*, *20*(1), 197–216. https://doi.org/10.1146/annurev.immunol.20.083001.084359

Jantsch, J., Chakravortty, D., Turza, N., Prechtel, A. T., Buchholz, B., Gerlach, R. G., Volke, M., Gläsner, J., Warnecke, C., Wiesener, M. S., Eckardt, K.-U., Steinkasserer, A., Hensel, M., & Willam, C. (2008). Hypoxia and Hypoxia-Inducible Factor-1α Modulate Lipopolysaccharide-Induced Dendritic Cell Activation and Function. *The Journal of Immunology*, *180*(7), 4697–4705. https://doi.org/10.4049/jimmunol.180.7.4697

Jao, C. Y., & Salic, A. (2008). Exploring RNA transcription and turnover *in vivo* by using click chemistry. *Proceedings of the National Academy of Sciences*, *105*(41), 15779–15784. https://doi.org/10.1073/pnas.0808480105

Jewell, J. L., Kim, Y. C., Russell, R. C., Yu, F.-X., Park, H. W., Plouffe, S. W., Tagliabracci, V. S., & Guan, K.-L. (2015). Metabolism. Differential regulation of mTORC1 by leucine and glutamine. *Science (New York, N.Y.)*, *347*(6218), 194–198. https://doi.org/10.1126/science.1259472

Johnson, D. C., Dean, D. R., Smith, A. D., & Johnson, M. K. (2005). STRUCTURE, FUNCTION, AND FORMATION OF BIOLOGICAL IRON-SULFUR CLUSTERS. *Annual Review of Biochemistry*, *74*(1), 247–281. https://doi.org/10.1146/annurev.biochem.74.082803.133518

Kakazu, E., Kanno, N., Ueno, Y., & Shimosegawa, T. (2007). Extracellular branched-chain amino acids, especially valine, regulate maturation and function of monocyte-derived dendritic cells. *Journal of Immunology (Baltimore, Md.: 1950)*, *179*(10), 7137–7146. https://doi.org/10.4049/jimmunol.179.10.7137

Kakazu, E., Kondo, Y., Kogure, T., Ninomiya, M., Kimura, O., Ueno, Y., & Shimosegawa, T. (2013). Plasma amino acids imbalance in cirrhotic patients disturbs the tricarboxylic acid cycle of dendritic cell. *Scientific Reports*, *3*, 3459. https://doi.org/10.1038/srep03459

Kakazu, E., Ueno, Y., Kondo, Y., Fukushima, K., Shiina, M., Inoue, J., Tamai, K., Ninomiya, M., & Shimosegawa, T. (2009). Branched chain amino acids enhance the maturation and function of myeloid dendritic cells

ex vivo in patients with advanced cirrhosis. *Hepatology (Baltimore, Md.)*, *50*(6), 1936–1945. https://doi.org/10.1002/hep.23248

Kaymak, I., Luda, K. M., Duimstra, L. R., Ma, E. H., Longo, J., Dahabieh, M. S., Faubert, B., Oswald, B. M., Watson, M. J., Kitchen-Goosen, S. M., DeCamp, L. M., Compton, S. E., Fu, Z., DeBerardinis, R. J., Williams, K. S., Sheldon, R. D., & Jones, R. G. (2022). Carbon source availability drives nutrient utilization in CD8+ T cells. *Cell Metabolism*, *34*(9), 1298-1311.e6. https://doi.org/10.1016/j.cmet.2022.07.012

Kc, W., Satpathy, A. T., Rapaport, A. S., Briseño, C. G., Wu, X., Albring, J. C., Russler-Germain, E. V., Kretzer, N. M., Durai, V., Persaud, S. P., Edelson, B. T., Loschko, J., Cella, M., Allen, P. M., Nussenzweig, M. C., Colonna, M., Sleckman, B. P., Murphy, T. L., & Murphy, K. M. (2014). L-Myc expression by dendritic cells is required for optimal T-cell priming. *Nature*, *507*(7491), 243–247. https://doi.org/10.1038/nature12967

Kedia-Mehta, N., & Finlay, D. K. (2019). Competition for nutrients and its role in controlling immune responses. *Nature Communications*, *10*(1), 2123. https://doi.org/10.1038/s41467-019-10015-4

Kelly, B., & Pearce, E. L. (2020). Amino Assets: How Amino Acids Support Immunity. *Cell Metabolism*, *32*(2), 154–175. https://doi.org/10.1016/j.cmet.2020.06.010

Kirkling, M. E., Cytlak, U., Lau, C. M., Lewis, K. L., Resteu, A., Khodadadi-Jamayran, A., Siebel, C. W., Salmon, H., Merad, M., Tsirigos, A., Collin, M., Bigley, V., & Reizis, B. (2018). Notch Signaling Facilitates In Vitro Generation of Cross-Presenting Classical Dendritic Cells. *Cell Reports*, *23*(12), 3658-3672.e6. https://doi.org/10.1016/j.celrep.2018.05.068

Krawczyk, C. M., Holowka, T., Sun, J., Blagih, J., Amiel, E., DeBerardinis, R. J., Cross, J. R., Jung, E., Thompson, C. B., Jones, R. G., & Pearce, E. J. (2010). Toll-like receptor–induced changes in glycolytic metabolism regulate dendritic cell activation. *Blood*, *115*(23), 4742–4749. https://doi.org/10.1182/blood-2009-10-249540

Kumar, B. V., Connors, T. J., & Farber, D. L. (2018). Human T Cell Development, Localization, and Function throughout Life. *Immunity*, *48*(2), 202–213. https://doi.org/10.1016/j.immuni.2018.01.007

Kumar, V., & McNerney, M. E. (2005). A new self: MHC-class-I-independent Natural-killer-cell self-tolerance. *Nature Reviews Immunology*, *5*(5), 363–374. https://doi.org/10.1038/nri1603

Laguerre, A., & Schultz, C. (2018). Novel lipid tools and probes for biological investigations. *Current Opinion in Cell Biology*, *53*, 97–104. https://doi.org/10.1016/j.ceb.2018.06.013

Laughlin, S. T., Baskin, J. M., Amacher, S. L., & Bertozzi, C. R. (2008). In Vivo Imaging of Membrane-Associated Glycans in Developing

Zebrafish. *Science*, *320*(5876), 664–667. https://doi.org/10.1126/science.1155106

Lawless, S. J., Kedia-Mehta, N., Walls, J. F., McGarrigle, R., Convery, O., Sinclair, L. V., Navarro, M. N., Murray, J., & Finlay, D. K. (2017). Glucose represses dendritic cell-induced T cell responses. *Nature Communications*, *8*(1), 15620. https://doi.org/10.1038/ncomms15620

Lelouard, H., Schmidt, E. K., Camosseto, V., Clavarino, G., Ceppi, M., Hsu, H.-T., & Pierre, P. (2007). Regulation of translation is required for dendritic cell function and survival during activation. *The Journal of Cell Biology*, *179*(7), 1427–1439. https://doi.org/10.1083/jcb.200707166

Lewis, K. L., Caton, M. L., Bogunovic, M., Greter, M., Grajkowska, L. T., Ng, D., Klinakis, A., Charo, I. F., Jung, S., Gommerman, J. L., Ivanov, I. I., Liu, K., Merad, M., & Reizis, B. (2011). Notch2 receptor signaling controls functional differentiation of dendritic cells in the spleen and intestine. *Immunity*, *35*(5), 780–791. https://doi.org/10.1016/j.immuni.2011.08.013

Leylek, R., Alcántara-Hernández, M., Lanzar, Z., Lüdtke, A., Perez, O. A., Reizis, B., & Idoyaga, J. (2019). Integrated Cross-Species Analysis Identifies a Conserved Transitional Dendritic Cell Population. *Cell Reports*, *29*(11), 3736-3750.e8. https://doi.org/10.1016/j.celrep.2019.11.042

Li, D., & Wu, M. (2021). Pattern recognition receptors in health and diseases. *Signal Transduction and Targeted Therapy*, *6*(1), 291. https://doi.org/10.1038/s41392-021-00687-0

Liao, Z., Wang, C., Tang, X., Yang, M., Duan, Z., Liu, L., Lu, S., Ma, L., Cheng, R., Wang, G., Liu, H., Yang, S., Xu, J., Tadese, D. A., Mwangi, J., Kamau, P. M., Zhang, Z., Yang, L., Liao, G., … Lai, R. (2024). Human transferrin receptor can mediate SARS-CoV-2 infection. *Proceedings of the National Academy of Sciences*, *121*(10), e2317026121. https://doi.org/10.1073/pnas.2317026121

Liberman, R., Bond, S., Shainheit, M. G., Stadecker, M. J., & Forgac, M. (2014). Regulated assembly of vacuolar ATPase is increased during cluster disruption-induced maturation of dendritic cells through a phosphatidylinositol 3-kinase/mTOR-dependent pathway. *The Journal of Biological Chemistry*, *289*(3), 1355–1363. https://doi.org/10.1074/jbc.M113.524561

Linke, M., Fritsch, S. D., Sukhbaatar, N., Hengstschläger, M., & Weichhart, T. (2017). mTORC1 and mTORC2 as regulators of cell metabolism in immunity. *FEBS Letters*, *591*(19), 3089–3103. https://doi.org/10.1002/1873-3468.12711

Lisci, M., Barton, P. R., Randzavola, L. O., Ma, C. Y., Marchingo, J. M., Cantrell, D. A., Paupe, V., Prudent, J., Stinchcombe, J. C., & Griffiths, G. M. (2021). Mitochondrial translation is required for sustained killing

by cytotoxic T cells. *Science*, *374*(6565), eabe9977. https://doi.org/10.1126/science.abe9977

Littwitz-Salomon, E., Moreira, D., Frost, J. N., Choi, C., Liou, K. T., Ahern, D. K., O'Shaughnessy, S., Wagner, B., Biron, C. A., Drakesmith, H., Dittmer, U., & Finlay, D. K. (2021). Metabolic requirements of NK cells during the acute response against retroviral infection. *Nature Communications*, *12*(1), 5376. https://doi.org/10.1038/s41467-021-25715-z

Liu, T.-T., Kim, S., Desai, P., Kim, D.-H., Huang, X., Ferris, S. T., Wu, R., Ou, F., Egawa, T., Van Dyken, S. J., Diamond, M. S., Johnson, P. F., Kubo, M., Murphy, T. L., & Murphy, K. M. (2022). Ablation of cDC2 development by triple mutations within the Zeb2 enhancer. *Nature*, *607*(7917), 142–148. https://doi.org/10.1038/s41586-022-04866-z

Liu, Z., Wang, H., Li, Z., Dress, R. J., Zhu, Y., Zhang, S., De Feo, D., Kong, W. T., Cai, P., Shin, A., Piot, C., Yu, J., Gu, Y., Zhang, M., Gao, C., Chen, L., Wang, H., Vétillard, M., Guermonprez, P., … Ginhoux, F. (2023). Dendritic cell type 3 arises from Ly6C+ monocyte-dendritic cell progenitors. *Immunity*, *56*(8), 1761-1777.e6. https://doi.org/10.1016/j.immuni.2023.07.001

Loftus, R. M., Assmann, N., Kedia-Mehta, N., O'Brien, K. L., Garcia, A., Gillespie, C., Hukelmann, J. L., Oefner, P. J., Lamond, A. I., Gardiner, C. M., Dettmer, K., Cantrell, D. A., Sinclair, L. V., & Finlay, D. K. (2018). Amino acid-dependent cMyc expression is essential for NK cell metabolic and functional responses in mice. *Nature Communications*, *9*(1), 2341. https://doi.org/10.1038/s41467-018-04719-2

Luber, C. A., Cox, J., Lauterbach, H., Fancke, B., Selbach, M., Tschopp, J., Akira, S., Wiegand, M., Hochrein, H., O'Keeffe, M., & Mann, M. (2010). Quantitative Proteomics Reveals Subset-Specific Viral Recognition in Dendritic Cells. *Immunity*, *32*(2), 279–289. https://doi.org/10.1016/j.immuni.2010.01.013

Lutz, M. B., Kukutsch, N., Ogilvie, A. L. J., Rößner, S., Koch, F., Romani, N., & Schuler, G. (1999). An advanced culture method for generating large quantities of highly pure dendritic cells from mouse bone marrow. *Journal of Immunological Methods*, *223*(1), 77–92. https://doi.org/10.1016/S0022-1759(98)00204-X

Mach, N., Gillessen, S., Wilson, S. B., Sheehan, C., Mihm, M., & Dranoff, G. (2000). Differences in dendritic cells stimulated in vivo by tumors engineered to secrete granulocyte-macrophage colony-stimulating factor or Flt3-ligand. *Cancer Research*, *60*(12), 3239–3246.

MacNabb, B. W., Kline, D. E., Albright, A. R., Chen, X., Leventhal, D. S., Savage, P. A., & Kline, J. (2019). Negligible Role for Deletion Mediated by cDC1 in CD8+ T Cell Tolerance. *Journal of Immunology*

(Baltimore, Md.: 1950), *202*(9), 2628–2635. https://doi.org/10.4049/jimmunol.1801621

Maldonado, S. D., Dai, J., Dutta, O., Hurley, H. J., Singh, S., Gittens-Williams, L., Kalyoussef, E., Edelblum, K. L., Rivera, A., & Fitzgerald-Bocarsly, P. (2022). Human Plasmacytoid Dendritic Cells Express C-Type Lectin Receptors and Attach and Respond to Aspergillus fumigatus. *Journal of Immunology (Baltimore, Md.: 1950)*, *209*(4), 675–683. https://doi.org/10.4049/jimmunol.2000632

Mantegazza, A. R., Savina, A., Vermeulen, M., Pérez, L., Geffner, J., Hermine, O., Rosenzweig, S. D., Faure, F., & Amigorena, S. (2008). NADPH oxidase controls phagosomal pH and antigen cross-presentation in human dendritic cells. *Blood*, *112*(12), 4712–4722. https://doi.org/10.1182/blood-2008-01-134791

Marchingo, J. M., & Cantrell, D. A. (2022). Protein synthesis, degradation, and energy metabolism in T cell immunity. *Cellular & Molecular Immunology*, *19*(3), 303–315. https://doi.org/10.1038/s41423-021-00792-8

Marchingo, J. M., Sinclair, L. V., Howden, A. J., & Cantrell, D. A. (2020). Quantitative analysis of how Myc controls T cell proteomes and metabolic pathways during T cell activation. *eLife*, *9*, e53725. https://doi.org/10.7554/eLife.53725

Martina, J. A., Chen, Y., Gucek, M., & Puertollano, R. (2012). MTORC1 functions as a transcriptional regulator of autophagy by preventing nuclear transport of TFEB. *Autophagy*, *8*(6), 903–914. https://doi.org/10.4161/auto.19653

Mayer, C. T., Ghorbani, P., Nandan, A., Dudek, M., Arnold-Schrauf, C., Hesse, C., Berod, L., Stüve, P., Puttur, F., Merad, M., & Sparwasser, T. (2014). Selective and efficient generation of functional Batf3-dependent CD103+ dendritic cells from mouse bone marrow. *Blood*, *124*(20), 3081–3091. https://doi.org/10.1182/blood-2013-12-545772

Mazel-Sanchez, B., Niu, C., Williams, N., Bachmann, M., Choltus, H., Silva, F., Serre-Beinier, V., Karenovics, W., Iwaszkiewicz, J., Zoete, V., Kaiser, L., Hartley, O., Wehrle-Haller, B., & Schmolke, M. (2023). Influenza A virus exploits transferrin receptor recycling to enter host cells. *Proceedings of the National Academy of Sciences*, *120*(21), e2214936120. https://doi.org/10.1073/pnas.2214936120

McNab, F., Mayer-Barber, K., Sher, A., Wack, A., & O'Garra, A. (2015). Type I interferons in infectious disease. *Nature Reviews Immunology*, *15*(2), 87–103. https://doi.org/10.1038/nri3787

Medzhitov, R. (2008). Origin and physiological roles of inflammation. *Nature*, *454*(7203), 428–435. https://doi.org/10.1038/nature07201

Mendes, A., Gigan, J. P., Rodriguez Rodrigues, C., Choteau, S. A., Sanseau, D., Barros, D., Almeida, C., Camosseto, V., Chasson, L., Paton, A. W., Paton, J. C., Argüello, R. J., Lennon-Duménil, A.-M.,

Gatti, E., & Pierre, P. (2021). Proteostasis in dendritic cells is controlled by the PERK signaling axis independently of ATF4. *Life Science Alliance*, *4*(2), e202000865. https://doi.org/10.26508/lsa.202000865

Michalski, A., Cox, J., & Mann, M. (2011). More than 100,000 detectable peptide species elute in single shotgun proteomics runs but the majority is inaccessible to data-dependent LC-MS/MS. *Journal of Proteome Research*, *10*(4), 1785–1793. https://doi.org/10.1021/pr101060v

Minutti, C. M., Piot, C., Pereira Da Costa, M., Chakravarty, P., Rogers, N., Huerga Encabo, H., Cardoso, A., Loong, J., Bessou, G., Mionnet, C., Langhorne, J., Bonnet, D., Dalod, M., Tomasello, E., & Reis E Sousa, C. (2024). Distinct ontogenetic lineages dictate cDC2 heterogeneity. *Nature Immunology*, *25*(3), 448–461. https://doi.org/10.1038/s41590-024-01745-9

Mkaddem, S. B., Christou, I., Rossato, E., Berthelot, L., Lehuen, A., & Monteiro, R. C. (2014). IgA, IgA Receptors, and Their Anti-inflammatory Properties. In M. Daeron & F. Nimmerjahn (Eds.), *Fc Receptors* (Vol. 382, pp. 221–235). Springer International Publishing. https://doi.org/10.1007/978-3-319-07911-0_10

Mogilenko, D. A., Haas, J. T., L'homme, L., Fleury, S., Quemener, S., Levavasseur, M., Becquart, C., Wartelle, J., Bogomolova, A., Pineau, L., Molendi-Coste, O., Lancel, S., Dehondt, H., Gheeraert, C., Melchior, A., Dewas, C., Nikitin, A., Pic, S., Rabhi, N., … Dombrowicz, D. (2019). Metabolic and Innate Immune Cues Merge into a Specific Inflammatory Response via the UPR. *Cell*, *178*(1), 263. https://doi.org/10.1016/j.cell.2019.06.017

Møller, S. H., Wang, L., & Ho, P.-C. (2022). Metabolic programming in dendritic cells tailors immune responses and homeostasis. *Cellular & Molecular Immunology*, *19*(3), 370–383. https://doi.org/10.1038/s41423-021-00753-1

Momburg, F., Roelse, J., Hämmerling, G. J., & Neefjes, J. J. (1994). Peptide size selection by the major histocompatibility complex-encoded peptide transporter. *The Journal of Experimental Medicine*, *179*(5), 1613–1623. https://doi.org/10.1084/jem.179.5.1613

Mossmann, D., Park, S., & Hall, M. N. (2018). mTOR signalling and cellular metabolism are mutual determinants in cancer. *Nature Reviews Cancer*, *18*(12), 744–757. https://doi.org/10.1038/s41568-018-0074-8

Nachef, M., Ali, A. K., Almutairi, S. M., & Lee, S.-H. (2021). Targeting SLC1A5 and SLC3A2/SLC7A5 as a Potential Strategy to Strengthen Anti-Tumor Immunity in the Tumor Microenvironment. *Frontiers in Immunology*, *12*, 624324. https://doi.org/10.3389/fimmu.2021.624324

Naik, S. H., Metcalf, D., van Nieuwenhuijze, A., Wicks, I., Wu, L., O'Keeffe, M., & Shortman, K. (2006). Intrasplenic steady-state dendritic cell

precursors that are distinct from monocytes. *Nature Immunology*, *7*(6), 663–671. https://doi.org/10.1038/ni1340

Naik, S. H., Sathe, P., Park, H.-Y., Metcalf, D., Proietto, A. I., Dakic, A., Carotta, S., O'Keeffe, M., Bahlo, M., Papenfuss, A., Kwak, J.-Y., Wu, L., & Shortman, K. (2007). Development of plasmacytoid and conventional dendritic cell subtypes from single precursor cells derived in vitro and in vivo. *Nature Immunology*, *8*(11), 1217–1226. https://doi.org/10.1038/ni1522

Nakaya, M., Xiao, Y., Zhou, X., Chang, J.-H., Chang, M., Cheng, X., Blonska, M., Lin, X., & Sun, S.-C. (2014). Inflammatory T cell responses rely on amino acid transporter ASCT2 facilitation of glutamine uptake and mTORC1 kinase activation. *Immunity*, *40*(5), 692–705. https://doi.org/10.1016/j.immuni.2014.04.007

Neefjes, J., Jongsma, M. L. M., Paul, P., & Bakke, O. (2011). Towards a systems understanding of MHC class I and MHC class II antigen presentation. *Nature Reviews Immunology*, *11*(12), 823–836. https://doi.org/10.1038/nri3084

Nemazee, D. (2017). Mechanisms of central tolerance for B cells. *Nature Reviews Immunology*, *17*(5), 281–294. https://doi.org/10.1038/nri.2017.19

Newsholme, P. (2021). Cellular and metabolic mechanisms of nutrient actions in immune function. *European Journal of Clinical Nutrition*, *75*(9), 1328–1331. https://doi.org/10.1038/s41430-021-00960-z

Norian, L. A., Rodriguez, P. C., O'Mara, L. A., Zabaleta, J., Ochoa, A. C., Cella, M., & Allen, P. M. (2009). Tumor-Infiltrating Regulatory Dendritic Cells Inhibit CD8+ T Cell Function via L -Arginine Metabolism. *Cancer Research*, *69*(7), 3086–3094. https://doi.org/10.1158/0008-5472.CAN-08-2826

O'Brien, K. L., & Finlay, D. K. (2019). Immunometabolism and natural killer cell responses. *Nature Reviews Immunology*, *19*(5), 282–290. https://doi.org/10.1038/s41577-019-0139-2

Ohtani, M., Hoshii, T., Fujii, H., Koyasu, S., Hirao, A., & Matsuda, S. (2012). Cutting Edge: mTORC1 in Intestinal CD11c+CD11b+ Dendritic Cells Regulates Intestinal Homeostasis by Promoting IL-10 Production. *The Journal of Immunology*, *188*(10), 4736–4740. https://doi.org/10.4049/jimmunol.1200069

Ohtani, M., Nagai, S., Kondo, S., Mizuno, S., Nakamura, K., Tanabe, M., Takeuchi, T., Matsuda, S., & Koyasu, S. (2008). Mammalian target of rapamycin and glycogen synthase kinase 3 differentially regulate lipopolysaccharide-induced interleukin-12 production in dendritic cells. *Blood*, *112*(3), 635–643. https://doi.org/10.1182/blood-2008-02-137430

Olson, G. S., Murray, T. A., Jahn, A. N., Mai, D., Diercks, A. H., Gold, E. S., & Aderem, A. (2021). Type I interferon decreases macrophage energy

metabolism during mycobacterial infection. *Cell Reports*, *35*(9), 109195. https://doi.org/10.1016/j.celrep.2021.109195

Onai, N., Kurabayashi, K., Hosoi-Amaike, M., Toyama-Sorimachi, N., Matsushima, K., Inaba, K., & Ohteki, T. (2013). A Clonogenic Progenitor with Prominent Plasmacytoid Dendritic Cell Developmental Potential. *Immunity*, *38*(5), 943–957. https://doi.org/10.1016/j.immuni.2013.04.006

Onai, N., Obata-Onai, A., Schmid, M. A., Ohteki, T., Jarrossay, D., & Manz, M. G. (2007). Identification of clonogenic common Flt3+M-CSFR+ plasmacytoid and conventional dendritic cell progenitors in mouse bone marrow. *Nature Immunology*, *8*(11), 1207–1216. https://doi.org/10.1038/ni1518

O'Neill, L. A. J., Kishton, R. J., & Rathmell, J. (2016). A guide to immunometabolism for immunologists. *Nature Reviews Immunology*, *16*(9), 553–565. https://doi.org/10.1038/nri.2016.70

Ong, S.-E., Blagoev, B., Kratchmarova, I., Kristensen, D. B., Steen, H., Pandey, A., & Mann, M. (2002). Stable Isotope Labeling by Amino Acids in Cell Culture, SILAC, as a Simple and Accurate Approach to Expression Proteomics. *Molecular & Cellular Proteomics*, *1*(5), 376–386. https://doi.org/10.1074/mcp.M200025-MCP200

Osorio, F., Tavernier, S. J., Hoffmann, E., Saeys, Y., Martens, L., Vetters, J., Delrue, I., De Rycke, R., Parthoens, E., Pouliot, P., Iwawaki, T., Janssens, S., & Lambrecht, B. N. (2014). The unfolded-protein-response sensor IRE-1α regulates the function of CD8α+ dendritic cells. *Nature Immunology*, *15*(3), 248–257. https://doi.org/10.1038/ni.2808

Palm, W., Park, Y., Wright, K., Pavlova, N. N., Tuveson, D. A., & Thompson, C. B. (2015). The Utilization of Extracellular Proteins as Nutrients Is Suppressed by mTORC1. *Cell*, *162*(2), 259–270. https://doi.org/10.1016/j.cell.2015.06.017

Paludan, S. R., Pradeu, T., Masters, S. L., & Mogensen, T. H. (2021). Constitutive immune mechanisms: Mediators of host defence and immune regulation. *Nature Reviews. Immunology*, *21*(3), 137–150. https://doi.org/10.1038/s41577-020-0391-5

Pandey, A., & Mann, M. (2000). Proteomics to study genes and genomes. *Nature*, *405*(6788), 837–846. https://doi.org/10.1038/35015709

Pantel, A., Teixeira, A., Haddad, E., Wood, E. G., Steinman, R. M., & Longhi, M. P. (2014). Direct Type I IFN but Not MDA5/TLR3 Activation of Dendritic Cells Is Required for Maturation and Metabolic Shift to Glycolysis after Poly IC Stimulation. *PLoS Biology*, *12*(1), e1001759. https://doi.org/10.1371/journal.pbio.1001759

Parcina, M., Wendt, C., Goetz, F., Zawatzky, R., Zähringer, U., Heeg, K., & Bekeredjian-Ding, I. (2008). *Staphylococcus aureus*- Induced Plasmacytoid Dendritic Cell Activation Is Based on an IgG-Mediated

Memory Response. *The Journal of Immunology*, *181*(6), 3823–3833. https://doi.org/10.4049/jimmunol.181.6.3823

Parrow, N. L., Fleming, R. E., & Minnick, M. F. (2013). Sequestration and scavenging of iron in infection. *Infection and Immunity*, *81*(10), 3503–3514. https://doi.org/10.1128/IAI.00602-13

Pasquini, S., Contri, C., Borea, P. A., Vincenzi, F., & Varani, K. (2021). Adenosine and Inflammation: Here, There and Everywhere. *International Journal of Molecular Sciences*, *22*(14), 7685. https://doi.org/10.3390/ijms22147685

Pearce, E. L., & Pearce, E. J. (2013). Metabolic Pathways in Immune Cell Activation and Quiescence. *Immunity*, *38*(4), 633–643. https://doi.org/10.1016/j.immuni.2013.04.005

Pearce, E. L., Poffenberger, M. C., Chang, C.-H., & Jones, R. G. (2013). Fueling Immunity: Insights into Metabolism and Lymphocyte Function. *Science*, *342*(6155), 1242454. https://doi.org/10.1126/science.1242454

Pelgrom, L. R., Davis, G. M., O'Shaughnessy, S., Wezenberg, E. J. M., Van Kasteren, S. I., Finlay, D. K., & Sinclair, L. V. (2023). QUAS-R: An SLC1A5-mediated glutamine uptake assay with single-cell resolution reveals metabolic heterogeneity with immune populations. *Cell Reports*, *42*(8), 112828. https://doi.org/10.1016/j.celrep.2023.112828

Pelgrom, L. R., Patente, T. A., Otto, F., Nouwen, L. V., Ozir-Fazalalikhan, A., Van Der Ham, A. J., Van Der Zande, H. J. P., Heieis, G. A., Arens, R., & Everts, B. (2022). mTORC1 signaling in antigen-presenting cells of the skin restrains CD8+ T cell priming. *Cell Reports*, *40*(1), 111032. https://doi.org/10.1016/j.celrep.2022.111032

Pelgrom, L. R., Patente, T. A., Sergushichev, A., Esaulova, E., Otto, F., Ozir-Fazalalikhan, A., van der Zande, H. J. P., van der Ham, A. J., van der Stel, S., Artyomov, M. N., & Everts, B. (2019). LKB1 expressed in dendritic cells governs the development and expansion of thymus-derived regulatory T cells. *Cell Research*, *29*(5), 406–419. https://doi.org/10.1038/s41422-019-0161-8

Pepper, M., Dzierszinski, F., Wilson, E., Tait, E., Fang, Q., Yarovinsky, F., Laufer, T. M., Roos, D., & Hunter, C. A. (2008). Plasmacytoid Dendritic Cells Are Activated by *Toxoplasma gondii* to Present Antigen and Produce Cytokines. *The Journal of Immunology*, *180*(9), 6229–6236. https://doi.org/10.4049/jimmunol.180.9.6229

Pereira, M., Chen, T.-D., Buang, N., Olona, A., Ko, J.-H., Prendecki, M., Costa, A. S. H., Nikitopoulou, E., Tronci, L., Pusey, C. D., Cook, H. T., McAdoo, S. P., Frezza, C., & Behmoaras, J. (2019). Acute Iron Deprivation Reprograms Human Macrophage Metabolism and Reduces Inflammation In Vivo. *Cell Reports*, *28*(2), 498-511.e5. https://doi.org/10.1016/j.celrep.2019.06.039

Persson, E. K., Uronen-Hansson, H., Semmrich, M., Rivollier, A., Hägerbrand, K., Marsal, J., Gudjonsson, S., Håkansson, U., Reizis, B., Kotarsky, K., & Agace, W. W. (2013). IRF4 transcription-factor-dependent CD103(+)CD11b(+) dendritic cells drive mucosal T helper 17 cell differentiation. *Immunity*, *38*(5), 958–969. https://doi.org/10.1016/j.immuni.2013.03.009

Piertney, S. B., & Oliver, M. K. (2006). The evolutionary ecology of the major histocompatibility complex. *Heredity*, *96*(1), 7–21. https://doi.org/10.1038/sj.hdy.6800724

Pitt, J. J. (2009). Principles and applications of liquid chromatography-mass spectrometry in clinical biochemistry. *The Clinical Biochemist. Reviews*, *30*(1), 19–34.

Platanias, L. C. (2005). Mechanisms of type-I- and type-II-interferon-mediated signalling. *Nature Reviews Immunology*, *5*(5), 375–386. https://doi.org/10.1038/nri1604

Poulin, L. F., Reyal, Y., Uronen-Hansson, H., Schraml, B. U., Sancho, D., Murphy, K. M., Håkansson, U. K., Ferreira Moita, L., Agace, W. W., Bonnet, D., & Reis E Sousa, C. (2012). DNGR-1 is a specific and universal marker of mouse and human Batf3-dependent dendritic cells in lymphoid and nonlymphoid tissues. *Blood*, *119*(25), 6052–6062. https://doi.org/10.1182/blood-2012-01-406967

Preite, N. W., Feriotti, C., Souza De Lima, D., Da Silva, B. B., Condino-Neto, A., Pontillo, A., Calich, V. L. G., & Loures, F. V. (2018). The Syk-Coupled C-Type Lectin Receptors Dectin-2 and Dectin-3 Are Involved in Paracoccidioides brasiliensis Recognition by Human Plasmacytoid Dendritic Cells. *Frontiers in Immunology*, *9*, 464. https://doi.org/10.3389/fimmu.2018.00464

Princiotta, M. F., Finzi, D., Qian, S.-B., Gibbs, J., Schuchmann, S., Buttgereit, F., Bennink, J. R., & Yewdell, J. W. (2003). Quantitating Protein Synthesis, Degradation, and Endogenous Antigen Processing. *Immunity*, *18*(3), 343–354. https://doi.org/10.1016/S1074-7613(03)00051-7

Purohit, V., Wagner, A., Yosef, N., & Kuchroo, V. K. (2022). Systems-based approaches to study immunometabolism. *Cellular & Molecular Immunology*, *19*(3), 409–420. https://doi.org/10.1038/s41423-021-00783-9

Qian, S.-B., Reits, E., Neefjes, J., Deslich, J. M., Bennink, J. R., & Yewdell, J. W. (2006). Tight linkage between translation and MHC class I peptide ligand generation implies specialized antigen processing for defective ribosomal products. *Journal of Immunology (Baltimore, Md.: 1950)*, *177*(1), 227–233. https://doi.org/10.4049/jimmunol.177.1.227

Radoshitzky, S. R., Abraham, J., Spiropoulou, C. F., Kuhn, J. H., Nguyen, D., Li, W., Nagel, J., Schmidt, P. J., Nunberg, J. H., Andrews, N. C., Farzan, M., & Choe, H. (2007). Transferrin receptor 1 is a cellular

receptor for New World haemorrhagic fever arenaviruses. *Nature*, *446*(7131), 92–96. https://doi.org/10.1038/nature05539

Raïch-Regué, D., Rosborough, B. R., Watson, A. R., McGeachy, M. J., Turnquist, H. R., & Thomson, A. W. (2015). mTORC2 Deficiency in Myeloid Dendritic Cells Enhances Their Allogeneic Th1 and Th17 Stimulatory Ability after TLR4 Ligation In Vitro and In Vivo. *The Journal of Immunology*, *194*(10), 4767–4776. https://doi.org/10.4049/jimmunol.1402551

Ratto, E., Chowdhury, S. R., Siefert, N. S., Schneider, M., Wittmann, M., Helm, D., & Palm, W. (2022). Direct control of lysosomal catabolic activity by mTORC1 through regulation of V-ATPase assembly. *Nature Communications*, *13*(1), 4848. https://doi.org/10.1038/s41467-022-32515-6

Reinfeld, B. I., Madden, M. Z., Wolf, M. M., Chytil, A., Bader, J. E., Patterson, A. R., Sugiura, A., Cohen, A. S., Ali, A., Do, B. T., Muir, A., Lewis, C. A., Hongo, R. A., Young, K. L., Brown, R. E., Todd, V. M., Huffstater, T., Abraham, A., O'Neil, R. T., … Rathmell, W. K. (2021). Cell-programmed nutrient partitioning in the tumour microenvironment. *Nature*, *593*(7858), 282–288. https://doi.org/10.1038/s41586-021-03442-1

Reits, E. A., Hodge, J. W., Herberts, C. A., Groothuis, T. A., Chakraborty, M., K.Wansley, E., Camphausen, K., Luiten, R. M., De Ru, A. H., Neijssen, J., Griekspoor, A., Mesman, E., Verreck, F. A., Spits, H., Schlom, J., Van Veelen, P., & Neefjes, J. J. (2006). Radiation modulates the peptide repertoire, enhances MHC class I expression, and induces successful antitumor immunotherapy. *The Journal of Experimental Medicine*, *203*(5), 1259–1271. https://doi.org/10.1084/jem.20052494

Reizis, B. (2019). Plasmacytoid Dendritic Cells: Development, Regulation, and Function. *Immunity*, *50*(1), 37–50. https://doi.org/10.1016/j.immuni.2018.12.027

Reizis, B., Bunin, A., Ghosh, H. S., Lewis, K. L., & Sisirak, V. (2011). Plasmacytoid Dendritic Cells: Recent Progress and Open Questions. *Annual Review of Immunology*, *29*(1), 163–183. https://doi.org/10.1146/annurev-immunol-031210-101345

Rieckmann, J. C., Geiger, R., Hornburg, D., Wolf, T., Kveler, K., Jarrossay, D., Sallusto, F., Shen-Orr, S. S., Lanzavecchia, A., Mann, M., & Meissner, F. (2017). Social network architecture of human immune cells unveiled by quantitative proteomics. *Nature Immunology*, *18*(5), 583–593. https://doi.org/10.1038/ni.3693

Robbins, S. H., Walzer, T., Dembélé, D., Thibault, C., Defays, A., Bessou, G., Xu, H., Vivier, E., Sellars, M., Pierre, P., Sharp, F. R., Chan, S., Kastner, P., & Dalod, M. (2008). Novel insights into the relationships between dendritic cell subsets in human and mouse revealed by

genome-wide expression profiling. *Genome Biology*, *9*(1), R17. https://doi.org/10.1186/gb-2008-9-1-r17

Rock, K. L., Farfán-Arribas, D. J., Colbert, J. D., & Goldberg, A. L. (2014). Re-examining class-I presentation and the DRiP hypothesis. *Trends in Immunology*, *35*(4), 144–152. https://doi.org/10.1016/j.it.2014.01.002

Rodrigues, P. F., Alberti-Servera, L., Eremin, A., Grajales-Reyes, G. E., Ivanek, R., & Tussiwand, R. (2018). Distinct progenitor lineages contribute to the heterogeneity of plasmacytoid dendritic cells. *Nature Immunology*, *19*(7), 711–722. https://doi.org/10.1038/s41590-018-0136-9

Rodrigues, P. F., Kouklas, A., Cvijetic, G., Bouladoux, N., Mitrovic, M., Desai, J. V., Lima-Junior, D. S., Lionakis, M. S., Belkaid, Y., Ivanek, R., & Tussiwand, R. (2023). pDC-like cells are pre-DC2 and require KLF4 to control homeostatic CD4 T cells. *Science Immunology*, *8*(80), eadd4132. https://doi.org/10.1126/sciimmunol.add4132

Rodrigues, P. F., & Tussiwand, R. (2020). Novel concepts in plasmacytoid dendritic cell (pDC) development and differentiation. *Molecular Immunology*, *126*, 25–30. https://doi.org/10.1016/j.molimm.2020.07.006

Ross, P. L., Huang, Y. N., Marchese, J. N., Williamson, B., Parker, K., Hattan, S., Khainovski, N., Pillai, S., Dey, S., Daniels, S., Purkayastha, S., Juhasz, P., Martin, S., Bartlet-Jones, M., He, F., Jacobson, A., & Pappin, D. J. (2004). Multiplexed protein quantitation in Saccharomyces cerevisiae using amine-reactive isobaric tagging reagents. *Molecular & Cellular Proteomics: MCP*, *3*(12), 1154–1169. https://doi.org/10.1074/mcp.M400129-MCP200

Ryans, K., Omosun, Y., McKeithen, D. N., Simoneaux, T., Mills, C. C., Bowen, N., Eko, F. O., Black, C. M., Igietseme, J. U., & He, Q. (2017). The immunoregulatory role of alpha enolase in dendritic cell function during Chlamydia infection. *BMC Immunology*, *18*(1), 27. https://doi.org/10.1186/s12865-017-0212-1

Sallusto, F., Cella, M., Danieli, C., & Lanzavecchia, A. (1995). Dendritic cells use macropinocytosis and the mannose receptor to concentrate macromolecules in the major histocompatibility complex class II compartment: Downregulation by cytokines and bacterial products. *The Journal of Experimental Medicine*, *182*(2), 389–400. https://doi.org/10.1084/jem.182.2.389

Samie, M., & Cresswell, P. (2015). The transcription factor TFEB acts as a molecular switch that regulates exogenous antigen-presentation pathways. *Nature Immunology*, *16*(7), 729–736. https://doi.org/10.1038/ni.3196

Satpathy, A. T., Briseño, C. G., Lee, J. S., Ng, D., Manieri, N. A., Kc, W., Wu, X., Thomas, S. R., Lee, W.-L., Turkoz, M., McDonald, K. G., Meredith,

M. M., Song, C., Guidos, C. J., Newberry, R. D., Ouyang, W., Murphy, T. L., Stappenbeck, T. S., Gommerman, J. L., … Murphy, K. M. (2013). Notch2-dependent classical dendritic cells orchestrate intestinal immunity to attaching-and-effacing bacterial pathogens. *Nature Immunology*, *14*(9), 937–948. https://doi.org/10.1038/ni.2679

Savina, A., Jancic, C., Hugues, S., Guermonprez, P., Vargas, P., Moura, I. C., Lennon-Duménil, A.-M., Seabra, M. C., Raposo, G., & Amigorena, S. (2006). NOX2 Controls Phagosomal pH to Regulate Antigen Processing during Crosspresentation by Dendritic Cells. *Cell*, *126*(1), 205–218. https://doi.org/10.1016/j.cell.2006.05.035

Savina, A., Peres, A., Cebrian, I., Carmo, N., Moita, C., Hacohen, N., Moita, L. F., & Amigorena, S. (2009). The Small GTPase Rac2 Controls Phagosomal Alkalinization and Antigen Crosspresentation Selectively in CD8+ Dendritic Cells. *Immunity*, *30*(4), 544–555. https://doi.org/10.1016/j.immuni.2009.01.013

Saxon, E., & Bertozzi, C. R. (2000). Cell Surface Engineering by a Modified Staudinger Reaction. *Science*, *287*(5460), 2007–2010. https://doi.org/10.1126/science.287.5460.2007

Saxton, R. A., Knockenhauer, K. E., Wolfson, R. L., Chantranupong, L., Pacold, M. E., Wang, T., Schwartz, T. U., & Sabatini, D. M. (2016). Structural basis for leucine sensing by the Sestrin2-mTORC1 pathway. *Science (New York, N.Y.)*, *351*(6268), 53–58. https://doi.org/10.1126/science.aad2087

Saxton, R. A., & Sabatini, D. M. (2017). mTOR Signaling in Growth, Metabolism, and Disease. *Cell*, *168*(6), 960–976. https://doi.org/10.1016/j.cell.2017.02.004

Schlitzer, A., McGovern, N., Teo, P., Zelante, T., Atarashi, K., Low, D., Ho, A. W. S., See, P., Shin, A., Wasan, P. S., Hoeffel, G., Malleret, B., Heiseke, A., Chew, S., Jardine, L., Purvis, H. A., Hilkens, C. M. U., Tam, J., Poidinger, M., … Ginhoux, F. (2013). IRF4 transcription factor-dependent CD11b+ dendritic cells in human and mouse control mucosal IL-17 cytokine responses. *Immunity*, *38*(5), 970–983. https://doi.org/10.1016/j.immuni.2013.04.011

Schlitzer, A., Sivakamasundari, V., Chen, J., Sumatoh, H. R. B., Schreuder, J., Lum, J., Malleret, B., Zhang, S., Larbi, A., Zolezzi, F., Renia, L., Poidinger, M., Naik, S., Newell, E. W., Robson, P., & Ginhoux, F. (2015). Identification of cDC1- and cDC2-committed DC progenitors reveals early lineage priming at the common DC progenitor stage in the bone marrow. *Nature Immunology*, *16*(7), 718–728. https://doi.org/10.1038/ni.3200

Schnorrer, P., Behrens, G. M. N., Wilson, N. S., Pooley, J. L., Smith, C. M., El-Sukkari, D., Davey, G., Kupresanin, F., Li, M., Maraskovsky, E., Belz, G. T., Carbone, F. R., Shortman, K., Heath, W. R., & Villadangos, J. A. (2006). The dominant role of CD8 $^{+}$ dendritic cells

in cross-presentation is not dictated by antigen capture. *Proceedings of the National Academy of Sciences*, *103*(28), 10729–10734. https://doi.org/10.1073/pnas.0601956103

Schoof, E. M., Furtwängler, B., Üresin, N., Rapin, N., Savickas, S., Gentil, C., Lechman, E., Keller, U. A. D., Dick, J. E., & Porse, B. T. (2021). Quantitative single-cell proteomics as a tool to characterize cellular hierarchies. *Nature Communications*, *12*(1), 3341. https://doi.org/10.1038/s41467-021-23667-y

Schubert, O. T., Röst, H. L., Collins, B. C., Rosenberger, G., & Aebersold, R. (2017). Quantitative proteomics: Challenges and opportunities in basic and applied research. *Nature Protocols*, *12*(7), 1289–1294. https://doi.org/10.1038/nprot.2017.040

Schuler, G., & Steinman, R. M. (1985). Murine epidermal Langerhans cells mature into potent immunostimulatory dendritic cells in vitro. *The Journal of Experimental Medicine*, *161*(3), 526–546. https://doi.org/10.1084/jem.161.3.526

Serbina, N. V., Salazar-Mather, T. P., Biron, C. A., Kuziel, W. A., & Pamer, E. G. (2003). TNF/iNOS-producing dendritic cells mediate innate immune defense against bacterial infection. *Immunity*, *19*(1), 59–70. https://doi.org/10.1016/s1074-7613(03)00171-7

Serwold, T., Gonzalez, F., Kim, J., Jacob, R., & Shastri, N. (2002). ERAAP customizes peptides for MHC class I molecules in the endoplasmic reticulum. *Nature*, *419*(6906), 480–483. https://doi.org/10.1038/nature01074

Shen, L., Sigal, L. J., Boes, M., & Rock, K. L. (2004). Important Role of Cathepsin S in Generating Peptides for TAP-Independent MHC Class I Crosspresentation In Vivo. *Immunity*, *21*(2), 155–165. https://doi.org/10.1016/j.immuni.2004.07.004

Shi, L., Chen, X., Zang, A., Li, T., Hu, Y., Ma, S., Lü, M., Yin, H., Wang, H., Zhang, X., Zhang, B., Leng, Q., Yang, J., & Xiao, H. (2019). TSC1/mTOR-controlled metabolic-epigenetic cross talk underpins DC control of CD8+ T-cell homeostasis. *PLoS Biology*, *17*(8), e3000420. https://doi.org/10.1371/journal.pbio.3000420

Shin, S., Han, M.-J., Jedrychowski, M. P., Zhang, Z., Shokat, K. M., Plas, D. R., Dephoure, N., & Yoon, S.-O. (2023). mTOR inhibition reprograms cellular proteostasis by regulating eIF3D-mediated selective mRNA translation and promotes cell phenotype switching. *Cell Reports*, *42*(8), 112868. https://doi.org/10.1016/j.celrep.2023.112868

Sichien, D., Scott, C. L., Martens, L., Vanderkerken, M., Van Gassen, S., Plantinga, M., Joeris, T., De Prijck, S., Vanhoutte, L., Vanheerswynghels, M., Van Isterdael, G., Toussaint, W., Madeira, F. B., Vergote, K., Agace, W. W., Clausen, B. E., Hammad, H., Dalod, M., Saeys, Y., … Guilliams, M. (2016). IRF8 Transcription Factor Controls Survival and Function of Terminally Differentiated

Conventional and Plasmacytoid Dendritic Cells, Respectively. *Immunity*, *45*(3), 626–640. https://doi.org/10.1016/j.immuni.2016.08.013

Sinclair, C., Bommakanti, G., Gardinassi, L., Loebbermann, J., Johnson, M. J., Hakimpour, P., Hagan, T., Benitez, L., Todor, A., Machiah, D., Oriss, T., Ray, A., Bosinger, S., Ravindran, R., Li, S., & Pulendran, B. (2017). mTOR regulates metabolic adaptation of APCs in the lung and controls the outcome of allergic inflammation. *Science*, *357*(6355), 1014–1021. https://doi.org/10.1126/science.aaj2155

Sinclair, L. V., Barthelemy, C., & Cantrell, D. A. (2020). Single Cell Glucose Uptake Assays: A Cautionary Tale. *Immunometabolism*, *2*(4), e200029. https://doi.org/10.20900/immunometab20200029

Sinclair, L. V., Howden, A. J., Brenes, A., Spinelli, L., Hukelmann, J. L., Macintyre, A. N., Liu, X., Thomson, S., Taylor, P. M., Rathmell, J. C., Locasale, J. W., Lamond, A. I., & Cantrell, D. A. (2019). Antigen receptor control of methionine metabolism in T cells. *eLife*, *8*, e44210. https://doi.org/10.7554/eLife.44210

Sinclair, L. V., Neyens, D., Ramsay, G., Taylor, P. M., & Cantrell, D. A. (2018). Single cell analysis of kynurenine and System L amino acid transport in T cells. *Nature Communications*, *9*(1), 1981. https://doi.org/10.1038/s41467-018-04366-7

Sinclair, L. V., Rolf, J., Emslie, E., Shi, Y.-B., Taylor, P. M., & Cantrell, D. A. (2013). Control of amino-acid transport by antigen receptors coordinates the metabolic reprogramming essential for T cell differentiation. *Nature Immunology*, *14*(5), 500–508. https://doi.org/10.1038/ni.2556

Sindrilaru, A., Peters, T., Wieschalka, S., Baican, C., Baican, A., Peter, H., Hainzl, A., Schatz, S., Qi, Y., Schlecht, A., Weiss, J. M., Wlaschek, M., Sunderkötter, C., & Scharffetter-Kochanek, K. (2011). An unrestrained proinflammatory M1 macrophage population induced by iron impairs wound healing in humans and mice. *Journal of Clinical Investigation*, *121*(3), 985–997. https://doi.org/10.1172/JCI44490

Sinha, S., Pereira-Reis, J., Guerra, A., Rivella, S., & Duarte, D. (2021). The Role of Iron in Benign and Malignant Hematopoiesis. *Antioxidants & Redox Signaling*, *35*(6), 415–432. https://doi.org/10.1089/ars.2020.8155

Snyder, J. P., & Amiel, E. (2019). Regulation of Dendritic Cell Immune Function and Metabolism by Cellular Nutrient Sensor Mammalian Target of Rapamycin (mTOR). *Frontiers in Immunology*, *9*, 3145. https://doi.org/10.3389/fimmu.2018.03145

Solt, L. A. (2022). Emerging insights and challenges for understanding T cell function through the proteome. *Frontiers in Immunology*, *13*, 1028366. https://doi.org/10.3389/fimmu.2022.1028366

Specht, H., Emmott, E., Petelski, A. A., Huffman, R. G., Perlman, D. H., Serra, M., Kharchenko, P., Koller, A., & Slavov, N. (2021). Single-cell proteomic and transcriptomic analysis of macrophage heterogeneity using SCoPE2. *Genome Biology*, *22*(1), 50. https://doi.org/10.1186/s13059-021-02267-5

Steinman, R. M., & Witmer, M. D. (1978). Lymphoid dendritic cells are potent stimulators of the primary mixed leukocyte reaction in mice. *Proceedings of the National Academy of Sciences*, *75*(10), 5132–5136. https://doi.org/10.1073/pnas.75.10.5132

Steward, K. F., Eilers, B., Tripet, B., Fuchs, A., Dorle, M., Rawle, R., Soriano, B., Balasubramanian, N., Copié, V., Bothner, B., & Hatzenpichler, R. (2020). Metabolic Implications of Using BioOrthogonal Non-Canonical Amino Acid Tagging (BONCAT) for Tracking Protein Synthesis. *Frontiers in Microbiology*, *11*, 197. https://doi.org/10.3389/fmicb.2020.00197

Stüve, P., Minarrieta, L., Erdmann, H., Arnold-Schrauf, C., Swallow, M., Guderian, M., Krull, F., Hölscher, A., Ghorbani, P., Behrends, J., Abraham, W.-R., Hölscher, C., Sparwasser, T. D., & Berod, L. (2018). De Novo Fatty Acid Synthesis During Mycobacterial Infection Is a Prerequisite for the Function of Highly Proliferative T Cells, But Not for Dendritic Cells or Macrophages. *Frontiers in Immunology*, *9*, 495. https://doi.org/10.3389/fimmu.2018.00495

Suazo, K. F., Park, K.-Y., & Distefano, M. D. (2021). A Not-So-Ancient Grease History: Click Chemistry and Protein Lipid Modifications. *Chemical Reviews*, *121*(12), 7178–7248. https://doi.org/10.1021/acs.chemrev.0c01108

Sukhbaatar, N., Hengstschläger, M., & Weichhart, T. (2016). mTOR-Mediated Regulation of Dendritic Cell Differentiation and Function. *Trends in Immunology*, *37*(11), 778–789. https://doi.org/10.1016/j.it.2016.08.009

Sulczewski, F. B., Maqueda-Alfaro, R. A., Alcántara-Hernández, M., Perez, O. A., Saravanan, S., Yun, T. J., Seong, D., Arroyo Hornero, R., Raquer-McKay, H. M., Esteva, E., Lanzar, Z. R., Leylek, R. A., Adams, N. M., Das, A., Rahman, A. H., Gottfried-Blackmore, A., Reizis, B., & Idoyaga, J. (2023). Transitional dendritic cells are distinct from conventional DC2 precursors and mediate proinflammatory antiviral responses. *Nature Immunology*, *24*(8), 1265–1280. https://doi.org/10.1038/s41590-023-01545-7

Swiecki, M., & Colonna, M. (2015). The multifaceted biology of plasmacytoid dendritic cells. *Nature Reviews Immunology*, *15*(8), 471–485. https://doi.org/10.1038/nri3865

Tan, H., Yang, K., Li, Y., Shaw, T. I., Wang, Y., Blanco, D. B., Wang, X., Cho, J.-H., Wang, H., Rankin, S., Guy, C., Peng, J., & Chi, H. (2017). Integrative Proteomics and Phosphoproteomics Profiling Reveals

Dynamic Signaling Networks and Bioenergetics Pathways Underlying T Cell Activation. *Immunity*, *46*(3), 488–503. https://doi.org/10.1016/j.immuni.2017.02.010

Tavernier, S. J., Osorio, F., Vandersarren, L., Vetters, J., Vanlangenakker, N., Van Isterdael, G., Vergote, K., De Rycke, R., Parthoens, E., van de Laar, L., Iwawaki, T., Del Valle, J. R., Hu, C.-C. A., Lambrecht, B. N., & Janssens, S. (2017). Regulated IRE1-dependent mRNA decay sets the threshold for dendritic cell survival. *Nature Cell Biology*, *19*(6), 698–710. https://doi.org/10.1038/ncb3518

Teh, M. R., Frost, J. N., Armitage, A. E., & Drakesmith, H. (2021). Analysis of Iron and Iron-Interacting Protein Dynamics During T-Cell Activation. *Frontiers in Immunology*, *12*, 714613. https://doi.org/10.3389/fimmu.2021.714613

Thompson, A., Schäfer, J., Kuhn, K., Kienle, S., Schwarz, J., Schmidt, G., Neumann, T., & Hamon, C. (2003). Tandem Mass Tags: A Novel Quantification Strategy for Comparative Analysis of Complex Protein Mixtures by MS/MS. *Analytical Chemistry*, *75*(8), 1895–1904. https://doi.org/10.1021/ac0262560

Thwe, P. M., & Amiel, E. (2018). The role of nitric oxide in metabolic regulation of Dendritic cell immune function. *Cancer Letters*, *412*, 236–242. https://doi.org/10.1016/j.canlet.2017.10.032

Thwe, P. M., Pelgrom, L. R., Cooper, R., Beauchamp, S., Reisz, J. A., D'Alessandro, A., Everts, B., & Amiel, E. (2017). Cell-Intrinsic Glycogen Metabolism Supports Early Glycolytic Reprogramming Required for Dendritic Cell Immune Responses. *Cell Metabolism*, *26*(3), 558-567.e5. https://doi.org/10.1016/j.cmet.2017.08.012

Toby, T. K., Fornelli, L., & Kelleher, N. L. (2016). Progress in Top-Down Proteomics and the Analysis of Proteoforms. *Annual Review of Analytical Chemistry (Palo Alto, Calif.)*, *9*(1), 499–519. https://doi.org/10.1146/annurev-anchem-071015-041550

Toby, T. K., Fornelli, L., Srzentić, K., DeHart, C. J., Levitsky, J., Friedewald, J., & Kelleher, N. L. (2019). A comprehensive pipeline for translational top-down proteomics from a single blood draw. *Nature Protocols*, *14*(1), 119–152. https://doi.org/10.1038/s41596-018-0085-7

Torrence, M. E., MacArthur, M. R., Hosios, A. M., Valvezan, A. J., Asara, J. M., Mitchell, J. R., & Manning, B. D. (2021). The mTORC1-mediated activation of ATF4 promotes protein and glutathione synthesis downstream of growth signals. *eLife*, *10*, e63326. https://doi.org/10.7554/eLife.63326

Trombetta, E. S., Ebersold, M., Garrett, W., Pypaert, M., & Mellman, I. (2003). Activation of lysosomal function during dendritic cell maturation. *Science (New York, N.Y.)*, *299*(5611), 1400–1403. https://doi.org/10.1126/science.1080106

Tussiwand, R., Everts, B., Grajales-Reyes, G. E., Kretzer, N. M., Iwata, A., Bagaitkar, J., Wu, X., Wong, R., Anderson, D. A., Murphy, T. L., Pearce, E. J., & Murphy, K. M. (2015). Klf4 expression in conventional dendritic cells is required for T helper 2 cell responses. *Immunity*, *42*(5), 916–928. https://doi.org/10.1016/j.immuni.2015.04.017

Urbiola-Salvador, V., Miroszewska, D., Jabłońska, A., Qureshi, T., & Chen, Z. (2022). Proteomics approaches to characterize the immune responses in cancer. *Biochimica et Biophysica Acta (BBA) - Molecular Cell Research*, *1869*(8), 119266. https://doi.org/10.1016/j.bbamcr.2022.119266

Van Kasteren, S., & Rozen, D. E. (2023). Using click chemistry to study microbial ecology and evolution. *ISME Communications*, *3*(1), 9. https://doi.org/10.1038/s43705-022-00205-5

Van Montfoort, N., Camps, M. G., Khan, S., Filippov, D. V., Weterings, J. J., Griffith, J. M., Geuze, H. J., Van Hall, T., Verbeek, J. S., Melief, C. J., & Ossendorp, F. (2009). Antigen storage compartments in mature dendritic cells facilitate prolonged cytotoxic T lymphocyte cross-priming capacity. *Proceedings of the National Academy of Sciences*, *106*(16), 6730–6735. https://doi.org/10.1073/pnas.0900969106

Veglia, F., Tyurin, V. A., Mohammadyani, D., Blasi, M., Duperret, E. K., Donthireddy, L., Hashimoto, A., Kapralov, A., Amoscato, A., Angelini, R., Patel, S., Alicea-Torres, K., Weiner, D., Murphy, M. E., Klein-Seetharaman, J., Celis, E., Kagan, V. E., & Gabrilovich, D. I. (2017). Lipid bodies containing oxidatively truncated lipids block antigen cross-presentation by dendritic cells in cancer. *Nature Communications*, *8*(1), 2122. https://doi.org/10.1038/s41467-017-02186-9

Verberk, S. G. S., De Goede, K. E., Gorki, F. S., Van Dierendonck, X. A. M. H., Argüello, R. J., & Van Den Bossche, J. (2022). An integrated toolbox to profile macrophage immunometabolism. *Cell Reports Methods*, *2*(4), 100192. https://doi.org/10.1016/j.crmeth.2022.100192

Villani, A.-C., Satija, R., Reynolds, G., Sarkizova, S., Shekhar, K., Fletcher, J., Griesbeck, M., Butler, A., Zheng, S., Lazo, S., Jardine, L., Dixon, D., Stephenson, E., Nilsson, E., Grundberg, I., McDonald, D., Filby, A., Li, W., De Jager, P. L., … Hacohen, N. (2017). Single-cell RNA-seq reveals new types of human blood dendritic cells, monocytes, and progenitors. *Science*, *356*(6335), eaah4573. https://doi.org/10.1126/science.aah4573

Voss, K., Hong, H. S., Bader, J. E., Sugiura, A., Lyssiotis, C. A., & Rathmell, J. C. (2021). A guide to interrogating immunometabolism. *Nature Reviews. Immunology*, *21*(10), 637–652. https://doi.org/10.1038/s41577-021-00529-8

Vremec, D., Hansen, J., Strasser, A., Acha-Orbea, H., Zhan, Y., O'Keeffe, M., & Shortman, K. (2015). Maintaining dendritic cell viability in culture. *Molecular Immunology*, *63*(2), 264–267. https://doi.org/10.1016/j.molimm.2014.07.011

Vremec, D., O'Keeffe, M., Wilson, A., Ferrero, I., Koch, U., Radtke, F., Scott, B., Hertzog, P., Villadangos, J., & Shortman, K. (2011). Factors determining the spontaneous activation of splenic dendritic cells in culture. *Innate Immunity*, *17*(3), 338–352. https://doi.org/10.1177/1753425910371396

Wang, Y., Du, X., Wei, J., Long, L., Tan, H., Guy, C., Dhungana, Y., Qian, C., Neale, G., Fu, Y.-X., Yu, J., Peng, J., & Chi, H. (2019). LKB1 orchestrates dendritic cell metabolic quiescence and anti-tumor immunity. *Cell Research*, *29*(5), 391–405. https://doi.org/10.1038/s41422-019-0157-4

Wang, Y., Huang, G., Zeng, H., Yang, K., Lamb, R. F., & Chi, H. (2013). Tuberous sclerosis 1 (Tsc1)-dependent metabolic checkpoint controls development of dendritic cells. *Proceedings of the National Academy of Sciences*, *110*(50). https://doi.org/10.1073/pnas.1308905110

Warburg, O. (1956). On the Origin of Cancer Cells. *Science*, *123*(3191), 309–314. https://doi.org/10.1126/science.123.3191.309

Ward, D. M., & Kaplan, J. (2012). Ferroportin-mediated iron transport: Expression and regulation. *Biochimica Et Biophysica Acta*, *1823*(9), 1426–1433. https://doi.org/10.1016/j.bbamcr.2012.03.004

Waskow, C., Liu, K., Darrasse-Jèze, G., Guermonprez, P., Ginhoux, F., Merad, M., Shengelia, T., Yao, K., & Nussenzweig, M. (2008). The receptor tyrosine kinase Flt3 is required for dendritic cell development in peripheral lymphoid tissues. *Nature Immunology*, *9*(6), 676–683. https://doi.org/10.1038/ni.1615

Wculek, S. K., Cueto, F. J., Mujal, A. M., Melero, I., Krummel, M. F., & Sancho, D. (2020). Dendritic cells in cancer immunology and immunotherapy. *Nature Reviews. Immunology*, *20*(1), 7–24. https://doi.org/10.1038/s41577-019-0210-z

Wculek, S. K., Khouili, S. C., Priego, E., Heras-Murillo, I., & Sancho, D. (2019). Metabolic Control of Dendritic Cell Functions: Digesting Information. *Frontiers in Immunology*, *10*, 775. https://doi.org/10.3389/fimmu.2019.00775

Weichhart, T., Costantino, G., Poglitsch, M., Rosner, M., Zeyda, M., Stuhlmeier, K. M., Kolbe, T., Stulnig, T. M., Hörl, W. H., Hengstschläger, M., Müller, M., & Säemann, M. D. (2008). The TSC-mTOR signaling pathway regulates the innate inflammatory response. *Immunity*, *29*(4), 565–577. https://doi.org/10.1016/j.immuni.2008.08.012

Weichhart, T., Haidinger, M., Katholnig, K., Kopecky, C., Poglitsch, M., Lassnig, C., Rosner, M., Zlabinger, G. J., Hengstschläger, M., Müller,

M., Hörl, W. H., & Säemann, M. D. (2011). Inhibition of mTOR blocks the anti-inflammatory effects of glucocorticoids in myeloid immune cells. *Blood*, *117*(16), 4273–4283. https://doi.org/10.1182/blood-2010-09-310888

Weigert, A., Weichand, B., Sekar, D., Sha, W., Hahn, C., Mora, J., Ley, S., Essler, S., Dehne, N., & Brüne, B. (2012). HIF-1α is a negative regulator of plasmacytoid DC development in vitro and in vivo. *Blood*, *120*(15), 3001–3006. https://doi.org/10.1182/blood-2012-03-417022

Weiss, G. (2015). Impact of Metals on Immune Response and Tolerance, and Modulation of Metal Metabolism during Infection. In J. O. Nriagu & E. P. Skaar (Eds.), *Trace Metals and Infectious Diseases*. MIT Press. http://www.ncbi.nlm.nih.gov/books/NBK569673/

Weiss, H. J., & Angiari, S. (2020). Metabolite Transporters as Regulators of Immunity. *Metabolites*, *10*(10), 418. https://doi.org/10.3390/metabo10100418

Wimmers, F., Subedi, N., Van Buuringen, N., Heister, D., Vivié, J., Beeren-Reinieren, I., Woestenenk, R., Dolstra, H., Piruska, A., Jacobs, J. F. M., Van Oudenaarden, A., Figdor, C. G., Huck, W. T. S., De Vries, I. J. M., & Tel, J. (2018). Single-cell analysis reveals that stochasticity and paracrine signaling control interferon-alpha production by plasmacytoid dendritic cells. *Nature Communications*, *9*(1), 3317. https://doi.org/10.1038/s41467-018-05784-3

Wiśniewski, J. R., Hein, M. Y., Cox, J., & Mann, M. (2014). A “proteomic ruler” for protein copy number and concentration estimation without spike-in standards. *Molecular & Cellular Proteomics: MCP*, *13*(12), 3497–3506. https://doi.org/10.1074/mcp.M113.037309

Wolowczuk, I., Verwaerde, C., Viltart, O., Delanoye, A., Delacre, M., Pot, B., & Grangette, C. (2008). Feeding our immune system: Impact on metabolism. *Clinical & Developmental Immunology*, *2008*, 639803. https://doi.org/10.1155/2008/639803

Worah, K., Mathan, T. S. M., Vu Manh, T. P., Keerthikumar, S., Schreibelt, G., Tel, J., Duiveman-de Boer, T., Sköld, A. E., van Spriel, A. B., de Vries, I. J. M., Huynen, M. A., Wessels, H. J., Gloerich, J., Dalod, M., Lasonder, E., Figdor, C. G., & Buschow, S. I. (2016). Proteomics of Human Dendritic Cell Subsets Reveals Subset-Specific Surface Markers and Differential Inflammasome Function. *Cell Reports*, *16*(11), 2953–2966. https://doi.org/10.1016/j.celrep.2016.08.023

Wu, D., Sanin, D. E., Everts, B., Chen, Q., Qiu, J., Buck, M. D., Patterson, A., Smith, A. M., Chang, C.-H., Liu, Z., Artyomov, M. N., Pearce, E. L., Cella, M., & Pearce, E. J. (2016). Type 1 Interferons Induce Changes in Core Metabolism that Are Critical for Immune Function. *Immunity*, *44*(6), 1325–1336. https://doi.org/10.1016/j.immuni.2016.06.006

Yewdell, J. W., Antón, L. C., & Bennink, J. R. (1996). Defective ribosomal products (DRiPs): A major source of antigenic peptides for MHC class

l molecules? *Journal of Immunology (Baltimore, Md.: 1950)*, *157*(5), 1823–1826.

Yoo, H. C., Yu, Y. C., Sung, Y., & Han, J. M. (2020). Glutamine reliance in cell metabolism. *Experimental & Molecular Medicine*, *52*(9), 1496–1516. https://doi.org/10.1038/s12276-020-00504-8

Zhang, Y., Fonslow, B. R., Shan, B., Baek, M.-C., & Yates, J. R. (2013). Protein analysis by shotgun/bottom-up proteomics. *Chemical Reviews*, *113*(4), 2343–2394. https://doi.org/10.1021/cr3003533